MASTER THESIS

FLEXURAL BEHAVIOUR OF REINFORCED CONCRETE BEAMS WITH A LAYER OF SHCC IN THE TENSION ZONE – Experimental Study

by

Zhekang Huang

To obtain the degree of Master of Science
at the Delft University of Technology

Student Number:	4504771	
Project Duration:	February 2017- November 2017	
Thesis Committee:	Prof.dr.ir. D.A. Hordijk (chair)	TU Delft - Structural and Building Engineering: Concrete Structures
	Dr. M. Luković (daily supervisor)	TU Delft - Structural and Building Engineering: Concrete Structures
	Prof.dr.ir. E. Schlangen	TU Delft – Materials and Environment
	Dr. H.M. Jonkers	TU Delft – Materials and Environment

Table of Content

LIST OF ABBRIVIATIONS

DIC	Digital image correlation
ECC	Engineered cementitious composite (different term used for SHCC)
GFRC	Glass fiber reinforced concrete
HPFRCC	High-performance fiber-reinforced cementitious composite
ImageJ	Image analysis software package
LVDT	Linear variable data transformer
RC	Reinforced concrete
R/SHCC	Reinforced strain hardening cementitious composite
SHCC	Strain hardening cementitious composite
SLS	Serviceability limit state
UHPC	Ultra-high performance concrete
UHP-SHCC	Ultra-high performance strain hardening cementitious composite
ULS	Ultimate limit state
w/c	Water cement ratio

LIST OF FIGURES

LIST OF TABLES

Abstract

In the structural design, both Ultimate Limit State (ULS) and Serviceability Limit State (SLS) should be satisfied. In SLS, maximum crack width for reinforced concrete structures is an important criterion. If the calculated crack width of a structure exceeds the maximum allowable crack width, extra reinforcement is required to control crack width. This extra steel is not required by the capacity criterions (ULS). Beside by adding the extra steel reinforcement, is there another possibly to control the crack widths in reinforced concrete structures? May recently developed innovative materials offer a solution?

Strain Hardening Cementitious Composite (SHCC) is a relatively new material, known for its ductility and crack control ability. Thus, the main idea of this research is to apply SHCC in the beam tension zone, which may help control the crack widths, without the need to add extra steel.

The aim of this experimental study is to investigate the crack control behavior of the reinforced concrete beam enhanced with SHCC layer in the tension zone. In order to investigate the influence of different thickness of the SHCC layer, reinforced concrete beams with two different thicknesses of SHCC layer are designed, 30 mm and 70 mm. In order to investigate whether adding self-healing agent in SHCC mixture will influence the crack width control ability, for each thickness, two beams are made. In one beam, self-healing agent is applied in the SHCC zone. The enhanced beams are compared to the regular reinforced concrete (control) beams with the same dimensions and rebar position. Specimens were tested in four-point bending while Digital Image Correlation (DIC) and an image analysis software package (ImageJ) were used to evaluate crack pattern development and crack widths. The procedure was developed to evaluate the displacements and crack widths during the loading from DIC. The results were verified with the measurement obtained by linear variable differential transformers (LVDTs) and Image J, respectively.

The experimental results show that SHCC enhanced beams have higher load carrying capacities and better cracking behavior compared to control beams. The thicker the SHCC layer is, the higher the load capacity is: beams with 70 mm SHCC layer have 26% higher capacity, while beams with 30 mm SHCC layer have 17% higher capacity compared to control beams.

Furthermore, beams with 70 mm SHCC layer have better crack control behavior: the maximum crack width exceeds 0.3 mm at 92% and 83% of their capacities (at 66 kN and 62 kN load), whereas the maximum crack width of the control beam reaches that crack width at 60% of its capacity (at 35 kN load). The beams with 30 mm SHCC layer show less benefits: the maximum crack width exceed 0.3 mm at 93% of their capacities (at 66 kN and 67 kN load), whereas the maximum crack width of the control beam reaches that crack width at 95% of its capacity (at 61 kN load). Finally, experimental results are also compared to numerical calculations and theoretical models. Based on the numerical calculations, the capacities of the beams with SHCC layer can be well predicted.

The conclusions can be drawn that maximum crack width of the beam can be controlled by thick SHCC layer (70 mm SHCC layer for beam with 200 mm height) in the beam tension zone. The thin SHCC layer (30 mm SHCC layer for the beam with 200 height) in the tension zone has no clear evidence of controlling the maximum crack width. However, the comparison group of beams with the SHCC layer of 30 mm and their control RC beam is not presentative, since 11 mm concrete cover, as applied in these cases, is not normative thickness. In addition, as the crack width of RC beam with concrete cover of 11 mm is already very small prior to yielding of the steel, there is no need to further reduce this maximum crack width. There is no difference on cracking behavior between the beam with SHCC layer and the beam with SHCC layer containing self-healing agents.

To summarize, applying SHCC in beam tension zone can increase the beam capacity. And there is a trend that the higher the SHCC layer is, the more the capacity increases. However, in reality, the beams would have higher height, thus the contribution of SHCC layer on their structural capacity will be lower, or negligible. The more important benefit of applying SHCC in the tension zone of the reinforced concrete structures is the

controlled crack width which can reduce the amount of additional reinforcement needed to satisfy SLS.

1

Introduction

In the structural design, there are two governing criteria for design, ultimate limit state (ULS) and serviceability limit state (SLS), which should be both satisfied. ULS focuses on the strength of the structural components to ensure the structural safety. While SLS focus on functionalities of the structure, deflection, cracking and vibration. In SLS, crack width is one very important criterion. If the maximum crack width of a structure is larger than 0.3 mm which is the recommended value in EC-2 for reinforcement concrete under quasi-permanent load for exposure classes except for X0 and XC1, the additional reinforcement must be added to control crack width and satisfy SLS criterion (2004,CEN). Even though the structure satisfies the ULS criterions. From ULS point of view, the extra reinforcement is partially wasted, because the strength is way beyond the required one.

For example, a 1.5-meter long beam need to be designed. The ULS load is 50 kN (the highest load the beam might suffer from, excluding the extreme conditions, such as a bomb-attack or a big earthquake) and the maximum crack width under serviceability load of 40 kN should be smaller than 0.3 mm. Based on the ULS load, a cross-section is designed with three 8 mm diameter rebars (Figure 1). The maximum crack width is found to be 0.4 mm under SLS load, which is larger than recommended value of 0.3 mm. To satisfy the maximum crack width criterion, an extra rebar with 8 mm diameter is added to control the crack width, which leads to the cross-section presented in Figure 2. Although the cross-section in Figure 2 satisfies both ULS and SLS criterions, its capacity is higher than what is required by ULS criteria. Figure 3 illustrates the Load-Deflection curve and the maximum crack width under serviceability load of the two beams with cross-sections in Figure 1 and 2. Beside by adding the extra steel reinforcement, is there another possibly to control the crack widths in reinforced concrete structures? May recently developed innovative materials offer a solution?

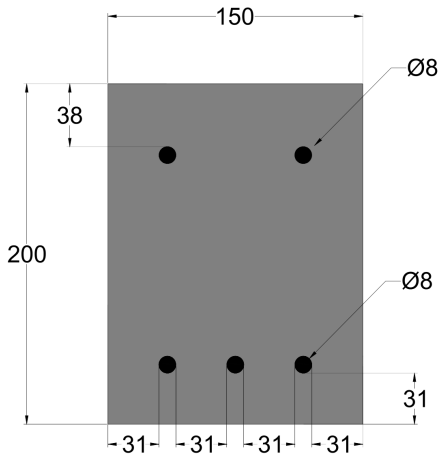

Figure 1 Cross-section with As=150.8 mm^2

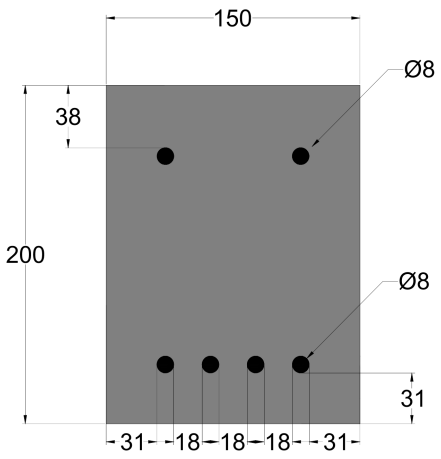

Figure 2 Cross-section with As=201.1 mm^2

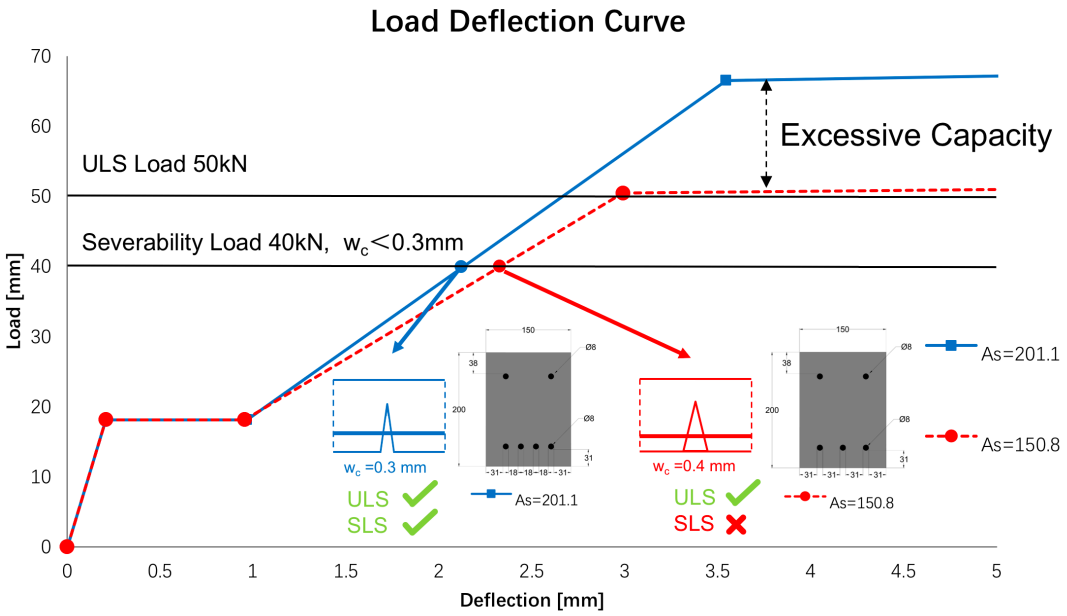

Figure 3 Conceptual Load-Deflection curves and maximum crack widths under SLS of the two beams cross-sections

Nowadays, many innovative building materials are developed. Strain-hardening cementitious composite (SHCC) is one of them. SHCC has the ability to control crack widths by smearing one large crack into many small cracks. This can be attributed to the bridge effect of fibers in the SHCC and special composition of SHCC matrix (almost no use of coarse aggregates but only fine sand). Therefore, SHCC can be placed in the tension zone of beams, around reinforcement, in the zone which is susceptible to large cracks and subsequently durability problems, to control crack widths. If this composite system, consisting of SHCC and concrete, is proved that it can control the crack widths,

the additional reinforcement, aimed to satisfy SLS criterion, but originally not needed for ULS requirements, might be either reduced or completely omitted.

Additional benefit of this hybrid SHCC-concrete system would be if its production procedure could be automatized. With the increase of labor price, due to economic reason, prefabricated concrete elements are getting more and more popular. Between the cast in-situ and prefabricated concrete, there is a third method, partially prefabricated and partly cast in-situ. This method is already implemented in wall and floor constructions. In wall construction, it is known as 'hollow walls' or 'Alvon walls' which consist of two reinforced, prefabricated shells approx. 60 mm thick interconnected with lattice girders (Figure 4). The shells act as formwork and concrete can be casted in between. In floor construction, an example is lattice girder floor, prefabricated slab with cast in-situ structural topping (Figure 5).

Figure 4 Hollow wall

Figure 5 Lattice girder floor

The same method can be applied to beam construction, creating a U-shape shell as formwork (Banthia *et al.*, 2012). SHCC might be an ideal material to make the shell in which the reinforcement will be embedded. This can be used as prefabricated stay-in-place mould, which, due to its lightness, can be easily transported to the construction site, where the remaining concrete is casted on site. Unlike the conventional concrete, SHCC is known for fine crack widths (crack widths smaller than 100 microns) and high ductility (around 500 times higher than that of the conventional concrete), and could provide the additional benefits of controlled crack widths only in zones where needed – in the concrete cover zones, in regions exposed to tensile stresses.

Provided that the system works, there are numerous advantages that could be achieved compared to the traditional way of construction. Besides the reinforcement saving (no additional reinforcement needed for controlling crack widths), stay-in-place SHCC mould with the embedded reinforcement within it allows faster and more precise construction and requires less man labour on site. With the man labour transferred from the construction site to the factory, working environment will also be improved.

With the 'durable shell', even with the less durable material inside it, the overall durability of the beam remains satisfactorily. Therefore, less durable materials, such as very porous concrete, recycled concrete or lightweight concrete, could be applied in the core, without compromising the overall durability.

2

Literature Review

2.1. Crack width

2.1.1. Eurocode serviceability limit states (SLS)

According to Eurocode 2 (CEN, 2004), cracking shall be limited to an extent that will not impair the proper functioning or durability of the structure or cause its appearance to be unacceptable. Thus, a limiting calculated crack width, w_{max}, should be established. The recommended w_{max} values are given in Table 1:

Table 1 Recommended maximum crack width under different exposure classes (CEN, 2004)

Exposure Class	Reinforced members and prestressed members with unbonded tendons	Prestressed members with bonded tendons
	Quasi-permanent load combination	Frequent load combination
X0, XC1	0,4[1]	0,2
XC2, XC3, XC4	0,3	0,2[2]
XD1, XD2, XS1, XS2, XS3		Decompression

Note 1: For X0, XC1 exposure classes, crack width has no influence on durability and this limit is set to guarantee acceptable appearance. In the absence of appearance conditions this limit may be relaxed.
Note 2: For these exposure classes, in addition, decompression should be checked under the quasi-permanent combination of loads.

The exposure classes mentioned above are related to environmental conditions, and the descriptions are shown in Table 2. The more hazardous environment requires usually the stricter crack width control.

Table 2 Description of the environment for different exposure classes (CEN, 2004)

Exposure Class	Description of the environment
X0	For concrete without reinforcement or embedded metal: all exposures except where there is freeze/thaw, abrasion or chemical attack. For concrete with reinforcement or embedded metal: very dry
XC1	Dry or permanently wet
XC2	Wet, rarely dry
XC3	Moderate humidity
XC4	Cyclic wet and dry
XD1	Moderate humidity
XD2	Wet, rarely dry
XS1	Exposed to airborne salt but not in direct contact with sea water
XS2	Permanently submerged
XS3	Tidal, splash and spray zones

2.1.2. Corrosion of rebar

Requirements related to the maximum crack width are usually related to susceptibility of reinforced concrete structures for the corrosion of the embed steel. Corrosion of a metal is an electrochemical process that requires an oxidizing agent, moisture, and electron flow within the metal; a series of chemical reactions take place on and adjacent to the surface of the metal (ACI 201.R2, 2016).

Although concrete provides cover and alkaline environment to the rebar, with carbonation of the concrete cover and cracks on the surface, which enable penetration of hazardous substances, such as chloride ions to the reinforcement, the corrosion may still occur.

After the corrosion, not only the cross-section area of steel is reduced, the rebar expands since the corroded substance has a much higher volume than steel (J. Verbeck and Erlin, 1975), which generates stress in the structure. This will lead to cracks, and even spalling of concrete. This is undesirable for both ultimate limit state and serviceability limit state (Koteš, 2013).

Crack and corrosion have the interaction. Cracks provide easy access for oxygen, moisture, and chlorides, and thus, surface cracks can create a condition in which corrosion and cracking are accelerated. Therefore, the usual requirements in concrete structures include limiting the maximum allowable crack width due to durability reasons. In more aggressive environment, the structure will be more susceptible to rebar corrosion and the maximum allowable crack widths are smaller. As indicated before, one conventional way of reducing maximum crack widths is by increasing the amount of the reinforcement. The question that imposes is whether recently developed innovative concrete-type materials can also offer opportunities for this specific problem?

2.2. SHCC

SHCC (in different literature also named as Engineered Cementitious composite, SHCC or HPFRCC) is a new type of concrete. It is called concrete, while it is not real concrete, but more paste or mortar because it contains only fine sand (no coarse aggregates) and usually around 2% of fibers. Beside mixture composition, the main difference between SHCC and conventional concrete is that SHCC has a pseudo-strain-hardening behavior: the load that sample can withstand, will not decrease after the first crack, but during the consecutive cracking would even further increase, until the specimen finally fails at very large deformations. SHCC is also known for its high ductility (Figure 6) and ability to have controlled crack width (multiple cracking behavior with crack widths usually smaller than 100 μm, Figure 7). This can be attributed to the mechanics of the fiber-matrix interaction within SHCC and the micro particle size. When a micro crack forms, the fibers will take over the tensile force. To further open the crack, the fibers need to be pulled out or broken, which requires higher force. And before pulling out or breaking of the fibers, a new micro crack will form at another location, which leads to a rise in deformation. This

successive cracking and crack bridging by fibers at increasing load leads to the strain-hardening behavior of SHCC.

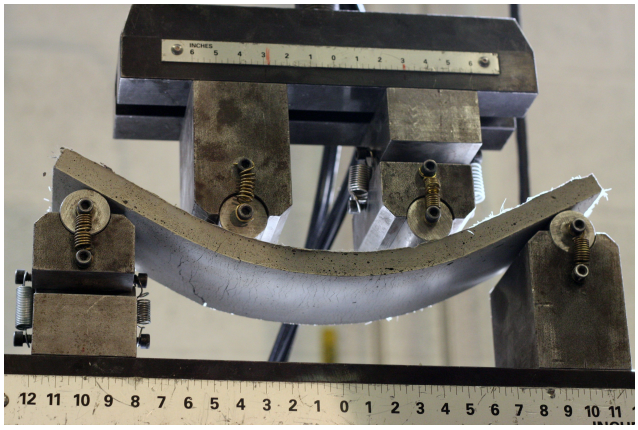

Figure 6 SHCC flexural specimen showing large deflection (University of Michigan, 2009)

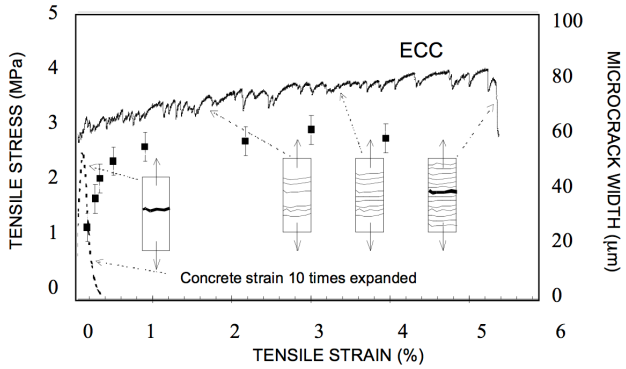

Figure 7 A tensile stress-strain curve of an SHCC, showing also the crack width development as a function of imposed tensile strain (Li, 2007).

2.2.1. Mechanical properties

SHCCs can be regarded as a family of materials whose mechanical properties vary due to different receipts and mixing procedures. The ranges of the major properties are shown in Table 3:

Table 3 Ranges of the Major Properties of SHCC (Li, 2007)

Compressive Strength [MPa]	**First Crack Strength [MPa]**	**Ultimate Tensile Strength [MPa]**	**Ultimate Tensile Strain [%]**	**Young' s Modulus [GPa]**	**Flexural Strength [MPa]**	**Density [g/cc]**
20 – 95	3–7	4 – 12	1–8	18 – 34	10 – 30	0.95 – 2.3

The most significant is that the ultimate tensile strain is hundreds of times larger than that of the conventional concrete.

Due to the large tensile ductility of SHCC, the combination of SHCC and steel reinforcement creates a synergistic load sharing capability in structural members. As a result, steel reinforcements in R/SHCC members are better utilized in enhancing structural performance (Li, 2007).

2.2.2. Durability

Transport properties

According to Li (2007), the transport properties of SHCC associated with permeability under hydraulic gradient, diffusion under ion concentration gradient, or sorption and absorption under capillary suction are all improved compared to concrete.

Water permeability

According to the tests of Lepech and Li (2005), the cracked SHCC strained in tension to several percent exhibited nearly the same water permeability ($k=5x10^{-11}$m/s) as uncracked concrete (Figure 8).

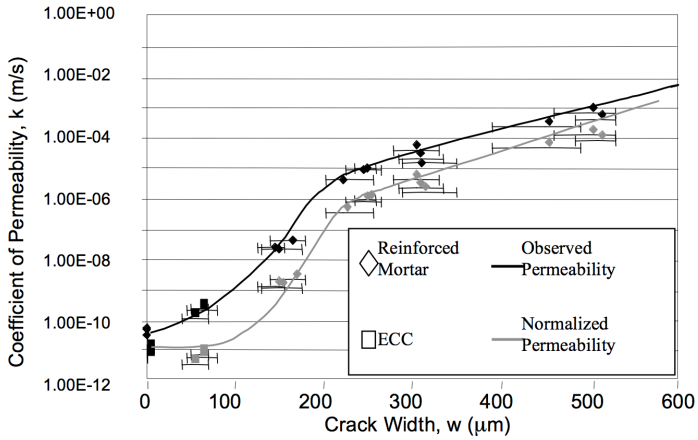

Figure 8 Permeability of precracked SHCC and reinforced mortar measured as a function of crack width (Lepech, M.D. & Li, 2005).

Capillary suction

Neville (1995) reported that typical sorptivity index is 0.09 mm/min$^{1/2}$ for conventional concrete with a water to cement (w/c) ratio of 0.4. According to Şahmaran and Li (2008), the sorptivity index of cracked and virgin SHCC specimens at w/c ratio of 0.27 was significantly lower than that of conventional concrete (Figure 9).

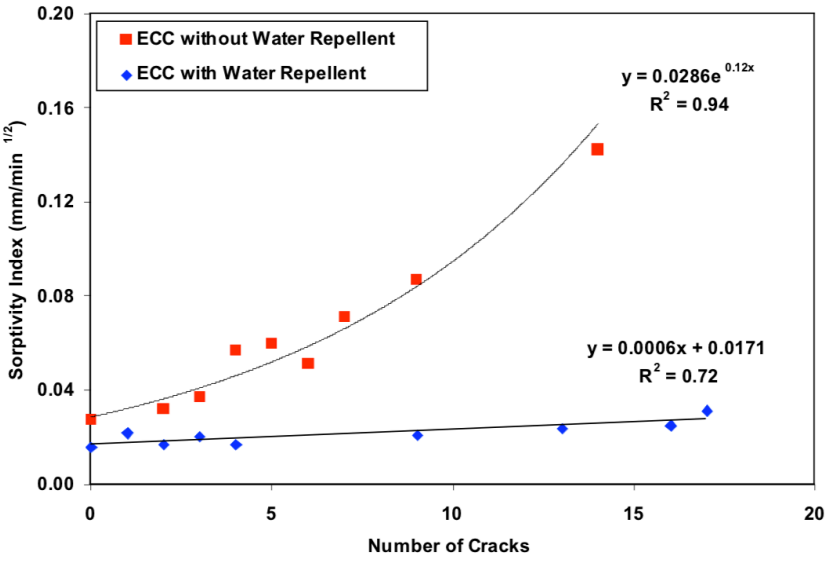

Figure 9 Capillary transport properties measured for preloaded SHCC beams, showing the effects of water repellent on sorptivity index as a function of the number of cracks (Şahmaran and Li, 2008).

Chloride diffusion

Şahmaran et al. (2011) investigated the chloride diffusion coefficients of SHCC. According to the tests on uncracked beams, the chloride diffusion coefficient of SHCC was found to be 6.75×10-12 m^2/s, and the chloride diffusion coefficient of steel reinforced mortar beam was 10.58×10-12 m^2/s. This indicates that SHCC has better chloride resistance than mortar under uncracked condition.

Under high imposed bending deformation, preloaded SHCC beam specimens exhibited microcracks less than 50 μm and an effective diffusion coefficient significantly lower than

that of similarly preloaded reinforced mortar control beams due to the tight crack widths inherent in SHCC (Figure 10).

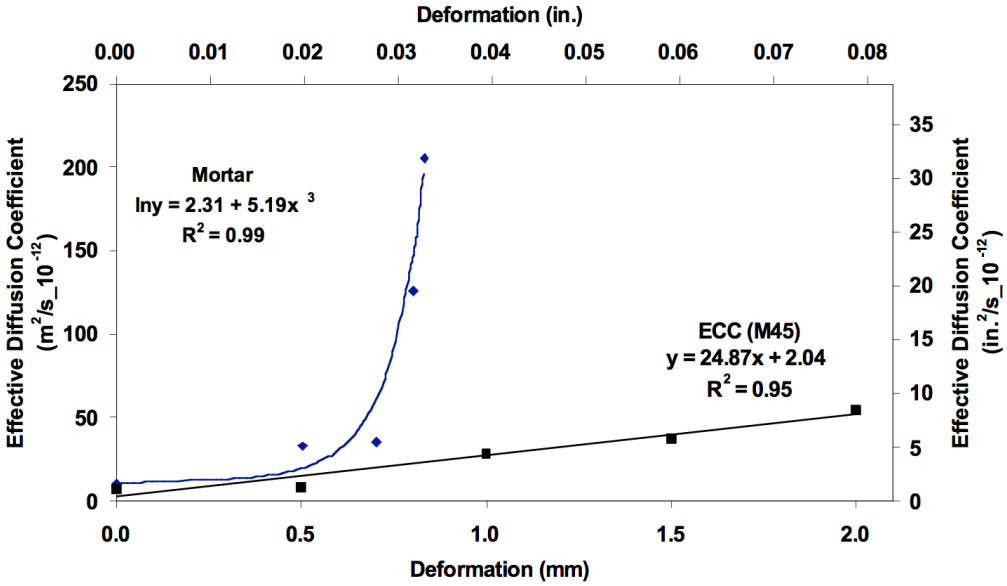

Figure 10 Diffusion coefficient versus pre-loading deformation level for SHCC and mortar (Sahmaran, Li and Li, 2011)

2.2.3. Corrosion resistance in R/SHCC

Miyazato and Hiraishi (2005) carried out a study on chloride penetration rate and corrosion rate of steel reinforcement. The experiment setups are shown in Figure 11. In the test, Reinforced SHCC beams (R/SHCC) and reinforced concrete beams (R/C) were preloaded to 20 kN for crack generation. In R/C beams, the deep crack with about 0.3-0.4mm width was generated. The multiple shallow cracks with the width of 0.1 mm or smaller were generated in R/SHCC specimen. And all crack widths were sustained (did not increase in width) during the exposure period. R/SHCC and R/C beams were exposed to 28 days chloride accelerated environment with wet (saltwater shower 90% RH – 2 days) and dry (60% RH – 5 days) cycles. The results showed that in the R/SHCC chloride penetration reaches 0-20 mm and that in the R/C beams it reaches 80-100 mm. Micro-cell and macro-cell corrosion are two types of corrosion in reinforced concrete structures (Hansson, Poursaee and Laurent, 2006). The total (macro and micro cell) steel

rebar corrosion rate in the R/SHCC was measured to be less than 0.0004 mm/year but in the R/C beams that exceeded 0.008 mm/year (Figure 12).

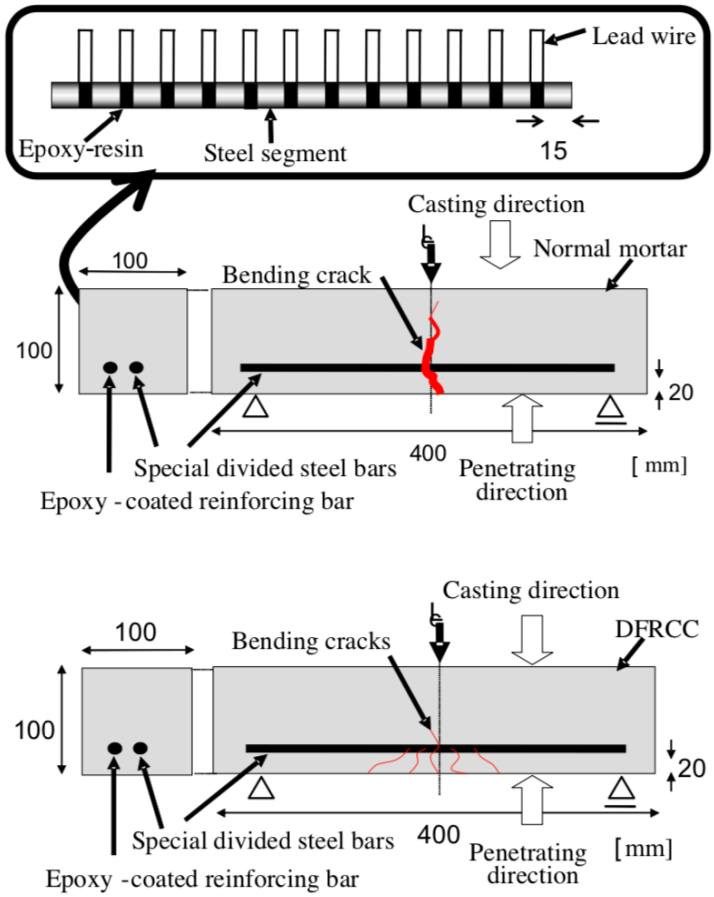

Figure 11 Specimen configurations and Experiment setups for corrosion test (Miyazato and Hiraishi, 2005).

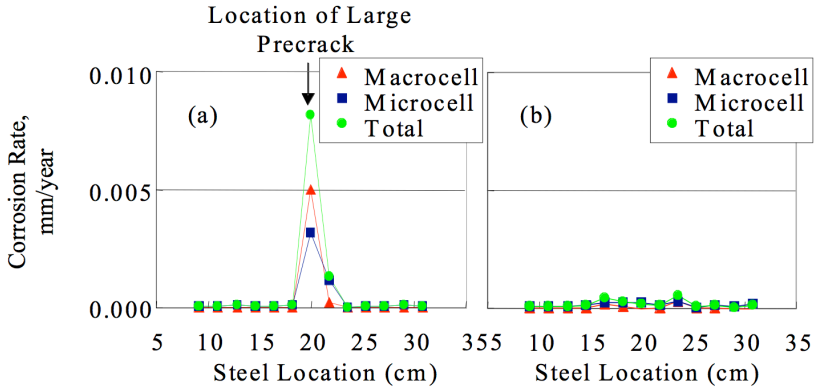

Figure 12 Measured corrosion rate along the steel rebar for preloaded (a) R/C, and (b) R/SHCC (Miyazato and Hiraishi, 2005).

2.2.4. Applications

Many full-scale applications of SHCC were achieved during the last decade. In the following part, examples of the most promising and known applications are given.

Expansion joint for bridge in Japan

Yuichi Ishikawa (2014) reported that damages or deteriorations of many RC bridges are observed at the girder ends and abutments during the inspections. This is caused from the water leakage, which contains deicing salts. And the leakage is due to the ageing of the expansion joints. Thus, a new highly durable jointless system is developed, named RC plug joint, for existing RC bridges with a bridge length less than 40 meters. The RC plug joint connects the abutment' s backwall and the superstructure' s deck using reinforcing steel bars embedded in SHCC. The new RC plug joint system can prevent water leakage and allow vehicles to ride smoothly over the joint. Figure 13 shows the side view of the RC plug joint. In this system, the old expansion joint is removed completely, and the space is filled by SHCC.

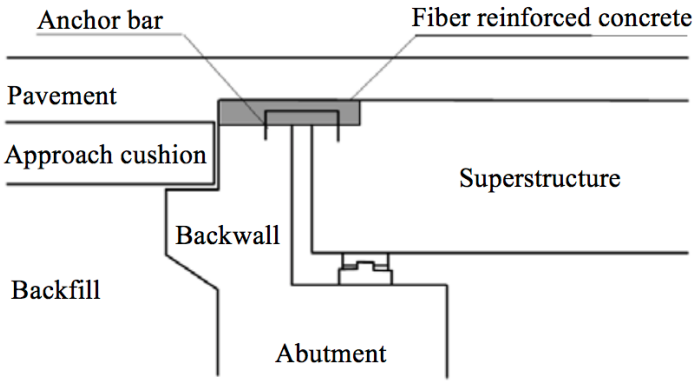

Figure 13 SHCC as expansion joint (Ishikawa *et al.*, 2014)

Coupling beams in the core of two high rises in Japan

Application of R/SHCC coupling beams in the core of two high rises in Japan was the first time that advanced concrete type material, such as SHCC, is applied as a seismic structural component. The super beam and oil damping devices mounted at the top of

building to absorb seismic energy are replaced by the R/SHCC coupling beams (Figure 14). Appearance and floor plan of Glorio Tower Roppongi, a 93m high and 27-story building in Tokyo and those of Nabule Yokohama Tower and Residence, a 150m high and 41-story building in Yokohama, are shown in Figure 15. This application exploits the high-energy absorption capability of R/SHCC to improve the seismic resistance of the two buildings mentioned above. Noticeably, after experiencing the large earthquake excitation in March 11, 2011, no visible damage evidence was observed on the two high rise buildings (Kanda *et al.*, 2011).

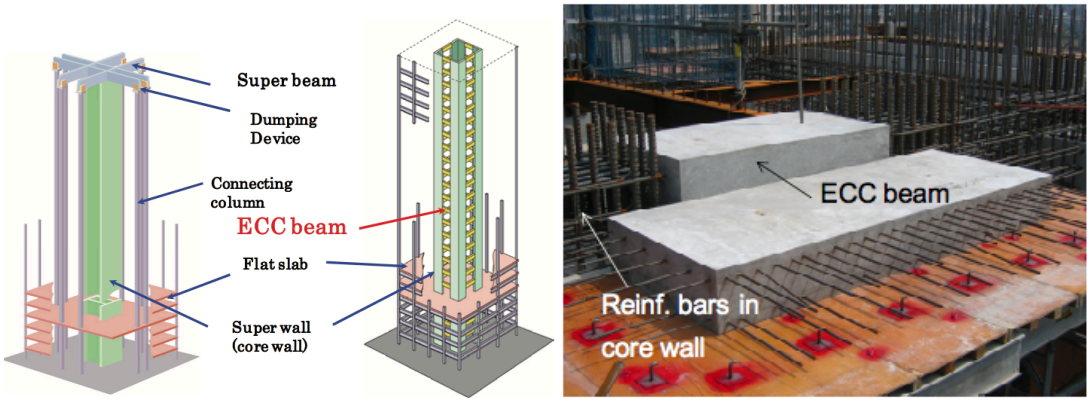

(a) (b)

Figure 14 (a) SHCC beam structural system, (b) Precasted SHCC elements (Kanda et al., 2011)

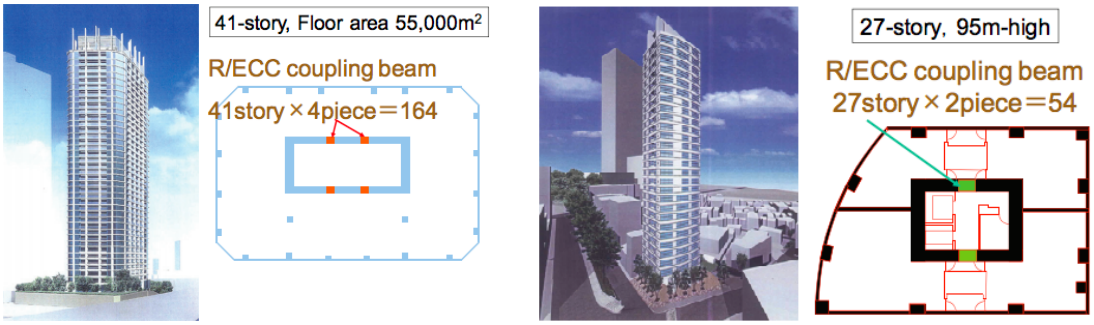

(a) (b)

Figure 15 (a) Glorio-tower Roppongi, (b) Nabule-Yokohama tower and residence (Kanda et al., 2011)

SHCC as repair material

Because of the small crack widths, SHCC is suitable for aesthetic repairs of surface cracked structure due to aesthetic. One of such applications is an irrigation channel repair in Japan (Kunieda and Rokugo, 2006).

After decades of service, the irrigation channels are suffering from deterioration due to abrasion. Central Main Channel in Shiga Prefecture and Seridanno Channel in Toyama Prefecture were severely deteriorated. After substrate treatment, SHCC were spayed and troweled on the cleared surface of the two channels. Conventional mortar and ultrahigh polymer cement mortar were also applied as comparison group. After one month of the application, cracks were observed on the conventional mortar and ultrahigh polymer cement mortar repaired surface, whereas not on the SHCC repaired surface (Figure 16).

(a) Before Repair (b) Surface Preparation

(c) Trowel (d) After Repair

Figure 16 Surface repair of irrigation channel (Kunieda and Rokugo, 2006)

2.3. Critical review on similar investigations

The idea of applying SHCC layer in the composite reinforced concrete structures is not new. Abd El-Hakim Khalil et al. (2017) investigated whether the ultra-high performance strain hardening cementitious composite (UHP-SHCC) strengthened beam has better

crack control behavior comparing to conventional reinforced concrete beam. In the study, five specimens were tested experimentally, which consisted of one conventional reinforced concrete beam as a control, labelled as BSC, and four UHP-SHCC strengthened beams with various reinforcement ratios in UHP-SHCC layer, labelled as BS0, BS1, BS2 and BS3, respectively. The beams were demoulded after 2 days of casting, and their bottom surface was washed out using a retarder to obtain a rough surface. After the wash-out process the specimens were covered with wet towels for 26 days. At the age of 28 days, UHP-SHCC strengthening layer was cast with 40mm thickness in the beams' tension side. The cross-sections of the beams are shown in Figure 17. The reinforcement alignment of the beams and experimental setups are shown in Figure 18. The tests showed that the cracks were much wider on the control beam, for all loads, compared with strengthened beams. At about maximum load, the crack widths of strengthened beams, BS0, BS1, BS2 and BS3, reached 1.9 mm, 1.6 mm, 1.25 mm and 1.2 mm respectively, and the crack width of the control beam was 6.5 mm. With 1.2% and 1.8% reinforcement ratio that is applied in strengthening layer (BS2 and BS3), the crack width of the control beam is reduced by 82% due to the fiber bridging action in the strengthening layer (Figure 19 (b)). The UHP-SHCC strengthened beams have higher capacity than the controlled beam (Figure 19 (a)). By adding the addition layer, the heights (and lever arm) of the cross sections are changed, which will also largely affect the capacity. In the research, the cracks are already too large to be compared. It is meaningless to compare large cracks which do not satisfy the crack width criterion. Comparing BS0 with BSC, the maximum crack width is significantly reduced by adding only SHCC layer, without reinforcement.

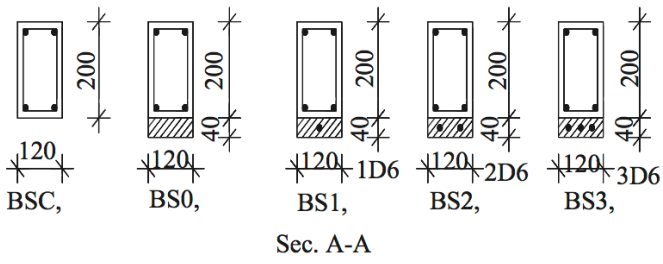

Figure 17 Cross sections of the beams (Khalil *et al.*, 2017)

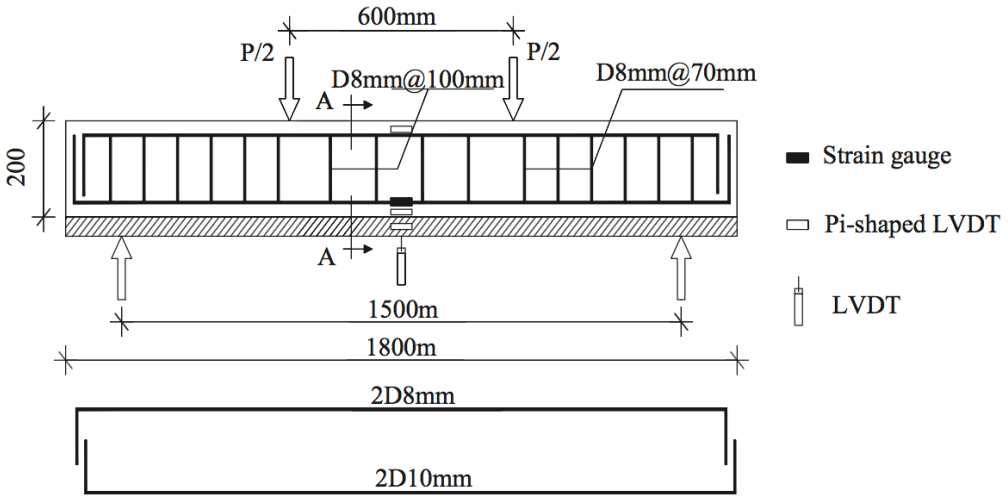

Figure 18 Reinforcement alignment and experiment setup (Khalil *et al.*, 2017)

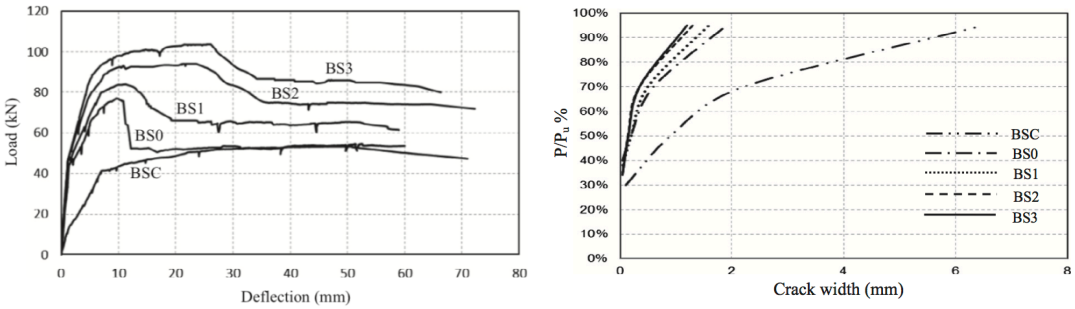

(a) (b)

Figure 19 Load-Deflection curve (a) and Load percentage-crack width curve (b) of 5 beams (Khalil *et al.*, 2017)

Chang-Geun Cho (2015) researched the behavior of cast in-situ SHCC and reinforced concrete composite slabs. Specimens were manufactured by casting in-situ an SHCC bottom layer after positioning of longitudinal, transverse, and vertical reinforcing bars and then casting a top layer of normal concrete that contains the upper part of the composite slab as shown in Figure 20. The failure loads for the enhanced slab with SHCC layer of 20 mm (SHCC-20), and the enhanced slab with SHCC layer of 40 mm (SHCC-40) are higher than that of the reinforced concrete slab (RC-180), which are 59.8 kN, 65.2 kN and 49.5 kN respectively (Figure 21). The enhanced slabs (SHCC-20 and SHCC-40) are stiffer than the reinforced concrete slab (RC-180). For the SHCC enhanced slab (SHCC-20 & SHCC-40), at the failure load, only one big crack was formed in the mid span with many small cracks. Compared to SHCC enhanced slab, RC slab has more big cracks (Figure 22). In this research only the crack patterns from three specimens at the failure load are compared, not the crack widths during the loading. It might be that crack

widths during the loading stage are smaller in SHCC-enhanced beams than in regular concrete beams.

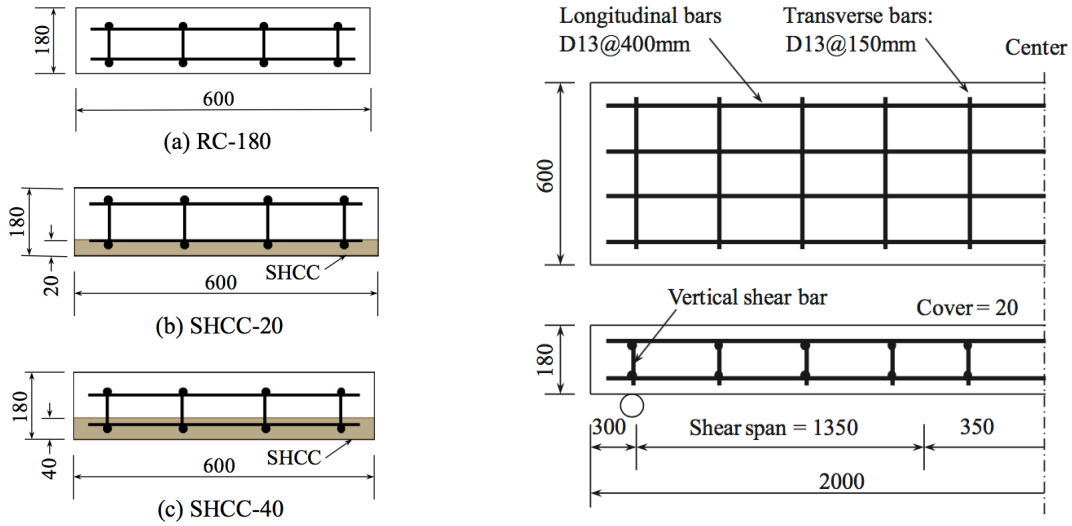

Figure 20 Dimensions and reinforcement details in cross-section (Cho *et al.*, 2015)

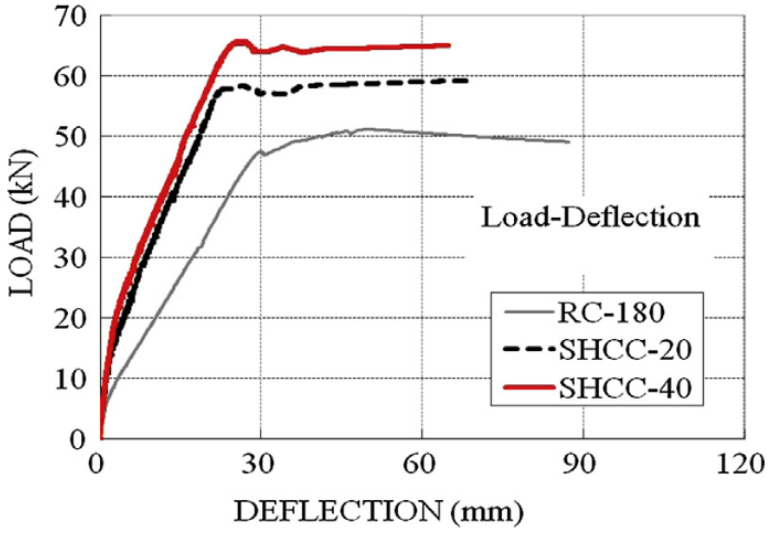

Figure 21 Load-Deflection curves at mid-span of the three specimens (Cho *et al.*, 2015)

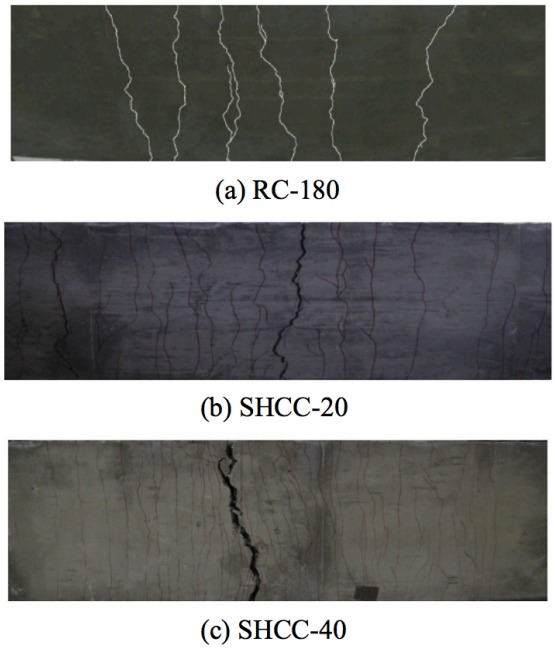

Figure 22 Cracks and failure patterns of three specimens (Cho *et al.*, 2015)

2.4. Semi-prefabrication

When making a composite structure, with a layer of SHCC in the tension zone, it would be good to simplify and automize procedure for the application. Therefore, the idea is to make prefabricated SHCC part, or, stay-in-place mould, in which regular concrete would be later cast in situ.

Prefabricated concrete construction means the concrete component is cast in factory or at fixed location on site, and the completed components are assembled to form structure. The featured point is that the same mould can be used for multiple times without modification (Warszawski, Avraham and Carmel, 1984). The partial application of the prefabrication technique in concrete construction is known as semi-prefab concrete construction (Mwamila and Karumuna, 1999).

There are numerous benefits of prefabrication and semi-prefabrication, which are stated below.

2.4.1. Quality of elements

The structures have designed life-time. During the life-time, the structure should not have any form of distress such as excessive cracks and deflection, corrosion etc. To prevent these from happening, concrete quality must be assured. For cast in-situ concrete, the quality highly depends on the workmanship of labour. The unskilled labour has higher possibility to deliver concrete with poor quality, which requires enormous repair afterwards.

While semi-prefabricated concrete elements require less skills, the procedure is automated and more quality control can be applied. A survey was conducted among government departments, developers, consultants and contractors in Hong Kong where many prefabricated building components had been introduced. Results of the survey shows that the most significant advantage for adopting prefabrication is "better supervision on improving the quality of prefabricated products". As the respondents claimed, better quality product is achieved by having better supervision, since the prefabricated components are tested and inspected before the installation (Tam *et al.*, 2007).

2.4.2. Faster construction

Structures with semi-prefabrication technique can be erected more quickly and efficiently than cast in-situ structures due to improved labor productivity and flexibility in construction sequence. For example, by implement semi-prefab construction, many different construction tasks can be performed at the same time while in-situ requires a linear production sequence.

2.4.3. Economical aspect

Mwamila (1999) reported that total construction cost savings by using semi prefab construction systems was 14% to 17% for office buildings and 16% to 19% for residential buildings respectively. With the increasing labour price, as expected in future, the amount of cost saving will even increase.

3

Experiment

3.1. Aims and objectives

Taking into account the susceptibility of reinforced concrete structures to durability problems due to large cracks, and potential of SHCC to keep the cracks small, the main aims and objectives of this study are:

- Investigate and compare the cracking pattern (crack spacing and crack widths) in reinforced concrete structure and in composite reinforced concrete structure where the reinforcement is embedded in SHCC layer.
- investigate if the thickness of the SHCC layer has the influence on crack control capacity of composite reinforced concrete beam.
- investigate if the crack control ability is affected by adding the self-healing agent in SHCC mixture.

Beside the main aim of this study, related to the ability of SHCC layer, applied in the tension zone of the reinforced concrete beam, to control crack widths, it was also investigated whether the layer of SHCC would have the influence on structural capacity of the beams. However, this was not the main aim of this study, as in reality, the beams would have higher height, and the contribution of SHCC layer on their structural capacity will be lower.

Experimental study was performed. Specimens were tested in four-point bending while Digital Image Correlation (DIC) and an image analysis software package (ImageJ) were used to evaluate crack pattern development and crack widths. Finally, experimental results are also compared to numerical calculations and theoretical models.

3.2. Design of the experiments

3.2.1. Cross sections

4 types of reinforced concrete cross-sections are designed. The controlled groups, Specimen 1 and 3 are conventional concrete beams with concrete covers of 31 mm and 11 mm, respectively. Group 2 and 4 are SHCC-concrete composite specimens where SHCC is applied in the tension zone. Group 2 and 4 have each 2 beams, one with pure SHCC layer and the other one with SHCC layer containing self-healing agents. With respect to concrete cover, Group 2 is correlated to the control Specimen 1 (both have concrete cover of 31 mm) and Group 4 is correlated to the control Specimen 3 (with concrete cover of 11 mm). The detailed dimensions are shown below:

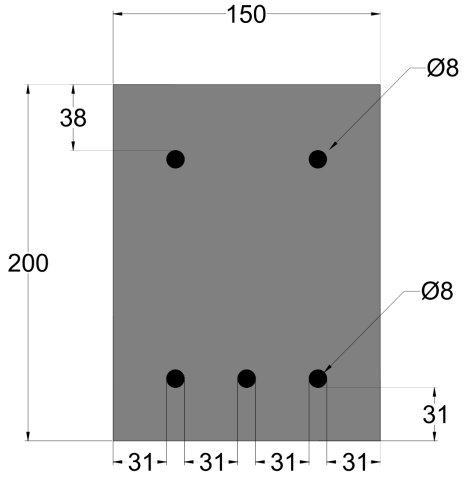

Specimen 1 (conventional RC beam 31 mm cover)

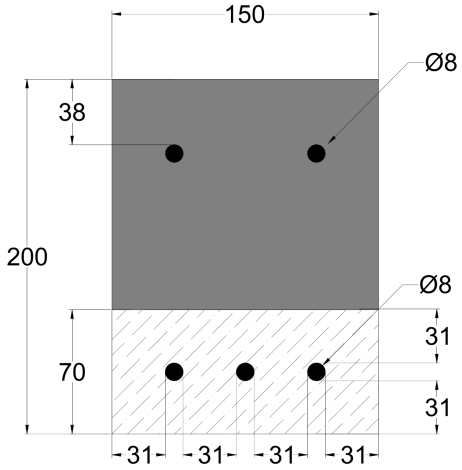

Group 2 (beam with composite system 31 mm cover)

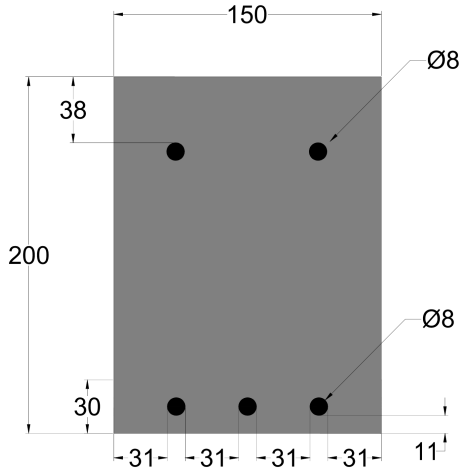

Specimen 3 (conventional RC beam 11 mm cover)

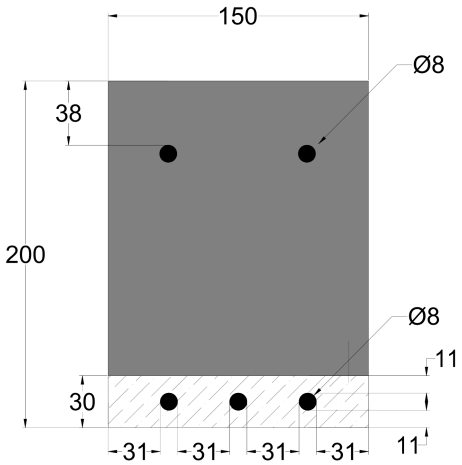

Group 4 (beam with composite system 11 mm cover)

Figure 23 Designed cross sections

3.2.2. Length of the beams

To analyze the crack behavior of different beams, a constant moment area is favorable. Therefore, a four-point bending test is designed. The beam should not be too long to handle and meanwhile, it should have enough constant moment region. Additionally, the length of the specimen should be longer than the distance between the supports, about 0.2 m on each side. Therefore, the length of the beams is set to be 1.9 m, which consists 0.4 m extra length (0.2 m on each side), 0.5 m between the loading point and the support and 0.5 m between loading points (Figure 24).

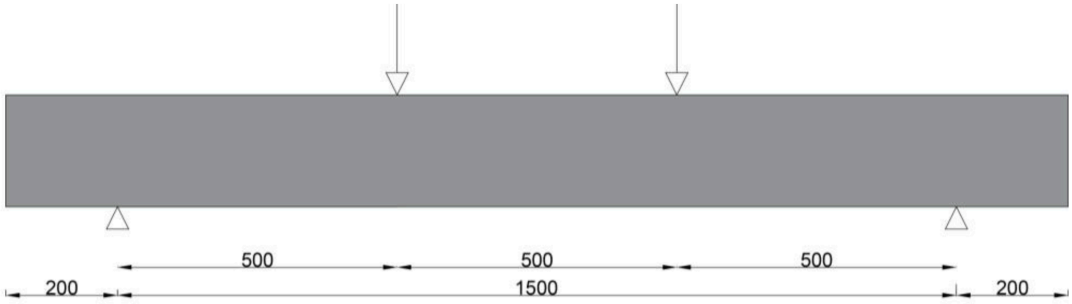

Figure 24 Experiment setup [Unit: mm]

3.2.3. Reinforcement

With respect to longitudinal reinforcement, the beams are designed such that the flexural failure occurs in the constant moment region. In order to have large crack widths, the percentage of reinforcement should be close to the minimum value. Therefore, only three tensile reinforcement with diameter of 8mm are placed in the tensile zone. The smallest reinforcement ratio among all the cross sections is 0.61 % (for specimen 3 and group 4)

In order to have flexural failure, shear failure should be avoided by applying shear reinforcement. The beam with SHCC layer of 70 mm has the highest capacity (76.36 kN) among all beams. The detailed calculations are shown in chapter 4.2.
The shear force diagram of beam under the force of 76.36 kN in four-point bending test is show below:

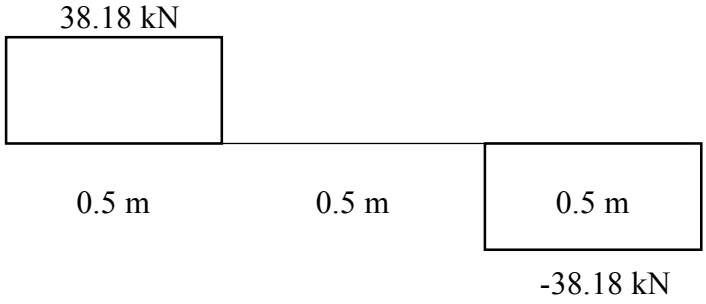

The shear force $V_{Ed} = 38.18\ \text{kN}$.

$$v_{Ed} = \frac{V_{Ed}}{b_w d} = \frac{38.18 * 1000}{150 * 165} = 1.54\ \text{MPa}$$

Where:

b_w is the width of the beam;

d is the effective depth, $d = h - c - \frac{\emptyset}{2} = 200 - 31 - \frac{8}{2} = 165\ \text{mm}$

$$v_{Rd,c} = 0.18k(100\rho_l f_{ck})^{\frac{1}{3}} = 0.18 * 2 * (100 * 0.0061 * 28)^{\frac{1}{3}} = 0.93\ \text{MPa}$$

Where:

ρ_l is longitudinal reinforcement ratio;

$k = 1 + \sqrt{200/d} \leq 2$;

$f_{ck} = f_{cm} - 8 = 28\ \text{MPa}$.

Since $v_{Rd,c} < v_{Ed}$, shear reinforcement is required.

The angle of shear crack, θ is:

$$\theta = \frac{1}{2}\arcsin\frac{2V_{Ed}}{(\alpha_{cw}\nu f_{cd})b_w z} = \frac{1}{2}\arcsin\left(\frac{2 * 38.18 * 1000}{1 * 0.7\left(1 - \frac{18.7}{250}\right) * 18.7 * 150 * 153.6}\right) = 7.94\ °$$

Where:

$\alpha_{cw} = 1$;

$\nu = 0.7 * (1 - \frac{f_{cd}}{250})$;

$f_{cd} = \frac{\alpha_{cc} f_{ck}}{\gamma_c} = \frac{1*28}{1.5} = 18.67\ \text{MPa}$;

$z = 165 - 27.12 * 0.42 = 153.6\ \text{mm}$, which is the distance between tensile reinforcement and center of compression zone (for detailed calculation see chapter 4.2).

The calculated shear crack angle is $7.94°$, which is smaller than $21.8°$. Therefore, the angle is limited to $21.8°$.

$$\theta = 21.8° \text{ and } \cot\theta = 2.5$$

$$z\cot\theta = 153.6 * 2.5 = 384.02 \text{ mm}$$

The shear reinforcement should be placed at 384.02mm distance from the supports.

The shear resistance of beams with shear reinforcement, $V_{Rd,s}$ is:

$$V_{Rd,s} = \frac{A_{sw} f_{ywd}}{s} \times z\cot\theta$$

Where:

A_{sw} is steel area

f_{ywd} steel yielding stress

s is spacing of shear reinforcement

The steel area per millimeter, $\frac{A_{sw}}{s}$ is:

$$\frac{A_{sw}}{s} = \frac{V_{Ed}}{f_{ywd} z\cot\theta} = \frac{38.18 * 1000}{500 * 384.02} = 0.198 \text{ mm}^2/\text{mm}$$

The spacing s, is set to be 150mm, then the steel area of $A_{sw} = 29.83 \text{ mm}^2$.

Six 2-leg stirrups with diameter 8mm are applied, 3 stirrups on each side. And the stirrups should be located in 384.02 mm ($z\cot\theta$) distance from the supports.

Shear capacity check:

$$A_s = 301.6 \text{ mm}^2$$

$$V_{Rd,s} = A_s * f_{ywd} = 150.8 \text{ kN} > 38.18 \text{ kN}$$

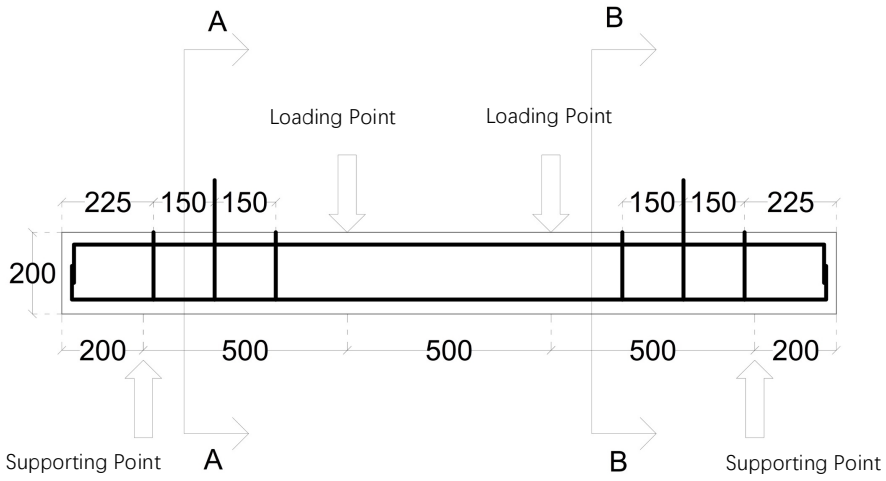

Figure 25 Vertical reinforcement alignment and experiment setups

The shear reinforcement protruding out of the beam will be used as anchor for the crane, since the beam is too heavy to be handled by man power. And the shear reinforcement is embedded into the SHCC layer to increase the structural integrity and avoid delamination between the layer of SHCC and regular concrete. The shear reinforcement was placed outside the constant moment region. The thickness of the concrete cover in constant moment region was controlled by placing spacers. At the cross sections where shear reinforcement was placed, the concrete cover is smaller, but this does not affect the cover depth or the crack pattern in the constant moment region. The figures of the cross sections are shown below:

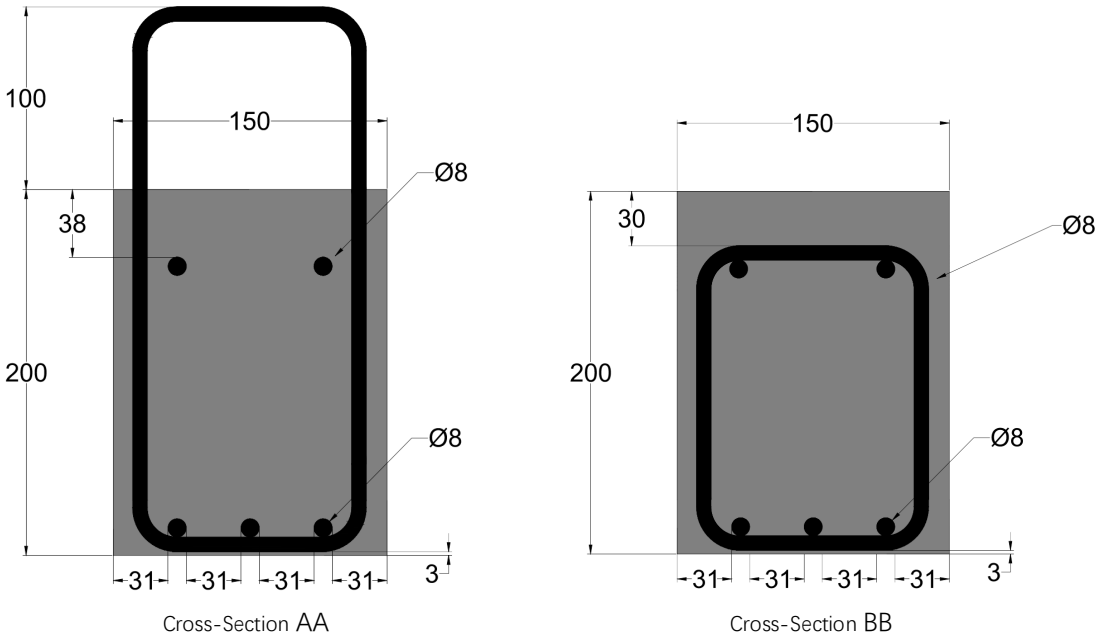

Figure 26 Cross sections of RC beam with cover 11 mm

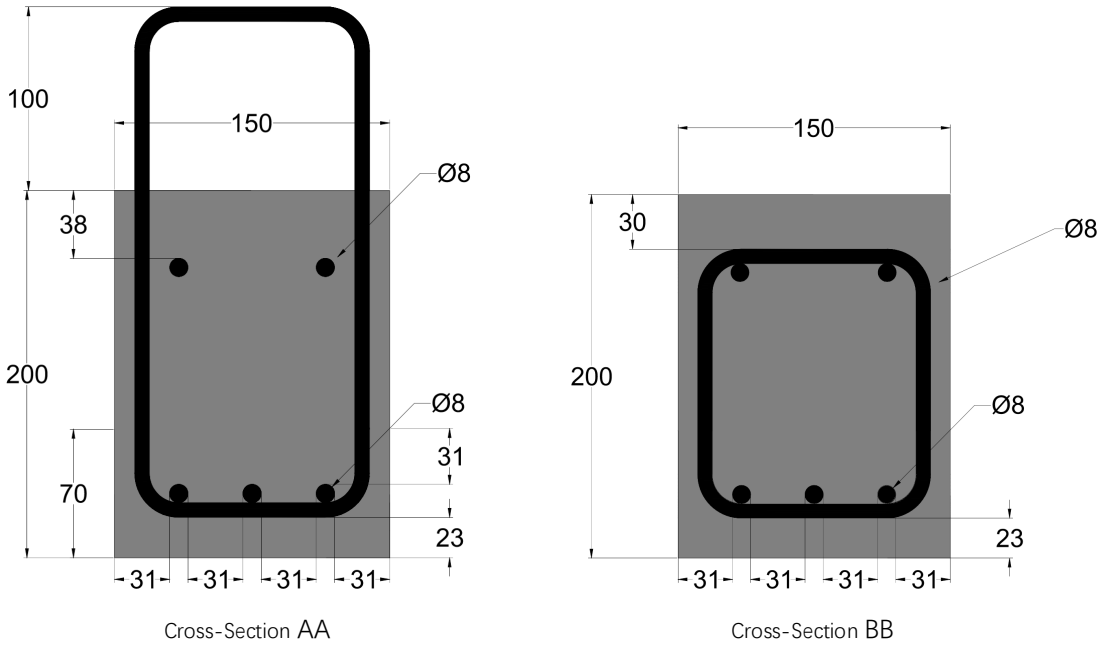

Figure 27 Cross sections of RC beam with cover 31 mm

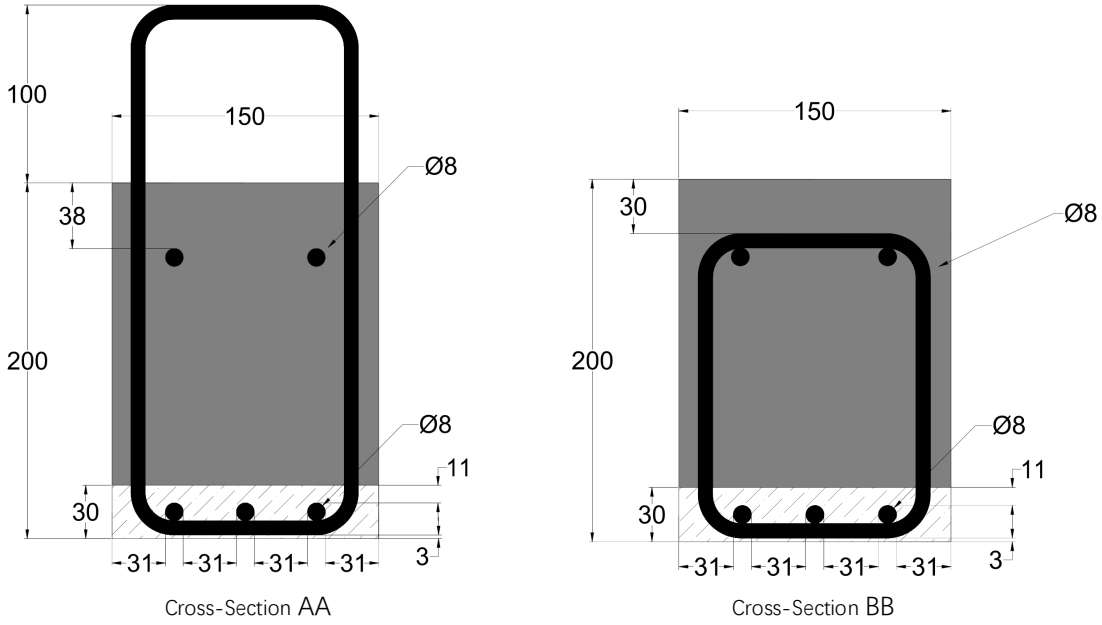

Figure 28 Cross section of beams with SHCC layer of 30 mm

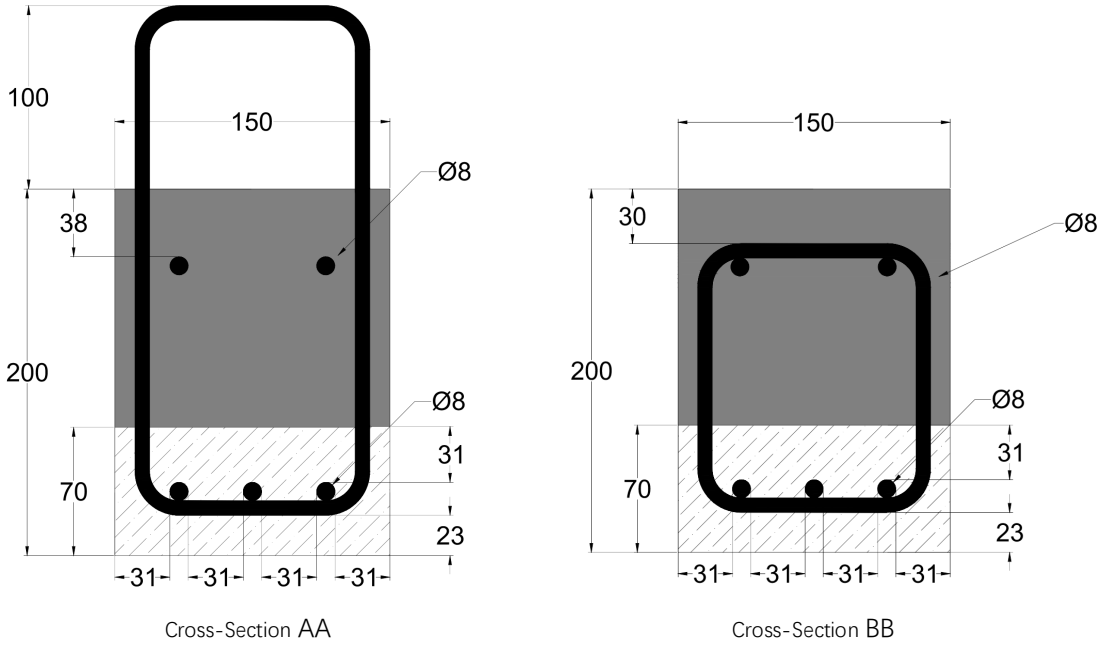

Figure 29 Cross section of beams with SHCC layer of 70 mm

3.3. Casting of the specimens

3.3.1. SHCC layer

The SHCC used in the experiment consists of cement (CEM III B), limestone powder, PVA fiber, superplasticizer and water (Figure 30). The detailed receipt is shown in Table 3. The properties of the PVA fiber are shown in Table 4. All ingredients should be mixed according to the designed mixing procedure. First limestone powder, PVA fibers and cement powder were added into the mixer and pre-mixed for 1 minute to achieve the uniform distribution of PVA fibers. Then the superplasticizer was mixed with the required amount of water in order to make sure that there is no residue, since the superplasticizer has strong impact on workability of SHCC. Finally, the superplasticizer water solution was added into the mixer and mixed for 4 minutes.

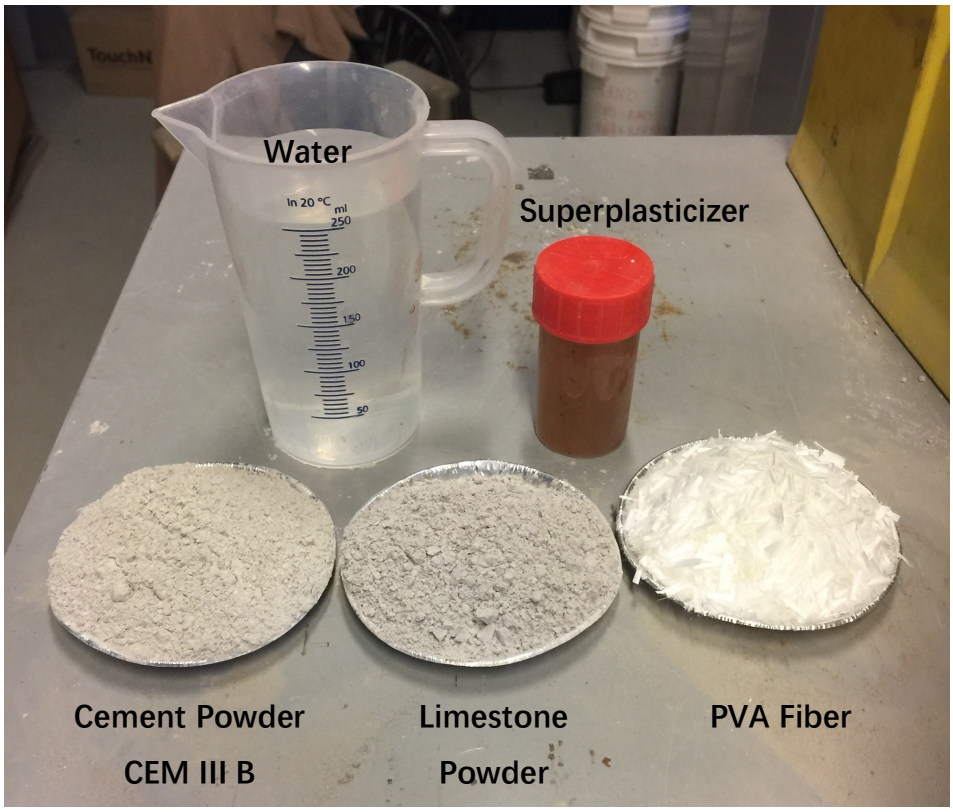

Figure 30 Ingredients of SHCC

Before casting the SHCC layer, spacers with different heights (11 mm and 31 mm, 4 spacers for each beam, 16 spacers in total) were casted first using the same receipt as SHCC mixture. They were tied with the reinforcement cage at the bottom near the supporting points (Figure 31 & Figure32). On the sides, only plastic spacers were used. After placing the reinforcement into the oiled mould, the unhardened SHCC mixture were poured into the mould with hand shovels (Figure 34). Then the SHCC layer was levelled with a designed tool (Figure 33). Since the thickness of the SHCC layer is small, it is not suitable to use vibration poker. And additionally, since the unhardened mixture has a relatively high viscosity, the SHCC mixture was only manually compacted to expel the air bubbles from the layer. Finally, the mould was covered with plastic sheet to keep the moisture in and left in the room temperature (around 20 C°) for 14 days.

Figure 31 SHCC spacers with height of 31 mm (left) and 11 mm (right)

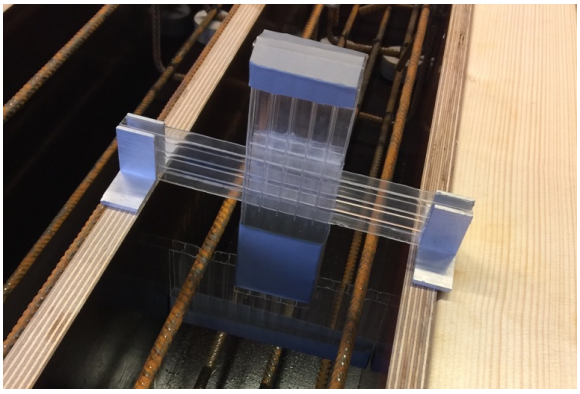

Figure 33 Designed leveling tool

Figure 32 Rebar cage in the mould with spacers

Figure 34 Spoons used in casting SHCC layer

Table 4 Receipt of SHCC and SHCC+SH

Recipe	**SHCC**	**SHCC+SH**
CEM III B [kg/m^3]	790	790
Limestone Powder [kg/m^3]	790	790
PVA Fiber [kg/m^3]	26	26
Superplasticizer [kg/m^3]	2.13	2.13
Water [kg/m^3]	410	410
Self-healing Powder [kg/m^3]	/	10

Table 5 PVA fiber properties

Material	**Length [mm]**	**Diameter [mm]**	**f_t [MPa]**	**E [GPa]**
PVA	8	0.04	1640	40

3.3.2. Interface treatment

After 14 days of curing for the SHCC layer, the plastic sheet was removed. The SHCC attached on the rebar was cleaned. The interface was first cleaned with air jet to blow away the dust. Then the interface was roughened with a steel bush to increase the bond between SHCC layer and concrete layer. Finally, the debris and powders brushed off from the interface were wiped out with ethanol.

3.3.3. Concrete layer

The planed concrete class is C20/25 and the receipt (Table 6) is based on the research of Blagojević (2016). However, the compressive strength results at the age of 33 days were higher than those reported by Blagojevic (2016). The average compressive strength measured on 150x150x150 mm^3 cubes is 45 MPa, which can be seen in Appendix D. This corresponds to the mean cylinder strength of 36 MPa ($f_{ck,cyl} = 0.8 * f_{ck,cube}$), and cylinder characteristic strength of 28 MPa, leading to the C25/30 strength class.

Table 6 The receipt of concrete (Blagojević, 2016)

Recipe	Dry Weight [kg/m^3]
CEM I B	260
Sand 0.125-0.25 mm	78.83
Sand 0.25-0.5 mm	256.199
Sand 0.5-1 mm	256.199
Sand 1-2 mm	157.661
Sand 2-4 mm	98.538
Gravel 4-8 mm	394.152
Gravel 8-16 mm	729.181
Water	156
Super plasticizer	0.26

The concrete was directly poured into the mould and on the top of the SHCC layer. Vibration poker was applied to expel the excessive air. The top surface was leveled and covered with plastic sheet to keep the humidity. The moulds are left in the room temperature (around 20 C°).

All the beams were demoulded after 33 days of concrete layer casting. The test dates can be seen in Appendix C.

3.4. Experiment setups

As stated above, all beams were tested in four-point bending (Figure 35). The experiment setups can be seen in Figure 24 and Figure 25. The beams were simply supported. The test was performed by displacement control of the jack, with a speed of 0.01 mm/sec. After yielding of the steel, the loads increased slowly, then the speed was increased to 0.05mm/sec. Capacity of the loading machine is 100 kN.

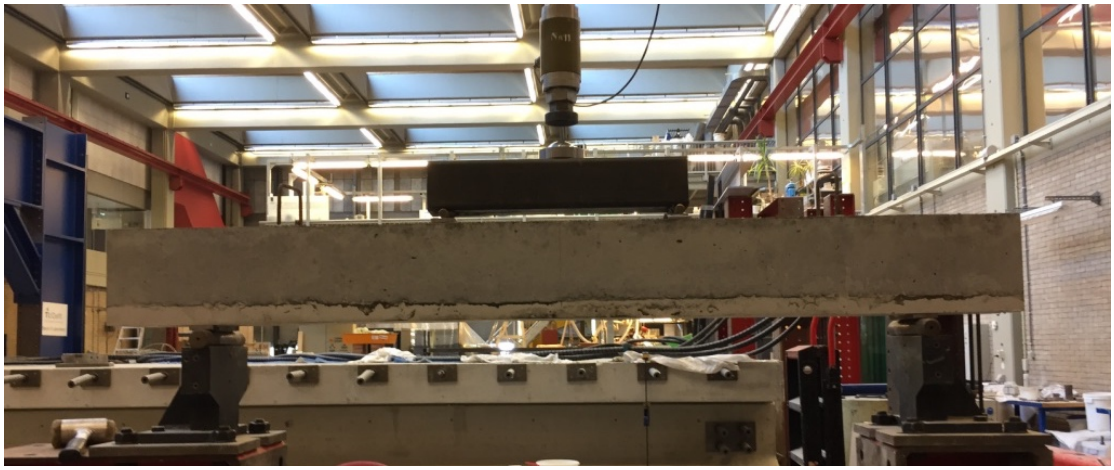

Figure 35 Experiment setup

3.4.1. Positions of LVDTs

Linear Variable Data Transformers (LVDTs) were placed at several locations on the beam: six at the bottom, three at the side and one to measure vertical deflection. In Figure 36 and Figure 37 locations of all LVDTs are given.

LVDT No.1 measures the deflection of the mid span. To measure the vertical deflection, a wooden beam was attached to the beam, spanning from one support to the other support at the height of the neutral axis before cracking, which is also the middle of the height.

LVDT No.2,3,4 measure the displacements at different height which will be compared with the Digital Image Correlation.

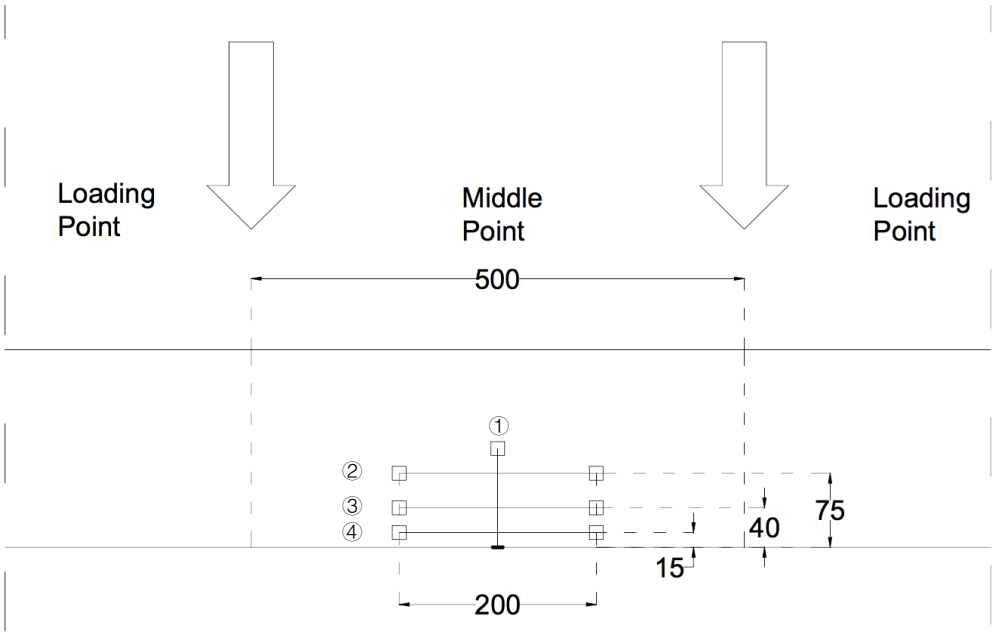

Figure 36 Positions of side LVDTs [Unit: mm]

LVDT from No.5 to No.10 measures the displacements at the bottom side of the beams. LVDT No.10 measures displacement over a measuring range of 500 mm. And rest of the LVDTs measure displacements over measuring range of 200 mm.

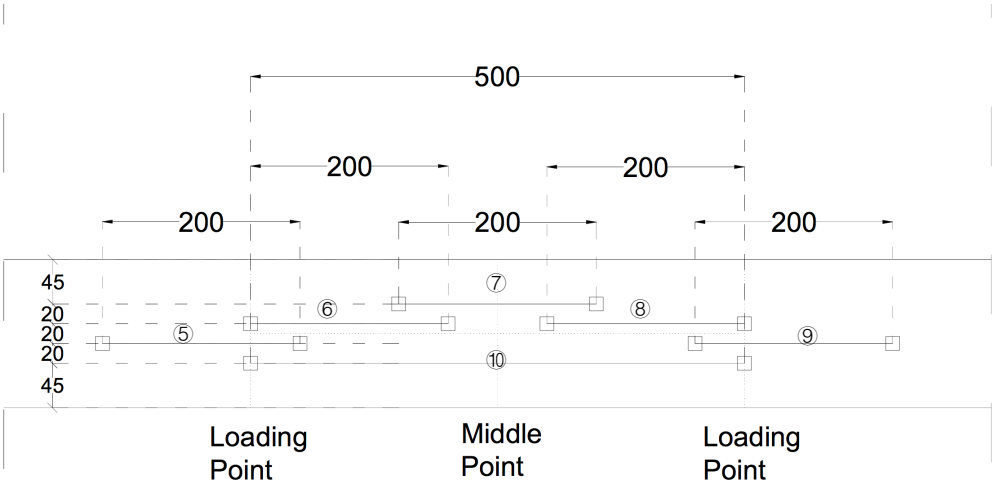

Figure 37 Positions of bottom LVDTs [Unit: mm]

3.5. Digital image correlation (DIC)

During the loading test, Digital Image Correlation (DIC) was applied to help assess the experiment data. This is a non-contact optical technique for measuring displacement and strain fields. This technique is considered ideally suited for study of crack

propagation, since it has the potential to become a cheap, simple yet accurate solution (Mccormick and Lord, 2010).

The displacement is obtained by comparing a series of the photos of the loaded specimen taken at different time intervals during the loading stage of the beams. The program will trace the movement of pixels during the experiment, and based on the relative displacement of points, the strains can be computed.

Surface preparation

To apply this technique, the surface of the specimen should be prepared in advance. Figure 38 is the original specimen surface. First, the specimen surface was painted white uniformly to give the specimen a ground colour (Figure 39). Notably, the painting of the ground colour should not be too thick, otherwise, it may cover small cracks and affect the measurements. Finally, random black patterns were painted with plastic roller (Figure 40). Black and white have strong contrast. The random black patterns are like the identities of different parts of specimen surface, which can help the program recognize the specimen.

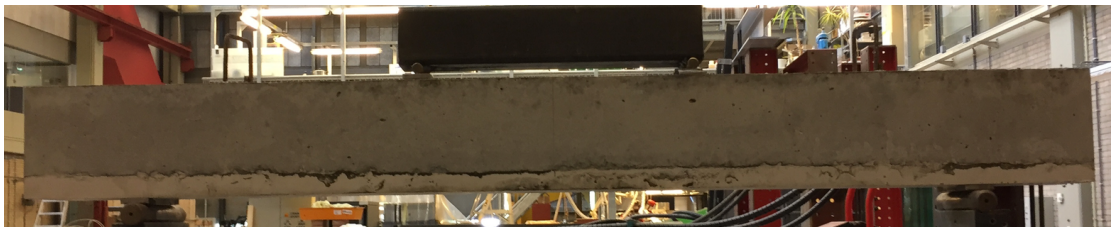

Figure 38 Original specimen surface

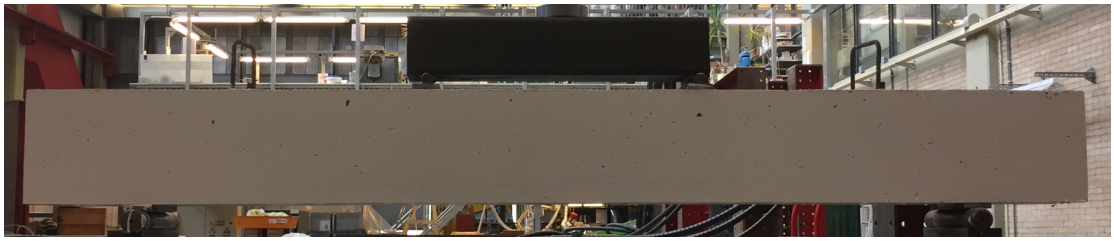

Figure 39 While ground colour

Figure 40 Random black patterns

Principle

Take an example given by Correlated Solutions, Inc. (2009). The specimen is marked with a cross –like pattern and the camera acquires 9x9 pixel image. The white pixels are gray level 100 and the black pixels are gray level 0.

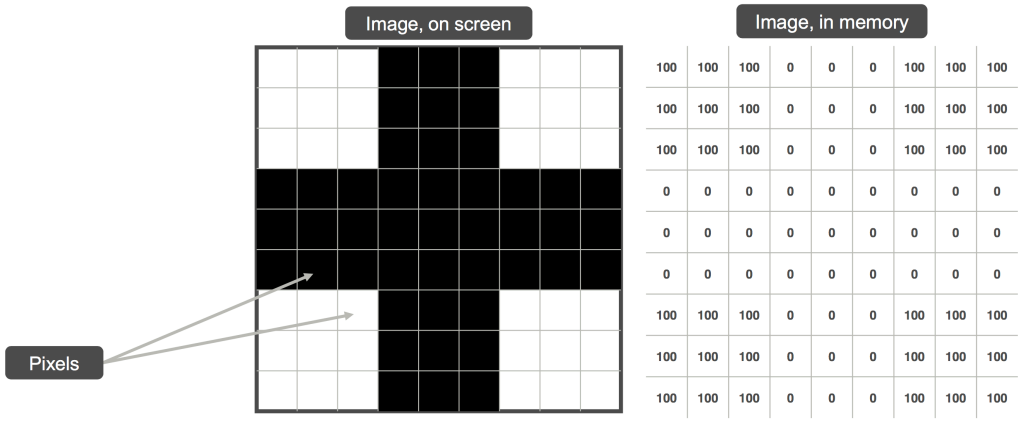

Figure 41 Unmoved image on screen and in momery (Correlated Solutions, Inc., 2009)

Then the specimen moves such that its image moves 1 pixel up.

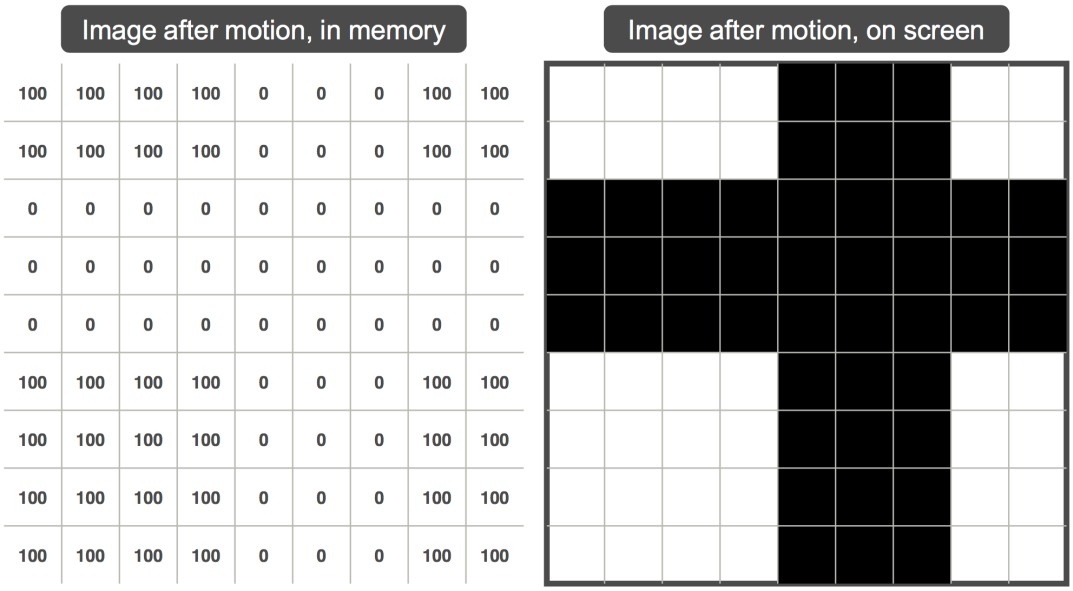

Figure 42 Unmoved image in momery and on screen (Correlated Solutions, Inc., 2009)

To find the movement, a 5x5 subset is defined in the reference image (before motion) and based on the equation given below, similarity scores of each 5x5 blocks in the search zone (defined by user, for example, here it can be 3) are calculated.

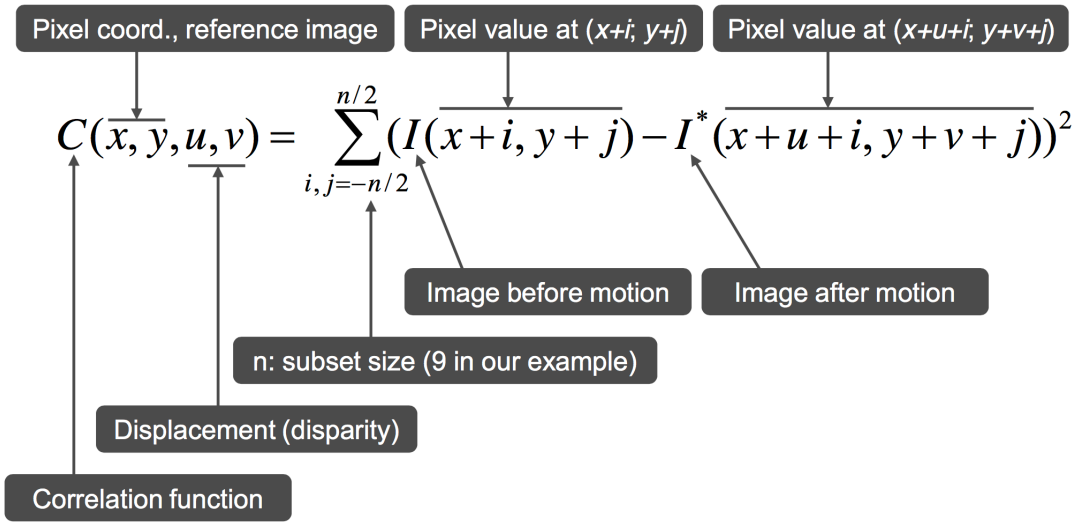

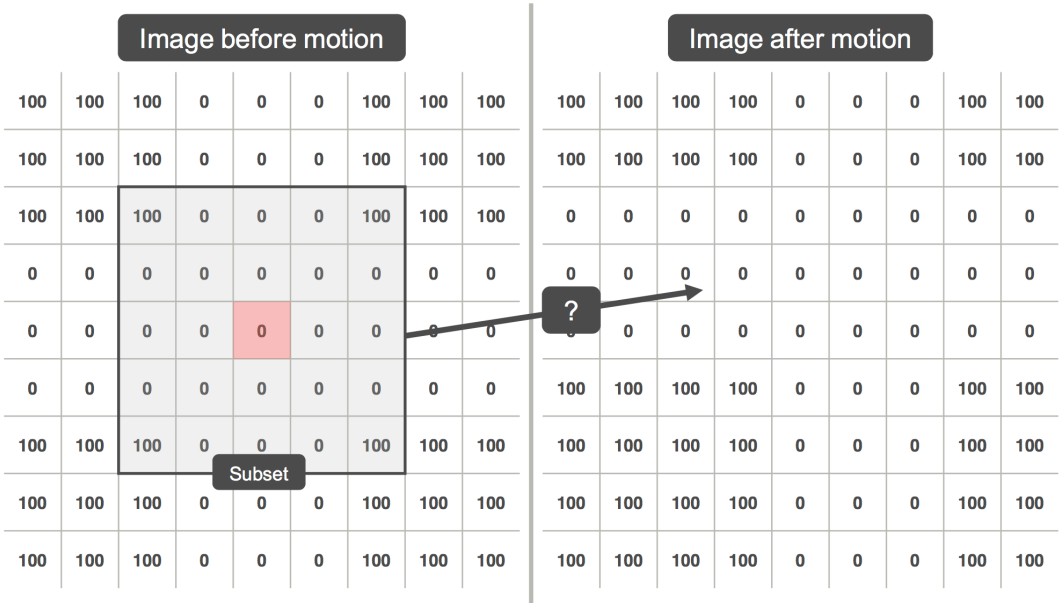

Figure 43 Images in gray scale and the subset (5;5) (Correlated Solutions, Inc., 2009)

For example, for subset at (x;y)=(5;5) first the displacement candidate (u;v)=(-2;-2) is checked:

$$C(5,5,-2,-2) = \sum_{i,j=-2}^{2} (I(5+i,5+j) - I^*(5-2+i,5-2+j))^2$$

$$= (100-0)^2 + (0-0)^2 + (0-0)^2 + (0-0)^2 + (100-0)^2 + (0-100)^2 + (0$$

$$-100)^2 + (0-100)^2 + (0-100)^2 + (0+0)^2 + (0-100)^2 + (0-100)^2 + (0-100)^2$$

$$+(0-100)^2 + (0+0)^2 + (0-100)^2 + (0-100)^2 + (0-100)^2 + (0-100)^2 + (0$$

$$+0)^2 + (0-100)^2 + (0-100)^2 + (0-100)^2 + (100-0)^2 = 18000$$

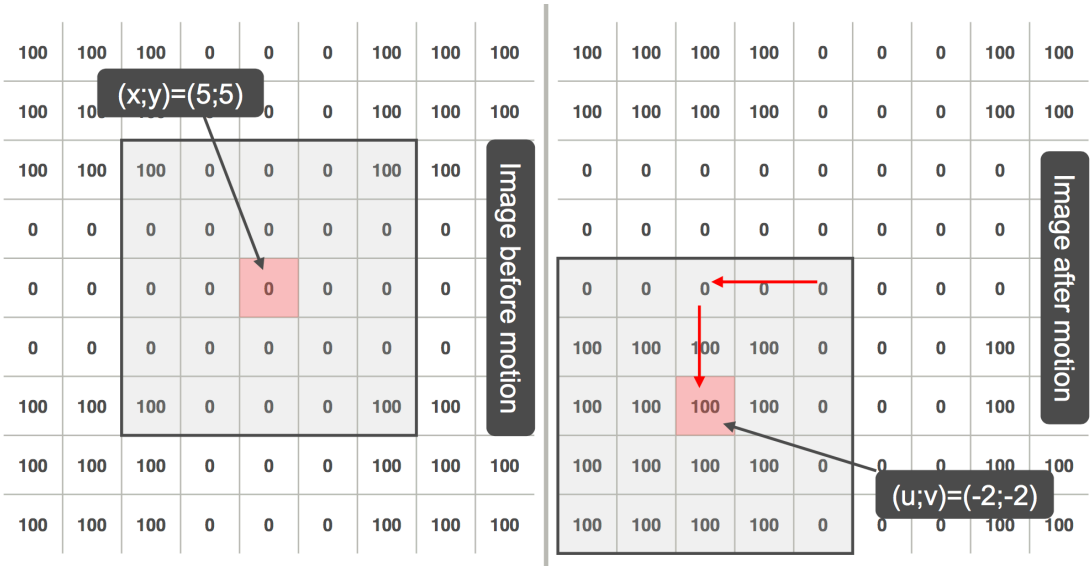

Figure 44 Subset (5;5) with displacement candidate (-2;-2) (Correlated Solutions, Inc., 2009)

Then, for the same subset at (x;y)=(5;5), displacement candidate (u;v)=(1;1) is chosen, for which C value is calculated.

$$C(5,5,1,1) = \sum_{i,j=-2}^{2} (I(5+i,5+j) - I^*(5+1+i,5+1+j))^2 = 0$$

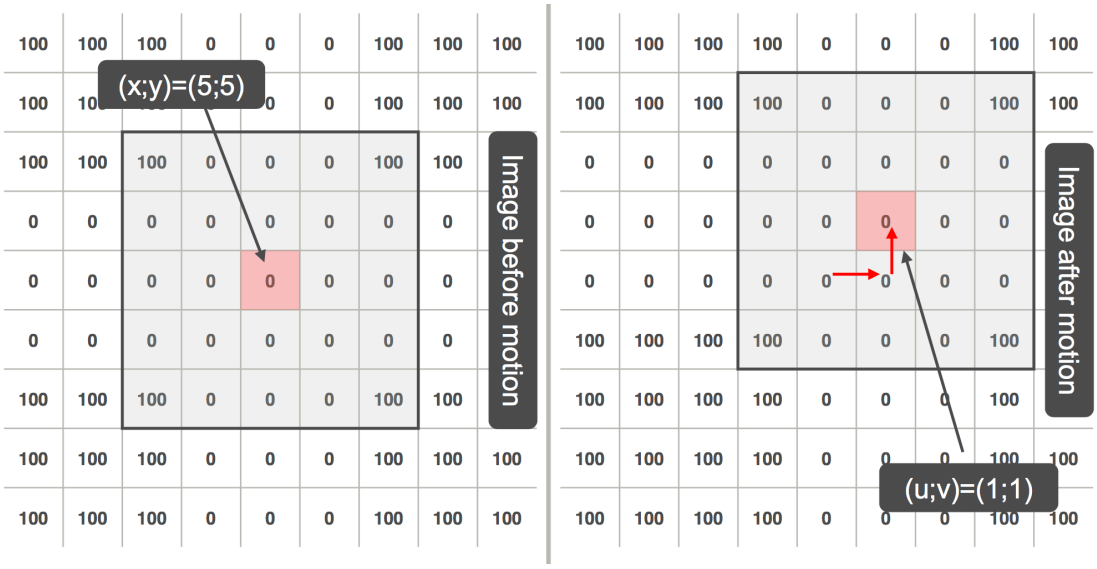

Figure 45 Subset (5;5) with displacement candidate (1;1) (Correlated Solutions, Inc., 2009)

After C values for the entire search zone are calculated, the program will choose the displacement candidate which has the smallest C value as the displacement of the pixel. In the example, the displacement of the pixel is (1;1). That means the horizontal displacement of the pixel is 1 and the vertical displacement of the pixel is also 1, with the

unit of pixel. The Subset size and search zone applied in the analysis for all tests will be shown in Appendix.

Requirements

To help the program recognize the pixel blocks, the specimen must have random and unique pattern with enough contrast and intense level on its surface. Otherwise, pre-treatment of the specimen is required.

Advantages

DIC is very cheap and easy to implement nondestructive measuring technique. It only requires a camera with high resolution and sometimes, pre-treatment of the specimen.

Different from the LVDT, DIC can analyze the entire area of element (provided that certain area is present in the photo) and achieve the displacement field and not only displacement between certain points. It can detect small changes which cannot be viewed by naked eyes.

Disadvantages

It is a relatively new method. There is no handbook to guide the users during the photographing and the processing of the photos. It more like trial and error. For instance, what is the optimal pattern size on the surface for an element with certain size is still not clear.

Processing the photos requires enormous computation. With personal laptop or computer, the process can be time-consuming.

DIC has inherent noise, though the analysis provides the smoothening function to mitigate the noise. The noise cannot be eliminated completely. This will affect the accuracy of results at low load with very small displacement.

3.6. ImageJ

ImageJ is a public domain, Java-based image processing program developed at the National Institution of Health. It' s widely used for processing biological graphs. For this experimental research, only basic functions are used for measuring the crack width. The minimum crack width that can be detected is related to the resolution of the image. With extremely small cracks, the resolution might not be high enough to measure the precise crack width.

For example, the width of the beam is 150mm and in the photo, the width of the beam is 1500 pixels. Then the length of one pixel (resolution) can be calculated as 150mm divided by 1500 pixels, which is 0.1mm. If a crack is 4 pixels wide, then the crack width is measured to be 0.4 mm. An example of measured photos is given in Figure 46.

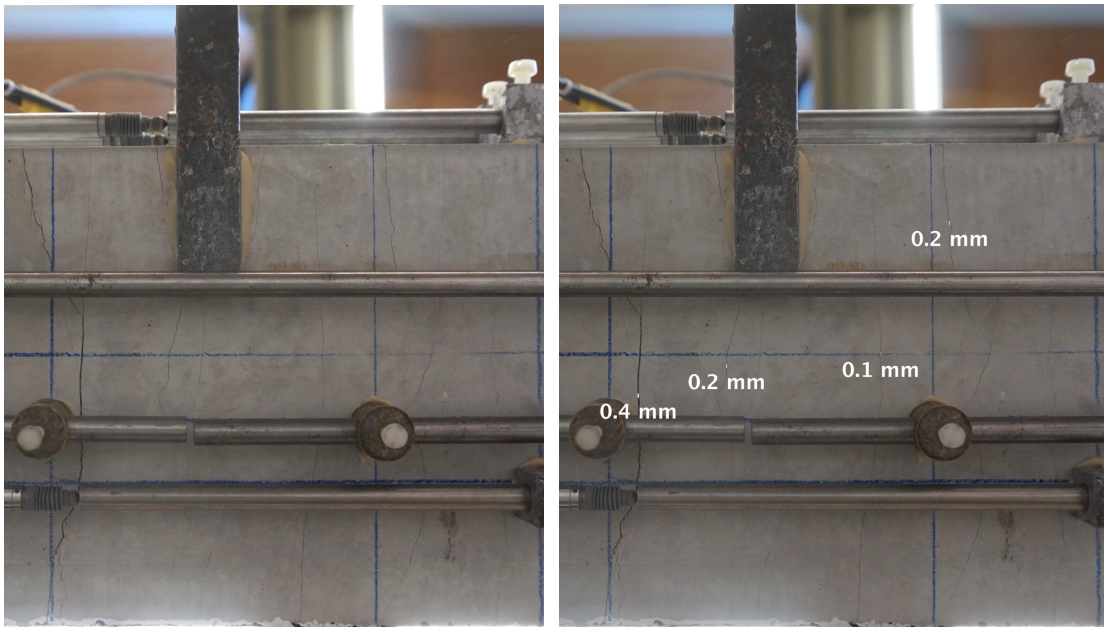

Figure 46 Original (left) and crack width marked (right) photo of the bottom side of the beam

4

Results

4.1. Load-Deflection curves

The Load-Deflection Curves of all the beams are shown below in Figure 47 and Figure 48. The complete deflections of the beams were not captured because the LVDT for measuring the deflection was mostly out of the range at deflections higher than 9 mm. Only for beam with SHCC+SH layer of 30 mm, the LVDT was adjusted such that it could measure during the whole experiment.

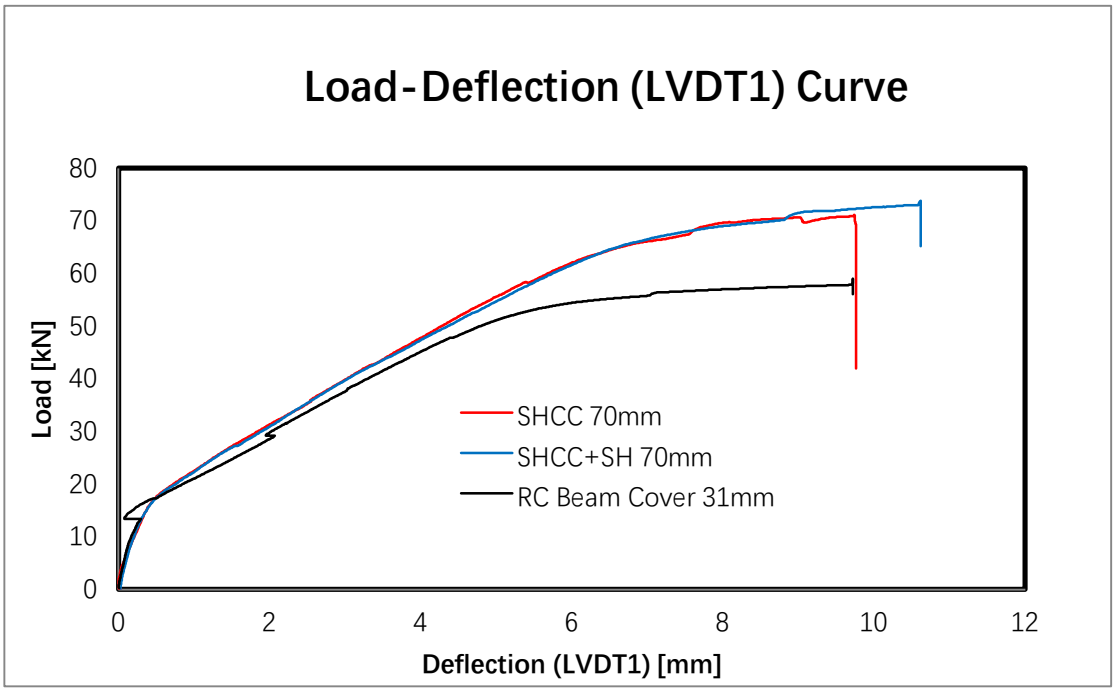

Figure 47 Load-Deflection (LVDT1) curves of beams with the concrete cover of 31 mm: composite beam with the SHCC layer of 70 mm (SHCC 70 mm), composite beam with the self-healing SHCC layer of 70 mm (SH+SHCC 70 mm) and corresponding conventional (control) reinforced concrete beam (RC beam cover 31 mm).

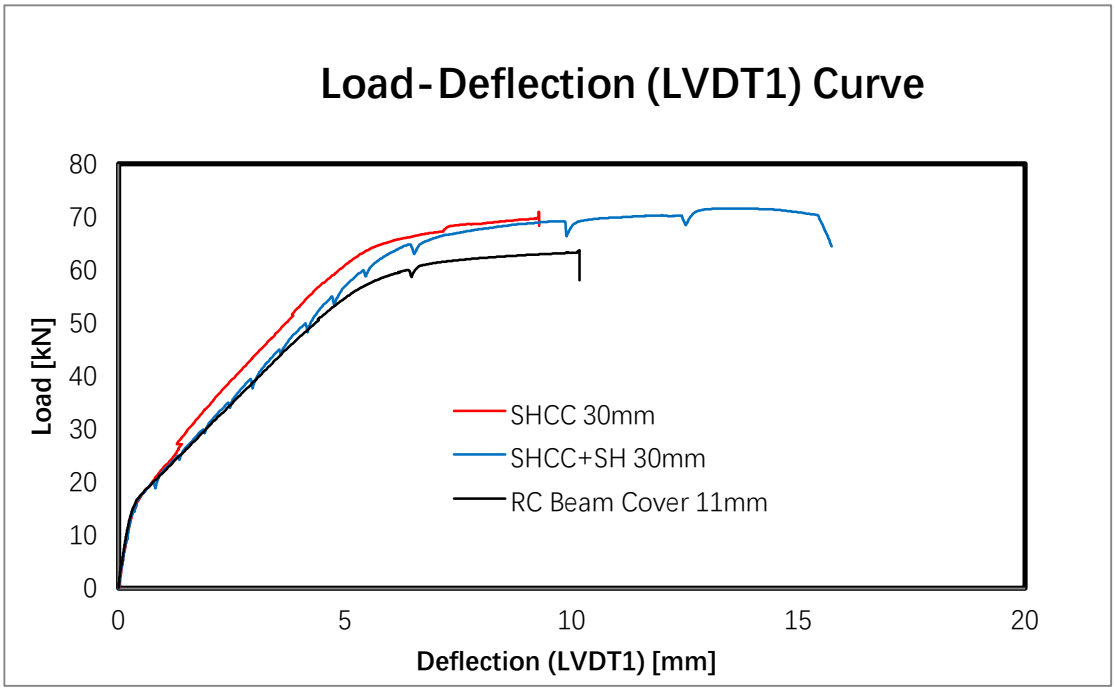

Figure 48 Load-Deflection (LVDT1) curves of beams with the concrete cover of 11 mm: composite beam with the SHCC layer of 30 mm (SHCC 30 mm), composite beam with the self-healing SHCC layer of 30 mm (SH+SHCC 30 mm) and corresponding conventional (control) reinforced concrete beam (RC beam cover 11 mm).

With the same reinforcement position, the beams with SHCC layer have higher load capacity than the conventional reinforced concrete beam. This is due to the tensile resistance of SHCC. Although the tensile stress of SHCC is only 3 MPa, the cross-sectional area is large, which also explains that the capacity difference for beam with 70 mm thickness SHCC layer is bigger than that for beam with 30 mm thickness SHCC layer. This can be elaborated by the following numerical calculation, where the contribution of SHCC to take tensile forces is taken into account. Since there was no effect on mechanical proprieties of SHCC mix due to the addition of self-healing agent, in the following calculations, both SHCC mixtures, with and without self-healing agent are considered in the same way.

4.2. Numerical calculations

4.2.1. Assumptions

The calculations are based on following assumptions related to the material properties:

Concrete properties:

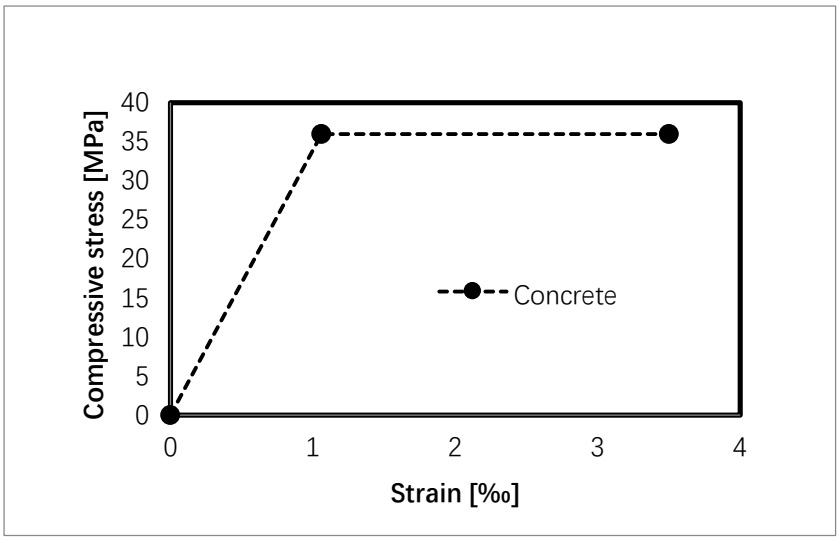

Figure 49 Concrete stress-stain curve

$f_{ctm,fl} = 4.536\ \text{MPa}$	Concrete Crack Stress
$f_{cm,cyl} = 36\ \text{MPa}$	Concrete Compressive Stress
$\varepsilon_c = 0.106\ \%$	Concrete Elastic Strain
$\varepsilon_{cu} = 0.35\ \%$	Concrete Ultimate Strain
$E_c = 34000\ \text{MPa}$	Concrete Young' s Modulus

Steel properties:

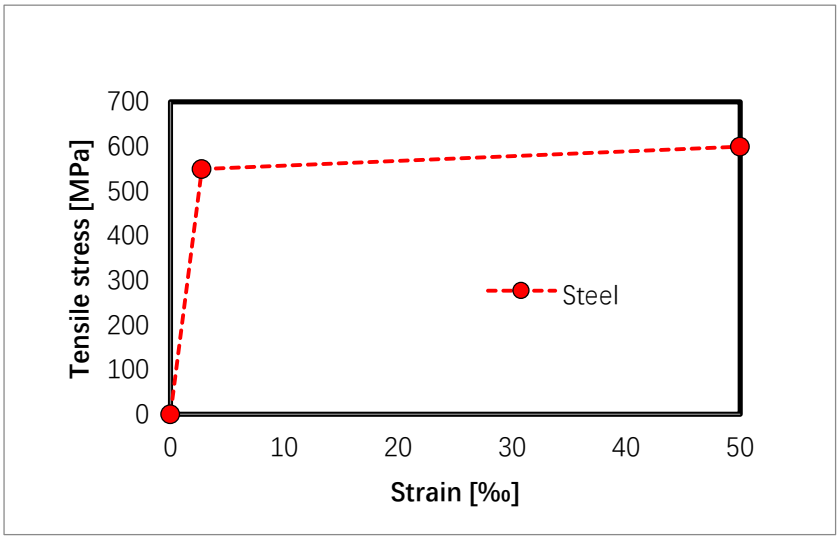

Figure 50 Steel stress-stain curve

$f_y = 550\ MPa$	Steel Yielding Stress
$f_u = 600\ MPa$	Steel Ultimate Stress
$\varepsilon_{sy} = 0.275\ \%$	Steel Yielding Strain
$\varepsilon_{su} = 5\ \%$	Steel Ultimate Strain
$E_s = 200000\ MPa$	Steel Young' s Modulus

SHCC properties:

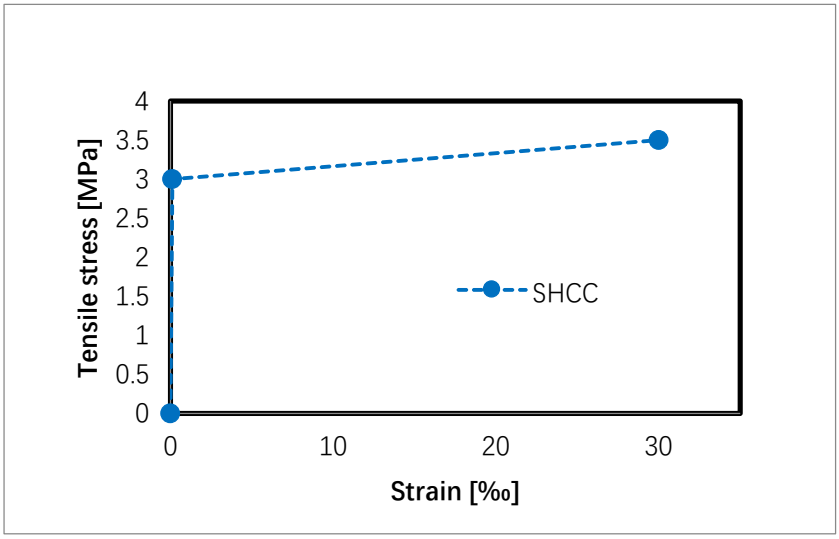

Figure 51 SHCC stress-stain curve

$\sigma_{SHCC,t,crack} = 3\ MPa$	SHCC Crack Stress
$\sigma_{SHCC,tu} = 3.5\ MPa$	SHCC Ultimate Tensile Stress
$\varepsilon_{SHCC,t,crack} = 0.01\%$	SHCC Crack Strain
$\varepsilon_{SHCC,tu} = 3\%$	SHCC Ultimate Tensile Strain
$E_{SHCC} = 18000MPa$	SHCC Young' s Modulus

Deflection at the mid span

The deflection at the mid span is estimated by two approaches. The first one is based on the geometry (Figure 52). With the same cross-section, under constant bending moment, the curvature is constant, which can be considered as a part of circle. Based on that, the deflection of the mid span can be estimated. However, the real deflection should be larger than this because the on the two sides of the constant moment area, the moment decreases linearly to the supports, but it is not zero. Thus, the deflection is underestimated. The deflection calculated by this approach is named w_1.

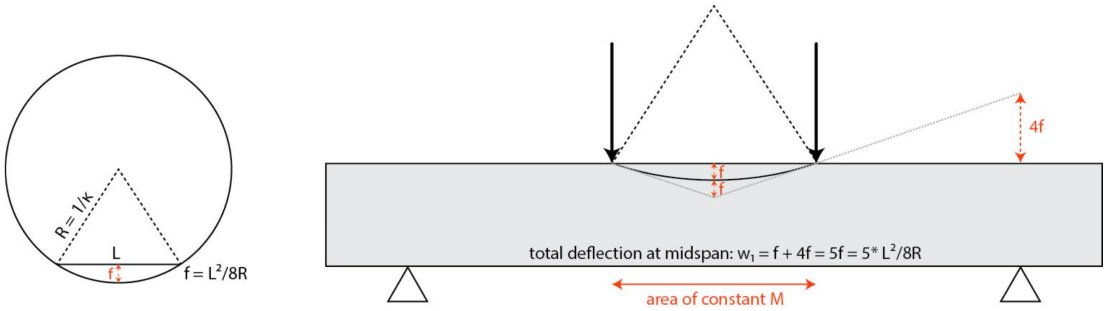

Figure 52 Estimation of the mid span deflection, w_1

$$w_1 = \frac{l^2}{8R} * 5$$

Another approach is based on the 'forget me not' equation from structural mechanics (Figure 53).

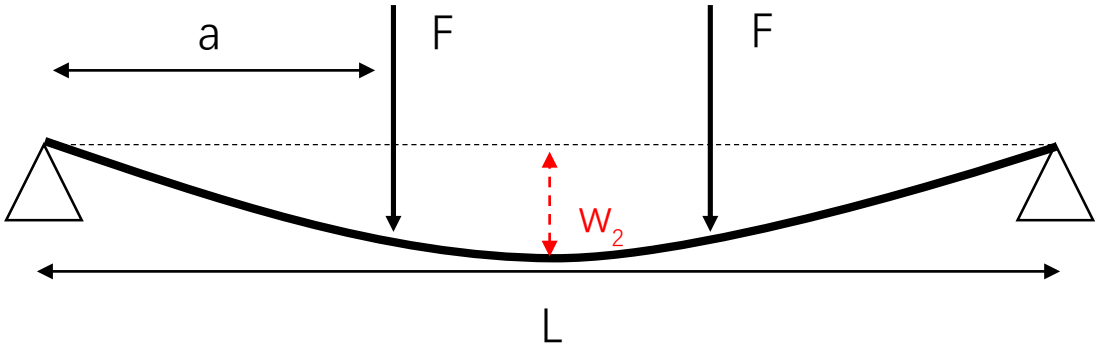

Figure 53 Estimation of the mid span deflection, w_2

$$w_2 = \frac{ML^2}{24EI} * (3 - 4 * \left(\frac{a^2}{L^2}\right))$$

Where EI can be calculated as moment divided by curvature:

$$EI = M/\kappa$$

And $\kappa = 1/R$.

Therefore, based on the specifications of the experiment setup the equation can be simplified as:

$$w_2 = \frac{ML^2}{24EI} * \left(3 - 4 * \left(\frac{a^2}{L^2}\right)\right) = \frac{L^2}{24R} * \left(3 - \frac{4}{9}\right) = \frac{23l^2}{24R}$$

In this approach, EI used in the equation is the crack EI of the cracked cross section. However, outside the constant moment region, the real EI is higher, since the concrete is not cracked. Therefore, w_2 might be overestimated.

4.2.2. Calculation of RC beam with cover of 31 mm

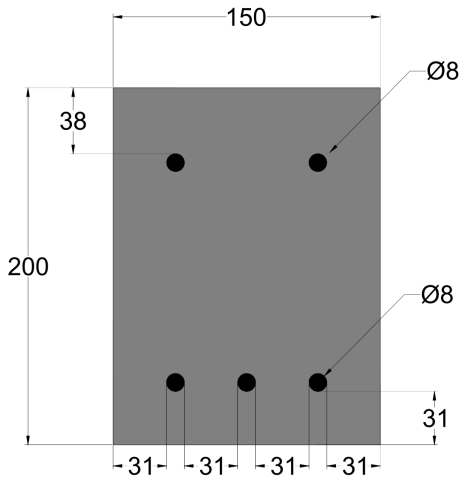

Figure 54 Specifications of the cross-section

Cross-section Geometry:

$b = 150\ mm$	Width of the Beam
$h = 200\ mm$	Height of the Beam
$A_s = 150.8\ mm^2$	Cross-sectional Area of the Steel
$c = 31\ mm$	Thickness of Concrete Cover
$\emptyset = 8\ mm$	Rebar Diameter
$l = 500\ mm$	Distance between Loading Points

During the loading, for RC beams, there are four significant points, which are:

1. Concrete cracks
2. Steel takes over the force
3. Steel yields
4. Concrete fails in compression

1. Concrete cracks

When tensile stress of concrete bottom fiber reaches 4.536 MPa, concrete cracks.

$$f_{ctm,fl} = 4.54\ MPa$$

$$\sigma = \frac{M}{W}$$

Where:

$W = \frac{bh^2}{6} = 10^6\ mm^3$ is Elastic Section Modulus.

For simplification, two layers of materials are considered as one and composite Elastic Section Modulus are not taken into account.

$$M_{concrete,crack} = \sigma_{ctm,fl} * W = 4.54\ kNm$$

$$Load = 2 * \frac{M}{0.5\ m} = 18.14\ kN$$

Curvature, κ is calculated based on cross sectional strains:

$$\kappa = \frac{0.0133\%}{h/2} = 1.33 * 10^{-6}\ 1/mm$$

$$R = \frac{1}{\kappa} = 7.52 * 10^{5}\ mm$$

$$w_1 = \frac{l^2}{8R} * 5 = 0.21\ mm$$

$$w_2 = \frac{23l^2}{24R} = 0.32\ mm$$

2. Steel takes over the force

Height of the compression zone x can be calculated as:

$$x = \left(\sqrt{(\alpha_e \rho)^2 + 2 * \alpha_e \rho} - \alpha_e \rho\right) * d$$

Where:

$\alpha_e = \frac{E_s}{E_c} = \frac{200000}{34000} = 5.88$ is ratio of young' s modulus

$d = h - c - \frac{\emptyset}{2} = 200 - 31 - \frac{8}{2} = 165\ mm$ is concrete effective depth

$\rho = \frac{A_s}{b*d} = \frac{150.8}{150*165} = 0.61\ \%$ is reinforcement ratio

$$x = \left(\sqrt{(5.88 * 0.61\%)^2 + 2 * 5.88 * 0.61\%} - 5.88 * 0.61\%\right) * 165 = 38.66\ mm$$

$$M = A_s E_s \varepsilon_s * (d - \frac{x}{3})$$

M remains the value of the last point. Steel strain, ε_s at this point can be calculated as:

$$\varepsilon_s = \frac{M}{A_s E_s * (d - \frac{x}{3})} = \frac{4.54 * 10^6}{150.8 * 200000 * (165 - \frac{38.66}{3})} = 0.099\ \%$$

Curvature, κ is calculated based on cross sectional strains:

$$\kappa = \frac{\varepsilon_s}{d - x} = \frac{0.099\%}{165 - 38.66} = 7.83 * 10^{-6}\ 1/\text{mm}$$

$$R = \frac{1}{\kappa} = 1.28 * 10^5\ \text{mm}$$

$$w_1 = \frac{l^2}{8R} * 5 = 1.22\ \text{mm}$$

$$w_2 = \frac{23l^2}{24R} = 1.88\ \text{mm}$$

3. Steel yields

Steel yields when $\varepsilon_s = 0.275\%$. Tensile force taken by steel, F_s is:

$$F_s = A_s E_s \varepsilon_{sy} = 150.8 * 200000 * 0.275\% = 82940\ \text{N}$$

The depth of concrete compression zone, x remains. Concrete compression force, F_{cc} is:

$$F_{cc} = \sigma_{cc} * x * b/2$$

According to Force Equilibrium:

$$F_{cc} = F_s$$

The compressive stress of concrete top fiber, σ_{cc} is:

$$\sigma_{cc} = \frac{F_s}{x * b/2} = \frac{82940}{38.66 * \frac{150}{2}} = 28.60\ \text{kN} < f_{cm,cyl} = 36\ \text{kN}$$

$$M = F_s * \left(d - \frac{x}{3}\right) = 82940 * \left(165 - \frac{38.66}{3}\right) = 12.62\ \text{kN}$$

$$\text{Load} = 2 * \frac{M}{0.5\ \text{m}} = 50.48\ \text{kN}$$

Curvature, κ is calculated based on cross sectional strains:

$$\kappa = \frac{\varepsilon_s}{d - x} = \frac{0.275\%}{165 - 38.66} = 2.18 * 10^{-5}\ 1/\text{mm}$$

$$R = \frac{1}{\kappa} = 4.59 * 10^5\ \text{mm}$$

$$w_1 = \frac{l^2}{8R} * 5 = 3.40\ \text{mm}$$

$$w_2 = \frac{23l^2}{24R} = 5.21\ \text{mm}$$

4. Concrete fails in compression

Concrete fails when then strain of concrete top fiber, ε_c reaches 0.35%. Compression forceF_{cc}, is:

$$F_{cc} = f_{cm,cyl} * x * b * coef.$$

where $coef.$ is calculated based on the concrete properties given above.

$$\varepsilon_c = \frac{f_{cm}}{E_c} = \frac{36}{34000} = 0.106\ \%$$

$$coef. = \frac{\varepsilon_{cu} - \varepsilon_c/2}{\varepsilon_{cu}} = \frac{0.35\% - 0.106\%/2}{0.35\%} = 0.85$$

According to Force Equilibrium:

$$F_{cc} = F_s$$

Tensile force taken by steel, F_s is:

$$F_s = A_s E_s \varepsilon_s = 150.8 * 600 = 90480\ N$$

The depth of the concrete compression zone, x is:

$$x = \frac{F_s}{0.85 * f_{cm,cyl} * b} = \frac{90480}{0.85 * 36 * 150} = 19.74\ mm$$

The barycenter of the compression force is at 42.79% of the compression zone from the top fiber (calculated based on the concrete properties), which can be calculated as:

$$\frac{\left[\frac{\varepsilon_{cu}}{2} * \left(\varepsilon_{cu} - \frac{2}{3}\varepsilon_c\right) + \frac{(\varepsilon_{cu} - \varepsilon_c)^2}{2}\right]}{coef. * \varepsilon_{cu}}$$

$$= \frac{\left[0.35\% * \left(0.35\% - \frac{2}{3} * 0.106\%\right) + \frac{(0.35\% - 0.106\%)^2}{2}\right]}{0.85 * 0.35\%}$$

$$= 42.79\ \%$$

$$M = F_s * (d - 42.79\% * x) = 90480 * (165 - 42.79\% * 19.74) = 14.16\ kNm$$

$$Load = 2 * \frac{M}{0.5\ m} = 56.65\ kN$$

Curvature, κ is calculated based on cross sectional strains:

$$\kappa = \frac{\varepsilon_{cu}}{x} = \frac{0.35\%}{19.74} = 1.77 * 10^{-4}\ 1/mm$$

$$R = \frac{1}{\kappa} = 5.64 * 10^3\ mm$$

$$w_1 = \frac{l^2}{8R} * 5 = 27.72 \text{ mm}$$

$$w_2 = \frac{23l^2}{24R} = 42.50 \text{ mm}$$

Table 7 Summary of the calculations for RC beam with 31 mm cover

	Mcr [kNm]	Kappa [1/mm]	Load [kN]	R [mm]	w_1 [mm]	w_2 [mm]
Stage 1	4.54	1.33E-06	18.14	749559.08	0.21	0.32
Stage 2	4.54	7.83E-06	18.14	127783.12	1.22	1.87
Stage 3	12.62	2.18E-05	50.46	45943.25	3.40	5.21
Stage 4	14.16	1.77E-04	56.65	5640.35	27.72	42.50

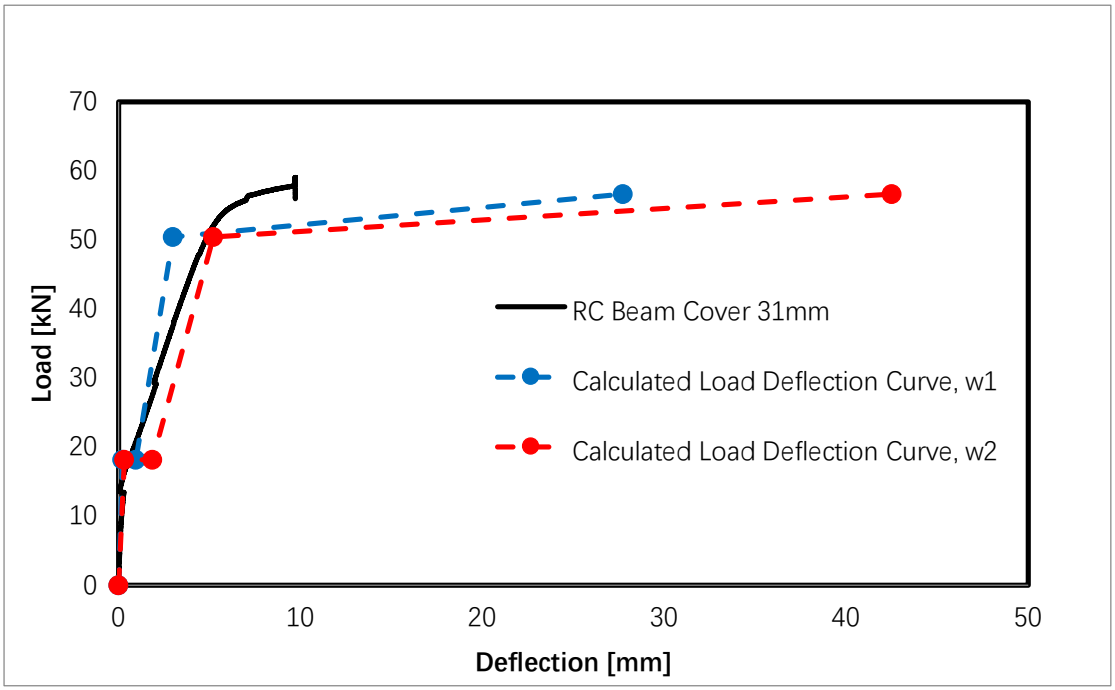

Figure 55 Calculated and experimental Load-Deflection curve of RB beam with 31 mm cover (the deflection after yielding of the steel during the experiment were not recorded as the LVDT was out of the range).

4.2.3. Calculation of beam with SHCC layer of 70 mm

The calculation is based on force equilibrium of the cross section.

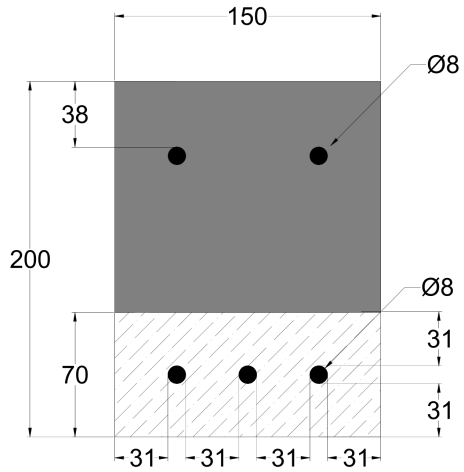

Figure 56 Specifications of the cross-section

Cross-section Geometry:

$b = 150\ mm$	Width of the Beam
$h = 200\ mm$	Height of the Beam
$h_{concrete} = 130\ mm$	Height of the concrete part
$h_{SHCC} = 70\ mm$	Height of the SHCC part
$A_s = 150.8\ mm^2$	Cross-sectional Area of the Steel
$A_{SHCC} = 10500\ mm^2$	Cross-sectional Area of the SHCC
$l = 500\ mm$	Distance between Loading Points

During the loading, for beams with SHCC layer, there are four significant points, which are:

1. SHCC first cracks
2. Concrete cracks
3. Steel yields
4. Concrete fails in compression

1. SHCC first cracks

   When tensile stress of SHCC reaches 3 MPa, SHCC cracks.

$$\sigma_{SHCC,t,crack} = 3\ MPa$$

Assume $\sigma_{SHCC,fl} = 1.5 * \sigma_{SHCC,t,crack} = 4.5$ MPa

$$\sigma_{fl} = \frac{M}{W}$$

Where:

$W = \frac{bh^2}{6} = \frac{150*200^2}{6} = 10^6\ mm^3$ Elastic Section Modulus.

$$M_{SHCC,crack} = \sigma_{SHCC,t,crack} * W = \frac{4.5 * 10^6}{1000 * 1000} = 4.5\ kNm$$

$$Load = 2 * \frac{M}{0.5\ m} = 18\ kN$$

Curvature, κ is calculated based on cross sectional strains:

$$\kappa = \frac{0.01\%}{h/2} = \frac{0.01\%}{200/2} = 1 * 10^{-6}\ 1/mm$$

Thus, the radius, R is:

$$R = \frac{1}{\kappa} = 1 * 10^6\ mm$$

$$w_1 = \frac{l^2}{8R} * 5 = \frac{500^2 * 5}{8 * 10^6} = 0.15625\ mm$$

$$w_2 = \frac{23l^2}{24R} = \frac{500^2 * 23}{24 * 10^6} = 0.25\ mm$$

2. Concrete cracks

Concrete cracks when tensile stress of the bottom concrete fiber reaches f_{ctm}

$$f_{ctm} = 4.536\ MPa$$

At the moment of cracking, there is a general Force Equilibrium which needs to be satisfied:

$$F_{cc} = F_{ct} + F_s + F_{SHCC}$$

Where F_{cc} is compression force taken by concrete:

$$\sigma_{cc} = \frac{\frac{f_{ctm}}{E_c}}{h_{conrete} - x} * x * E_c$$

$$F_{cc} = \sigma_{cc} * x * b/2$$

F_{ct}, $F_s$and F_{SHCC} are tensile forces taken by concrete, steel and SHCC, respectively:

$$F_{ct} = f_{ctm} * (h_{conrete} - x) * b/2$$

$$F_s = \sigma_s A_s$$

$$\sigma_s = \varepsilon_s E_s$$

$$\varepsilon_s = \frac{\varepsilon_{ctm}}{h_{conrete} - x}\left(h_{conrete} + \frac{h_{SHCC}}{2} - x\right)$$

$$F_{SHCC} = \sigma_{SHCC} * A_{SHCC}$$

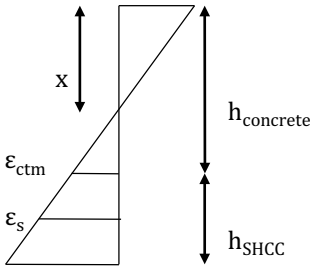

$$F_{cc} = F_{ct} + F_s + F_{SHCC}$$

With solving the equation of Force Equilibrium, $x = 86.60\ \text{mm}$, which is the height of the compression zone.

In order to calculate M-κ, diagram and deflections, further calculations were performed: x is substituted into the equations in order to calculate equilibrium forces and resulting cross sectional moment:

$$F_{cc} = \frac{\frac{f_{ctm}}{E_c}}{h_{conrete} - x} * x * E_c * x * \frac{b}{2} = \frac{4.536 * 86.6}{130 - 86.6} * 86.6 * 150/2 = 58519.95\ \text{N}$$

$$L_{cc} = \frac{2}{3}(h_{conrete} - x) = \frac{2}{3}(130 - 86.6) = 57.33\ \text{mm}$$

$$F_{SHCC} = \sigma_{SHCC} * A_{SHCC} = 3.5 * 10500 = 36750\ \text{N}$$

$$L_{SHCC} = h_{conrete} + \frac{h_{SHCC}}{2} - x = 130 + \frac{70}{2} - 86.6 = 78.4\ \text{mm}$$

$$F_s = A_s \varepsilon_s E_s = 150.8 * \frac{\frac{4.536}{34000}}{130 - 86.6}\left(130 + \frac{70}{2} - 86.6\right) * 200000 = 7238.4\ \text{N}$$

$$L_s = 130 + \frac{70}{2} - 86.6 = 78.4\ \text{mm}$$

$$F_{ct} = 4.536 * (130 - 86.6) * 86.6/2 = 14764.86\ \text{N}$$

$$L_{ct} = \frac{2}{3}x = \frac{2}{3} * 86.6 = 28.93\ \text{mm}$$

$$M_{Concrete,crack} = F_{cc} * L_{cc} + F_{ct} * L_{ct} + F_{SHCC} * L_{SHCC} + F_s * L_s = 7.254\ \text{kNm}$$

$$\text{Load} = 2 * \frac{M}{0.5\text{m}} = 29.016\ \text{kN}$$

Curvature, κ is calculated based on cross sectional strains:

$$\kappa = \frac{0.0133\%}{x} = \frac{0.0133\%}{86.6} = 3.0645 * 10^{-6}\ 1/\text{mm}$$

Thus, the radius, R is:

$$R = \frac{1}{\kappa} = \frac{1}{3.0645 * 10^{-6}} = 326315.79 \text{ mm}$$

$$w_1 = \frac{l^2}{8R} * 5 = \frac{500^2 * 5}{8 * 326315.79} = 0.4788 \text{ mm}$$

$$w_2 = \frac{23l^2}{24R} = \frac{500^2 * 23}{24 * 326315.79} = 0.74 \text{ mm}$$

3. Steel yields:

Steel yields when $\varepsilon_s = 0.275\%$, At the moment of yielding, the following Force Equilibrium is fulfilled:

$$F_{cc} = F_s + F_{SHCC}$$

Since the concrete is already cracked, tensile force that can be taken by concrete, F_{ct}, is neglected, while the compression force taken by concrete, F_{cc} is:

$$F_{cc} = \sigma_{cc} * x * b/2$$

$$\sigma_{cc} = \varepsilon_{cc} E_c$$

$$\varepsilon_{cc} = \frac{0.275\%}{h_{conrete} + \frac{h_{SHCC}}{2} - x} x$$

And tensile forces taken by SHCC and steel, F_{SHCC}, and F_s are:

$$F_{SHCC} = \sigma_{SHCC} * A_{SHCC}$$

$$F_s = \sigma_s A_s$$

$$\sigma_s = \varepsilon_s E_s$$

$$F_{cc} = F_s + F_{SHCC}$$

By solving the equation of Force Equilibrium, $x = 45.22 \text{ mm}$, which is the height of the compression zone.

Substitute x into the equations to calculate equilibrium forces and resulting cross sectional moment:

$$F_{cc} = \varepsilon_{cc} E_c * x * \frac{b}{2} = \frac{0.275\%}{130 + \frac{70}{2} - 45.22} * 34000 * 150/2 = 119692.82 \text{ N}$$

$$L_{cc} = \frac{2}{3} x = \frac{2}{3} * 45.2 = 30.15 \text{ mm}$$

$$F_{SHCC} = \sigma_{SHCC} * A_{SHCC} = 3.5 * 10500 = 36750 \text{ N}$$

$$L_{SHCC} = h_{conrete} + \frac{h_{SHCC}}{2} - x = 130 + \frac{70}{2} - 45.22 = 119.78\ \text{mm}$$

$$F_s = A_s \varepsilon_s E_s = 150.8 * 0.275\% * 200000 = 82940\ \text{N}$$

$$L_s = h_{conrete} + \frac{h_{SHCC}}{2} - x = 130 + \frac{70}{2} - 45.22 = 119.78\ \text{mm}$$

$$M_{Concrete,crack} = F_{cc} * L_{cc} + F_{SHCC} * L_{SHCC} + F_s * L_s = 17.96\ \text{kNm}$$

$$\text{Load} = 2 * \frac{M}{0.5\ \text{m}} = 71.83\ \text{kN}$$

Curvature, κ is calculated based on cross sectional strains:

$$\kappa = \frac{0.275\%}{h_{conrete} + \frac{h_{SHCC}}{2} - x} = \frac{0.275\%}{130 + \frac{70}{2} - 45.22} = 2.296 * 10^{-5}\ 1/\text{mm}$$

Thus, the radius, R is:

$$R = \frac{1}{\kappa} = 43557.82\ \text{mm}$$

$$w_1 = \frac{l^2}{8R} * 5 = \frac{500^2 * 5}{8 * 43557.82} = 3.587\ \text{mm}$$

$$w_2 = \frac{23l^2}{24R} = \frac{500^2 * 23}{24 * 43557.82} = 5.50\ \text{mm}$$

4. Concrete fails in compression

Concrete top fiber fails when strain reaches 0.35%,$\varepsilon_{cc} = 0.35\%$. At the moment of concrete compression failure, the equation of Force Equilibrium is fulfilled:

$$F_{cc} = F_s + F_{SHCC}$$

According to the stress-strain curve concrete, the ratio is 0.85. The compression force taken by concrete, F_{cc} is:

$$F_{cc} = f_{cm,cyl} * x * b * 0.85$$

Tensile force taken by SHCC, F_{SHCC} is:

$$F_{SHCC} = \sigma_{SHCC} * A_{SHCC}$$

And according to the geometry of the beam cross section, the strain of the steel, σ_s can be calculated as:

$$\sigma_s = \left(\left(\frac{\varepsilon_{cc}}{x} * \left(h_{conrete} + \frac{h_{SHCC}}{2} - x\right) - \varepsilon_{sy}\right) * \left(\frac{f_u - f_y}{\varepsilon_{su} - \varepsilon_{sy}}\right) + f_y\right)$$

Then the tensile force taken by steel, F_s is:

$$F_s = \sigma_s A_s$$

Solve the equation of Force Equilibrium, $x = 27.12\ \text{mm}$, which is the height of the compression zone.

Substitute x into the equations:

$$F_{cc} = f_{cm,cyl} * x * b * 0.85 = 36 * 27.12 * 150 * 0.85 = 124480.8\ \text{N}$$

$$L_{cc} = (1 - 0.429) * x = (1 - 0.429) * 27.12 = 15.49\ \text{mm}$$

Where $0.429\,x$ is the position of barycenter of the compression zone from top fiber.

$$F_{SHCC} = \sigma_{SHCC} * A_{SHCC} = 3.5 * 10500 = 36750\ \text{N}$$

$$L_{SHCC} = h_{conrete} + \frac{h_{SHCC}}{2} - x = 130 + \frac{70}{2} - 27.12 = 137.88\ \text{mm}$$

$$F_s = A_s \sigma_s$$

$$F_s = 150.8 * \left(\left(\frac{0.35\%}{27.12} * \left(130 + \frac{70}{2} - 27.12 \right) - 0.275\% \right) * \left(\frac{650 - 550}{5\% - 0.275\%} \right) + 550 \right)$$

$$F_s = 87743\ \text{N}$$

$$L_s = h_{conrete} + \frac{h_{SHCC}}{2} - x = 130 + \frac{70}{2} - 27.12 = 137.88\ \text{mm}$$

$$M_{Concrete,crack} = F_{cc} * L_{cc} + F_{SHCC} * L_{SHCC} + F_s * L_s = 19.09\ \text{kNm}$$

$$\text{Load} = 2 * \frac{M}{0.5\ \text{m}} = 76.36\ \text{kN}$$

Curvature, κ is calculated based on cross sectional strains:

$$\kappa = \frac{0.35\%}{x} = \frac{0.35\%}{27.12} = 1.29 * 10^{-4}\ 1/\text{mm}$$

$$R = \frac{1}{\kappa} = 7748.57\ \text{mm}$$

$$w_1 = \frac{l^2}{8R} * 5 = \frac{500^2 * 5}{8 * 7748.57} = 20.165\ \text{mm}$$

$$w_2 = \frac{23l^2}{24R} = \frac{500^2 * 23}{24 * 7748.57} = 30.93\ \text{mm}$$

Table 8 Summary of the calculations for beams with 70 mm SHCC layer

	Mcr [kNm]	Kappa [1/mm]	Load [kN]	R [mm]	w_1 [mm]	w_2 [mm]
Stage 1	3.00	0.00E+00	18.00	1000000.00	0.16	0.25
Stage 2	7.25	1.00E-06	29.02	326315.79	0.48	0.74
Stage 3	17.94	3.06E-06	71.78	43556.36	3.59	5.50
Stage 4	19.09	2.30E-05	76.36	7748.57	20.17	30.93

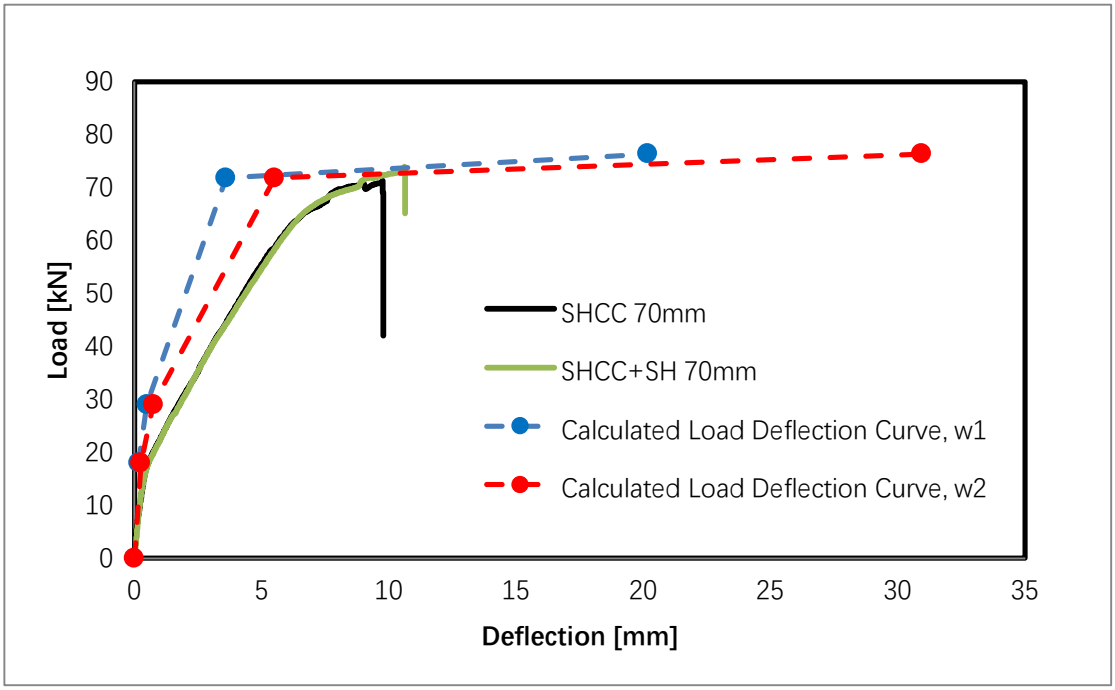

Figure 57 Calculated and experimental Load-Deflection curve of beams with 70 mm SHCC layer (the deflections after yielding of the steel during the experiment were not recorded as the LVDT was out of the range).

Calculation of RC beam with cover 11 mm

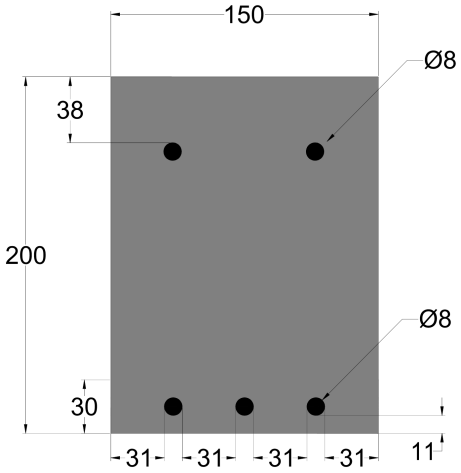

Figure 58 Specifications of the cross-section

Cross-section Geometry:

$b = 150\ mm$	Width of the Beam
$h = 200\ mm$	Height of the Beam
$A_s = 150.8\ mm^2$	Cross-sectional Area of the Steel
$c = 11\ mm$	Thickness of Concrete Cover
$\emptyset = 8\ mm$	Rebar Diameter
$l = 500\ mm$	Distance between Loading Points

Table 9 Summary of the calculations for RC beam with 11 mm cover

	Mcr [kNm]	Kappa [1/mm]	Load [kN]	R [mm]	w_1 [mm]	w_2 [mm]
Stage 1	4.54	1.33E-06	18.14	749559.08	0.21	0.32
Stage 2	4.54	6.11E-06	18.14	163698.29	0.95	1.46
Stage 3	14.20	1.91E-05	56.81	52278.15	2.99	4.58
Stage 4	15.97	1.77E-04	63.89	5640.35	27.72	42.50

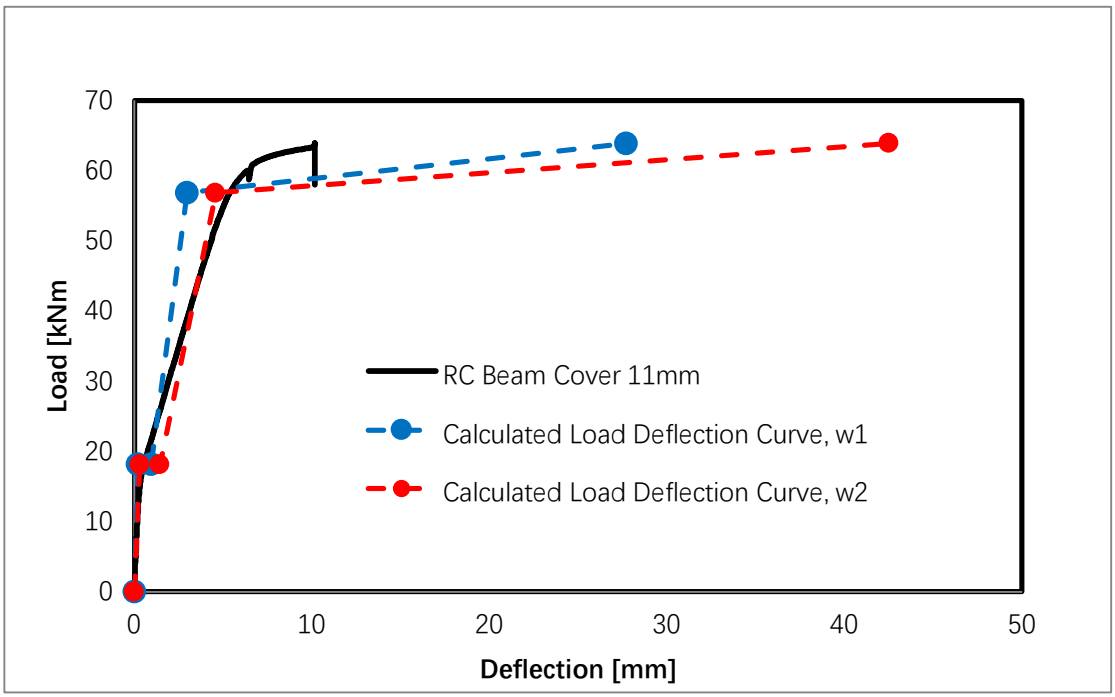

Figure 59 Calculated and experimental Load-Deflection curve of RB beam with 11 mm cover (the deflection after yielding of the steel during the experiment were not recorded as the LVDT was out of the range).

Calculation of beam with SHCC layer of 30 mm

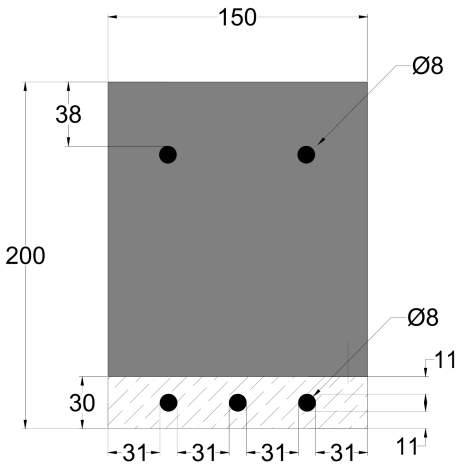

Figure 60 Specifications of the cross-section

Cross-section Geometry:

$b = 150\ mm$	Width of the Beam
$h = 200\ mm$	Height of the Beam
$h_{concrete} = 170\ mm$	Height of the Concrete Part
$h_{SHCC} = 30\ mm$	Height of the SHCC Part
$A_s = 150.8\ mm^2$	Cross-sectional Area of the Steel
$A_{SHCC} = 4500\ mm^2$	Cross-sectional Area of the SHCC
$l = 500\ mm$	Distance between Loading Points

Table 10 Summary of the calculations for beams with 30 mm SHCC layer

	Mcr [kNm]	Kappa [1/mm]	Load [kN]	R [mm]	w_1 [mm]	w_2 [mm]
Stage 1	3.00	1.00E-06	12.00	1000000.00	0.16	0.25
Stage 2	5.89	1.84E-06	23.57	542481.20	0.29	0.44
Stage 3	16.80	1.96E-05	67.20	51101.82	3.06	4.69
Stage 4	18.53	1.52E-04	74.12	6577.14	23.77	36.45

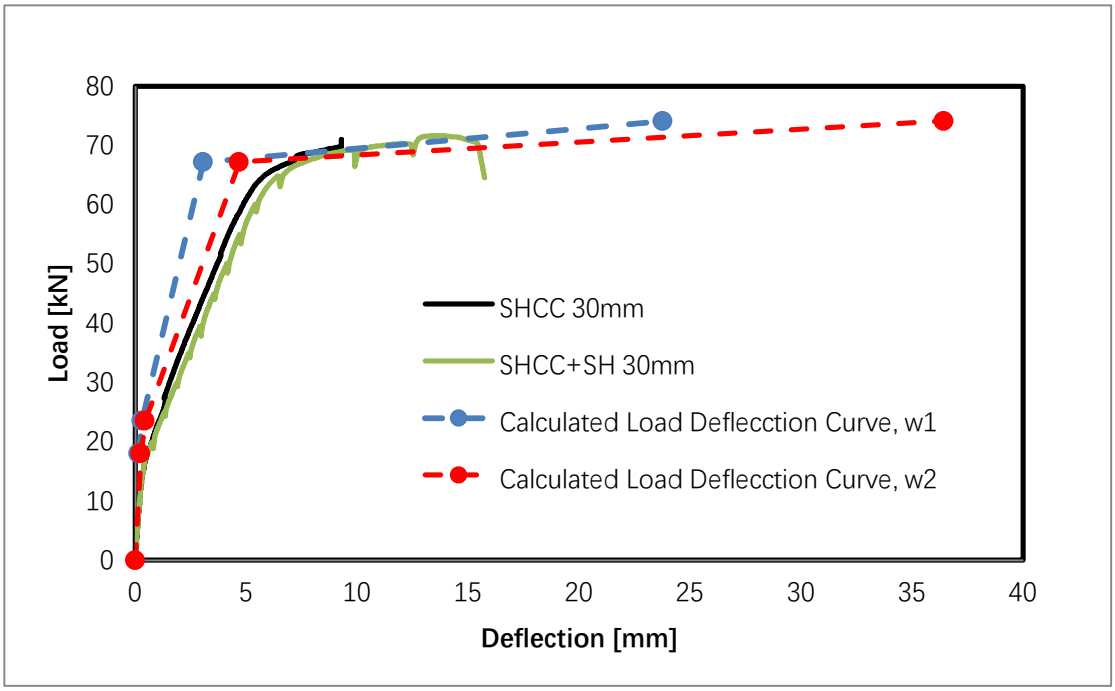

Figure 61 Calculated and experimental Load-Deflection curve of beams with 30 mm SHCC layer (the deflection after yielding of the steel during the experiment were not recorded as the LVDT was out of the range)

Discussion on the results of numerical calculation

The capacity of composite beam with SHCC layer in the tension can be well predicted by theoretical calculation. However, the deflection of the beam could not be reliably predicted because of measuring range of LVDT (except for one beam which has SHCC+SH layer of 30 mm). The overestimation of deflection may be caused by lower concrete compressive stress. The beams were in compression, thus, if the actual concrete stress is lower than the value used in the calculation, the deflection will be significantly influenced. In the Load-Deflection curves, w_2 seems to be closer to the experimental results, but the accurate theoretical results should be between w_1 and w_2.

4.3. Verification of DIC displacement measurement (comparison with LVDTs)

To verify the accuracy DIC, the results from LVDTs on one side of the beam (LVDT 02, 03 and 04) and the results from DIC on the other side are compared.

The LVDT only measures the displacement between two fixed points. Before loading the specimens, the positions of LVDTs are marked with red dots on the opposite side where the DIC photos are taken, which helps to find the data from DIC results.

Figure 62 LVDT No.2, 3 & 4 (from top to bottom)

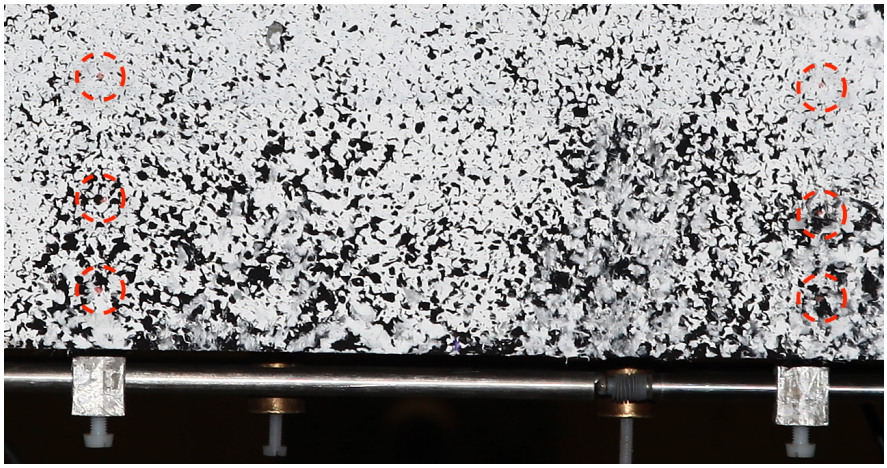

Figure 63 Red dots on the painted surface used during DIC to verify with the LVDT measurements

Two methods are developed to calculate the displacements of the LVDTs from DIC results:

1. Method based on displacement field. The procedure can be described as follows:

First find the coordinates of the pair of red dots on the first image. Then use the coordinates to find the displacements of the red dots at different loads. The differences between the horizontal displacements of two red dots at different loading levels should be equal to the displacements recorded by LVDTs.

2. Method based on the strain field computed from displacement field. It starts with the same procedure as the first method: find the coordinates of the pairs of red dots. Then, the strains between the two coordinates are summed up and multiplied with the length of a grid. The results should also be equal to the displacements recorded by LVDTs. At higher loads, some points are missing, since cracks generate new patterns on the element surface, which cannot be find in the previous photo. That leads to non-correlated points around the cracks that have no data. The missing data make the sum of the strain smaller than the actual value, which also leads to a small displacement. Therefore, these points are not included in the comparison.

One group of comparisons between the data of DIC and LVDTs from Test No.1 (beam with SHCC layer of 30 mm) is shown below (Figure 64, Figure 65 and Figure 66). The rest of the comparisons can be seen in Appendix.

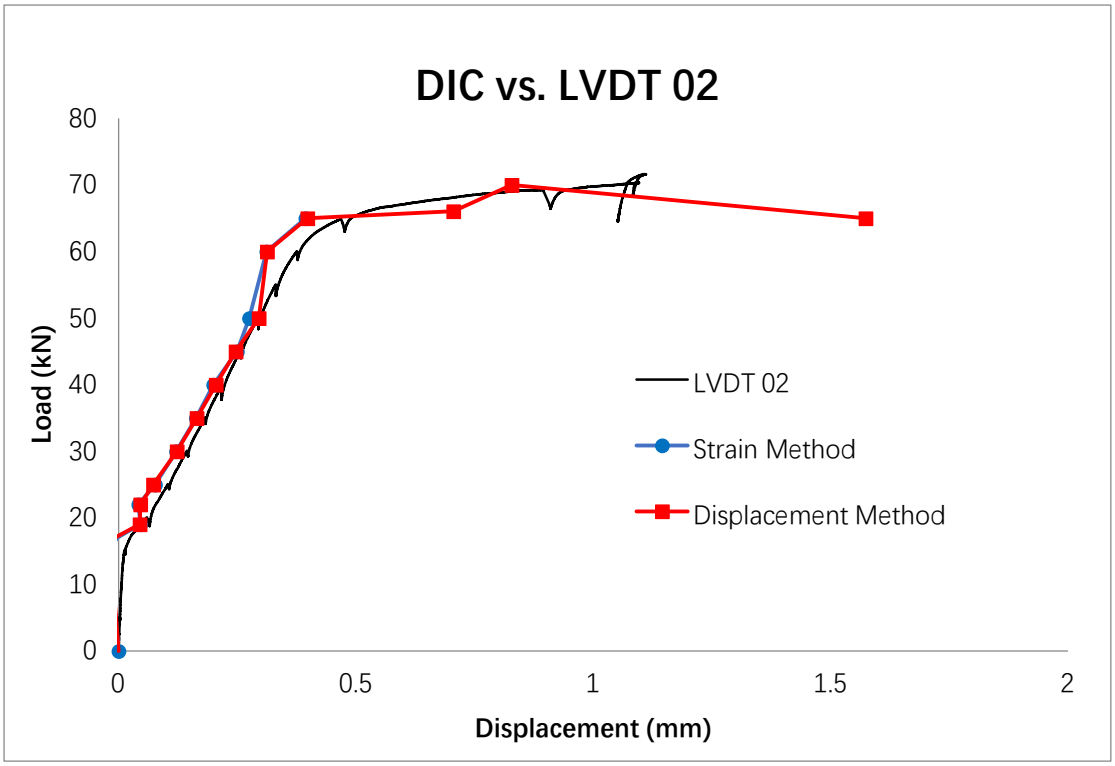

Figure 64 Comparison between DIC and LVDT No.2 from beam with SHCC layer of 30 mm

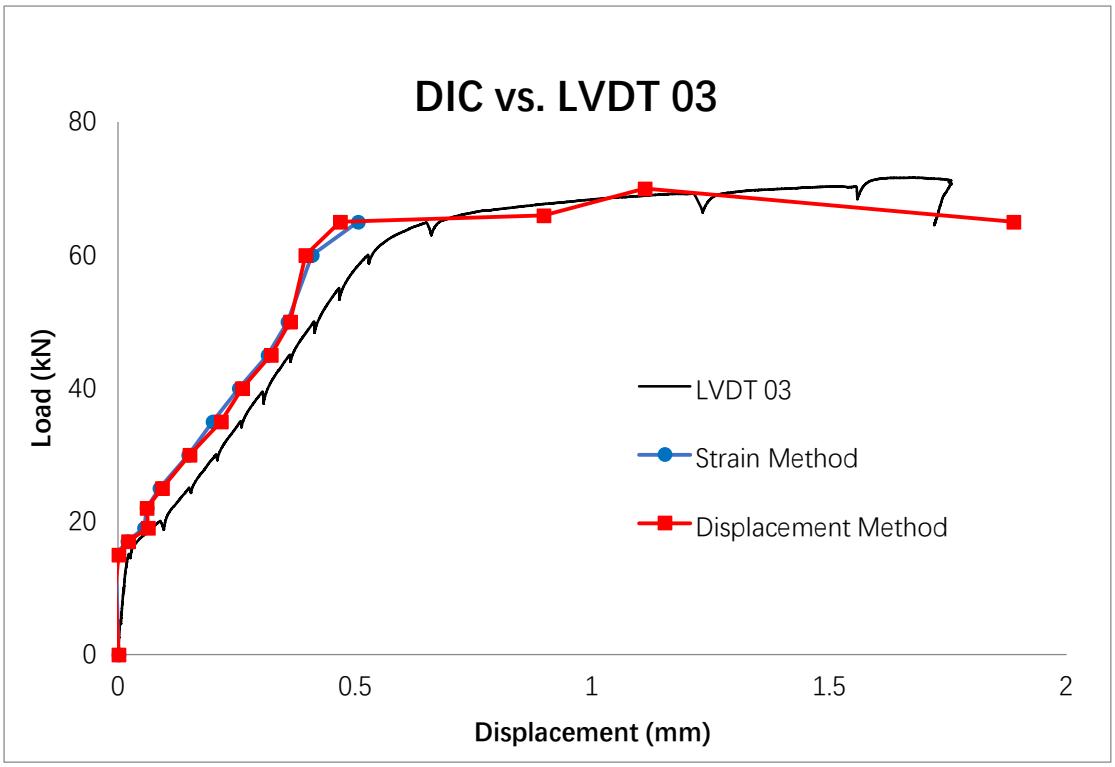

Figure 65 Comparison between DIC and LVDT No.3 from beam with SHCC layer of 30 mm

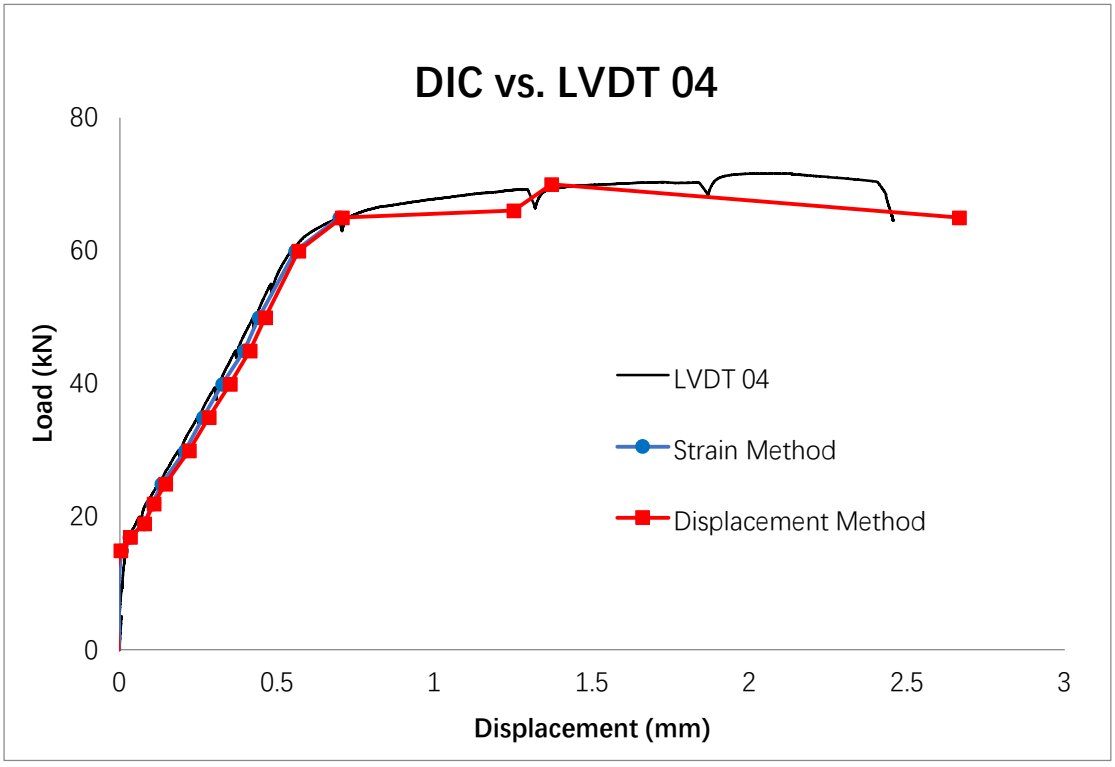

Figure 66 Comparison between DIC and LVDT No.4 from beam with SHCC layer of 30 mm

4.4. Measuring the maximum crack width with DIC

The comparisons between the DIC and LVDTs show that the results from the DIC have high accuracy and the results are reliable. In this case, the displacement is measured over the large length, i.e. the length of 20 mm. The next step is to check if the displacements can be reliably evaluated in the discrete points of the beam, i.e. if crack widths can also be accurately evaluated.

To evaluate the maximum crack width at different loads, first the overall analysis of the whole beam should be performed to find out at which locations the crack localized. In order to save the computation time. The initial analysis can be performed with coarse mesh and large load intervals. The analyzed DIC Images of the whole beam from Test 04 (SHCC layer of 70 mm with self-healing agents) and together with the photos of the failed beam are shown below:

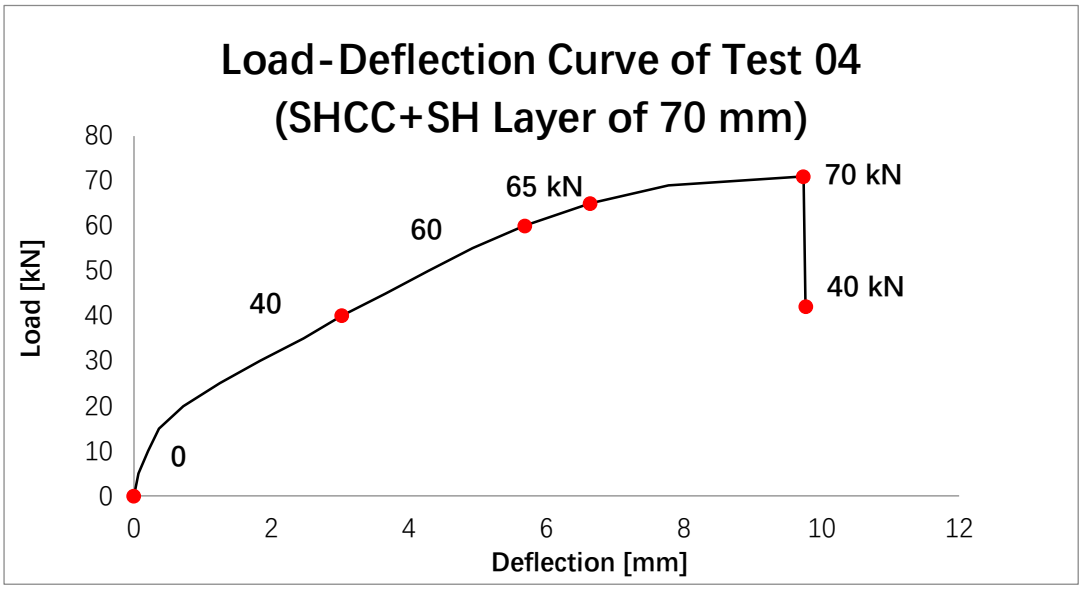

Figure 67 Load-Deflection curve of beam with SHCC+SH layer of 70 mm) and the analyzed loads (red dots)

Figure 68 DIC images of the whole beam from beam with SHCC+SH layer of 70 mm under 0 kN

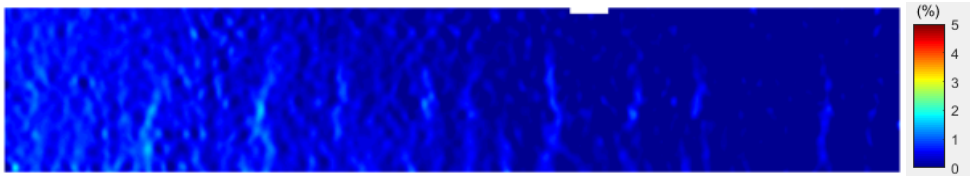

Figure 69 DIC images of the whole beam from beam with SHCC+SH layer of 70 mm under 40 kN

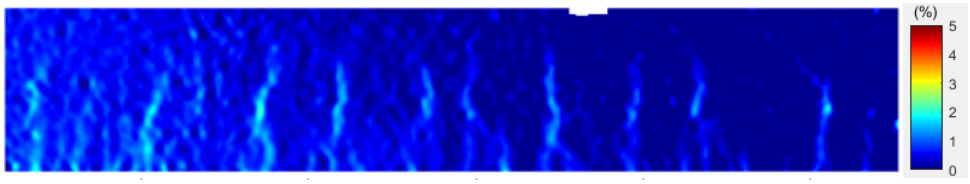

Figure 70 DIC images of the whole beam from beam with SHCC+SH layer of 70 mm under 60 kN

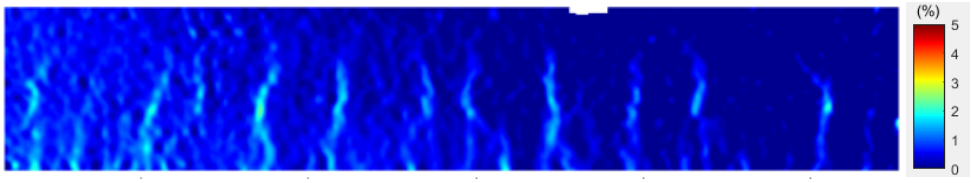

Figure 71 DIC images of the whole beam from beam with SHCC+SH layer of 70 mm under 65 kN

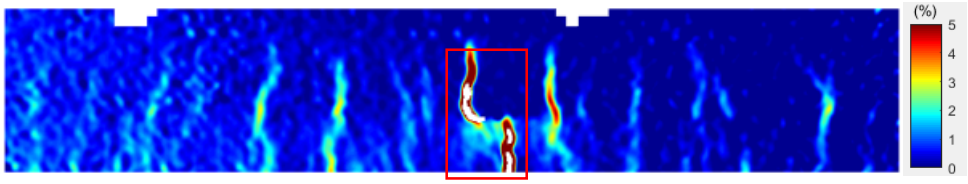

Figure 72 DIC images of the whole beam from beam with SHCC+SH layer of 70 mm under 70 kN, where the crack localized first is marked with the red box

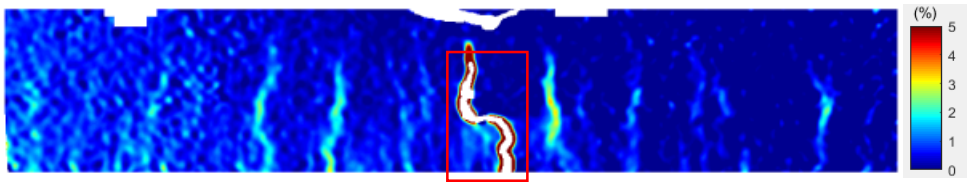

Figure 73 DIC images of the whole beam from beam with SHCC+SH layer of 70 mm, after failure, under 40 kN, where the crack localized first is marked with red box

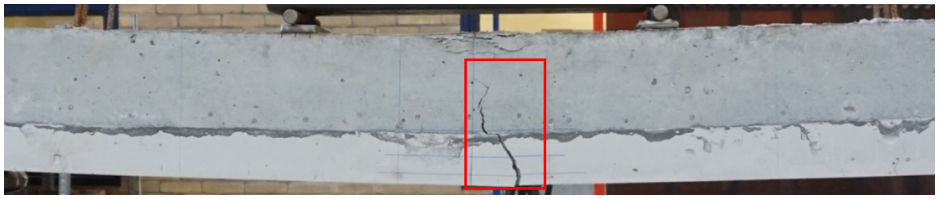

Figure 74 Beam with SHCC+SH layer of 70 mm, after failure, under the load of 40 kN

Once the location of the localized crack is determined (red box), the analyzing area is narrowed to the first localized crack. And then the small area is analyzed with the finer mesh and small load interval to see how the crack developed with load. On the analyzed small area, the crack can be clearly seen. The following step is to find the X and Y coordinates of two points at the bottom of the image (corresponding to the bottom of the beam where the crack is largest), one near the left of the crack and one near the right of the crack. From the displacement field, the horizontal displacements of the two points can be found. The difference between their horizontal displacement is the crack width from DIC.

For example, on the DIC image of the localized crack area under 71 kN (Figure 75 (right)), the crack is seen clearly and the x and y coordinates of two points, one on the left side of the crack and the other one on the right edge of the crack, are recorded as $\mathrm{x}_1, \mathrm{y}_1$ and$\mathrm{x}_2, \mathrm{y}_2$. Then the crack width under 69 kN can be calculated as the absolute value of the horizontal movement of the left pixel under 69 kN ($\mathrm{u}_{\mathrm{horizontal}}(69\ \mathrm{kN}, \mathrm{x}_1, \mathrm{y}_1)$) minus the horizontal movement of the right pixel under 69 kN ($\mathrm{u}_{\mathrm{horizontal}}(69\ \mathrm{kN}, \mathrm{x}_2, \mathrm{y}_2)$). This can be summarized as the equation shown below.

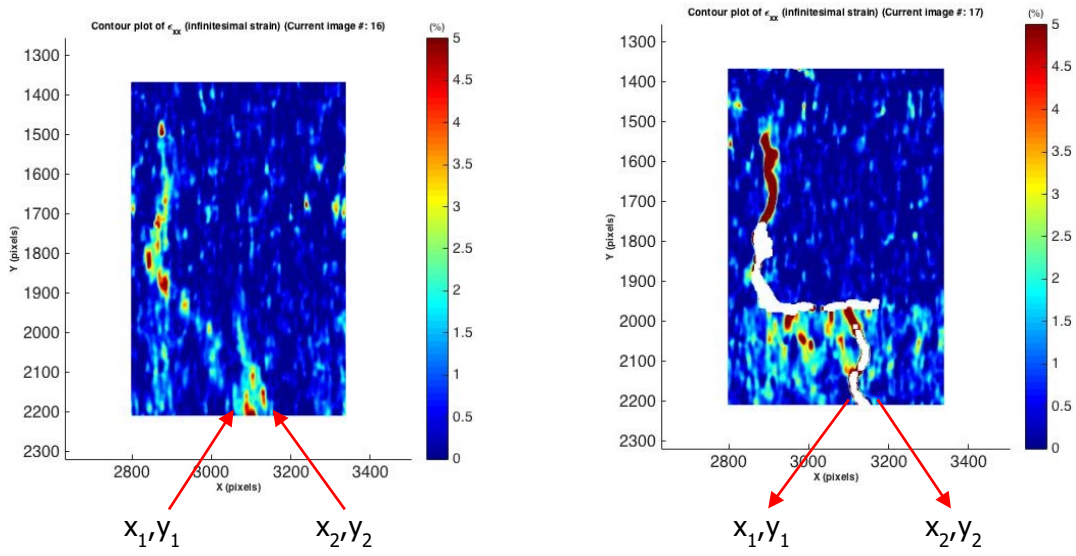

Figure 75 DIC image of localized crack area under 69 kN (left) and 71 kN (right) from beam with SHCC+SH layer of 70 mm

$$\text{Crack Width}(\text{Load}) = |u_{\text{horizontal}}(\text{Load}, x_1, y_1) - u_{\text{horizontal}}(\text{Load}, x_2, y_2)|$$

The photo of the first localized crack under the force of 40 kN, after failure taken from the other side of the beam is also shown in Figure 76 for comparison.

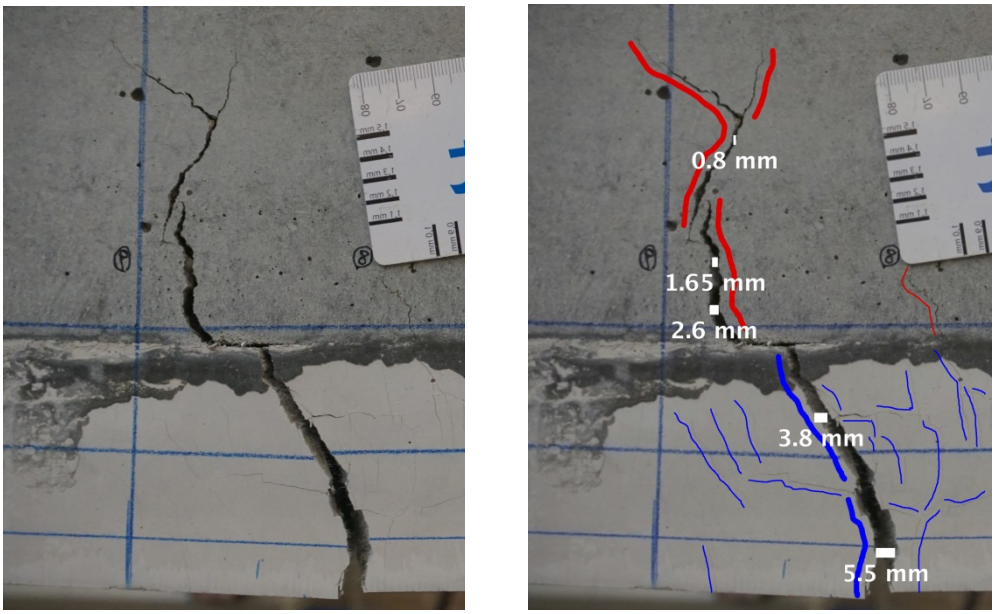

Figure 76 First localized crack, after failure, under the force of 40 kN from beam with SHCC+SH layer of 70 mm without labelled crack width (left) and with labelled crack width (right)

The analyzed images of the target area are shown below. The principle is the same as the first method used to compare LVDTs and DIC. Due to the inaccuracy at higher loads, the strain field based calculation was not performed.

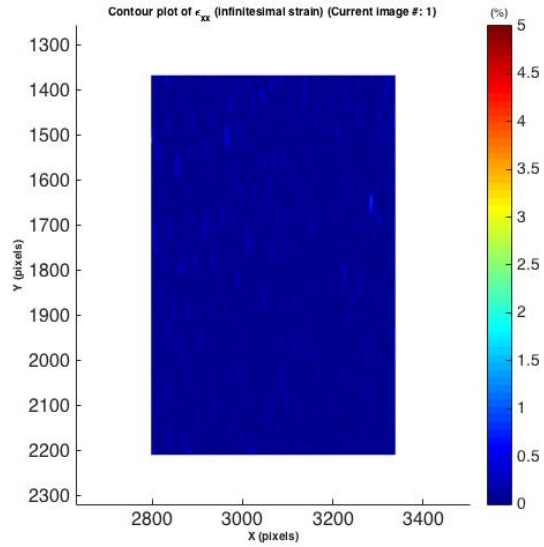

Figure 77 DIC image of the localized crack area from beam with SHCC+SH layer of 70 mm at 0 kN

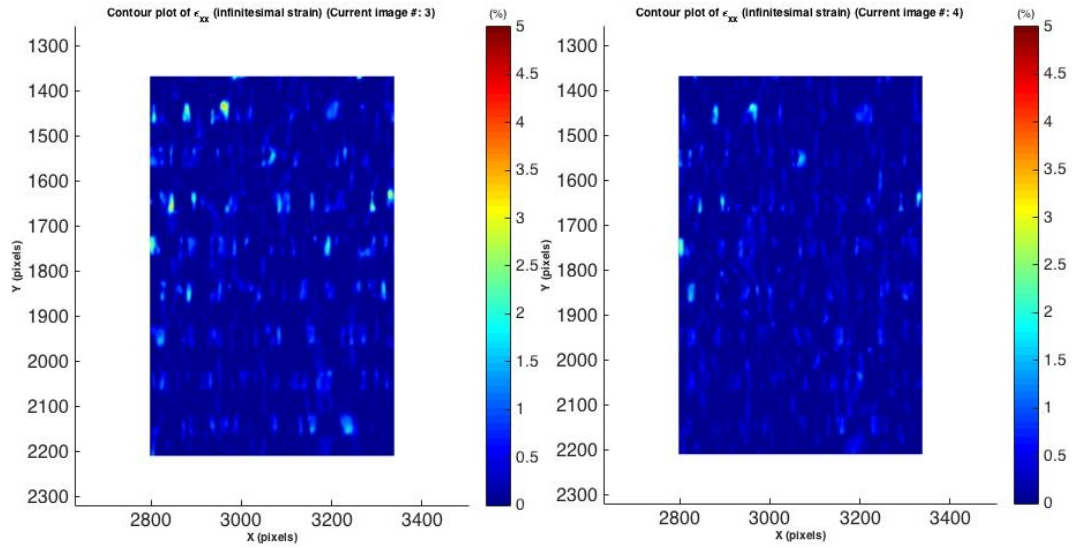

Figure 78 DIC image of the localized crack area from beam with SHCC+SH layer of 70 mm at 5 kN and 10 kN

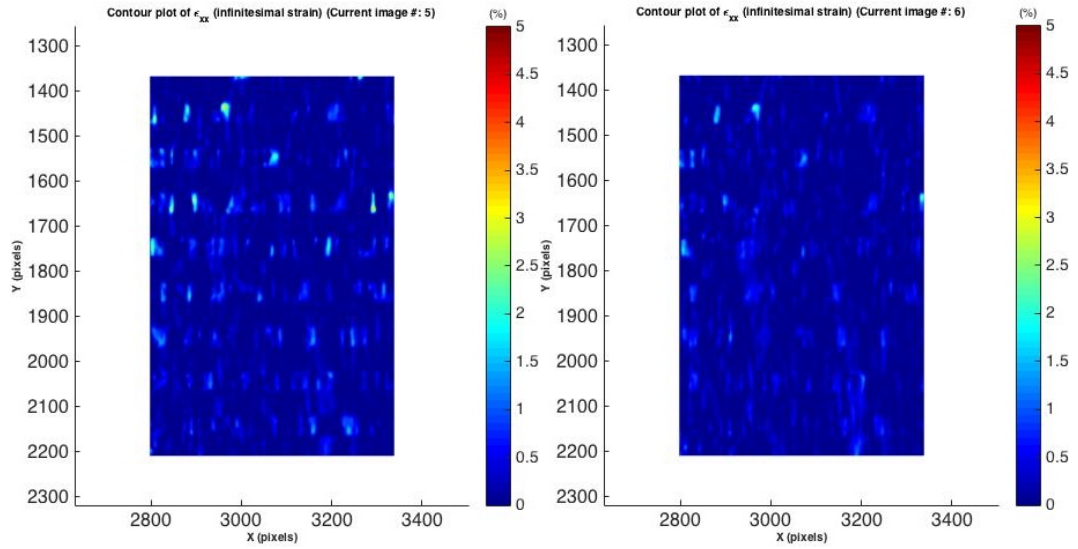

Figure 79 DIC image of the localized crack area from beam with SHCC+SH layer of 70 mm at 15 kN and 20 kN

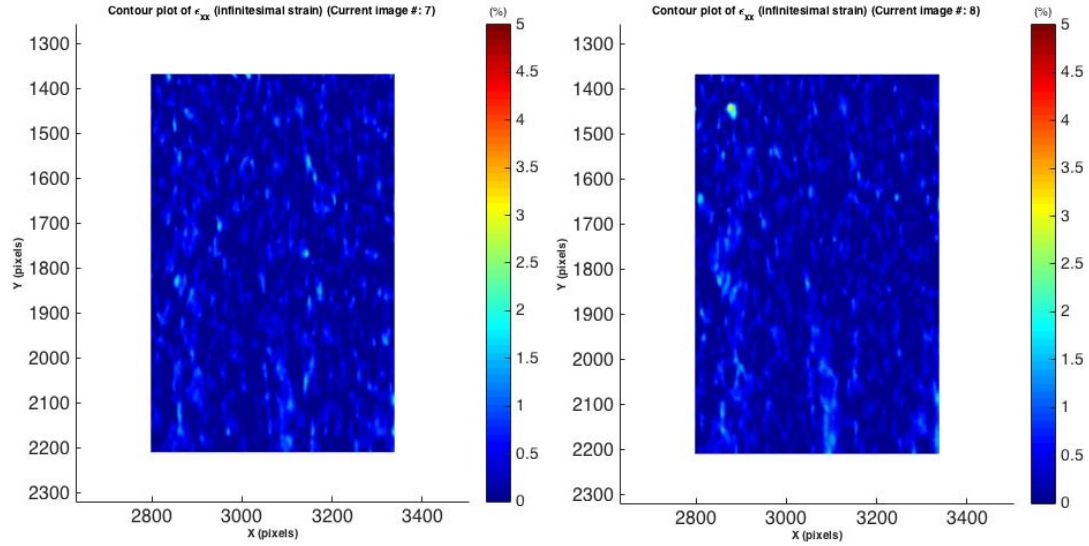

Figure 80 DIC image of the localized crack area from beam with SHCC+SH layer of 70 mm at 25 kN and 30 kN

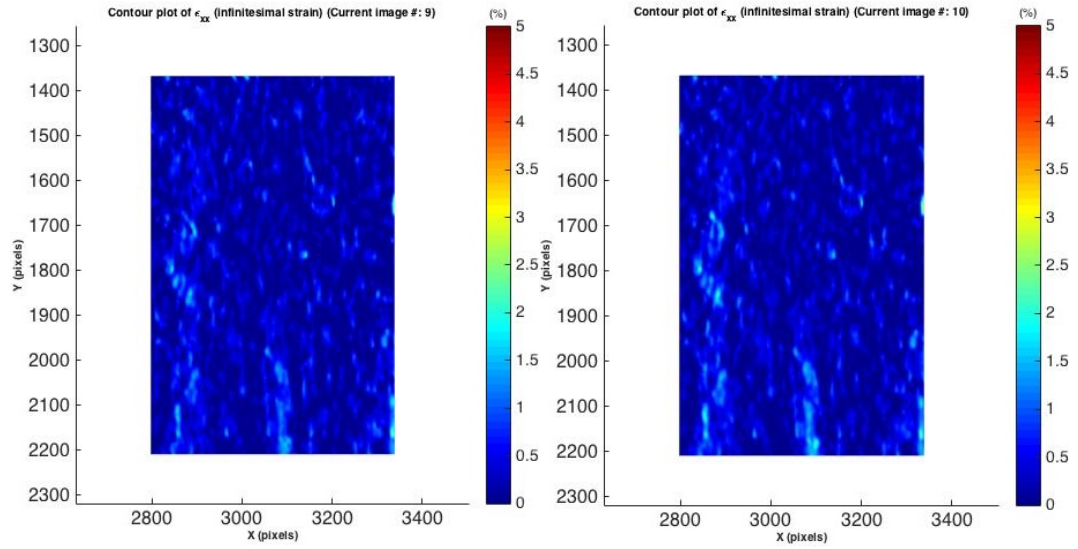

Figure 81 DIC image of the localized crack area from beam with SHCC+SH layer of 70 mm at 35 kN and 40 kN

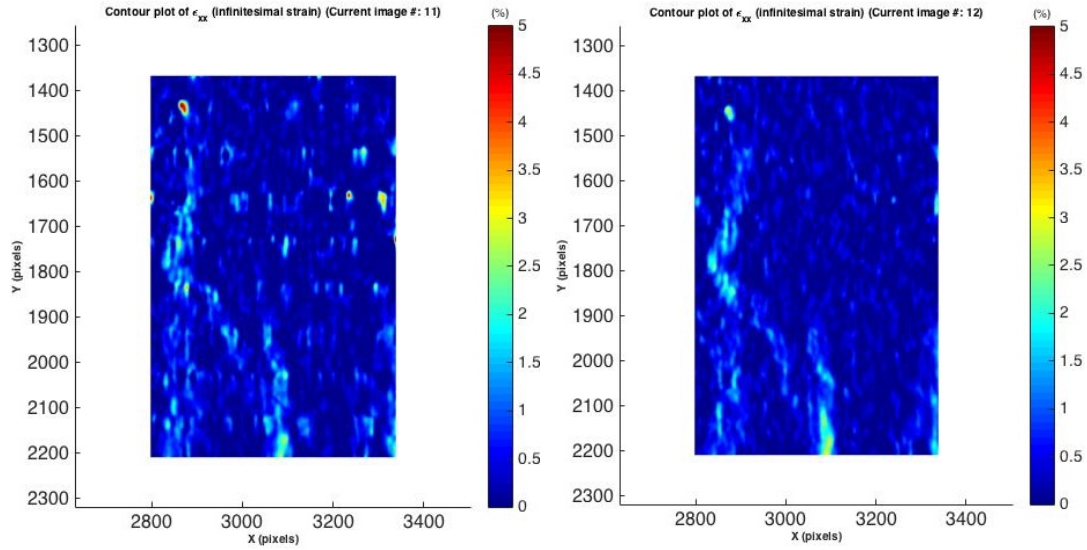

Figure 82 DIC image of the localized crack area from beam with SHCC+SH layer of 70 mm at 45 kN and 50 kN

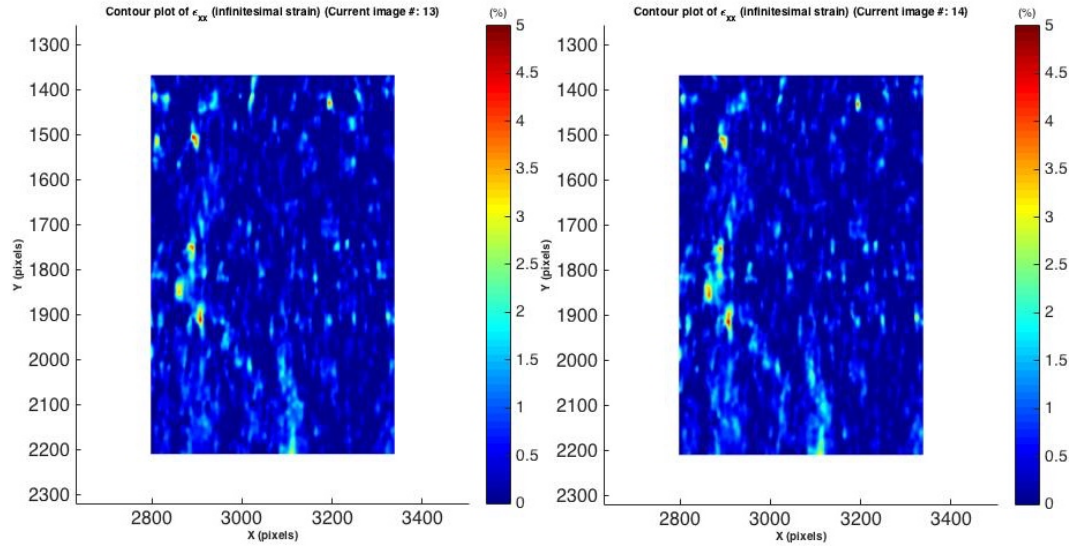

Figure 83 DIC image of the localized crack area from beam with SHCC+SH layer of 70 mm at 55 kN and 60 kN

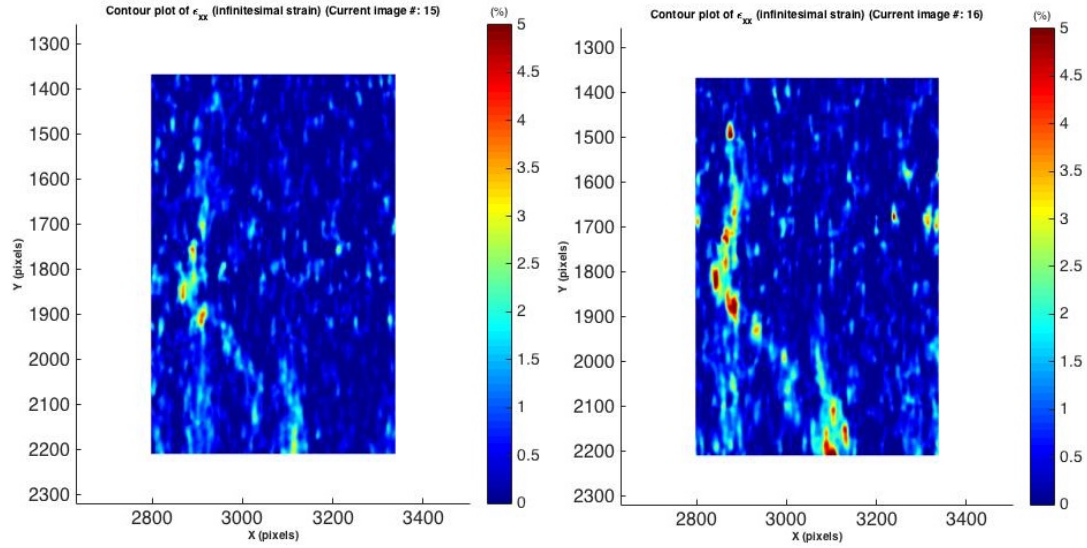

Figure 84 DIC image of the localized crack area from beam with SHCC+SH layer of 70 mm at 65 kN and 69 kN

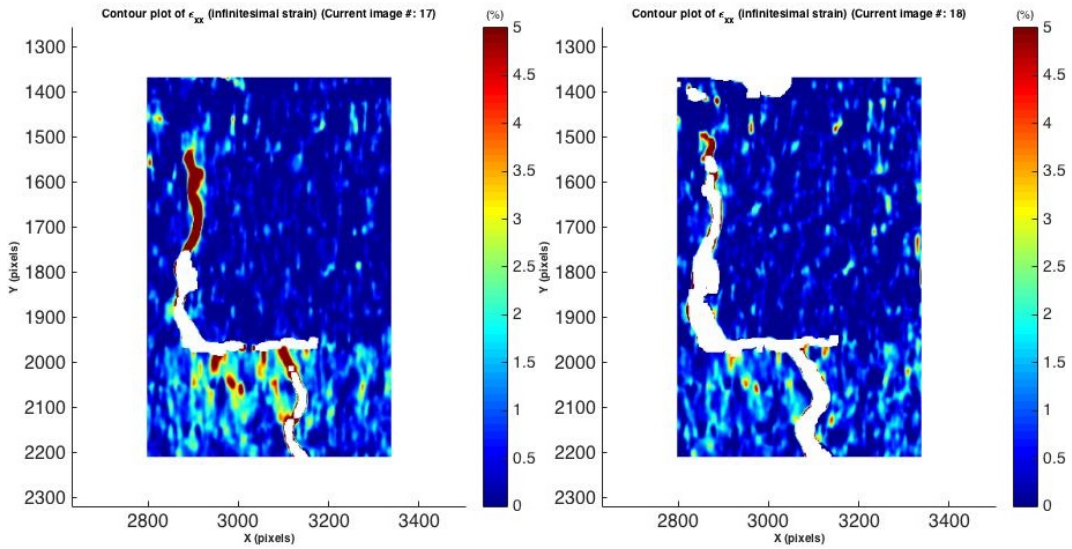

Figure 85 DIC image of the localized crack area from beam with SHCC+SH layer of 70 mm at 71 kN and 40 kN

The displacements of the two points at two sides of the crack will arise inaccuracy as the points are not exactly on the crack edges. Therefore, some elastic deformation is included in the crack width calculation. To see how much the elastic deformation affects the results, the distance between the two points is changed from original 90 pixels, to+10 pixels and +30 pixels (Figure 86).

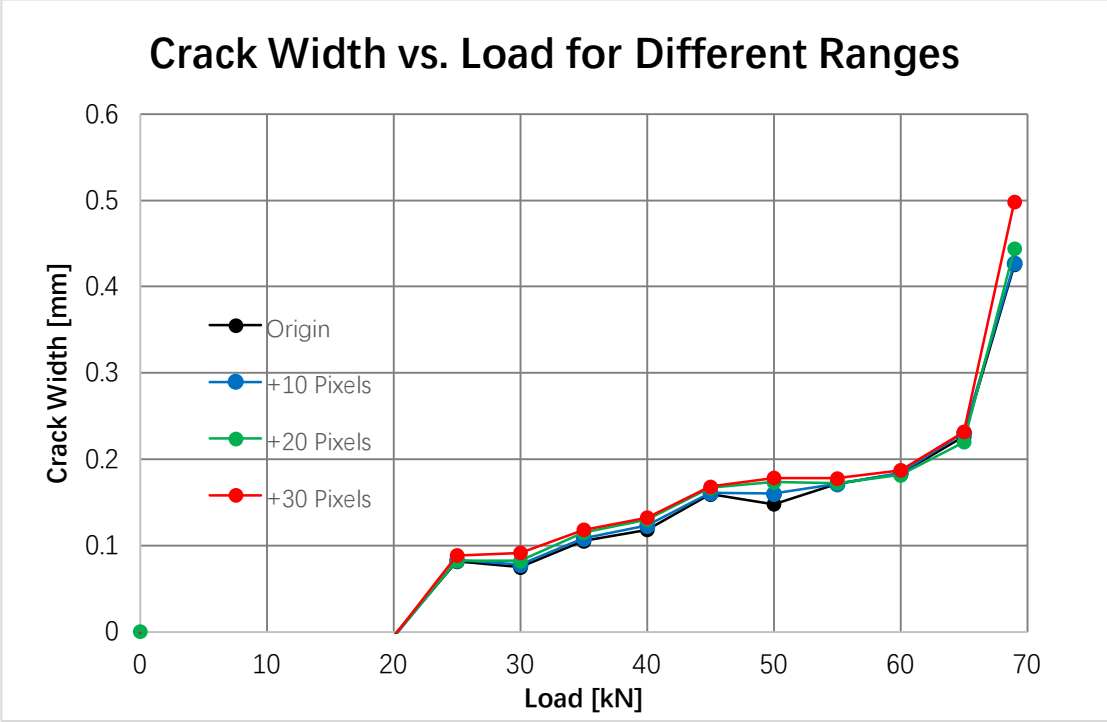

Figure 86 Crack width from different ranges and crack width differences

The differences between the crack widths drawn from different range are very small comparing with the crack width. That means when the range changes, only some elastic deformation is included. When load reaches 69 kN, the differences tend to increase. However, the elastic deformation does not affect the result, especially at low loads. When the load reaches higher level, the crack width is already beyond 0.3 mm, which is not the interest of the research.

4.4.1. Verification of DIC for crack width measurement (comparison with ImageJ)

In order to verify the results obtained by DIC, photos were also taken from the bottom side of the beam during the experiment, and the crack widths was measured by ImageJ at different load levels. The pictorial and quantitative comparisons between the photos measured by ImageJ and DIC are shown below in Table 11.

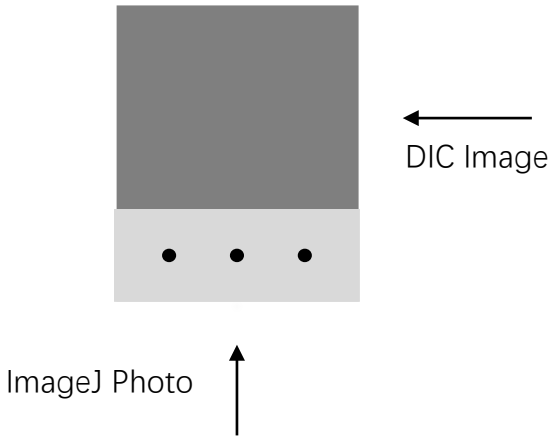

Table 11 Pictorial comparison between photos measured by ImageJ and DIC Images

Load	DIC Images	Photos Measured by ImageJ
0 kN	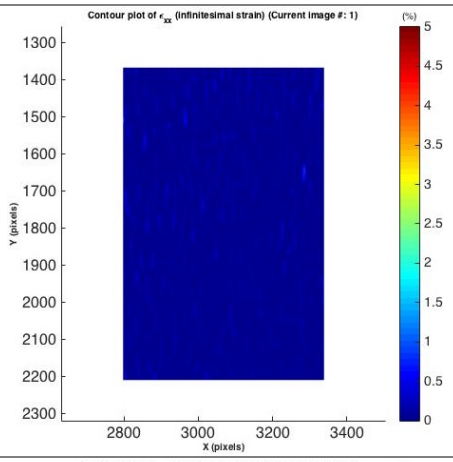	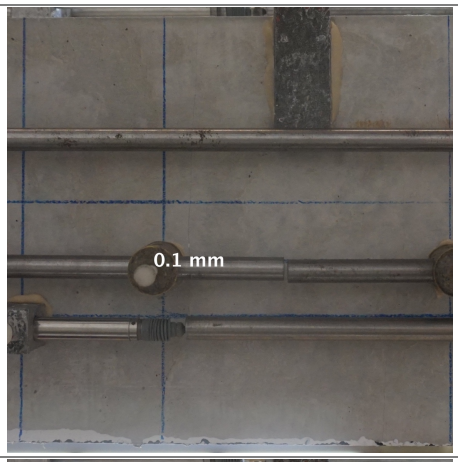
50 kN	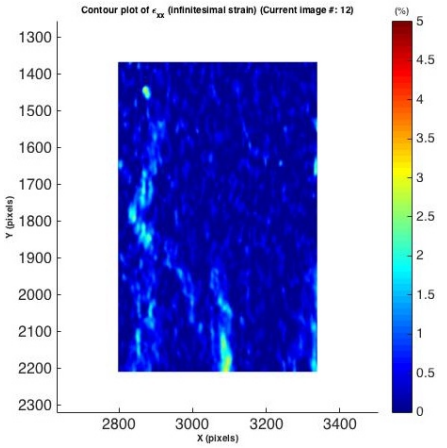	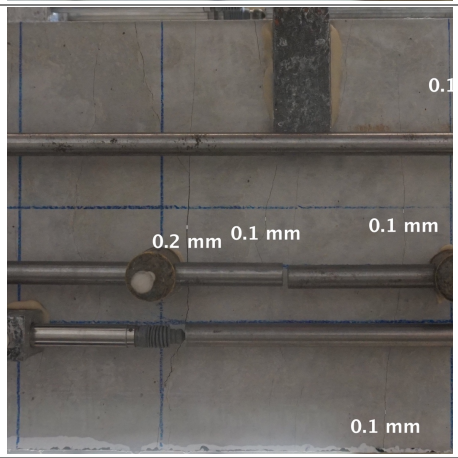
69 kN	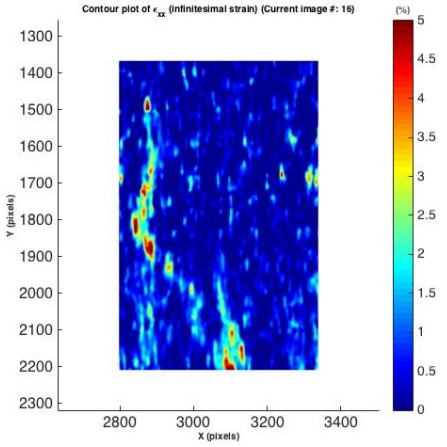	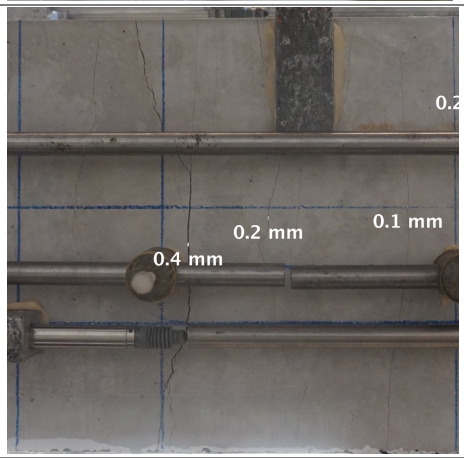

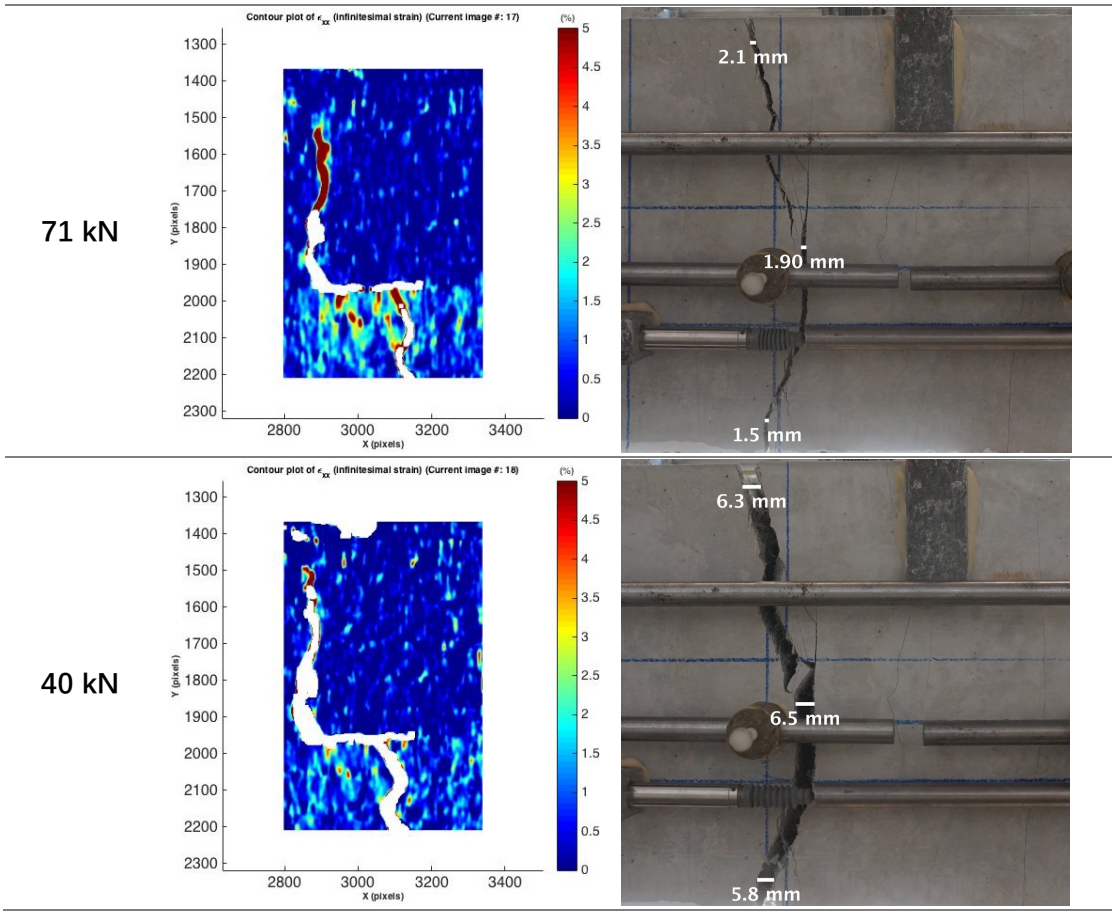

The numerical comparison of crack width form DIC and ImageJ is shown below in Figure 87, Figure 88 and Figure 89.

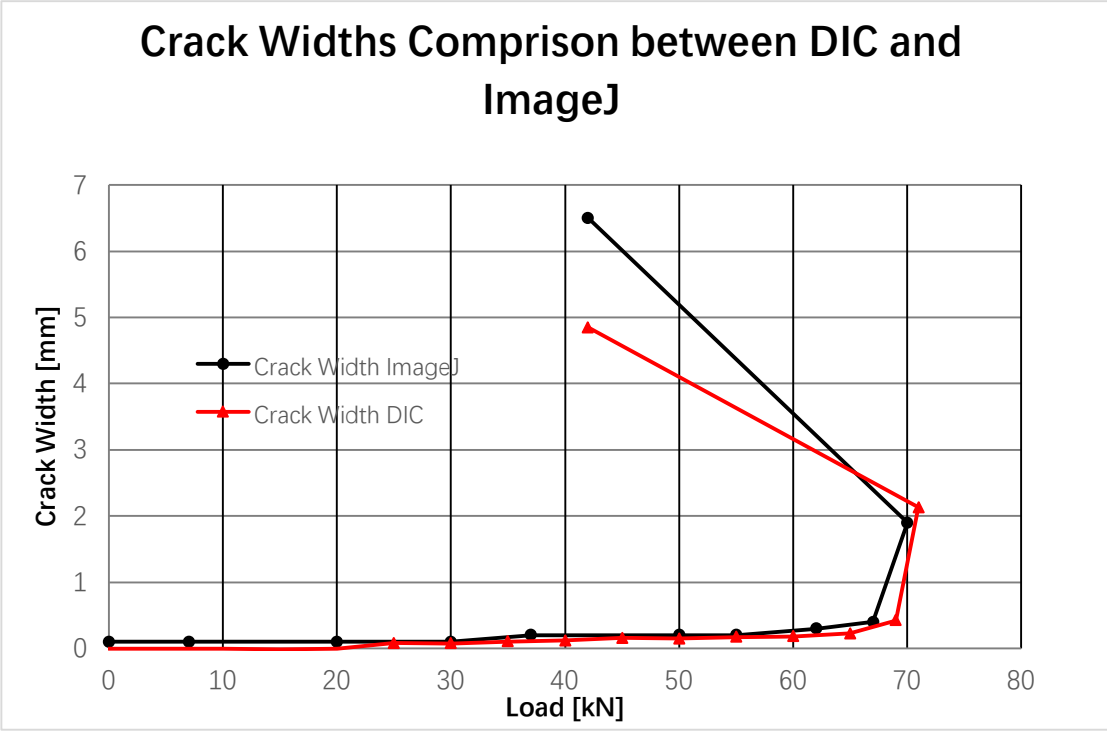

Figure 87 Comparison between crack width measured by DIC and that measured by ImageJ

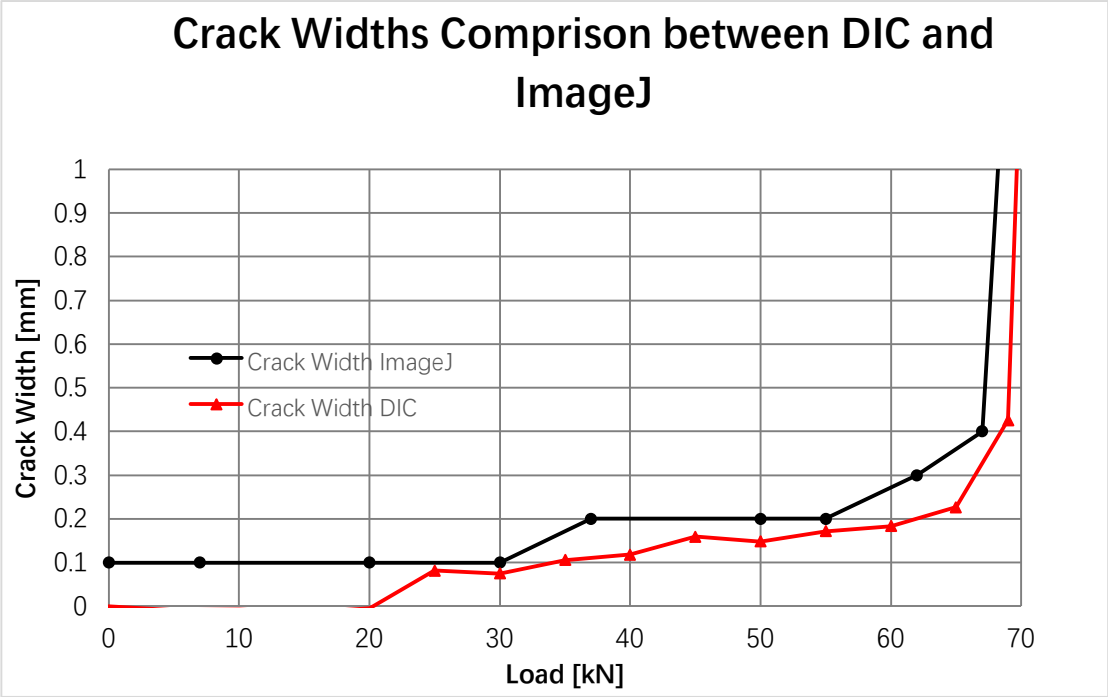

Figure 88 Comparison between crack width measured by DIC and that measured by ImageJ (crack width up to 1 mm)

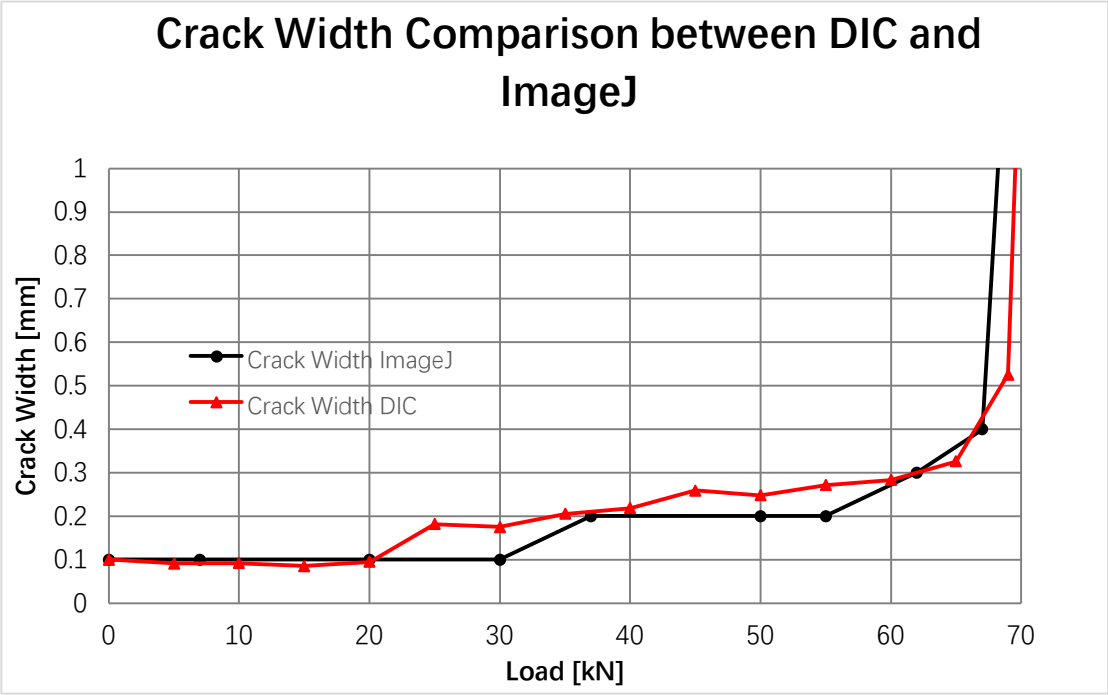

Figure 89 Comparison between crack width measured by DIC and that measured by ImageJ (DIC crack width is shifted 0.1 mm for initial shrinkage crack) (crack width up to 1 mm)

The crack width measured by ImageJ for Test 04 at low loads already existed before starting the test and increasing the load. They were constant and with the crack width of

0.1mm. That is due to the shrinkage induced crack (Which will be discussed in more details in the later chapter). This, however, cannot be captured by DIC, since only the photos during the loading were taken. In Figure 89, the crack width measured by DIC is shifted up for 0.1 mm. he maximum difference between the crack width evaluated by DIC and that of ImageJ is always smaller than 0.1mm under the same load. That means the crack width measured by DIC is reliable.

4.5. Maximum crack width for RC beams

For RC beams, it was observed that not only one crack opened at the final stage. All the cracks will open quite simultaneously. Therefore, the biggest crack cannot be found easily by observing the development of cracks on the DIC images. Take Test 06 for instance where the conventional reinforced beam, with concrete cover of 31 mm was tested:

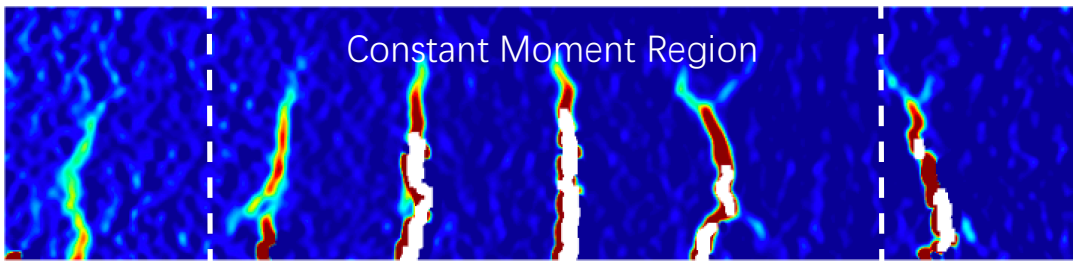

Figure 90 DIC image of Test 06 (RC beam with 31 mm cover) under 60 kN

There are four cracks in the constant moment region (Figure 90). To find which crack localized first, all four cracks were analyzed.

0.3 mm is considered as the critical crack width. In Figure 91, Crack No. 3 first reached the critical crack width. Therefore, Crack No. 3 in Test 04 is used to compare with the results of corresponding beams with the SHCC layer.

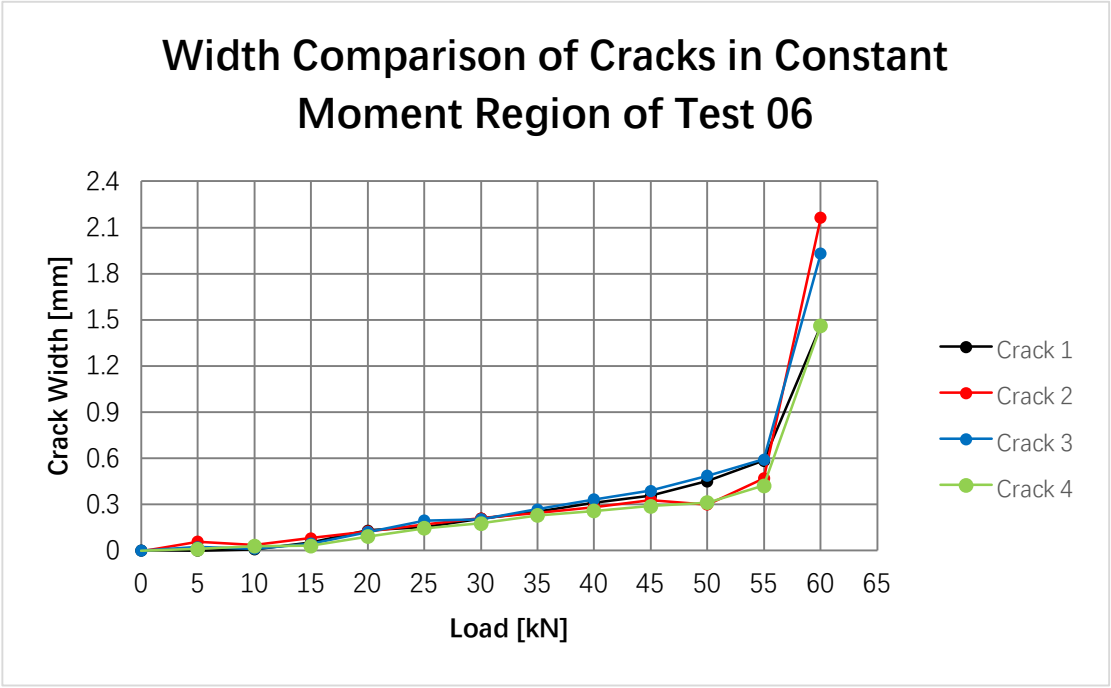

Figure 91 Crack Widths of the four cracks in the constant moment region zone for Test 06 (RC beam with 31 mm cover)

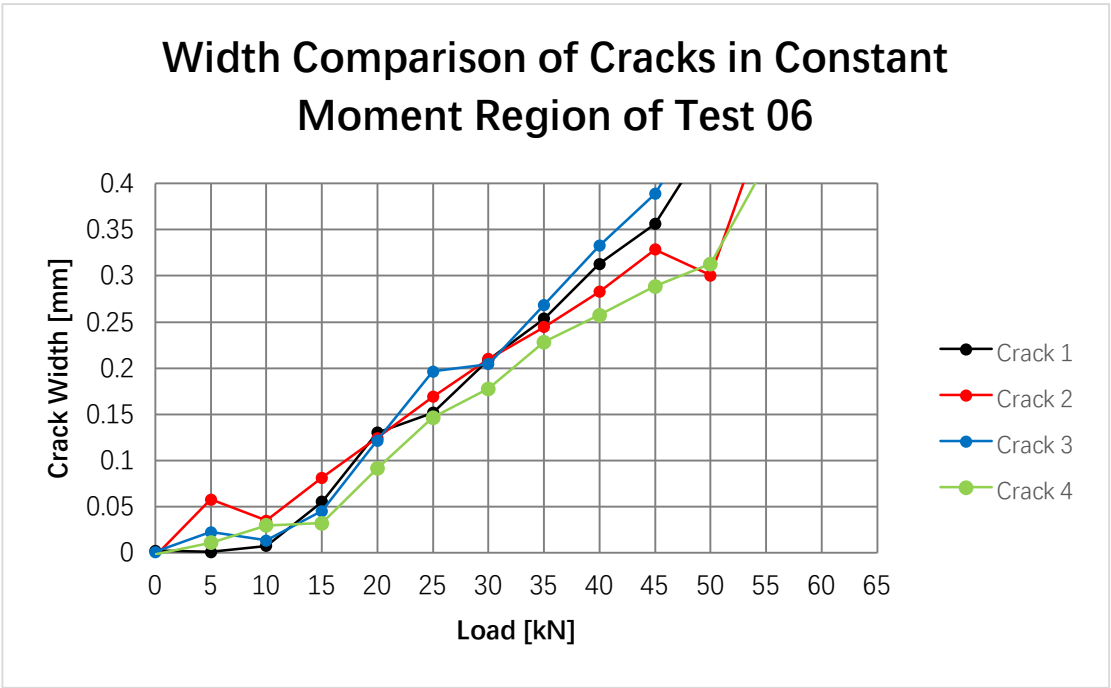

Figure 92 Crack Widths of the four cracks in the constant moment region zone for Test 06 (RC beam with 31 mm cover) (crack width up to 0.4 mm)

4.6. Load vs. Deflection vs. Max. Crack Width

In the following two graphs, Load-Deflection curve and Crack-Deflection curve are presented together for better comparison between three variables: load, deflection and maximum crack width. The first graph (Figure 93) shows the results from the comparison of RC beam with concrete 31 mm and SHCC beam with SHCC layer of 70 mm. And the second graph (Figure 94) shows the results from the comparison of RC beam with concrete 11 mm and SHCC beam with SHCC layer of 30 mm.

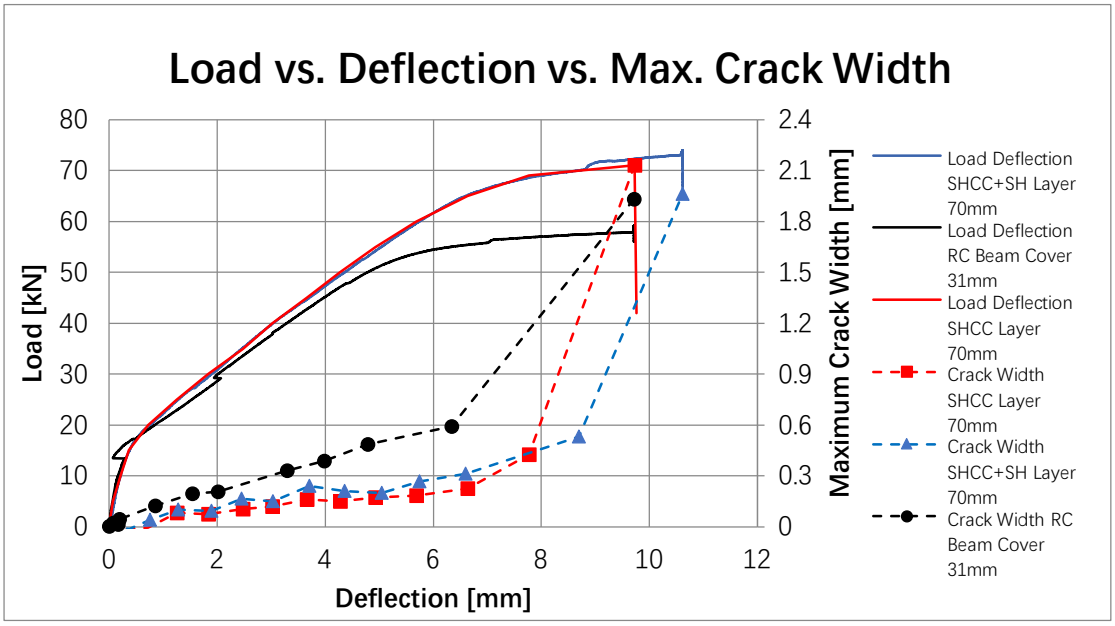

Figure 93 Load-Deflection and Crack-Deflection curves of beams with 70 mm SHCC layer and RC beam with 31 mm cover

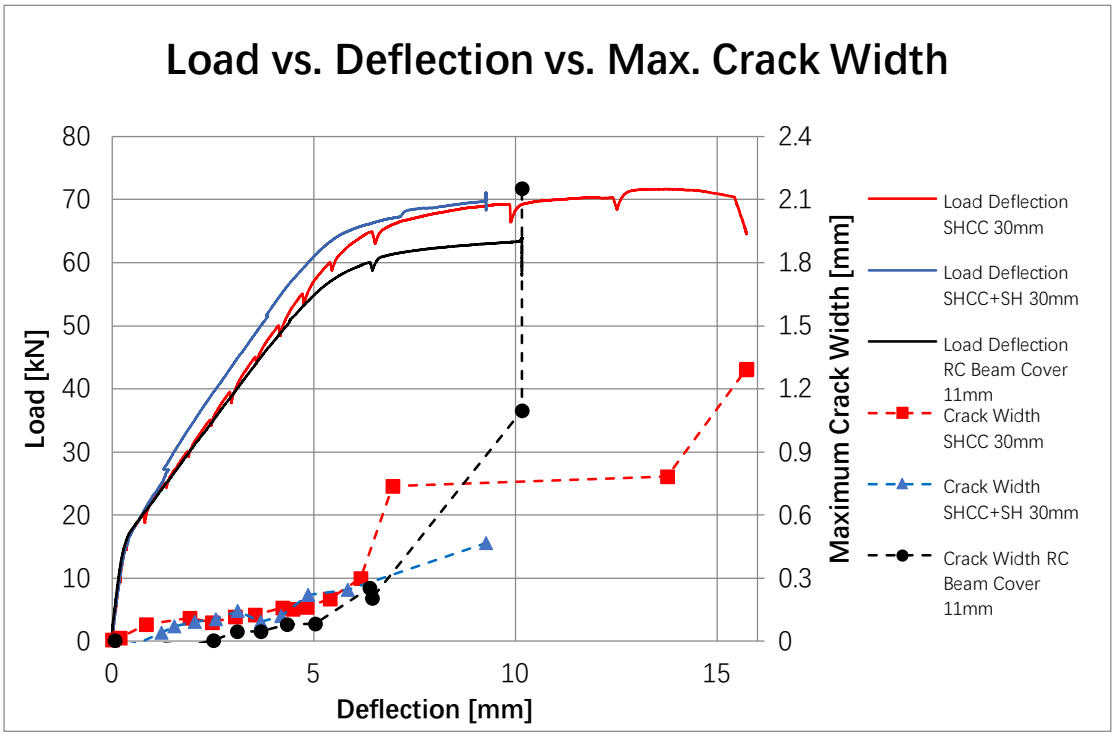

Figure 94 Load-Deflection and Crack-Deflection curves of beams with 30 mm SHCC layer and RC beam with 11 mm cover

4.7. Crack pattern

The procedure for acquiring photos and evaluating crack patterns is shown below. The side images were taken from one side of the beam and photos for DIC were taken from the other side of the beam. Bottom images were taken from downside. Together, they form the crack patterns.

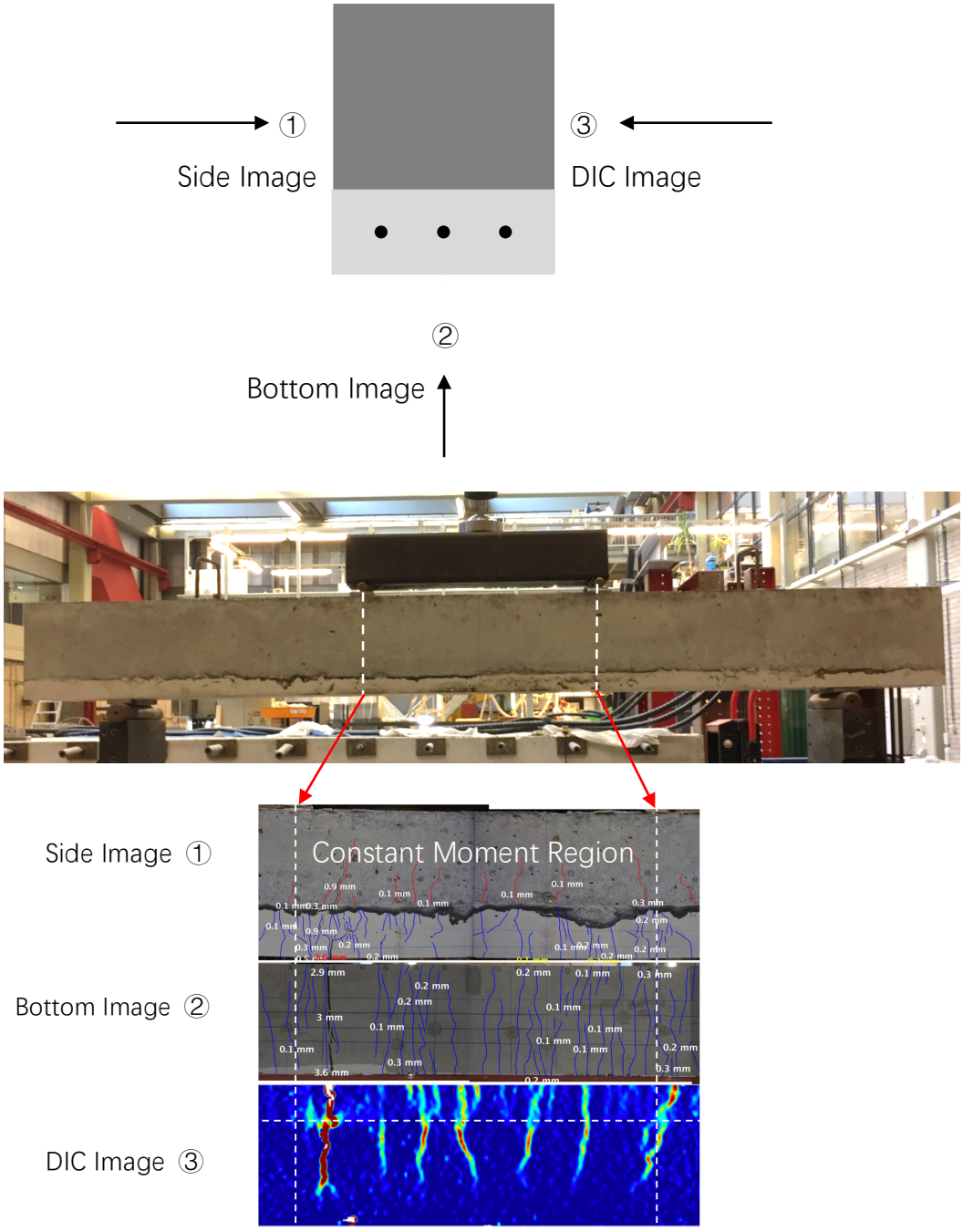

Figure 95 Conceptual drawing of the procedure of crack patterns

For all tested beams, crack patterns and crack width distributions are given below.

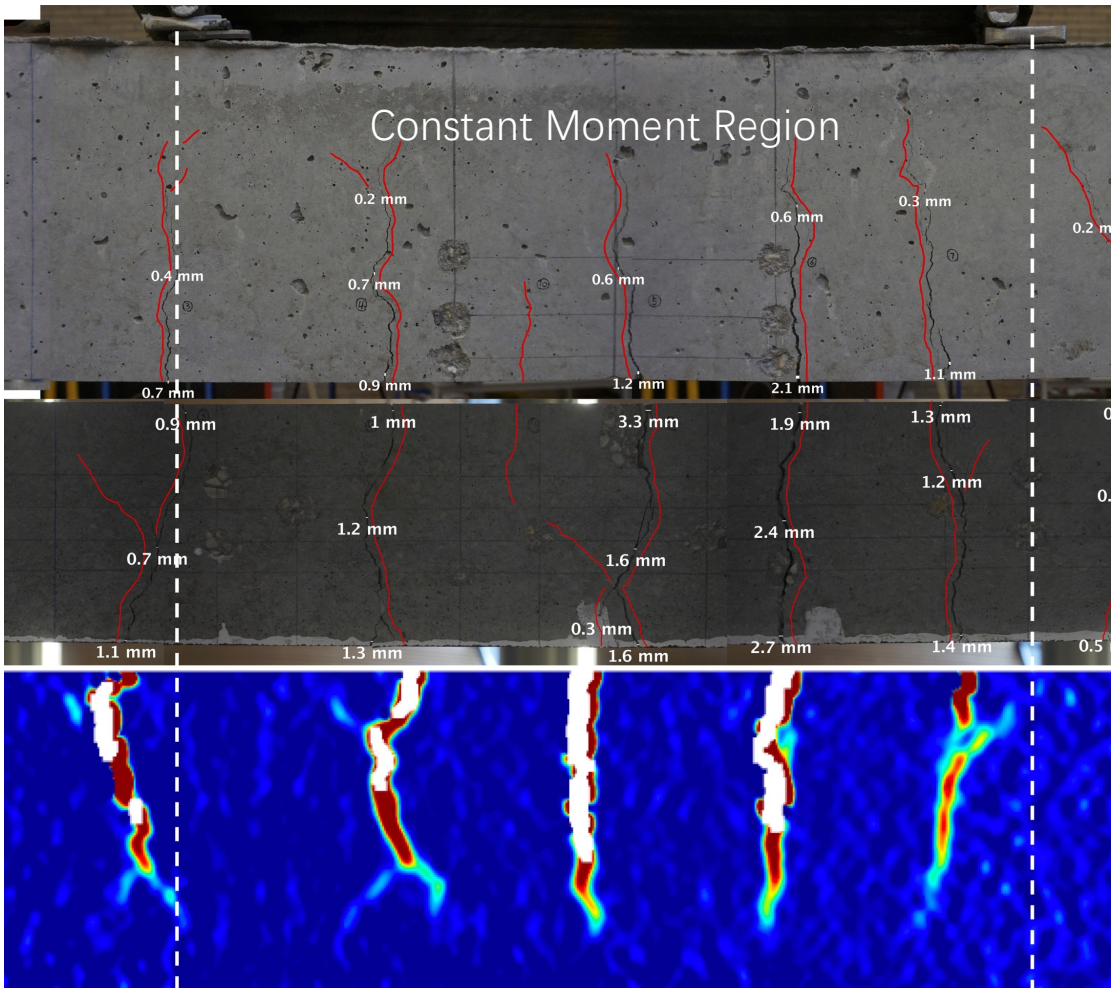

Figure 96 Crack pattern of Test 06 (RC beam with cover of 31 mm)

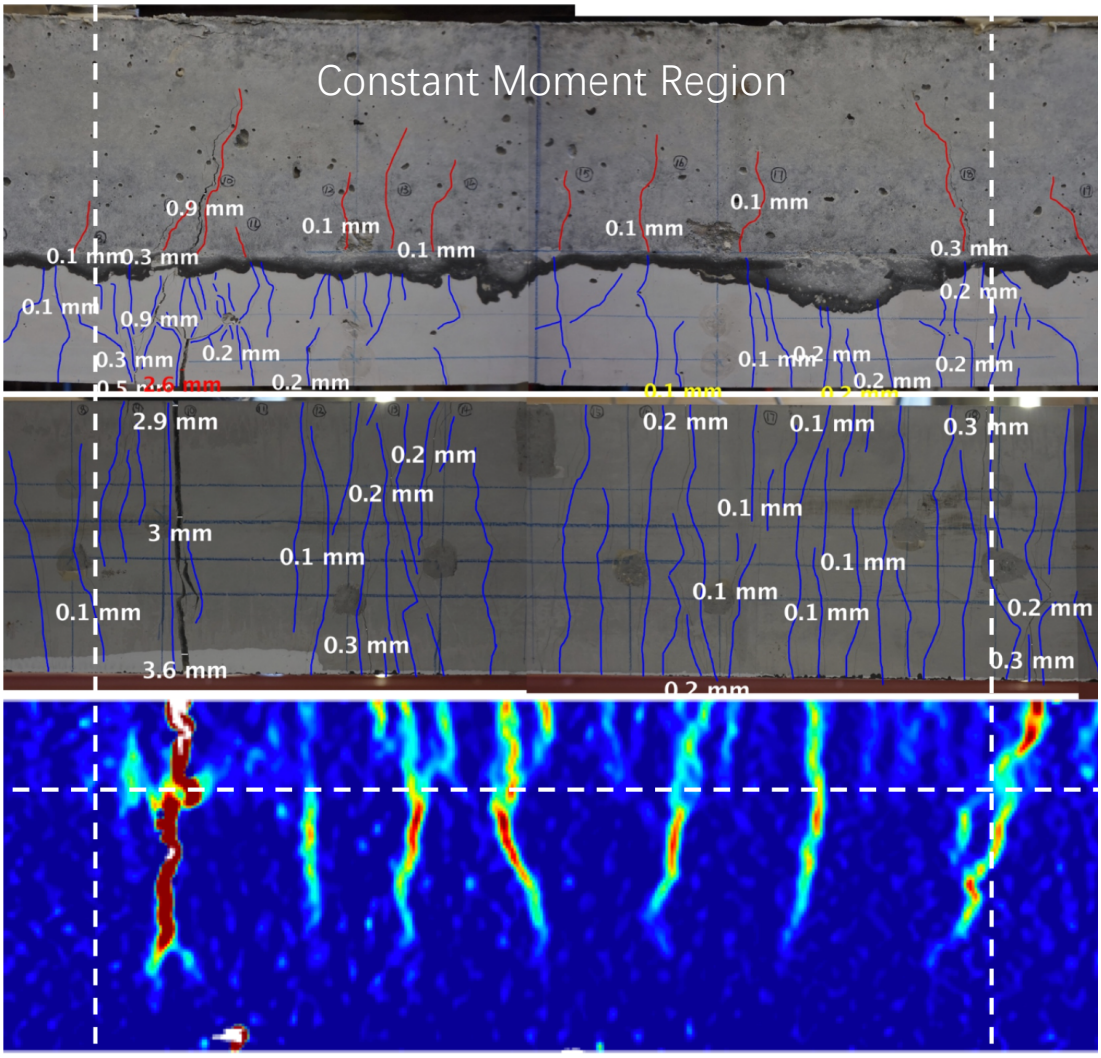

Figure 97 Crack pattern of Test 03 (beam with SHCC layer of 70 mm)

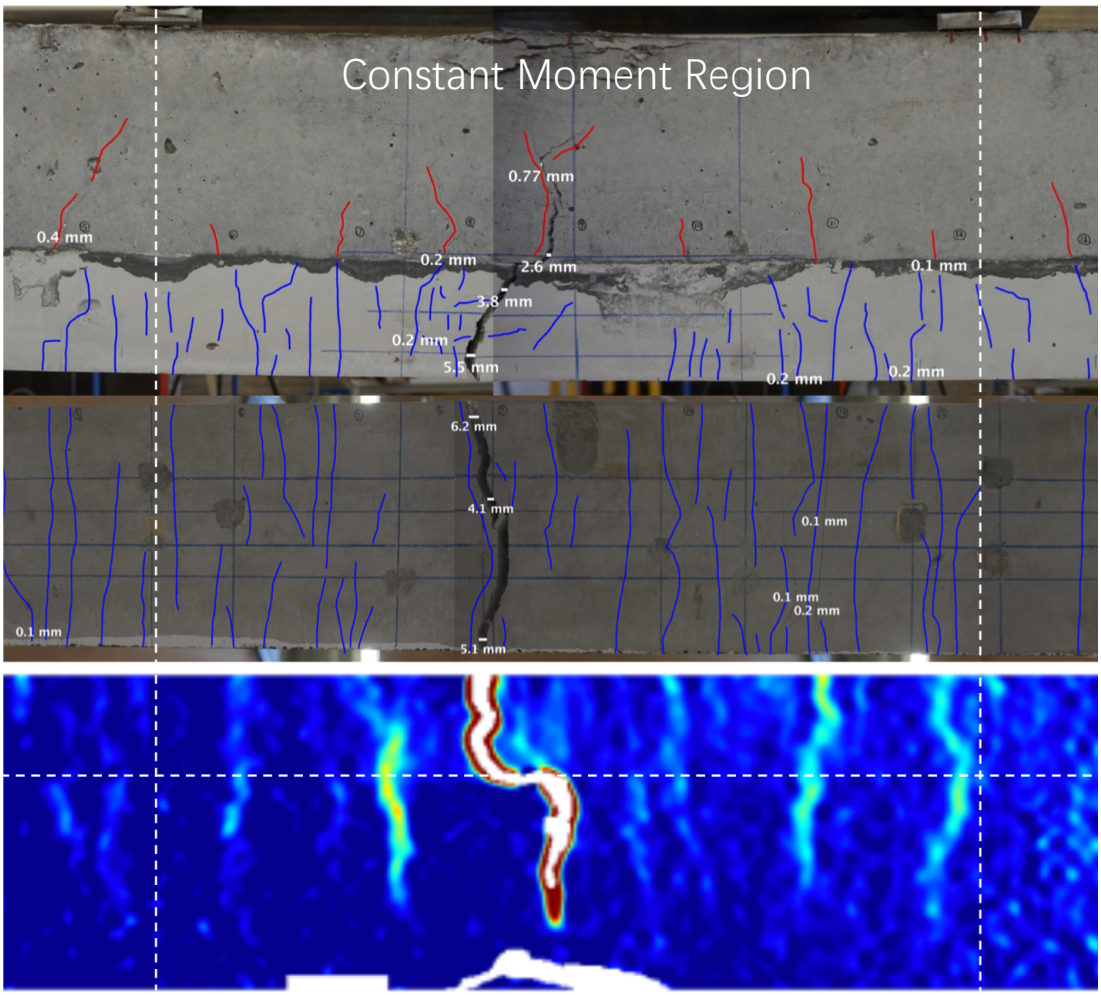

Figure 98 Crack pattern of Test 04 (beam with SHCC+SH layer of 70 mm)

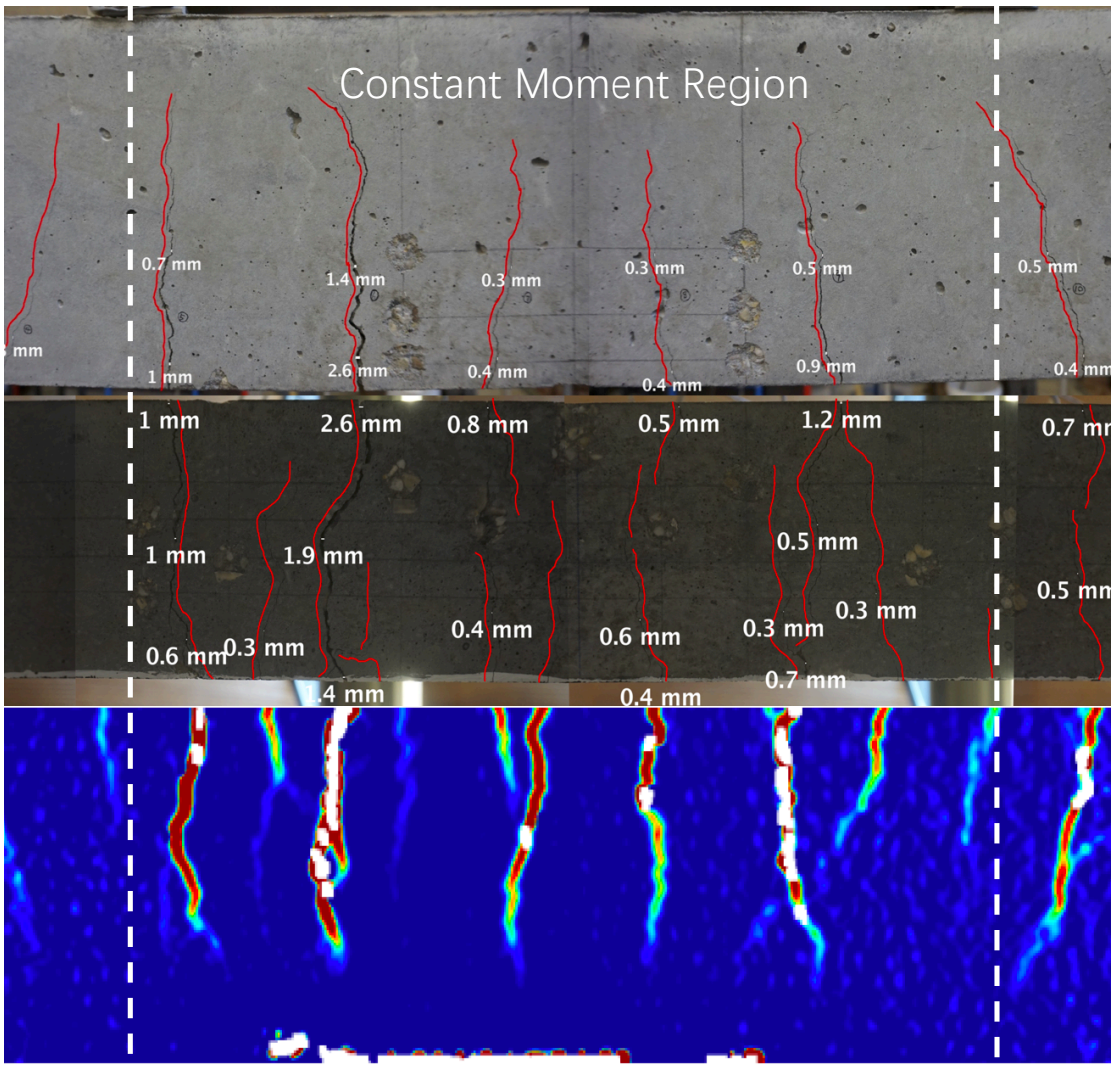

Figure 99 Crack pattern of Test 02 (RC beam with cover of 11 mm)

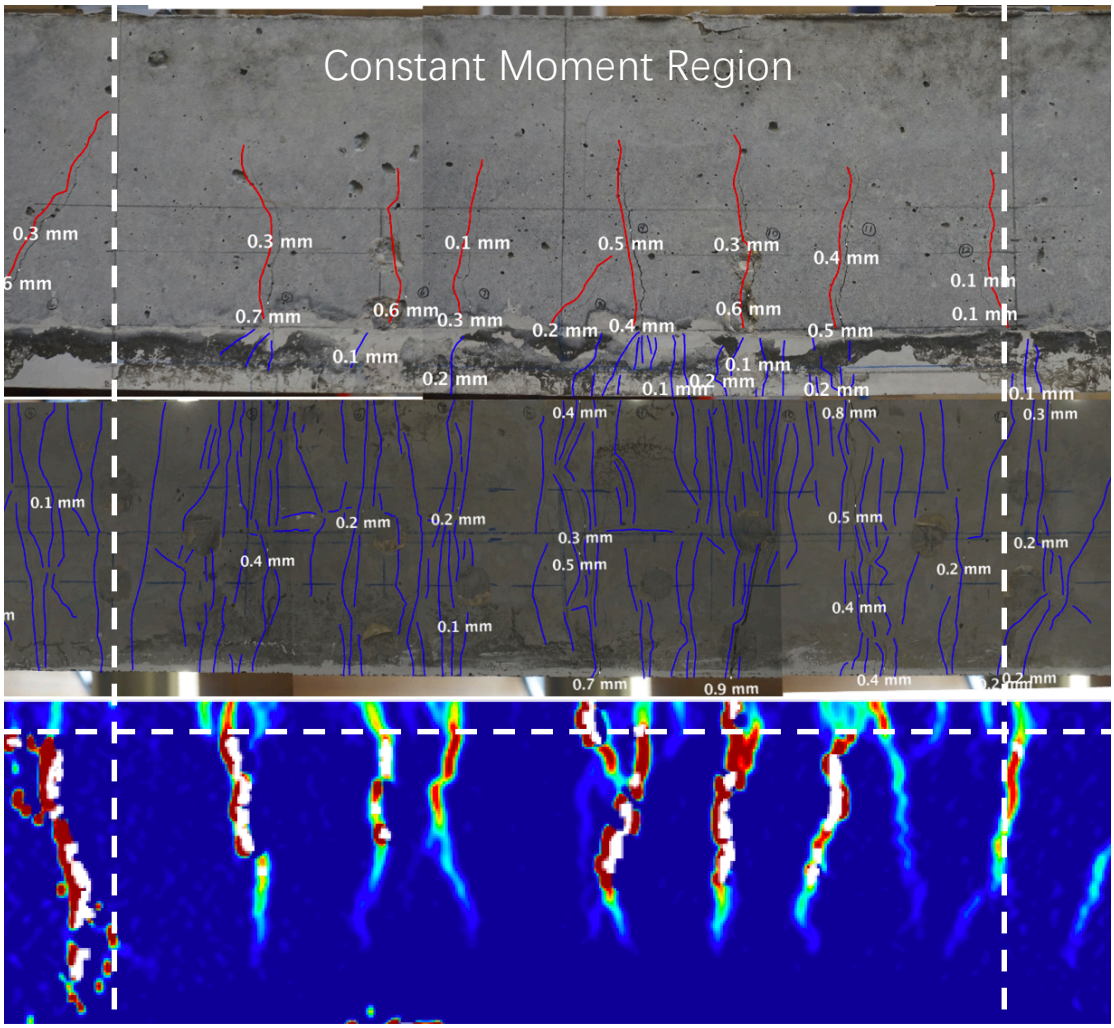

Figure 100 Crack pattern of Test 01 (beam with SHCC+SH layer of 30 mm)

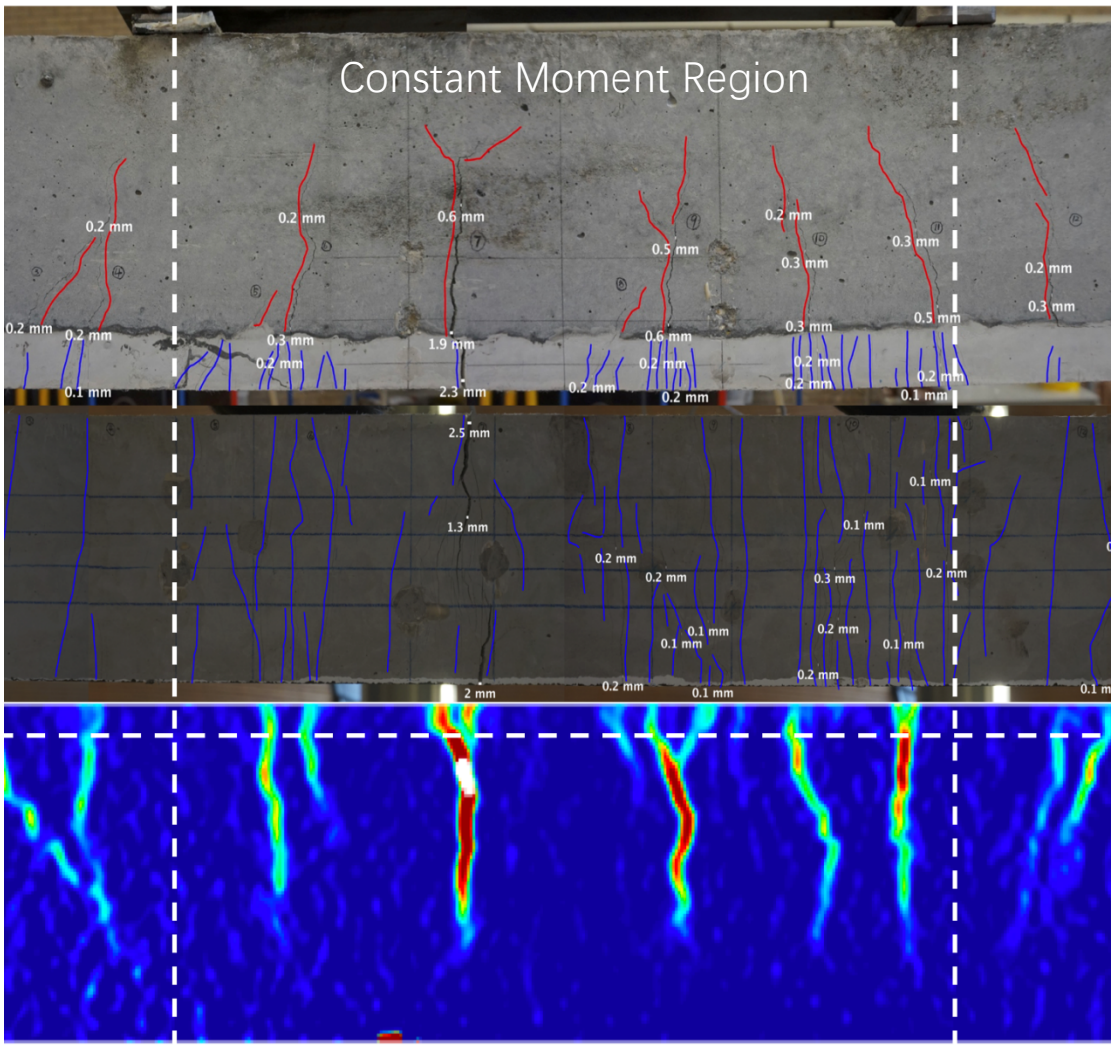

Figure 101 Crack pattern of Test 05 (beam with SHCC layer of 30 mm)

4.7.1. Calculation of the maximum crack spacing

According to the Eurocode 2, the crack spacing for two RC beams are calculated below and compared to the experimental measurements. The experimental crack spacings for all beams were measured from the crack pattern by ImageJ (Table 12). More detailed can be found in Appendix I.

$$s_{r,max} = 3.4c + 0.425k_1k_2\frac{\emptyset}{\rho_{p,eff}}$$

Where:

c is nominal cover,

$k_1 = 0.8$

$k_2 = 1.0$ for tension (e.g. from restraint)

$= 0.5$ for bending

The mean crack spacing is calculated as:

$s_{r,mean} = 1.5 * l_t$

Where l_t is the transfer length, $l_t = \frac{f_{ctm}}{\rho}(1 + \alpha_e \rho)$

For RC beam with cover 11 mm,

$s_{r,max} = 88.15\ mm$

$s_{r,mean} = 55.95\ mm$

For RC beam with cover 31 mm,

$s_{r,max} = 223.76\ mm$

$s_{r,mean} = 130.55\ mm$

Table 12 Experimental and theoretical mean and maximum crack spacing

Label of Beams		Mean Crack Spacing [mm]	Maximum Crack Spacing [mm]
RC 11mm	Experimental	94.151	107.601
	Theoretical	55.95	88.15
SHCC 30 mm	Experimental	82.418	98.095
	Theoretical	/	/
SHCC+SH 30 mm	Experimental	63.59	136.406
	Theoretical	/	/
RC 31mm	Experimental	116.294	149.739
	Theoretical	130.55	223.76
SHCC 70 mm	Experimental	57.972	102.362
	Theoretical	/	/
SHCC+SH 70 mm	Experimental	69.309	78.388
	Theoretical	/	/

The experimentally measured crack spacing of RC beam with cover 31 mm is consistent with the theoretically calculated value. While the experimentally measured crack spacing of RC beam with cover 11 mm is smaller than the theoretically calculated value. The

calculation is based on the equation given in Eurocode 2. However, 11 mm concrete cover is not normative in Eurocode 2. Therefore, the equation used above might not be applicable for the RC beam with cover 11 mm, which leads to the deviation.

5

Discussions

5.1. Comparison between beams with SHCC layer and RC beams

The load carrying capacity of the beams with SHCC layer of 70 mm are larger (72 kN for SHCC and 74 kN for SHCC+SH) than that of the RC beam with cover 31 mm (58 kN) (Figure 93). The difference of the capacity can be attributed the tensile resistance of SHCC, which was also shown by numerical calculation in chapter 4.2. Additionally, according to the cube compression tests of SHCC and SHCC containing self-healing agents, the self-healing agents have no influence on the mechanical properties of SHCC. However, this was not the main aim of this study as the beams presented do not have realistic heights. With higher beams, the contribution of 70 mm thick SHCC layer on the flexural capacity would be significantly reduced. The main aim of this study was to investigate if crack widths could be controlled by adding a SHCC layer in the tension zone of the reinforced concrete beam.

In Eurocode, for quasi-permanent load combination, the recommended maximum crack width is 0.3 mm (see Table 1). Therefore, we hereby take 0.3 mm as critical crack width. For RC beam with 31 mm cover, its maximum crack width exceeds 0.3 mm when load reaches 35 kN, which is about 60% of the capacity (Figure 93). For beams with 70 mm SHCC layer, the crack widths exceed 0.3 mm at 66 kN (SHCC) and 62 kN (SHCC+SH), which are 92% and 83% respectively of their capacities (Figure 93). That shows that beams with 70 mm SHCC layer have a better crack control behavior, which allows the beams to

utilize 32% and 23% of the capacity additionally. In other words, there is no need to add the additional reinforcement to control crack widths.

The crack pattern of the RC beam with 31 mm cover is normative. Five cracks occurred in the constant moment region. And the crack widths are at the same magnitude (Figure 96). The crack patterns of the beams with SHCC layer of 70 mm are different (Figure 97 Figure 98). From the bottom, many small cracks were generated with one large crack which localized at high load. From the side, more cracks were observed on the concrete part with smaller crack spacing, comparing to the RC beam. When one crack reaches SHCC layer, it was smeared into several small cracks. That also proves the crack control ability of the thick SHCC layer.

If the beams with SHCC layer of 30 mm and the RC beam with cover 11 mm are compared, the maximum load carrying capacity of the beams with SHCC layer of 30 mm are 72 kN for SHCC and 71 kN for SHCC+SH, respectively and the maximum load of the RC beam with cover 11 mm is 64 kN (Figure 94). The differences on the ultimate capacity and the stiffness of this comparison group are smaller than that between SHCC layer of 70 mm and the RC beam with cover 31 mm. The small differences are due to reduction on the cross-sectional area of SHCC. That also shows that SHCC does contribute to the ultimate capacity of the beams, as also confirmed by theoretical calculations.

For the beams with SHCC layer of 30 mm, the maximum crack width exceeds 0.3 mm at 93% of their capacities (at 66 kN and 67 kN load), whereas the maximum crack width of the RC beam with cover 11 mm reaches that crack width at 95% of its capacity (at 61 kN load) (Figure 94).

The smearing behavior was also observed on the beams with SHCC layer of 30 mm. However, the number of cracks on concrete layer is the same comparing with the RC beam with cover 11 mm.

The comparisons show that applying SHCC in the beam tension can increase the capacity of the beam. And with 70 mm SHCC layer, the maximum crack width is successfully controlled, while with 30 mm SHCC layer, there is no evidence of crack control behavior.

5.2. Delamination between two layers

The beams with SHCC layer is not a monolithic beam. It is a composite beam which consist of two parts, the SHCC layer and the conventional concrete cast on top of it. The two parts are bonded together by friction and hydration product of the cement. In general, one may think the better the bond is, the stronger the element will be. Because the bond can increase the structural integrity. Whereas, it might not be the case for SHCC system. Lukovic (2016) compared the crack pattern in SHCC when it is applied as repair material on smooth surface and grooved surface old concrete.

The specimen in Figure 102 (left) has a smooth surface which has larger debonding length. After the one crack in concrete reaches the interface, due to low bond strength, the interface breaks. The strain will be allocated along the debonding length. Thus, the crack can be more uniformly distributed. In the case of grooved surface (Figure 102 (right)), due to the high bonding strength, the debonding length is short, which can be attributed to the grooves. The strain is concentrated around the short debonding length. The cracks in SHCC is developed more intensively, which is less favorable comparing to smooth surface.

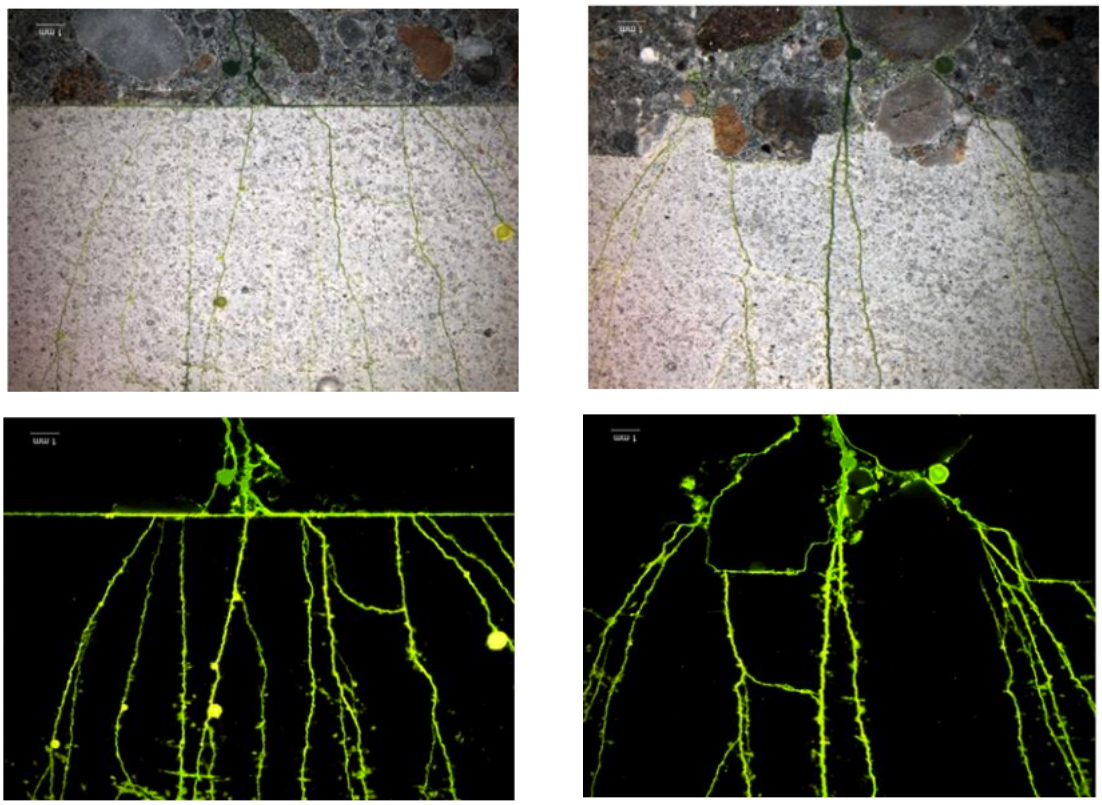

Figure 102 Crack patterns of specimens with smooth interface (left) and with grooved interface (right) (Lukovic, 2016)

Therefore, low bonding stress between two layers is more favorable, which allows delamination to develop. However, if the stress is too low, the delamination may develop too early. The structural integrity may be impaired, which will affect the stiffness and capacity of the structure.

Not only the delamination will influence the distribution of the crack between two layers, the fiber content will also influence that. Abdel Zaher et al. (2008) reported that when applying UHP-SHCC as repair material on cracked concrete substrate, by increasing the fiber volume content in UHP-SHCC, more cracks were found the on the UHP-SHCC layer. That means the cracked is more distributed.

Delamination was also found in this research. In Test 04, for the beam with SHCC layer of 70 mm, the delamination was formed around the failure load (71 kN). That means the bonding strength is high enough, which prevents the delamination from developing when load is lower than 70 kN. Before the developing of the delamination (Figure 103 (a)), there is trend to form a traverse crack, which links the crack in concrete and the crack in SHCC. However, after the developing of the delamination, the strain was

released. And near the end of the debonding length, one crack in SHCC layer localized (Figure 103 (b) & (c)).

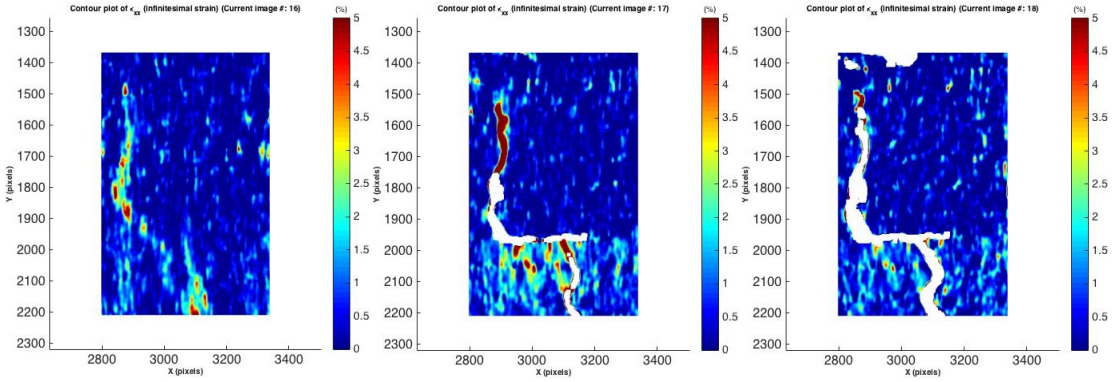

(a) (b) (c)

Figure 103 DIC image of Test 04 (beam with SHCC layer of 70 mm) under (a) 69 kN, (b) 71 kN and (c) 40 kN

5.3. Shrinkage cracks on SHCC layer

SHCC shrinks more than conventional concrete, due to its high cement content, which needs water to hydrate. All beams with SHCC are demoulded after 47 days of the casting of SHCC layer (33 days after the casting of concrete layer). After one day of exposure in the room condition, shrinkage cracks were observed on the SHCC layer (Figure 104). That is due to different shrinkage ratio between SHCC and conventional concrete after exposure. SHCC layer trends to shrink, but it was constrained by its bond with concrete. When the stress reaches a certain value, SHCC layer cracks.

The shrinkage cracks may lead to stress concentration, which prevent the cracks from uniformly distributing and make the crack localize at earlier stage.

To avoid the shrinkage crack, the SHCC can be exposed to air in advance. In this way, the SHCC layer will shrink freely and subsequently, the normal concrete will be cast on top of it (after the largest part of shrinkage is finished).

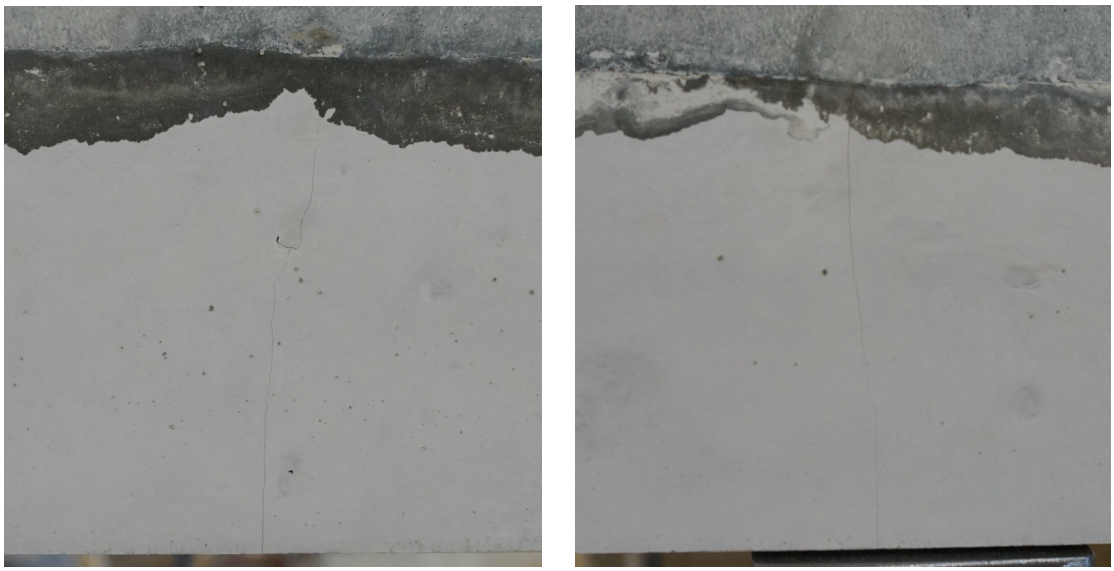

Figure 104 Shrinkage cracks on the SHCC layer of the beam with SHCC layer of 70 mm

5.4. Problems during casting

As shown above, the SHCC layers were poured into the mould by spoons. And due to the small thickness of the SHCC layer, vibration porker was not applied. Therefore, between one spoon of SHCC and another, there is a weak 'wet to wet' interface that has less fibers to bridge the two parts together.

In Japanese Recommendation of SHCC (JSCE, 2008), the same problem is called overlaying (horizontal interface) and merging (vertical interface) (Figure 105). And suggestions are made that vibration porker should be applied to eliminate the weak interface.

For thin SHCC layer, using rake before leveling to break the interface can be possible solution and may also help orient the fibers.

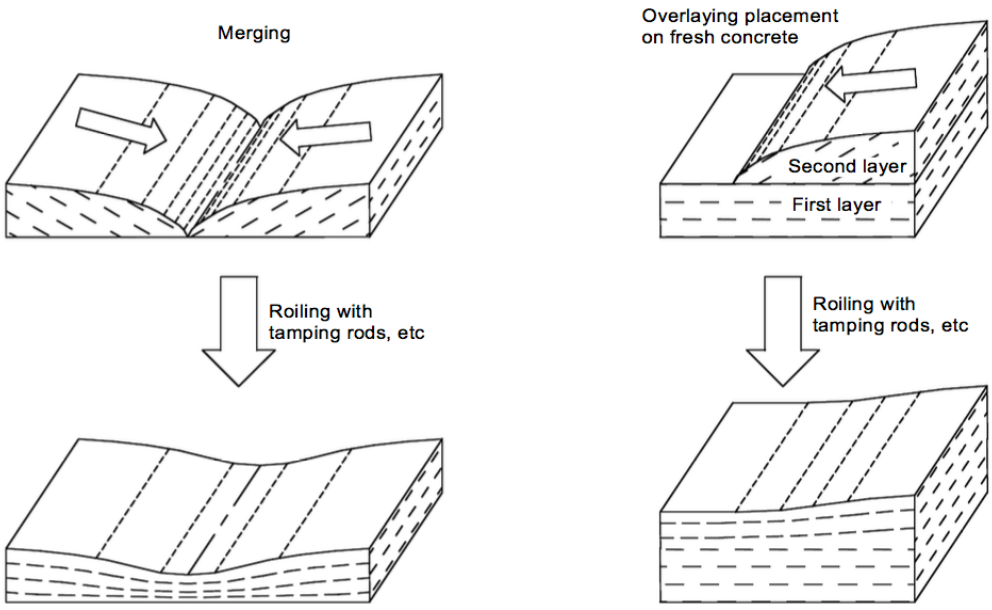

Figure 105 Conceptual drawing of overlaying and merging (JSCE, 2008)

On the SHCC layer of the failed specimens, unusual crack pattern (Figure 106), longitudinal cracks were observed, especially on the 70 mm SHCC layers, which have high possibility to form a horizontal weak interface. That shows the weak interface due to non-uniformly distributed fiber may cause the initialization of the cracks.

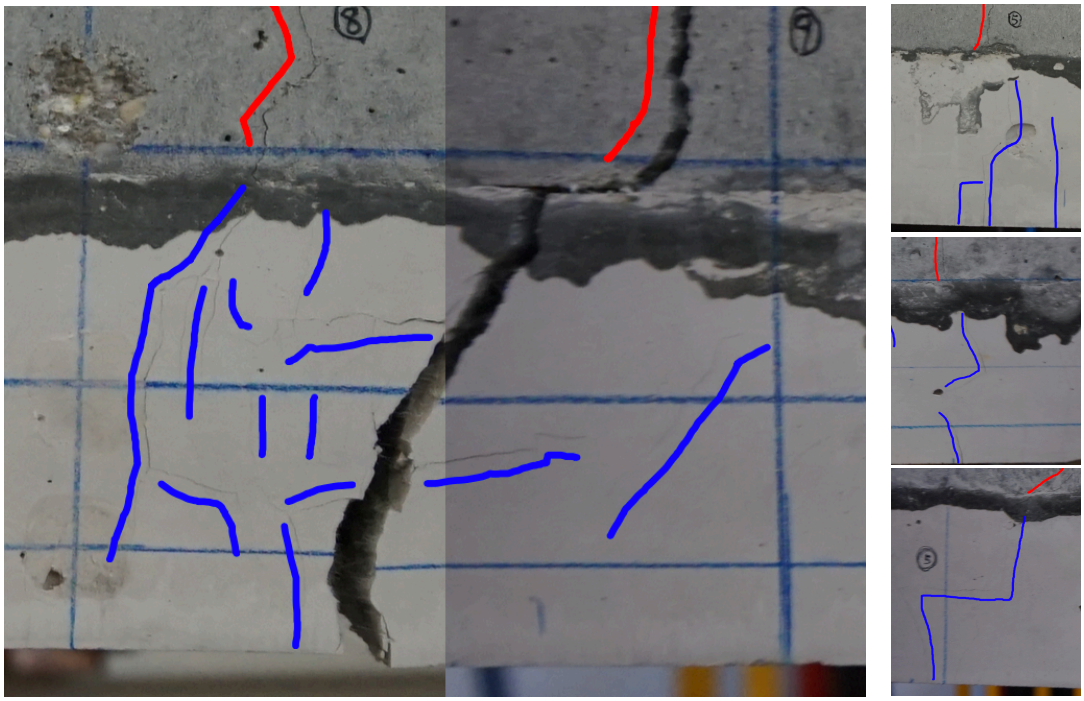

Figure 106 Unusual crack pattern, longitudinal cracks on SHCC layer of the beam with SHCC layer of 70 mm

6

Further Research

For further research, the SHCC layer with embedded reinforcement system can be designed as a semi-prefabricated element for beam construction. Figure 107 shows the lab-scale protocol model with SHCC layer of 70 mm and embedded reinforcement.

Figure 107 Lab-scale protocol section of SHCC layer with embedded reinforcement system

The manufacture procedure of the element is 'folding'. This was inspired by the beams constructed in Puerto Rico. Banthia *et al.*, (2012) reported that the hotel structure was to be poured using permanent glass fiber reinforced concrete (GFRC) forms for the beams and columns. The U-shaped beam forms were manufactured using folding steel molds (Figure 108).

Figure 108 GFRC permanent formwork for beams in Puerto Rico. Courtesy of Nippon Electric Glass America Inc (Banthia *et al.*, 2012).

The detailed manufacture procedures of the U-shape element were shown as follows (Figure 109):

① Firstly, a layer of SHCC about 10 mm thick is poured into the special mould.

② Then the side panels are flipped over and the reinforcement cage is put into the special.

③ After that, the SHCC mixture is poured into the mould to fill the empty part.

④ Let SHCC harden for 60 minutes to gain some stiffness which is enough for the flanges to support themselves. Finally, erect the two sides of the mould and cover it with plastic sheet for curing.

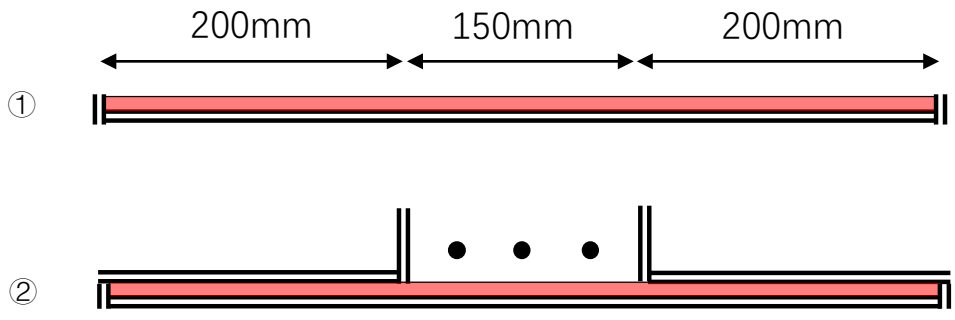

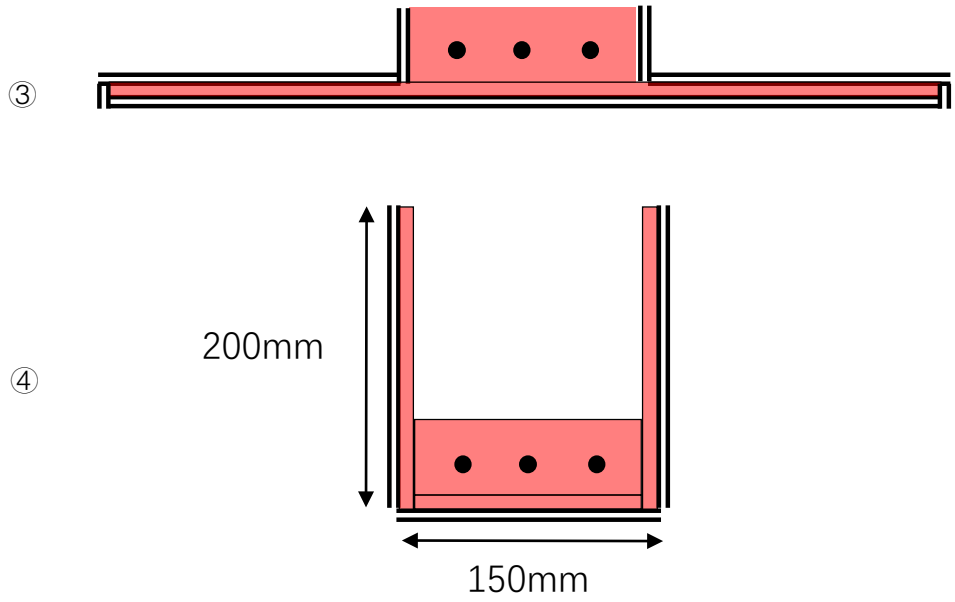

Figure 109 Manufacture procedures of the U-shape channel

The special mould (Figure 110 (a)) and the erected element (Figure 110 (b)) are shown below:

(a) (b)

Figure 110 (a) Special mould made of plastic plate. (b) Folded element

The key point of the procedure is the time of erection. If the element is folded when the SHCC mixture does not have enough stiffness, and the flange will fall or creep down. However, if the element is folded when the SHCC mixture is too stiff, the folded corners will crack. For the element with height of 200 mm and width of 150 mm (bottom layer of

70 mm and flange thickness 10mm), the optimal time is around 60 minutes after pouring the SHCC, since no cracks were found at the bottom corners (Figure 111).

Figure 111 Bottom corners of the element folded after 60 minutes from pouring

The advantages of the system are summarized below:

- The reinforcement required by crack width control can be spared.
- The capacity of the structure can be further utilized before reaching the limited crack width.
- Applying the prefabricated element, the construction speed and quality will be promoted. And SHCC is lighter than conventional concrete, thus easier for transport.

7

Conclusions

The aims of the research were to investigate whether applying SHCC layer in beam tension zone with embedded reinforcement can help control the maximum crack width, and whether the crack control ability will be affected by adding a self-healing agent or varying the thickness of the SHCC layer. The results and the main conclusion from the research are summarized as follows:

- Applying SHCC in beam tension zone can increase the beam capacity. For the beams with the thickness of 30 mm the capacity was increased by 8 kN (SHCC) and 7 kN (SHCC+SH) and for the beams with the SHCC thickness of 70 mm the capacity was increased by 14 kN (SHCC) and 16 kN (SHCC+SH). However, this was not the main goal of this research, as the beams in reality will have higher height and contribution of SHCC layer on the structural capacity will be lower or negligible.
- The capacity of the SHCC-concrete composite beam can be well predicted by theoretical calculations. However, the deflection of the beam cannot be accurately predicted.
- Maximum crack width of the beam can be control by thick SHCC layer (70 mm SHCC layer for beam with 200 height) in the beam tension zone.
- Thin SHCC layer (30 mm SHCC layer for beam with 200 height) in tension zone has no clear evidence of controlling the maximum crack width. However, the comparison between the SHCC-concrete composite beam and RC beam is not representative, as 11 mm is not normative thickness for the concrete cover.
- Adding self-healing agents in SHCC mixture did not affect the crack control ability of the SHCC layer or the capacity of the SHCC-concrete composite beam.
- The accuracy of DIC is verified with the measurement obtained by the linear

variable differential transformer (LVDTs) when measuring the displacement over a length of 200 mm.

- The procedure of measuring crack width by DIC is developed. In the research, the procedure was done manually, but it has the potential to be automized. The results were verified by measurements obtained by Image J (image software).
- The procedure of casting U-shape stay-in-place mould is developed. The optimal folding time for the SHCC mixture, in order for the mix to reach appropriate stiffness but to avoid cracking after folding, is found to be around 1 hour.

References

Abdel Zaher, A., Kunieda, M., Ueda, N. and Nakamura, H. (2008) *Evaluation of crack opening performance of a repair material with strain hardening behavior*, *Cement and Concrete Composites*. doi: 10.1016/j.cemconcomp.2008.08.003.

American Concrete Institution Committee 201 (2016) 'Guide to Durable Concrete'.

Banthia, N., Bindiganavile, V., Jones, J. and Novak, J. (2012) *Fiber-reinforced concrete in precast concrete application. Research leads to innovative products*, *PCI Journal*. doi: 10.15554/pcij.06012012.33.46.

Blagojević, A. (2016) *The Influence of Cracks on the Durability and Service Life of Reinforced Concrete Structures in relation to Chloride-Induced Corrosion*. Technische Universiteit Delft. Available at: http://repository.tudelft.nl/.

Cho, C.-G., J. Kappos, A., Moon, H.-J. and Lim, H.-J. (2015) *Experiments and Failure Analysis of SHCC and Reinforced Concrete Composite Slabs*, *Engineering Failure Analysis*. doi: 10.1016/j.engfailanal.2015.01.009.

Hansson, C. M., Poursaee, A. and Laurent, A. (2006) *Macrocell and Microcell Corrosion of Steel in OPC and High Performance Concrete*, *Cement and Concrete Research*. doi: 10.1016/j.cemconres.2006.07.005.

Ishikawa, Y., Aoyama, M., Kuroyanagi, M., Nagai, M. and Miyashita, T. (2014) *Proposition of a new type of jointless system for existing concrete bridges*, *J. Phys. Sci. Appl.*

J. Verbeck, G. and Erlin, B. (1975) 'Corrosion of Metals in Concrete-Needed Research', *ACI Materials Journal*, 49, pp. 39–46.

JSCE (2008) *Recommendations for Design and Construction of High Performance Fiber Reinforced Cement Composites with Multiple Fine Cracks (HPFRCC)*.

Kanda, T., Nagai, S., Maruta, M., Yamamoto, Y., Toledo Filho, R. D., Silva, F., Koenders, E. and Fairbairn, E. M. R. (2011) *New high-rise R/C structure using ECC coupling beams*, *2nd International RILEM Conference on Strain Hardening Cementitious Composites (SHCC2-Rio)*.

Khalil, A. E., Etman, E., Atta, A. and Essam, M. (2017) 'Behavior of RC beams strengthened with strain hardening cementitious composites (SHCC) subjected to monotonic and repeated loads' , *Engineering Structures*. Elsevier Ltd, 140, pp. 151–163. doi: 10.1016/j.engstruct.2017.02.049.

Koteš, P. (2013) 'Influence of Corrosion on Crack Width and Pattern in an RC Beam' , *Procedia Engineering*, 65(Complete), pp. 311–320. doi: 10.1016/j.proeng.2013.09.048.

Kunieda, M. and Rokugo, K. (2006) *Recent Progress on HPFRCC in Japan Required Performance and Applications*, *Journal of Advanced Concrete Technology - J ADV CONCR TECHNOL*. doi: 10.3151/jact.4.19.

Lepech, M.D. & Li, V. C. (2005) 'WATER PERMEABILITY OF CRACKED CEMENTITIOUS COMPOSITES' .

Li, V. C. (2007) 'Engineered Cementitious Composites (ECC) – Material , Structural , and Durability Performance' .

Lukovic, M. (2016) *INFLUENCE OF INTERFACE AND STRAIN HARDENING CEMENTITIOUS COMPOSITE (SHCC) PROPERTIES ON THE PERFORMANCE OF CONCRETE REPAIRS*. Technische Universiteit Delft. Available at: http://repository.tudelft.nl/.

Mccormick, N. and Lord, J. (2010) 'Digital Image Correlation' , *Materials Today*. Elsevier Ltd, 13(12), pp. 52–54. doi: 10.1016/S1369-7021(10)70235-2.

Miyazato, S. and Hiraishi, Y. (2005) 'Transport properties and steel corrosion in ductile fiber reinforced cement composites' .

Mwamila, B. L. M. and Karumuna, B. L. (1999) 'Semi-prefabrication concrete techniques in developing countries' , *Building Research & Information*. Routledge, 27(3), pp. 165–182. doi: 10.1080/096132199369507.

Sahmaran, M., Li, M. and Li, V. (2011) *Transport Properties of Engineered Cementitious Composites Under Chloride Exposure*, *ACI Materials Journal*.

Şahmaran, M. and Li, V. (2008) *Influence of microcracking on water absorption and sorptivity of ECC*, *Materials and Structures/Materiaux et Constructions*. doi: 10.1617/s11527-008-9406-6.

Tam, V., Tam, C., Zeng, S. and C.Y. Ng, W. (2007) *Towards adoption of prefabrication in construction*, *Building and Environment*. doi: 10.1016/j.buildenv.2006.10.003.

Warszawski, A., Avraham, M. and Carmel, D. (1984) *Utilization of Precast Concrete Elements in Building*, *Journal of Construction Engineering and Management-asce - J CONSTR ENG MANAGE-ASCE*. doi: 10.1061/(ASCE)0733-9364(1984)110:4(476).

Appendix A. Mould design

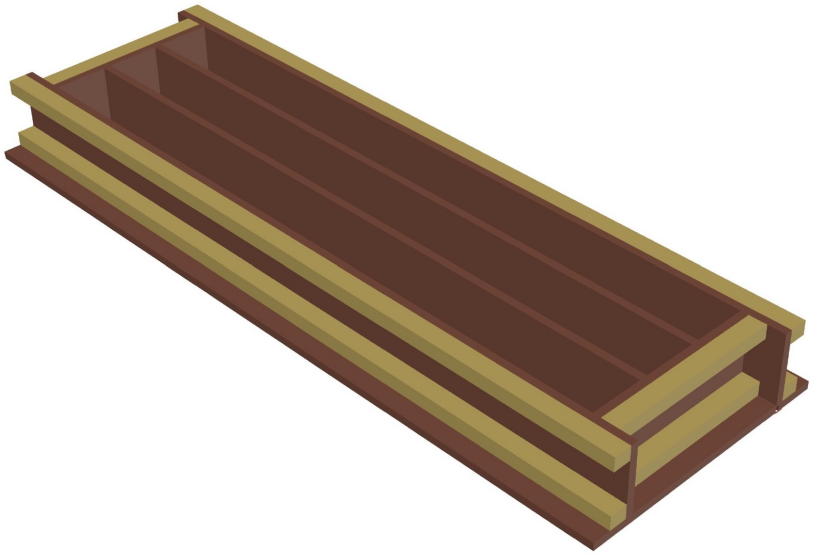

Figure 112 3D Model of the mould

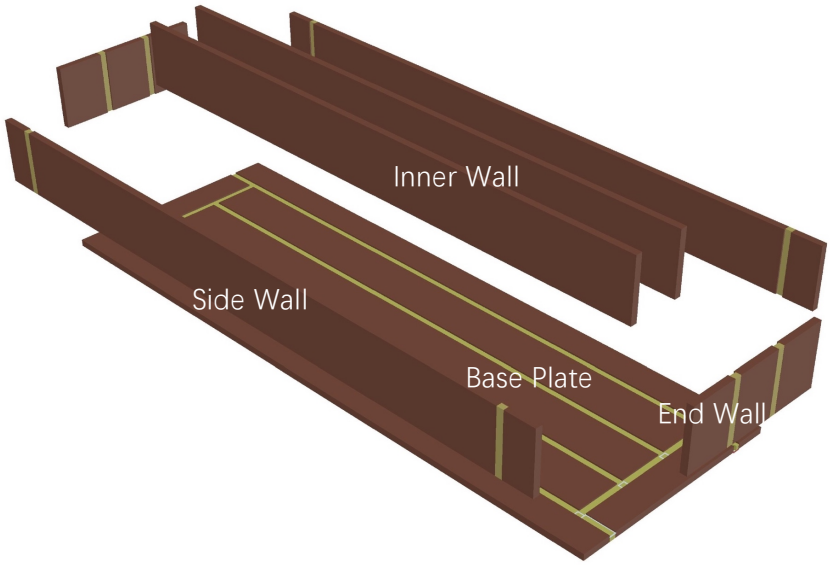

Figure 113 Elements of the mould

One mould consists of 7 elements, 2 inner walls, 2 side walls, 2 end walls and 1 end plate. Wooden beams are applied to constrain the plates and help reducing deflection.

The Required Materials are listed below:

Table 13 Material list (for two moulds)

Material	Amount
Base Plate	2
Side Wall	4
Inner Wall	4
End Wall	4
Wood Beam	22 (21.184) meters

The dimensions of the plates are shown below:

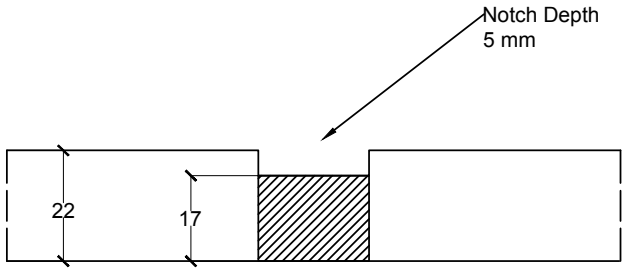

Figure 114 PS: Hatched area means notch (Unit: mm)

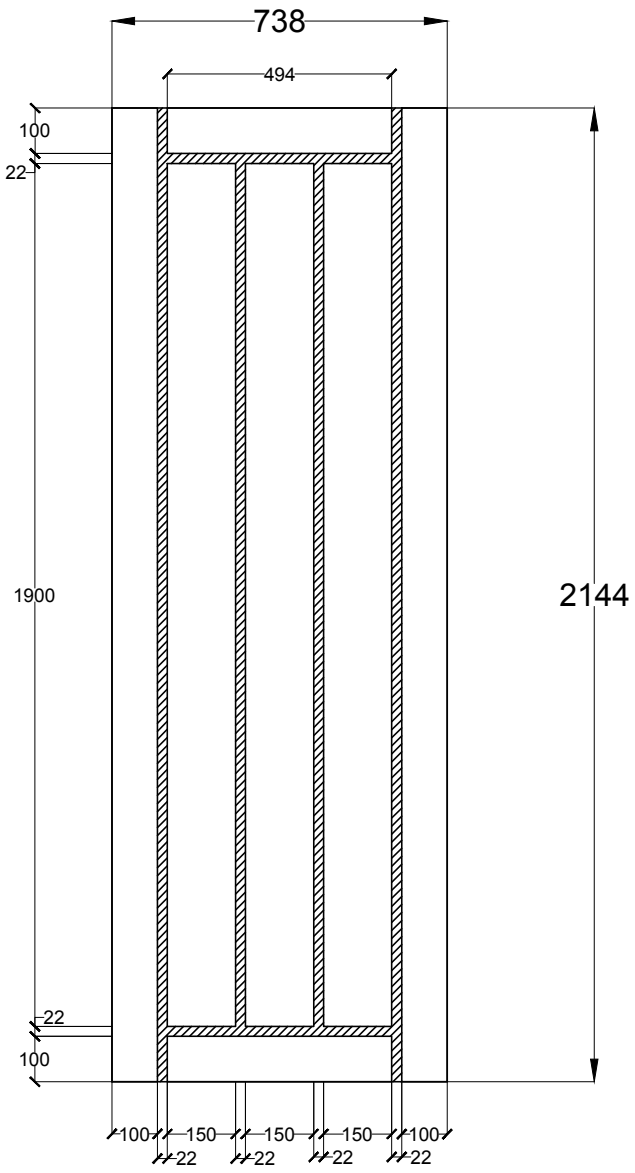

Figure 115 Dimensions of the base plate (notch is hatched)

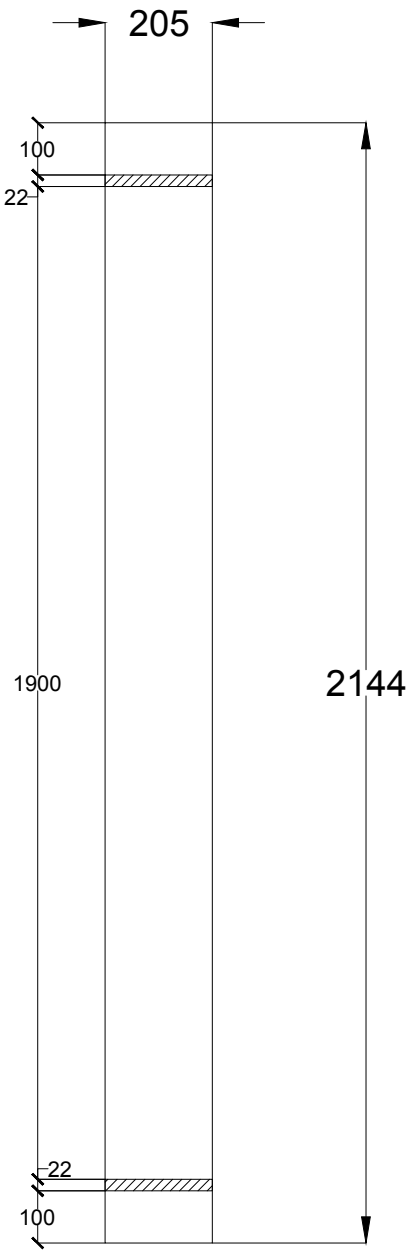

Figure 116 Dimensions of the side wall [mm].

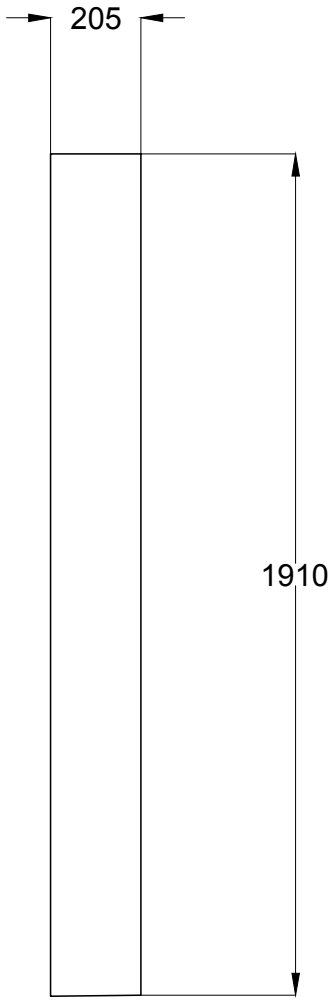

Figure 117 Dimensions of the inner wall [mm]

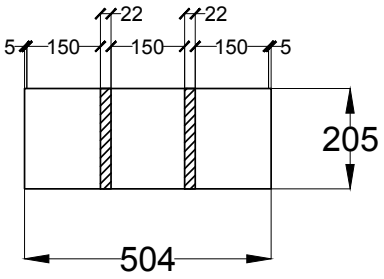

Figure 118 Dimensions of the end wall [mm]

Appendix B. Experiment setups

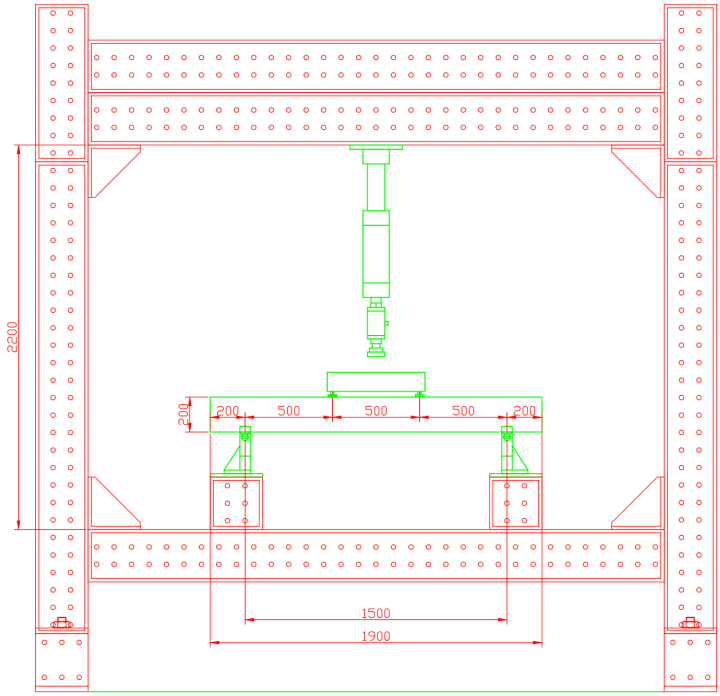

Figure 119 Loading frame and experiment setups

Appendix C. Test dates

Table 14 Test dates

Test No.	Cross-section	Test date
Test 01	SHCC+SH 30 mm	23-05-17
Test 02	RC Cover 11 mm	24-05-17
Test 03	SHCC 70 mm	29-05-17
Test 04	SHCC+SH 70 mm	29-05-17
Test 05	SHCC 30 mm	30-05-17
Test 06	RC Cover 31 mm	31-05-17

Appendix D. Cube compression tests

Concrete cube compression tests

Table 15 Results of concrete cube compression tests (casted on 20-04-2017 and tested on 23-04-2017)

Number	Size [cm]	Loading speed [kN/s]	Load [kN]	Stress [MPa]	Concrete age [days]	Average [Mpa]	Standard Deviation
1	15x15x15	13.5	904.3	40.19	33	45.74	3.44
2	15x15x15	13.5	1025.7	45.59	33		
3	15x15x15	13.5	1103.7	49.05	33		
4	15x15x15	13.5	1082.8	48.12	33		

SHCC and SHCC+SH cube compression tests

Table 16 Results of SHCC and SHCC+SH cube compression tests (casted on 07-04-2017 and tested on 30-10-2017)

Label	Size [cm]	Loading Speed [kN/s]	Load [kN]	Stress [MPa]	SHCC age [days]	Average [MPa]	Standard Deviation
SHCC 1	15x15x15	13.5	1403.1	62.36	190	62.67	1.01
SHCC 2	15x15x15	13.5	1440.7	64.03	190		
SHCC 3	15x15x15	13.5	1386.4	61.62	190		
SHCC+SH 4	15x15x15	13.5	1454.7	64.65	190	63.57	0.91
SHCC+SH 5	15x15x15	13.5	1404.4	62.42	190		
SHCC+SH 6	15x15x15	13.5	1432.2	63.65	190		

Appendix E. DIC vs. LVDTs for all tests

Test 01, beam with SHCC+SH layer of 30 mm

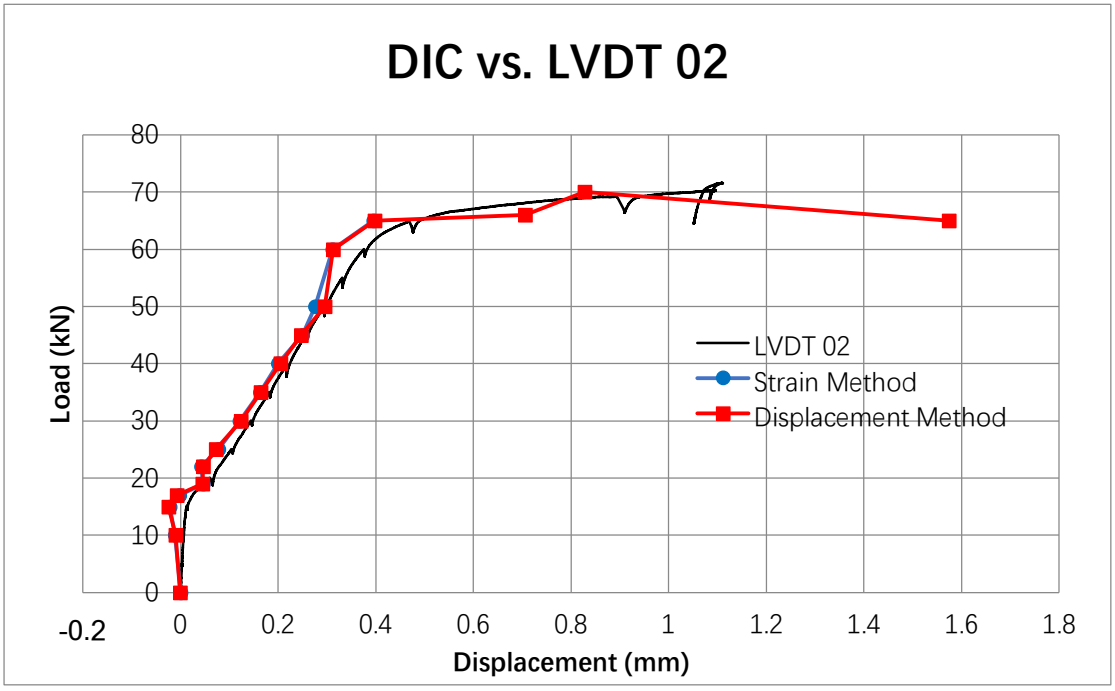

Figure 120 DIC vs. LVDT 02 Test 01, beam with SHCC+SH layer of 30 mm

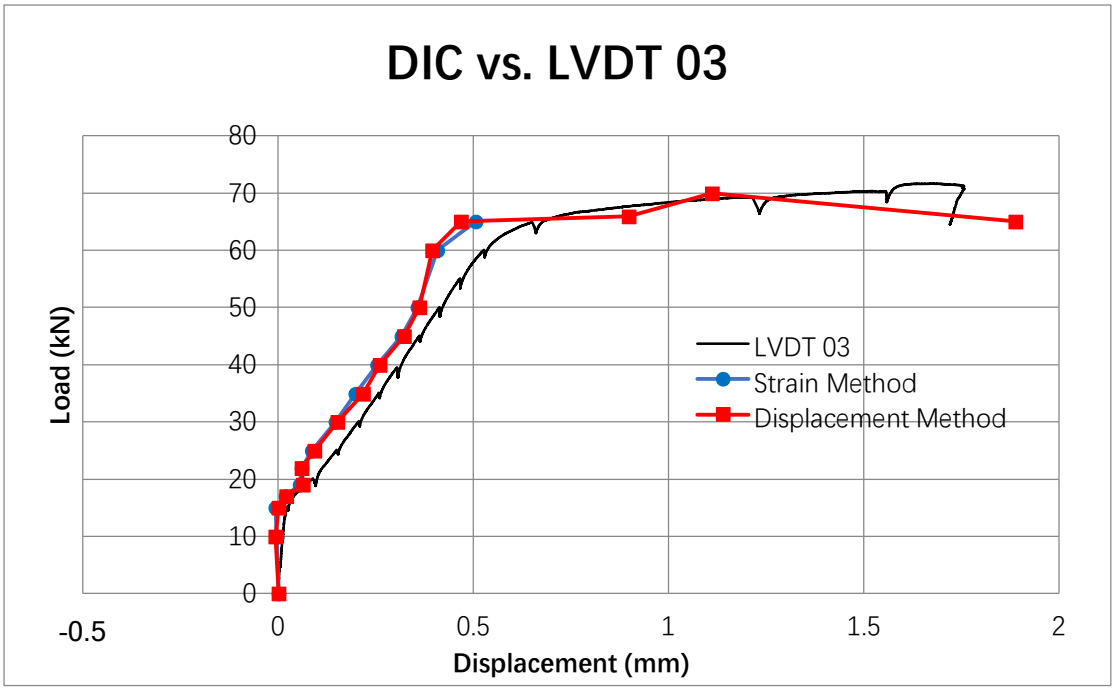

Figure 121 DIC vs. LVDT 03 Test 01, beam with SHCC+SH layer of 30 mm

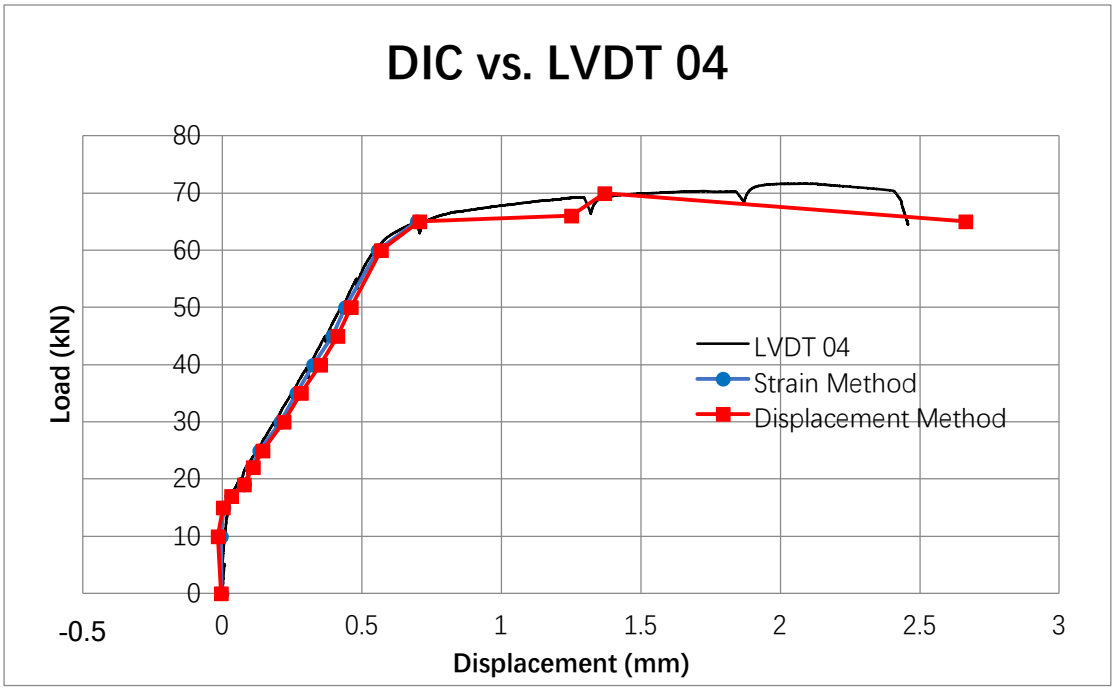

Figure 122 DIC vs. LVDT 04 Test 01, beam with SHCC+SH layer of 30 mm

Test 02, RC beam with cover of 11 mm

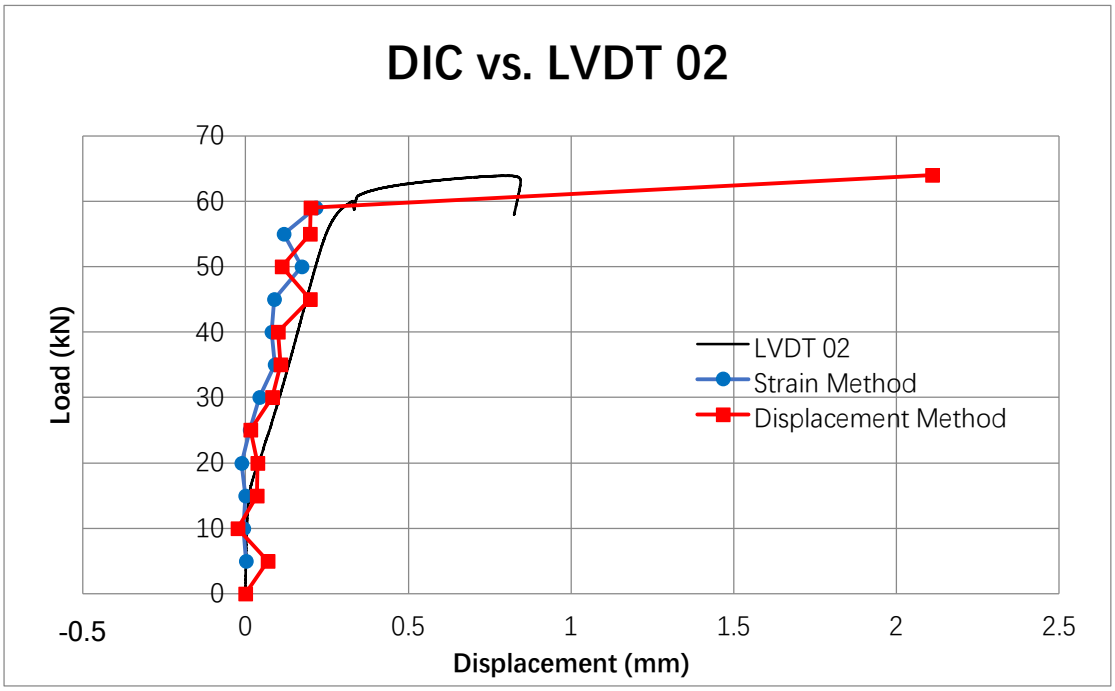

Figure 123 DIC vs. LVDT 02 Test 01, RC beam with cover of 30 mm

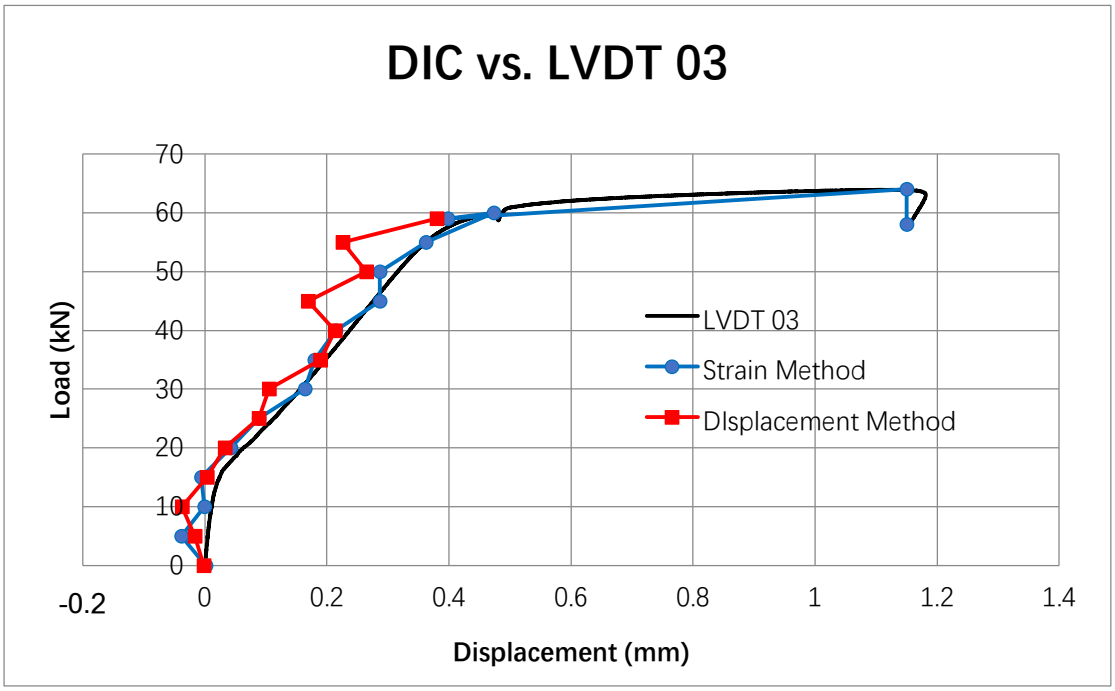

Figure 124 DIC vs. LVDT 03 Test 02, RC beam with cover of 30 mm

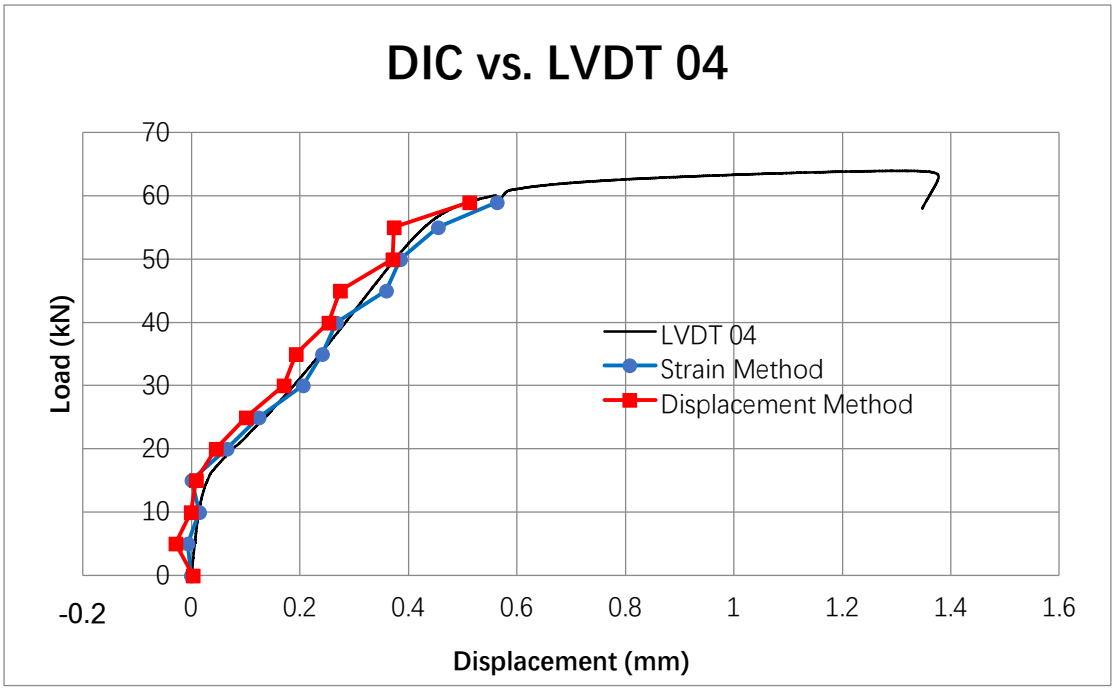

Figure 125 DIC vs. LVDT 04 Test 02, RC beam with cover of 30 mm

Test 03, beam with SHCC layer of 70 mm

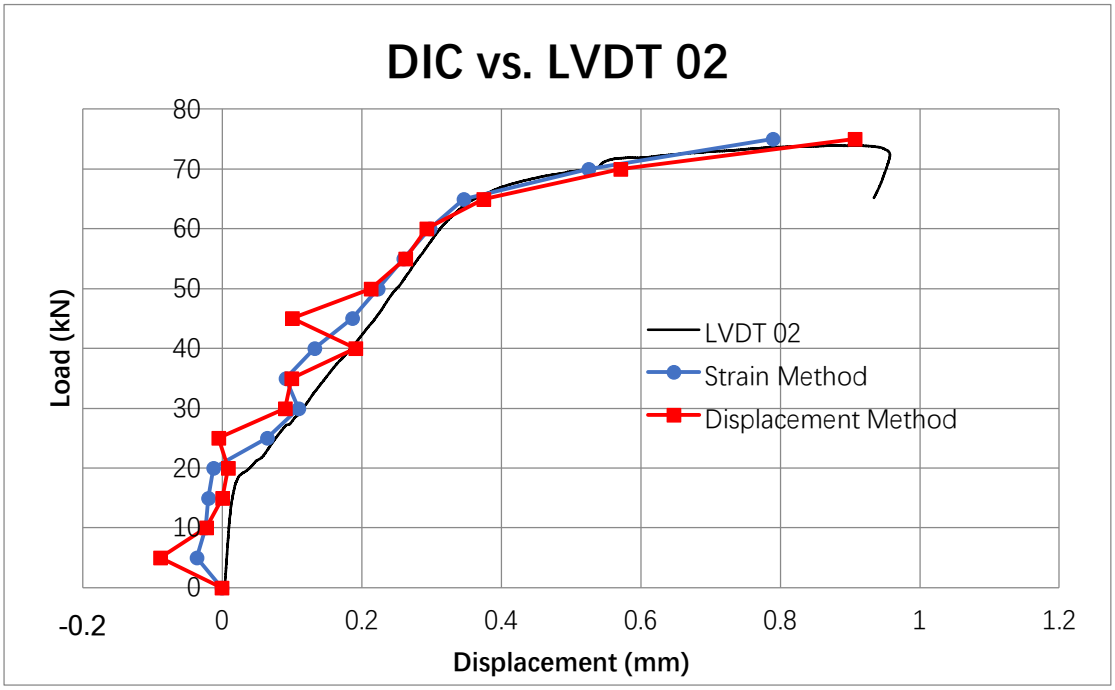

Figure 126 DIC vs. LVDT 03 Test 02, beam with SHCC layer of 70 mm

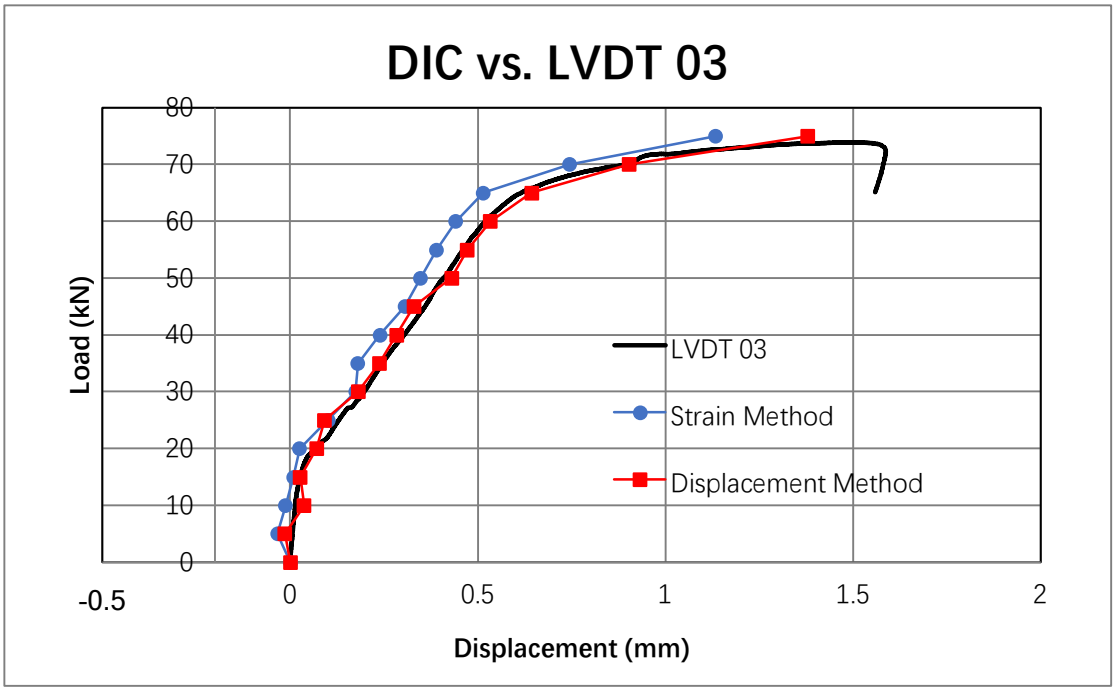

Figure 127 DIC vs. LVDT 03 Test 03, beam with SHCC layer of 70 mm

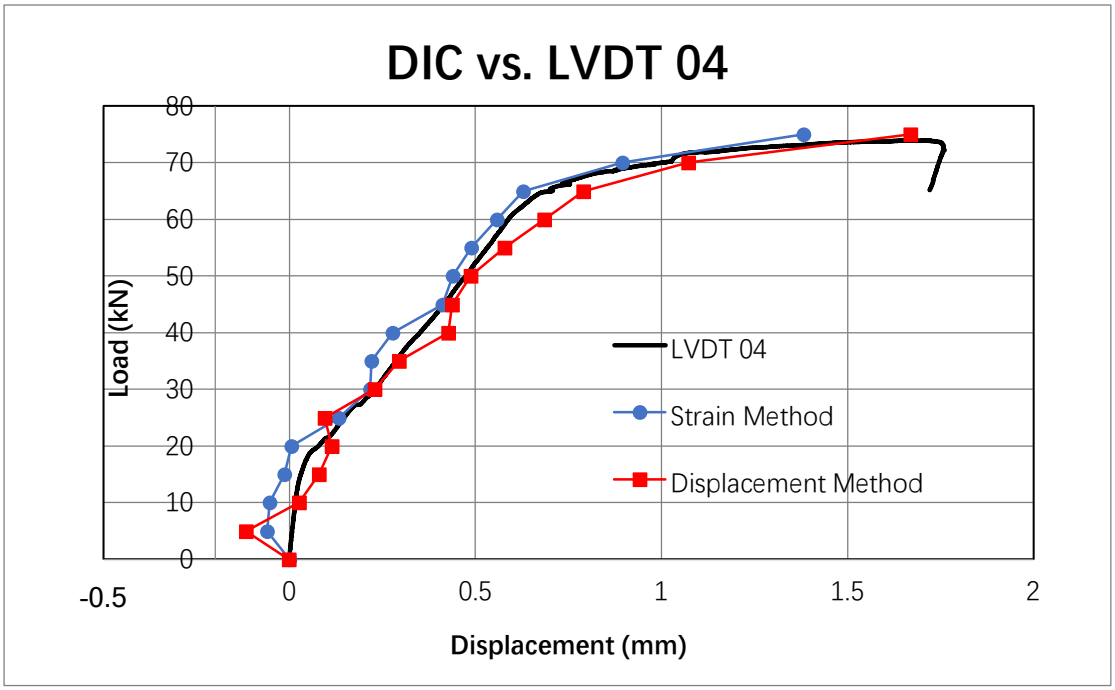

Figure 128 DIC vs. LVDT 04 Test 03, beam with SHCC layer of 70 mm

Test 04, beam with SHCC+SH layer of 70 mm

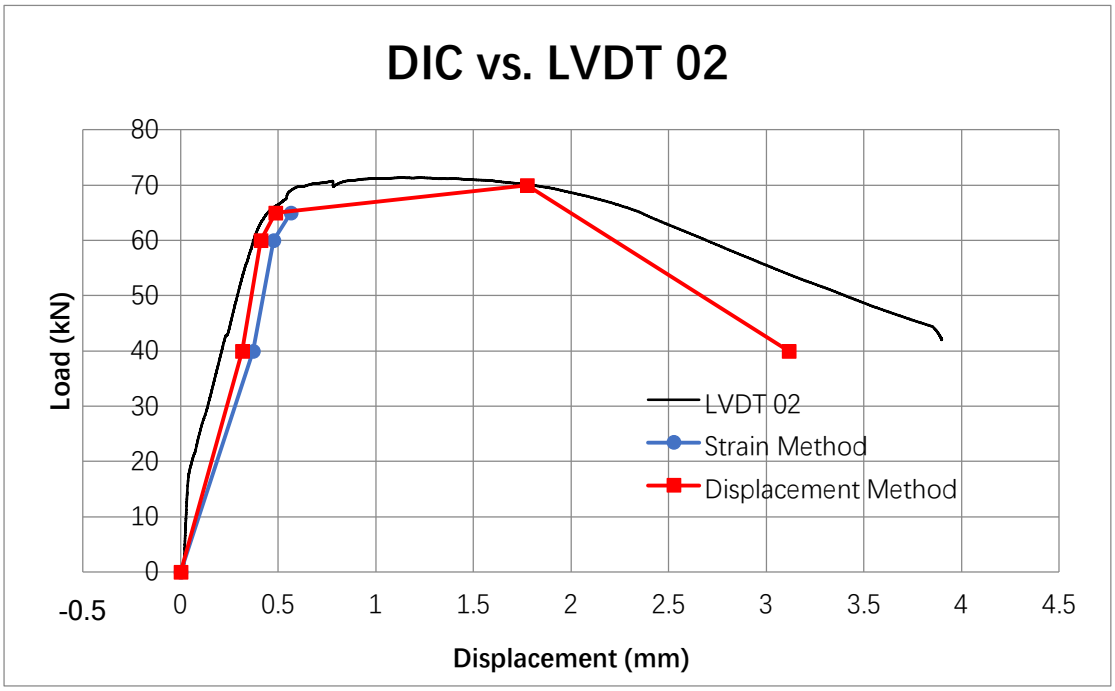

Figure 129 DIC vs. LVDT 02 Test 04, beam with SHCC+SH layer of 70 mm

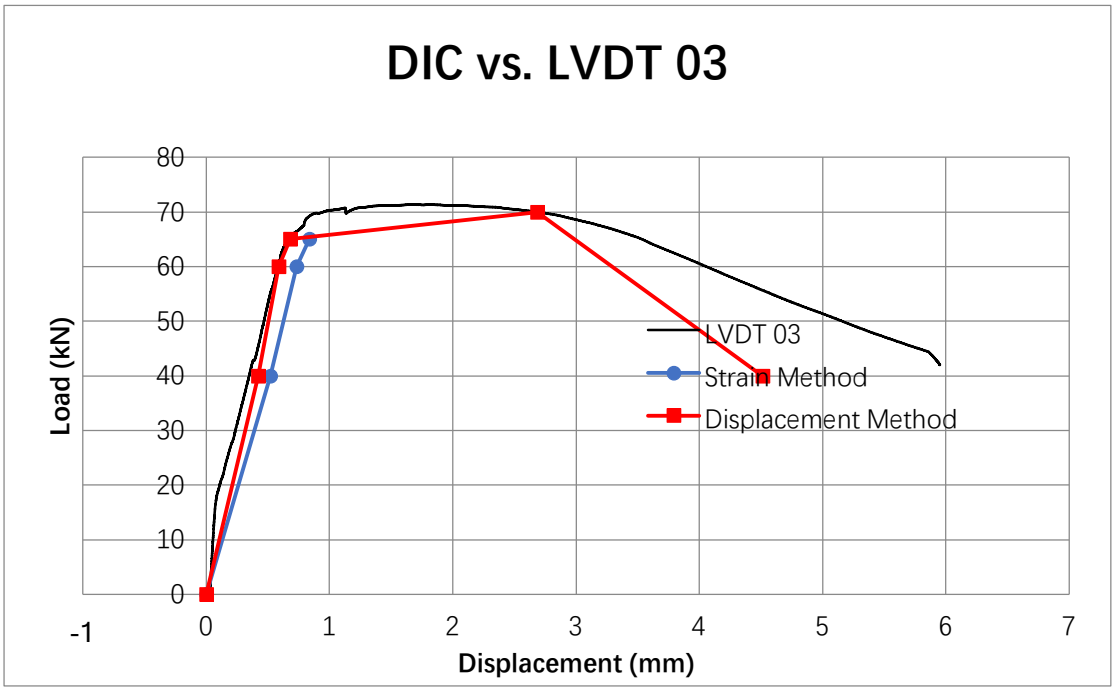

Figure 130 DIC vs. LVDT 03 Test 04, beam with SHCC+SH layer of 70 mm

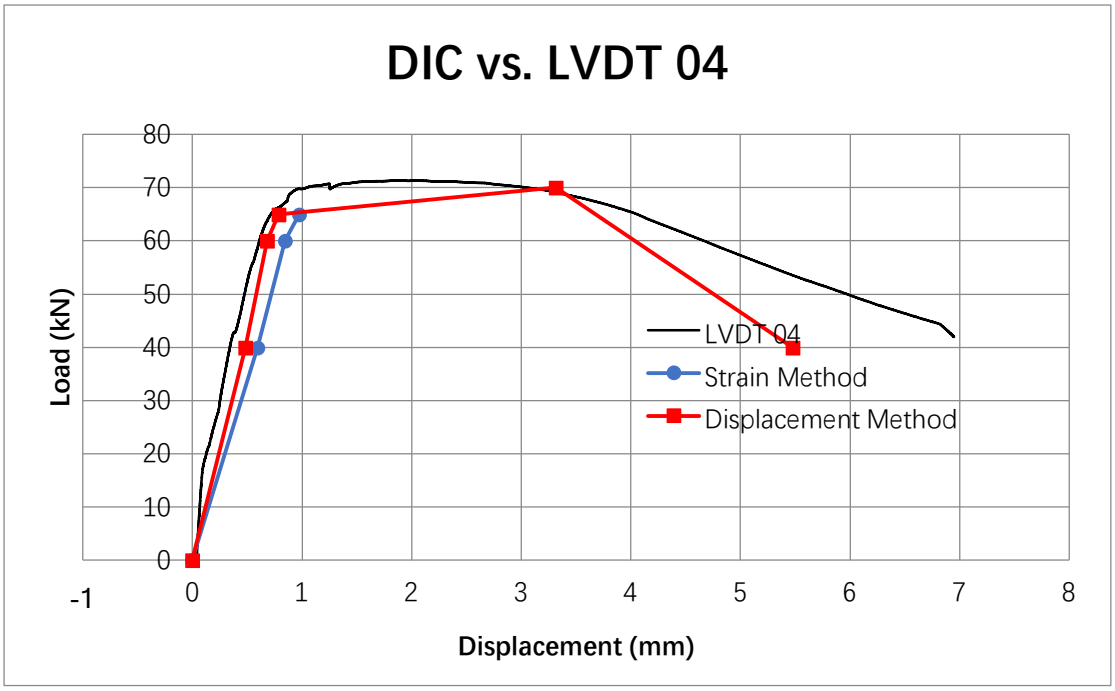

Figure 131 DIC vs. LVDT 04 Test 04, beam with SHCC+SH layer of 70 mm

Test 05, beam with SHCC layer of 30 mm

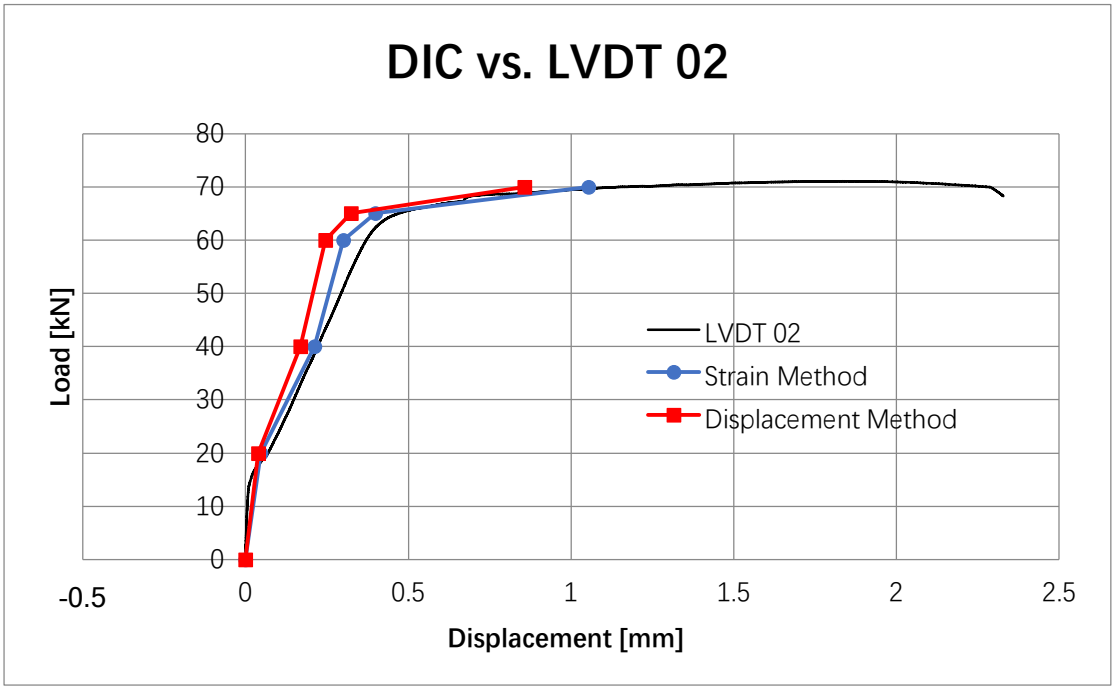

Figure 132 DIC vs. LVDT 02 Test 05, beam with SHCC layer of 30 mm

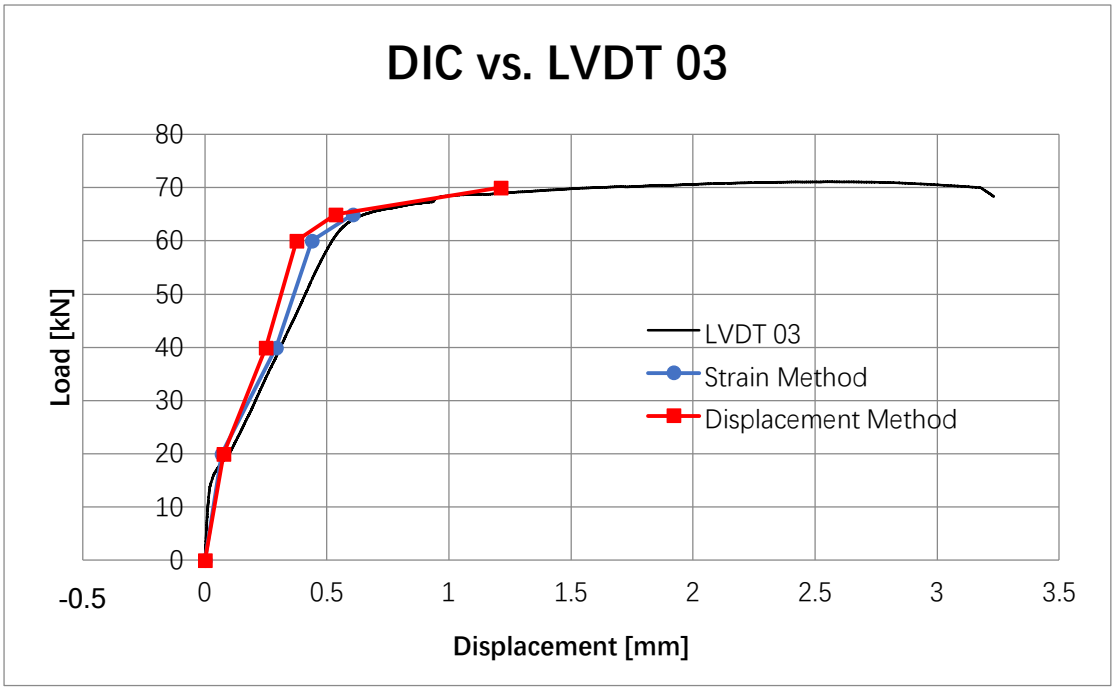

Figure 133 DIC vs. LVDT 03 Test 05, beam with SHCC layer of 30 mm

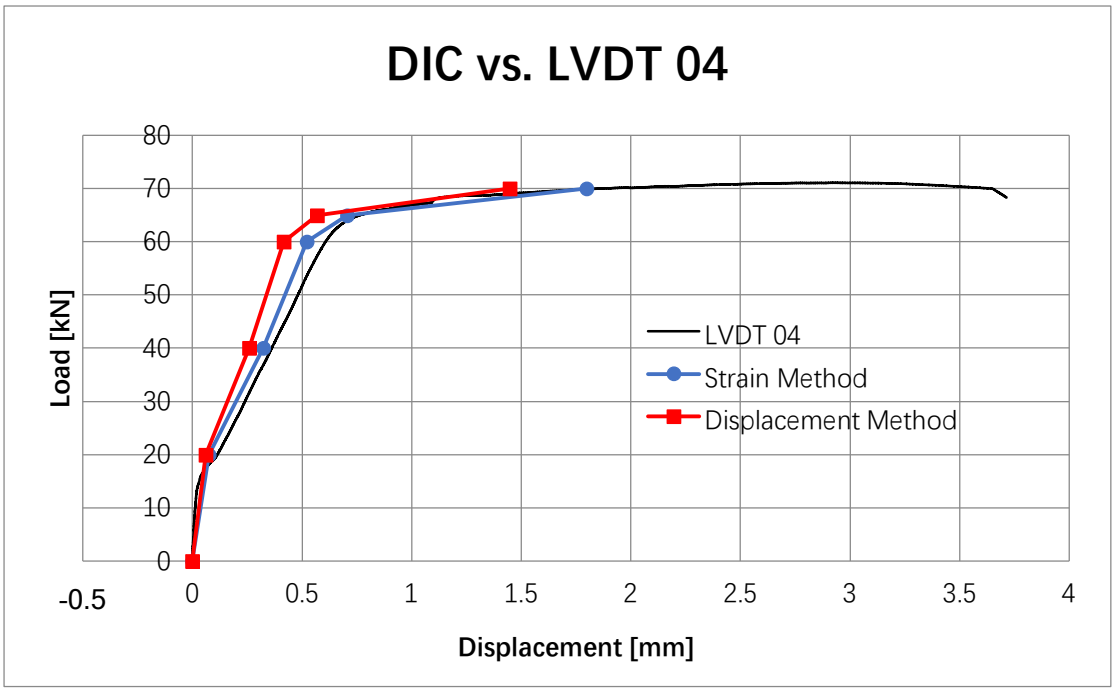

Figure 134 DIC vs. LVDT 04 Test 05, beam with SHCC layer of 30 mm

Test 06, RC beam with cover of 31 mm

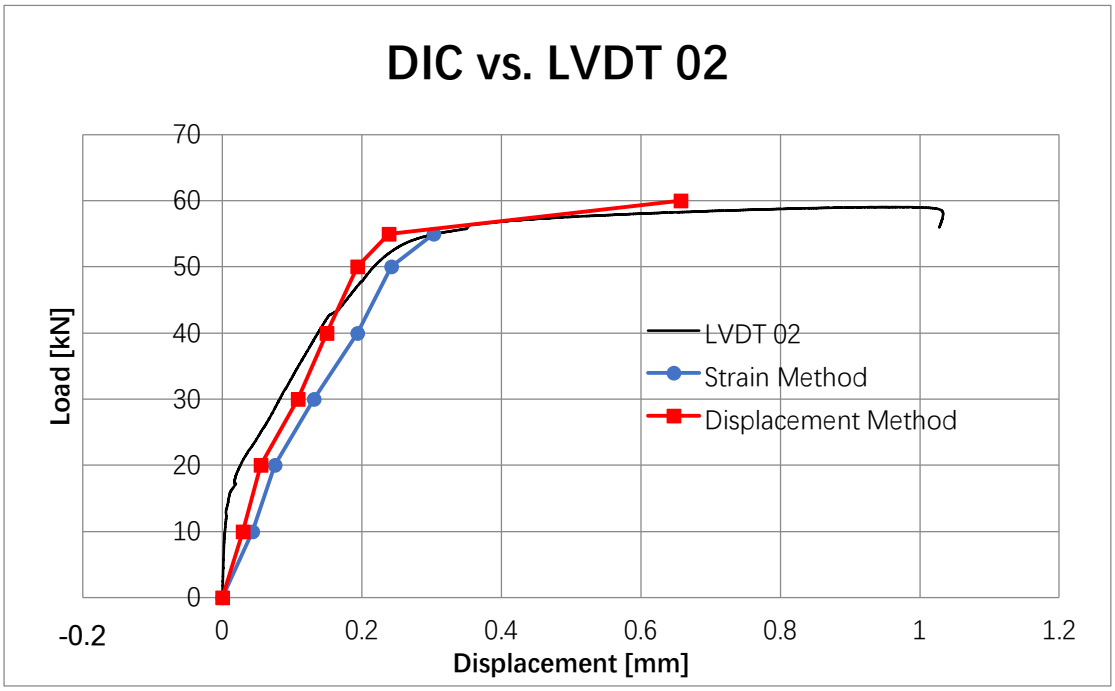

Figure 135 DIC vs. LVDT 02 Test 06, RC beam with cover of 31 mm

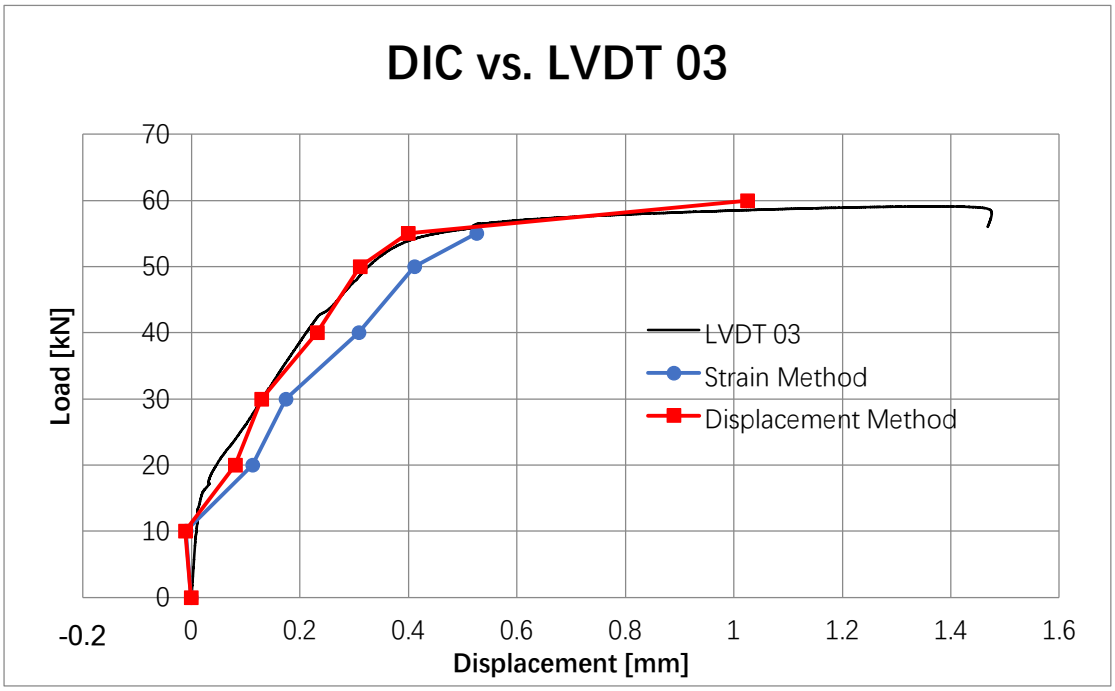

Figure 136 DIC vs. LVDT 03 Test 06, RC beam with cover of 31 mm

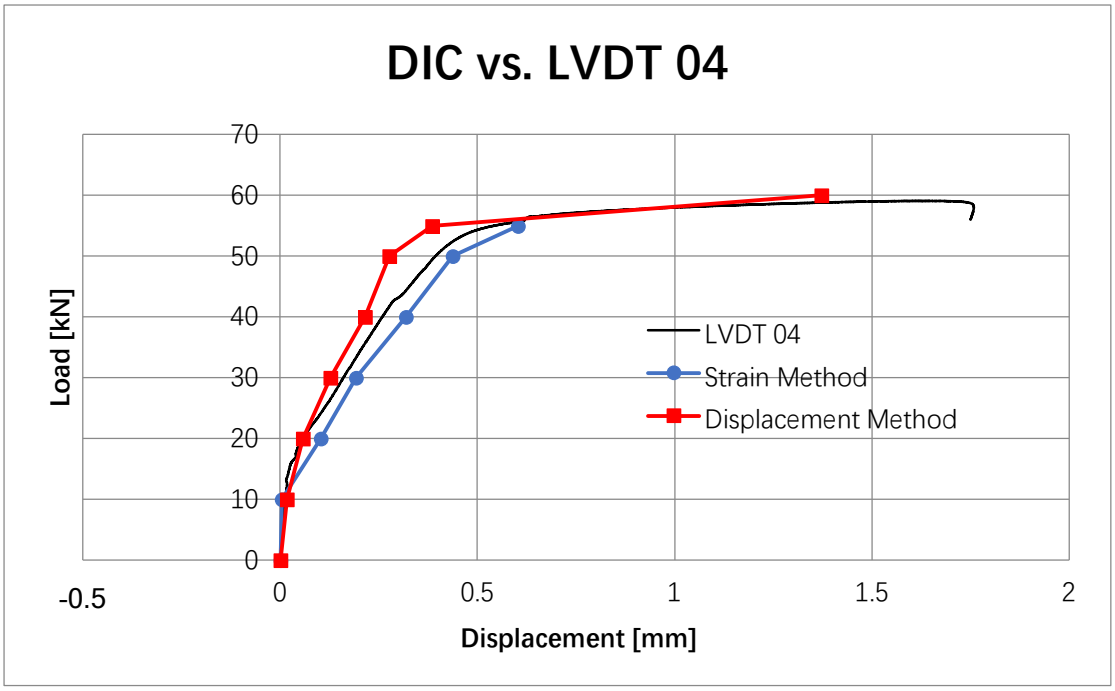

Figure 137 DIC vs. LVDT 04 Test 06, RC beam with cover of 31 mm

Appendix F. Crack widths comparison for RC beam with cover of 11 mm

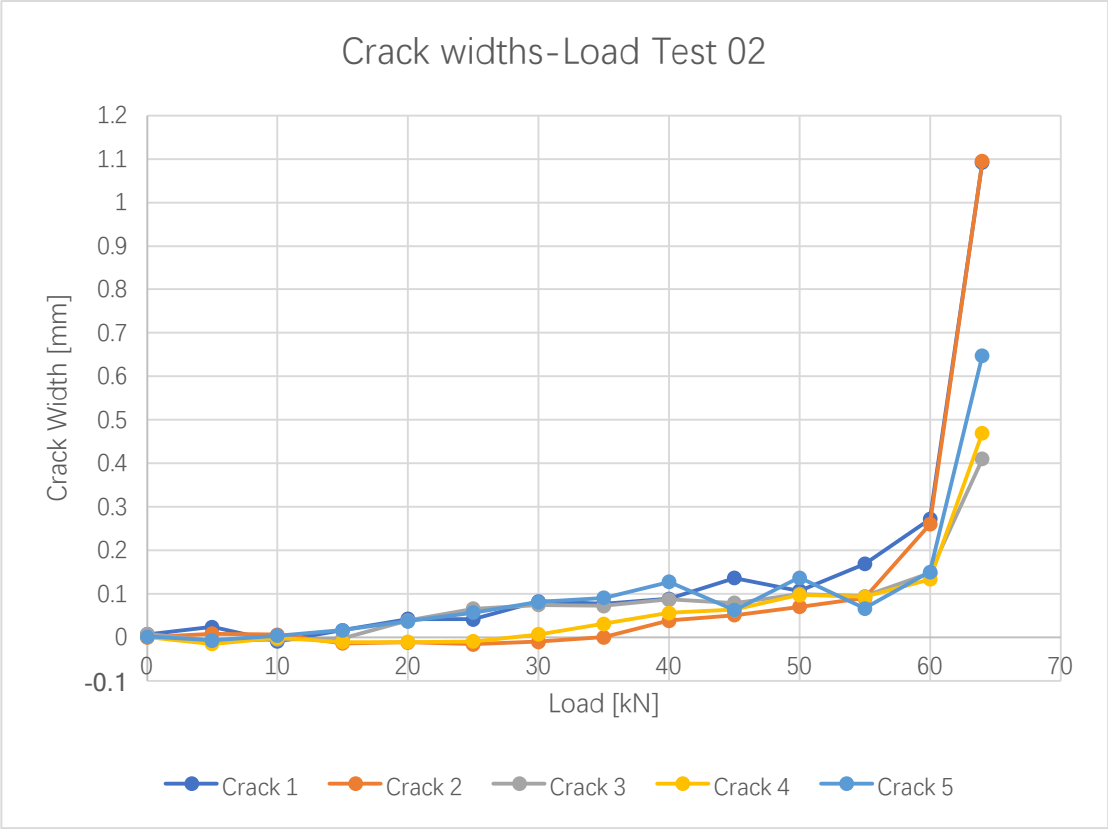

Figure 138 Crack widths comparison of five cracks of Test 02, RC beam with cover of 11 mm

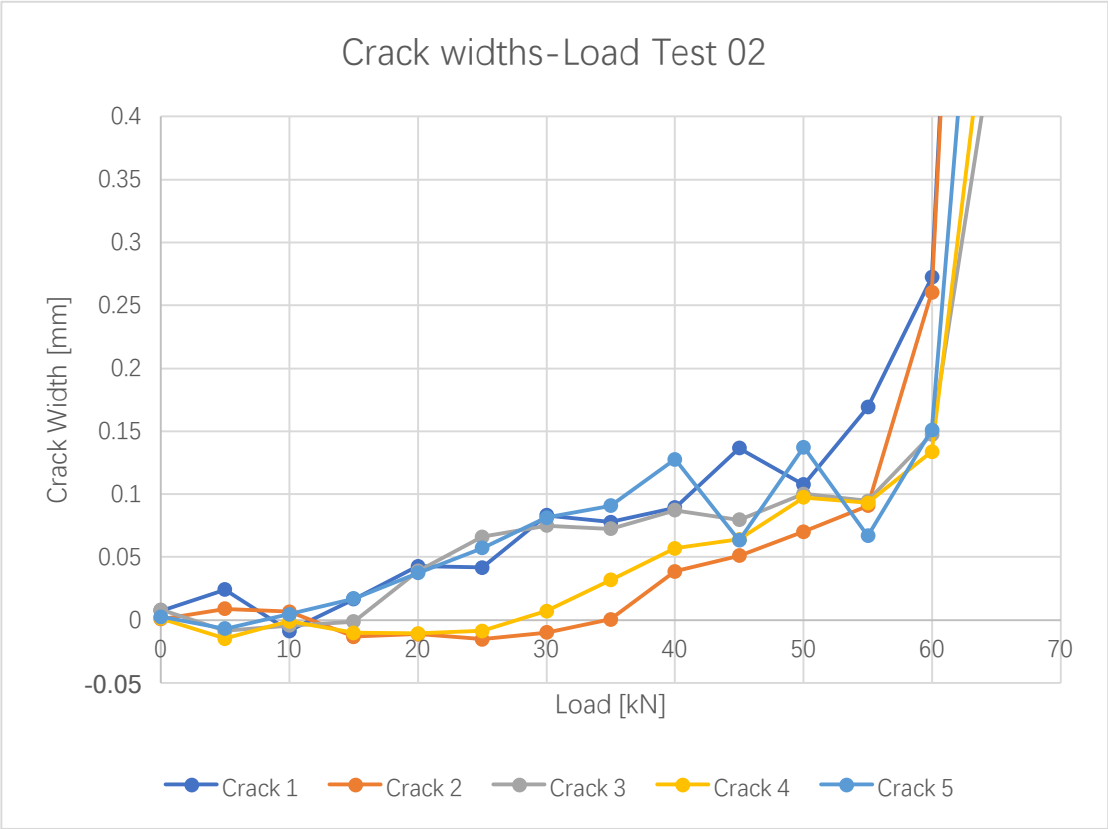

Figure 139 Crack widths comparison of five cracks of Test 02, RC beam with cover of 11 mm for crack width up to 0.4 mm

Appendix G. DIC parameters used in the analysis

Table 17 DIC parameters used in the analysis for whole beam

Whole Beam	Subset Size	Search Zone
Test 01	31	7
Test 02	31	6
Test 03	51	5
Test 04	61	3
Test 05	31	5
Test 06	31	7

Table 18 DIC parameters used in the analysis for localized cracke area

Cracked Area	Subset Size	Search Zone
Test 01	31	7
Test 02 Crack No.1	31	8
Test 02 Crack No.2	31	8
Test 02 Crack No.3	31	8
Test 02 Crack No.4	31	8
Test 02 Crack No.5	31	8
Test 03	27	10
Test 04	41	7
Test 05	51	3
Test 06 Crack No.1	51	3
Test 06 Crack No.2	51	3
Test 06 Crack No.3	51	3
Test 06 Crack No.4	51	3

Figure 140 Crack widths comparison of five cracks of Test 02, RC beam with cover of 11 mm

Appendix H. DIC images for all beams

Test 01, beam with SHCC+SH layer of 30 mm

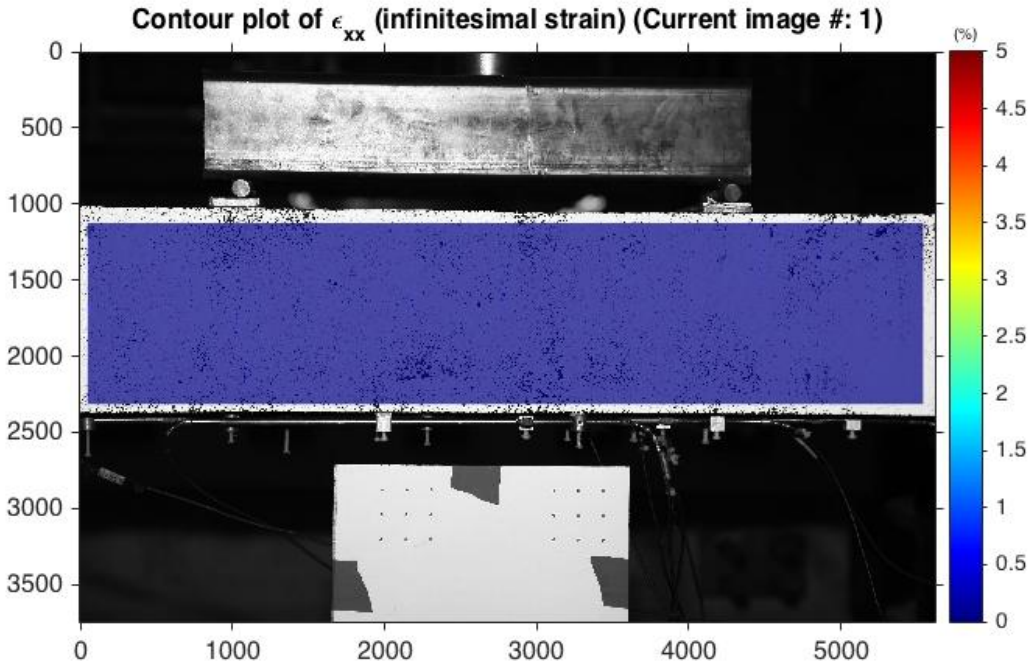

Figure 141 DIC image under 0 kN of Test 01, beam with SHCC layer of 30 mm

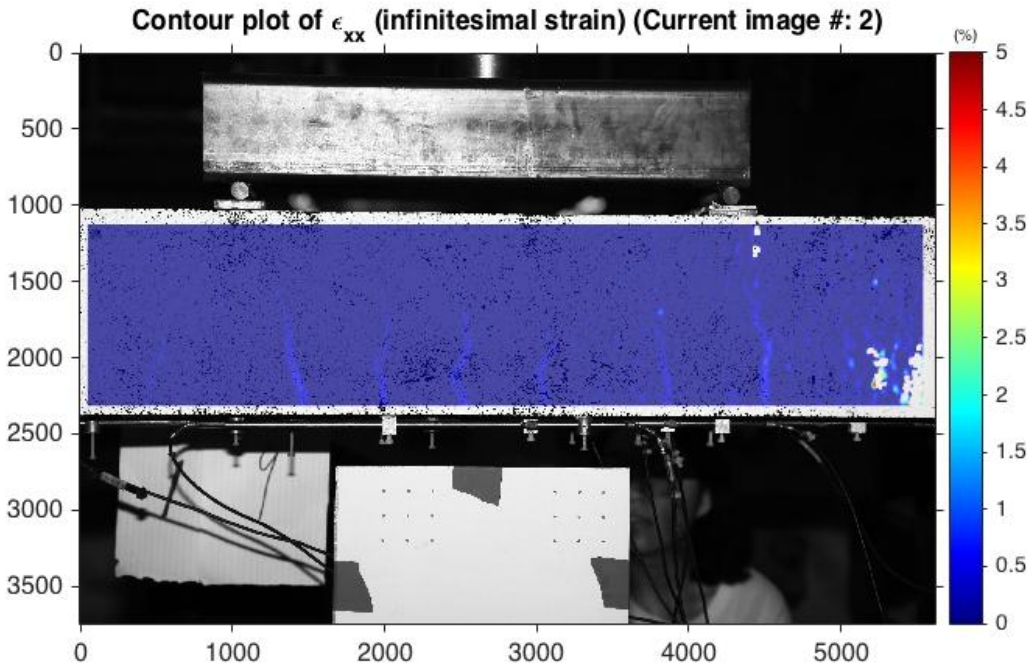

Figure 142 DIC image under 19 kN of Test 01, beam with SHCC layer of 30 mm

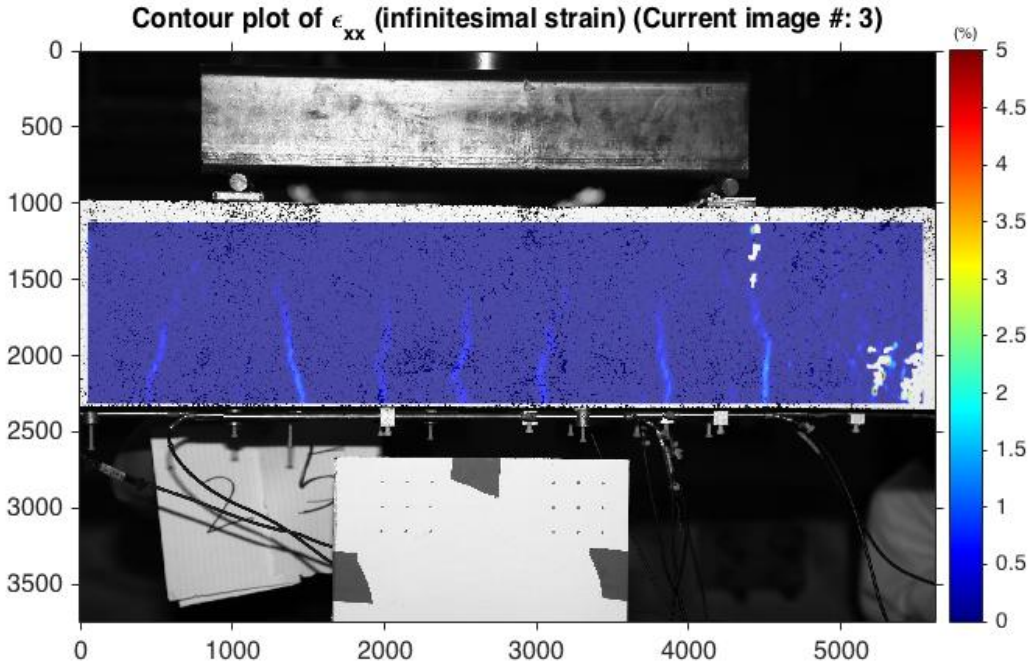

Figure 143 DIC image under 25 kN of Test 01, beam with SHCC layer of 30 mm

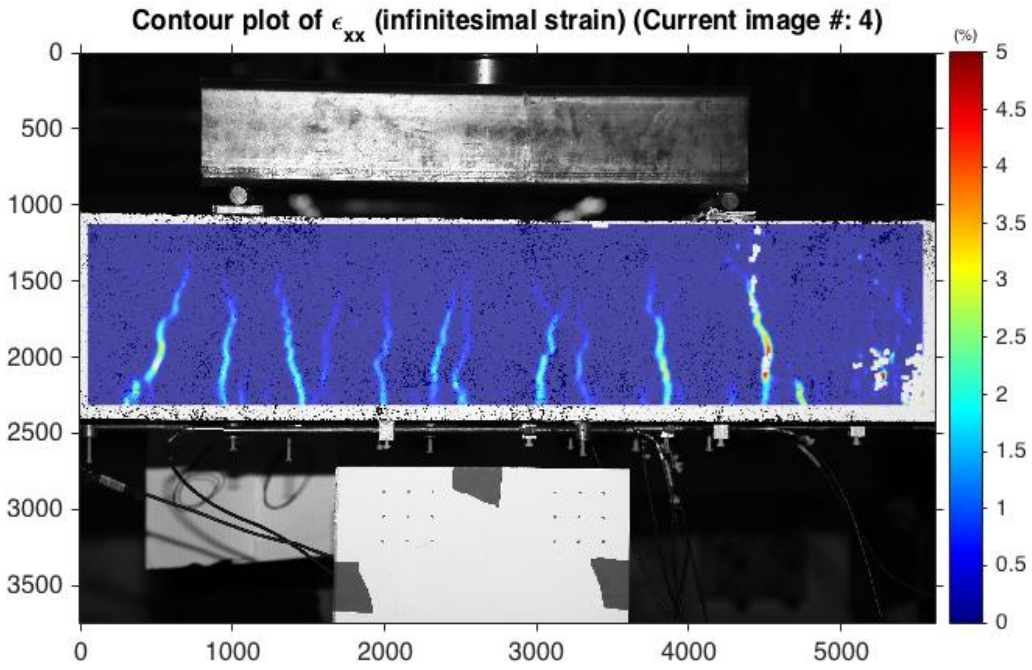

Figure 144 DIC image under 60 kN of Test 01, beam with SHCC layer of 30 mm

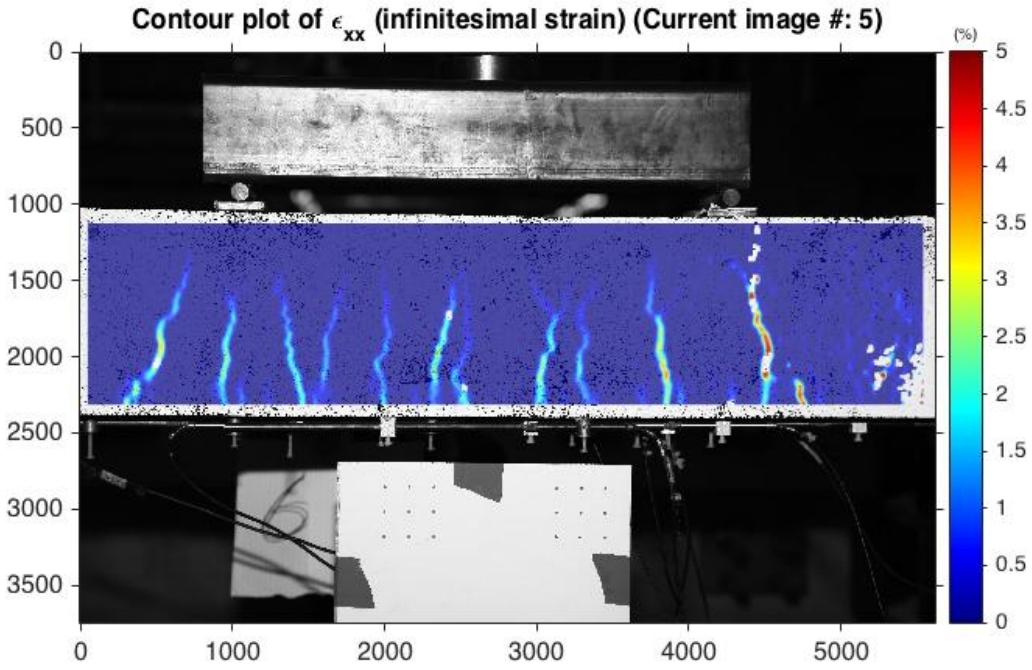

Figure 145 DIC image under 64 kN of Test 01, beam with SHCC layer of 30 mm

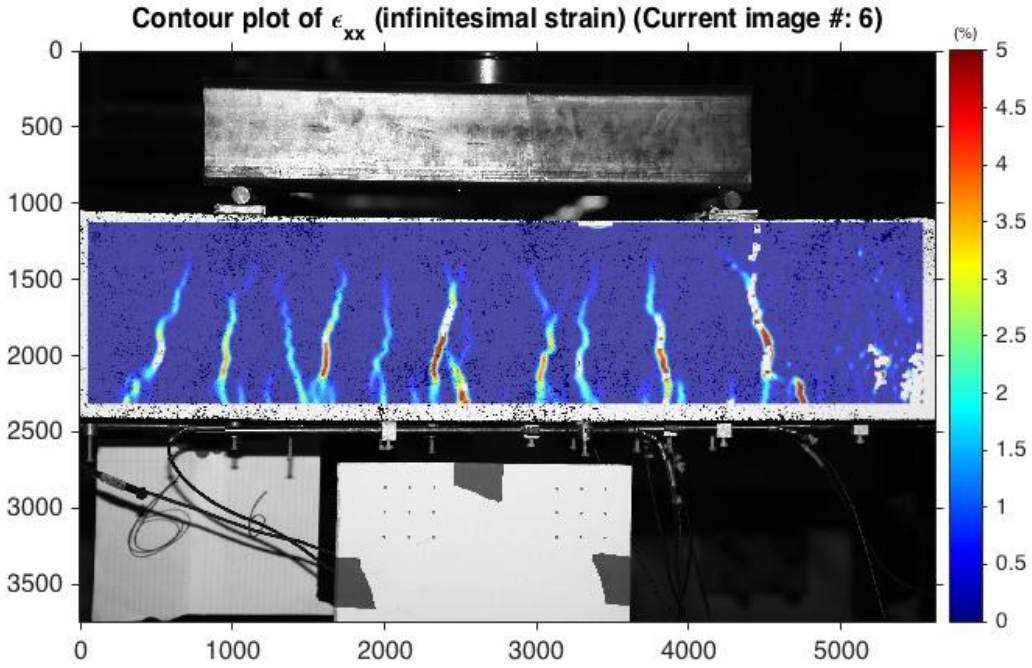

Figure 146 DIC image under 66 kN of Test 01, beam with SHCC layer of 30 mm

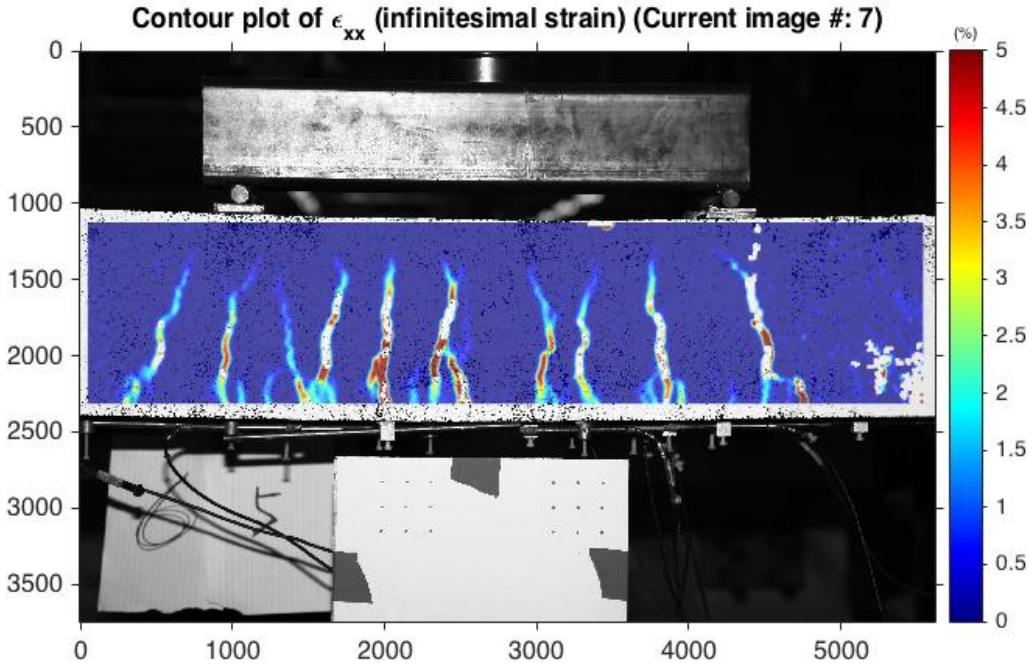

Figure 147 DIC image under 65 kN (decrease) of Test 01, beam with SHCC layer of 30 mm

Test 02, RC beam with cover of 11 mm

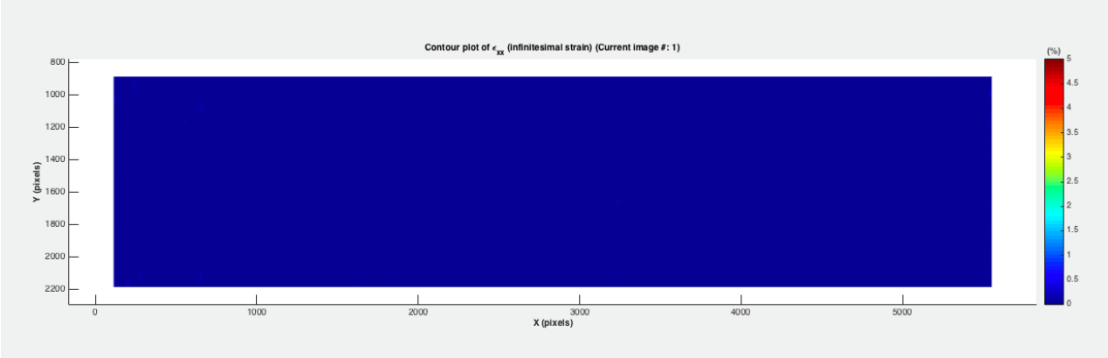

Figure 148 DIC image under 0 kN of Test 02, RC beam with cover of 11 mm

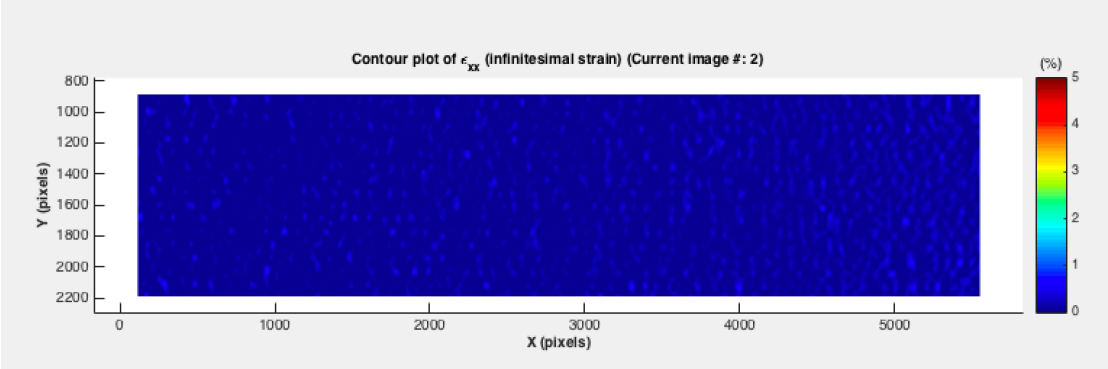

Figure 149 DIC image under 10 kN of Test 02, RC beam with cover of 11 mm

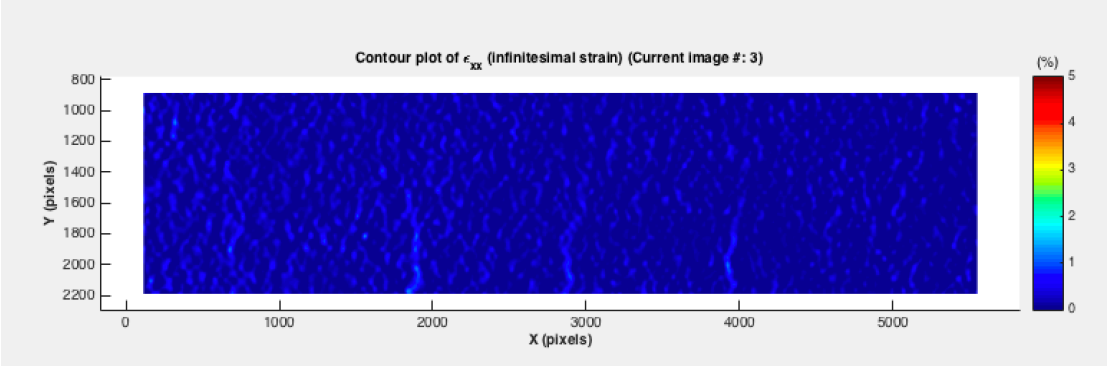

Figure 150 DIC image under 20 kN of Test 02, RC beam with cover of 11 mm

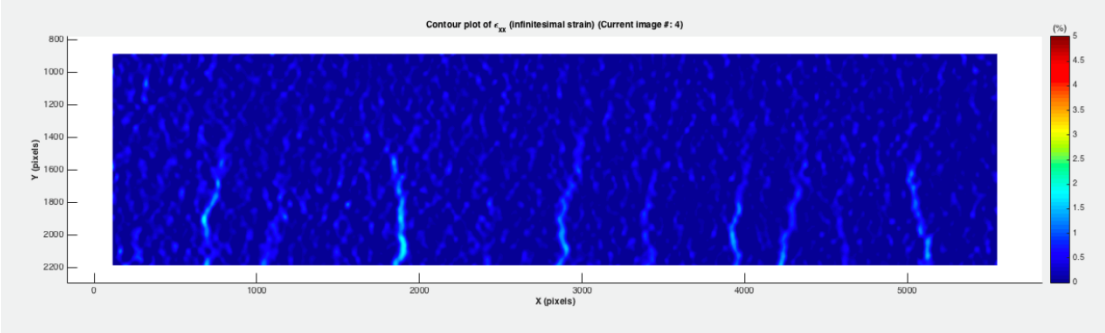

Figure 151 DIC image under 30 kN of Test 02, RC beam with cover of 11 mm

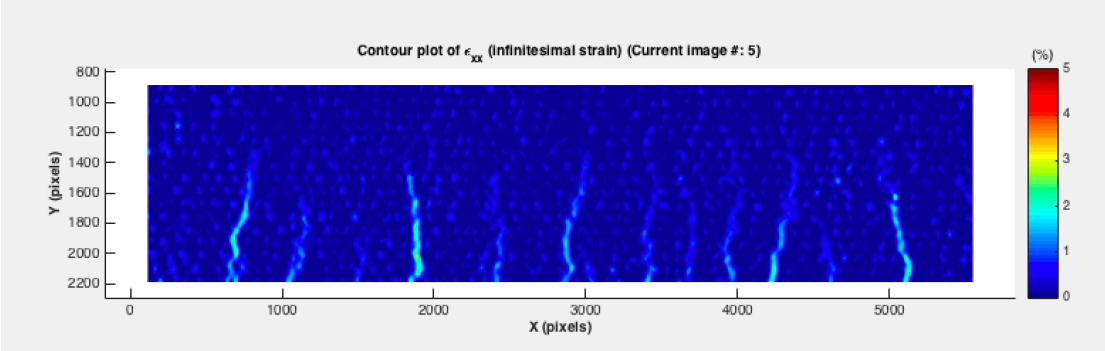

Figure 152 DIC image under 40 kN of Test 02, RC beam with cover of 11 mm

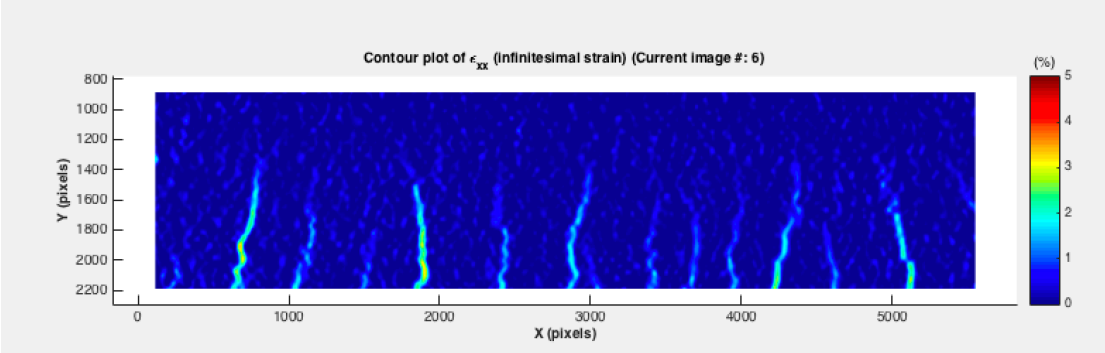

Figure 153 DIC image under 50 kN of Test 02, RC beam with cover of 11 mm

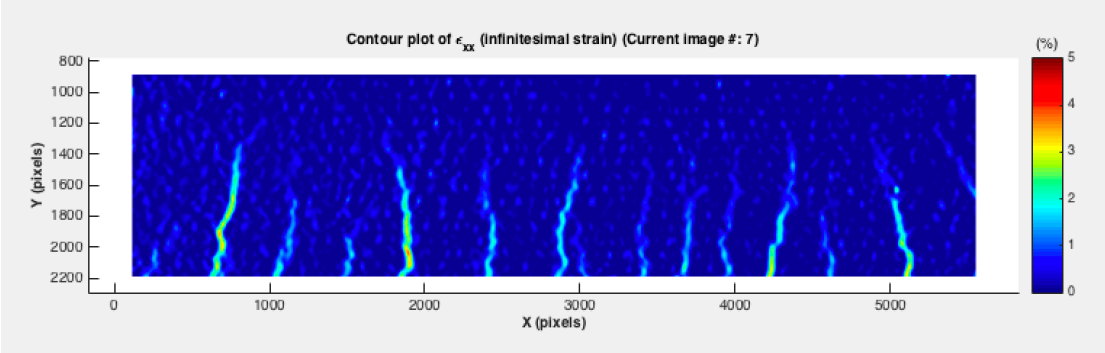

Figure 154 DIC image under 55 kN of Test 02, RC beam with cover of 11 mm

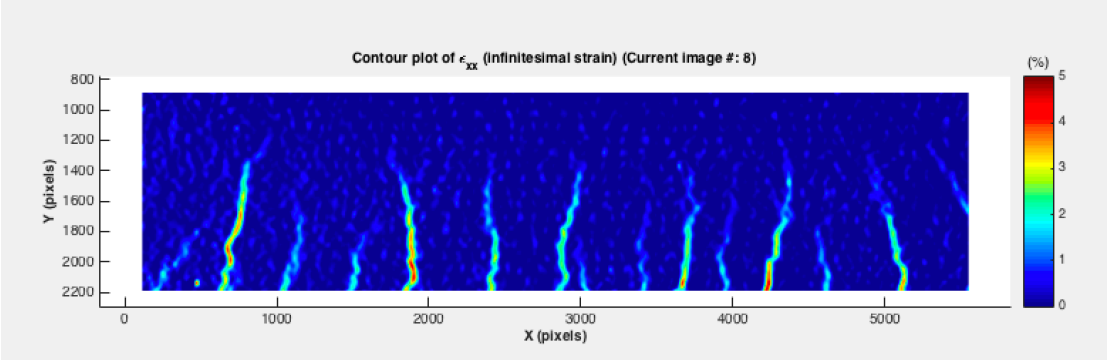

Figure 155 DIC image under 60 kN of Test 02, RC beam with cover of 11 mm

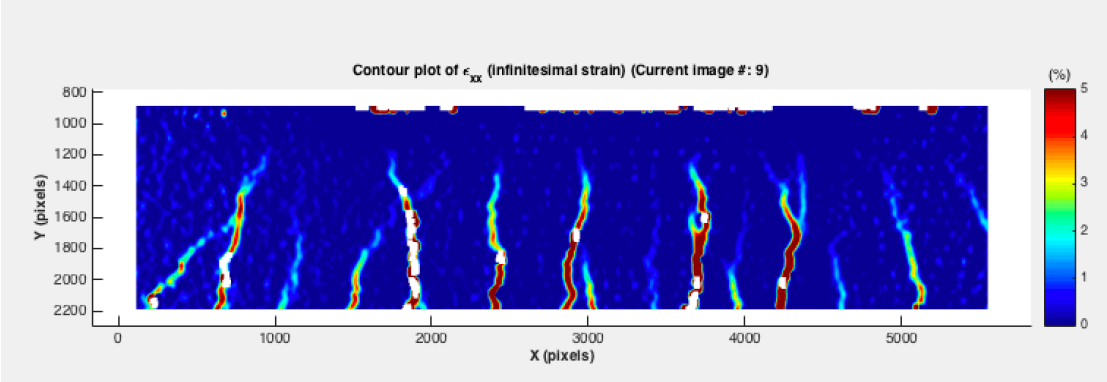

Figure 156 DIC image under 64 kN of Test 02, RC beam with cover of 11 mm

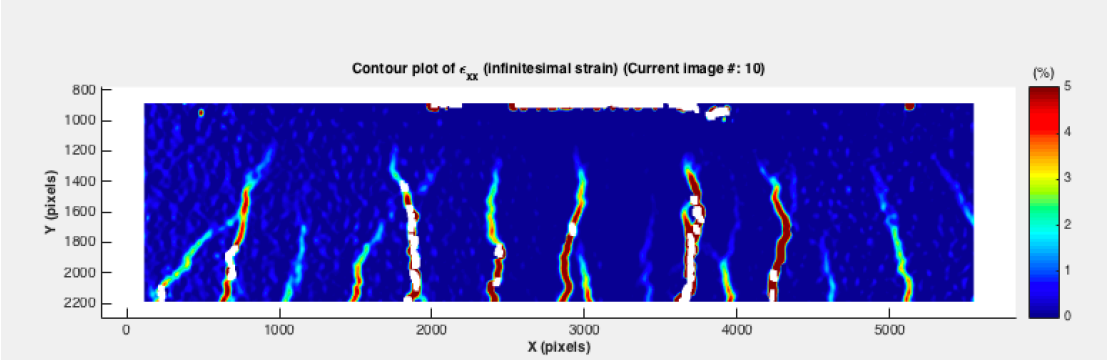

Figure 157 DIC image under 58 kN (decrease) of Test 02, RC beam with cover of 11 mm

Test 03, beam with SHCC layer of 70 mm

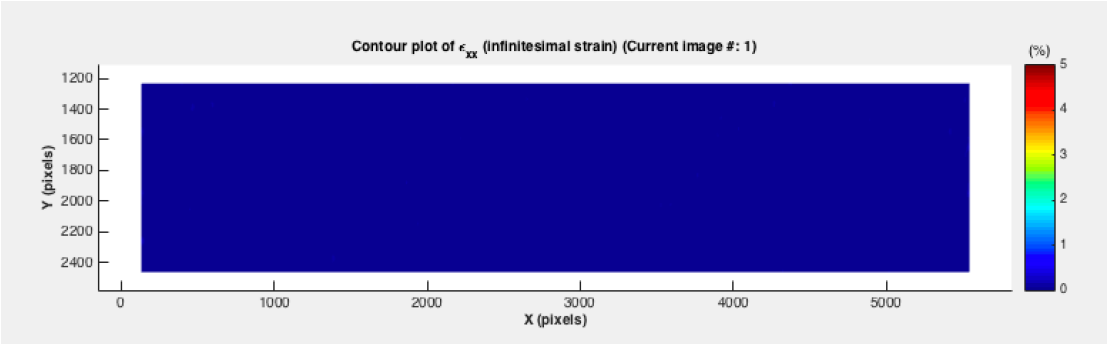

Figure 158 DIC image under 0 kN of Test 03, beam with SHCC layer of 70 mm

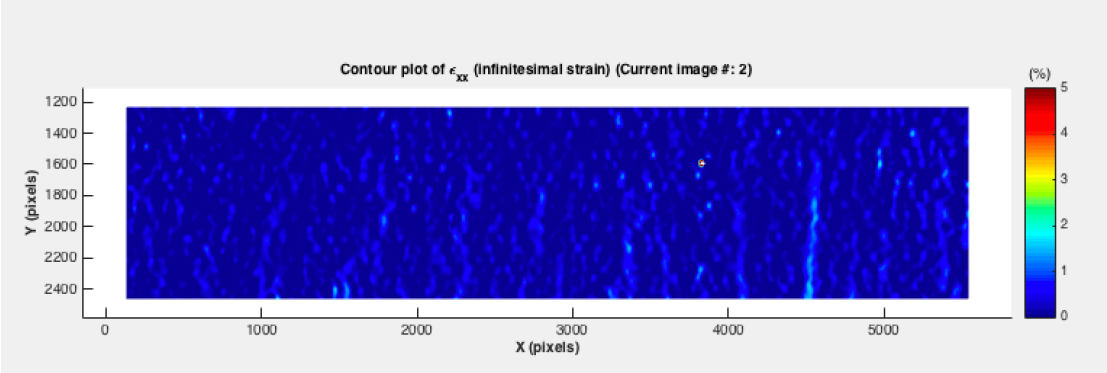

Figure 159 DIC image under 30 kN of Test 03, beam with SHCC layer of 70 mm

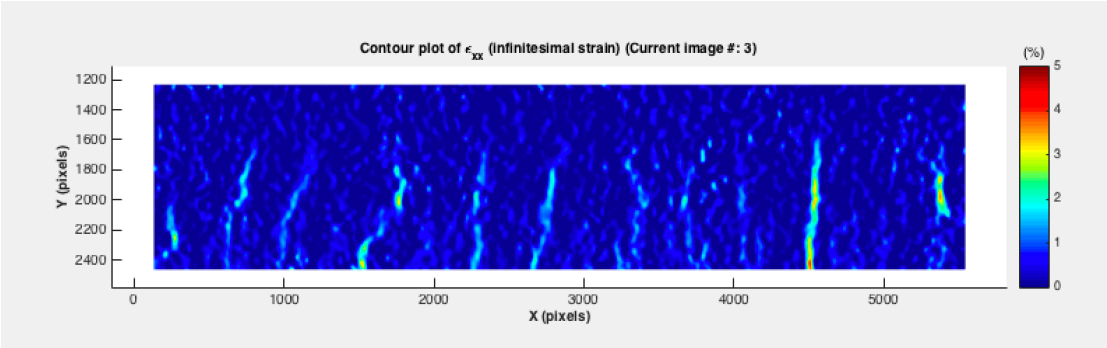

Figure 160 DIC image under 60 kN of Test 03, beam with SHCC layer of 70 mm

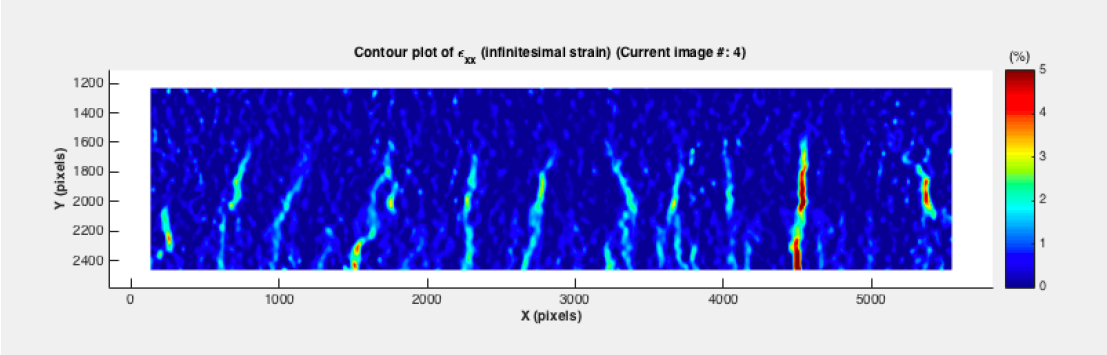

Figure 161 DIC image under 70 kN of Test 03, beam with SHCC layer of 70 mm

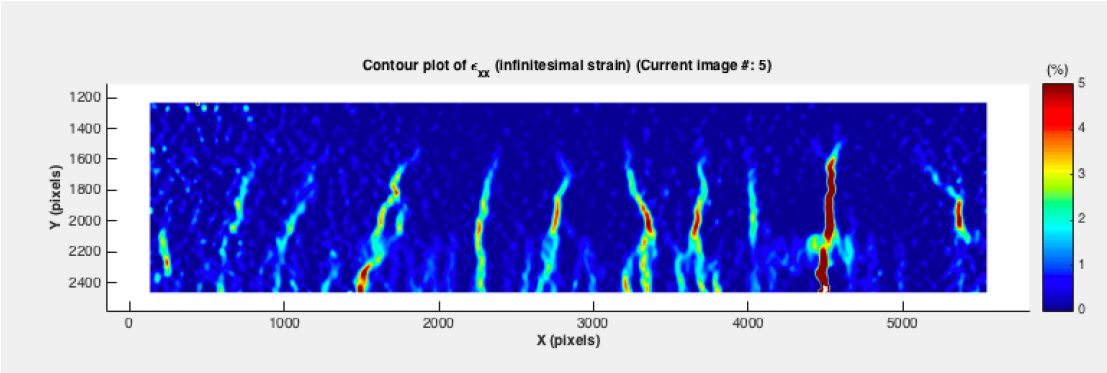

Figure 162 DIC image under 74 kN of Test 03, beam with SHCC layer of 70 mm

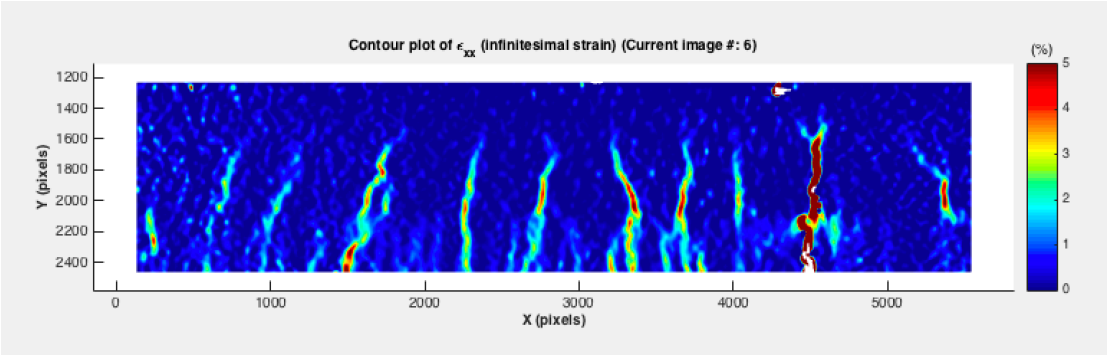

Figure 163 DIC image under 75 kN of Test 03, beam with SHCC layer of 70 mm

Test 04, beam with SHCC+SH layer of 70 mm

Figure 164 DIC image under 0 kN of Test 04, beam with SHCC+SH layer of 70 mm

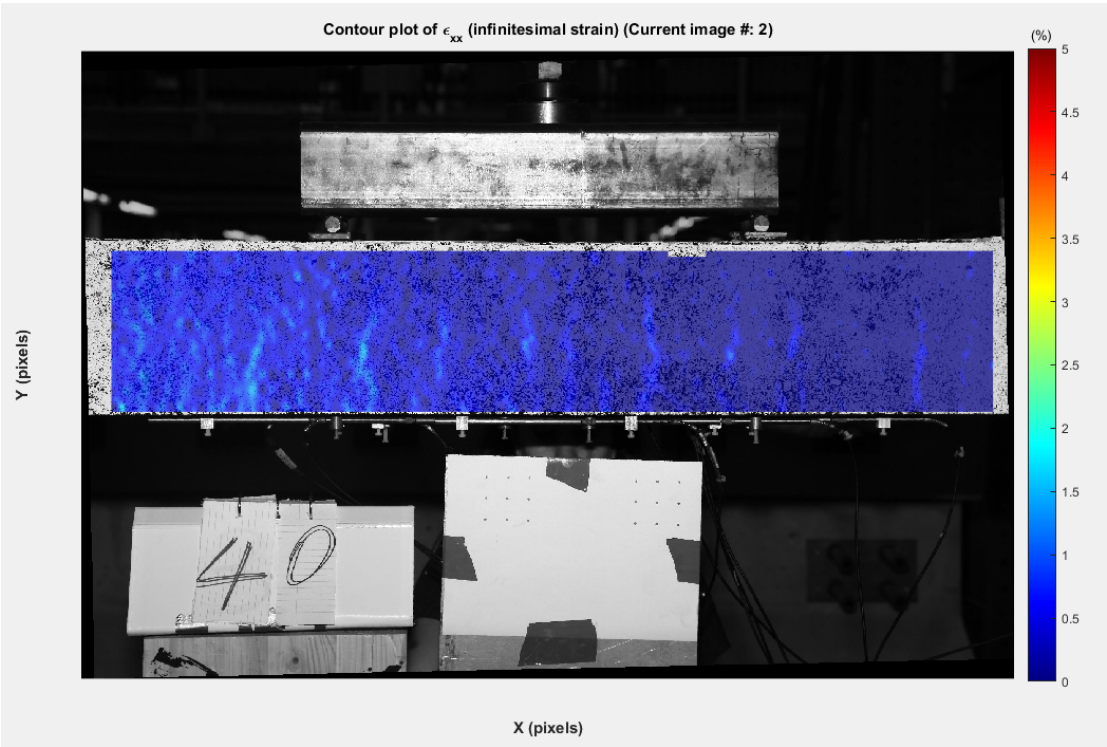

Figure 165 DIC image under 40 kN of Test 04, beam with SHCC+SH layer of 70 mm

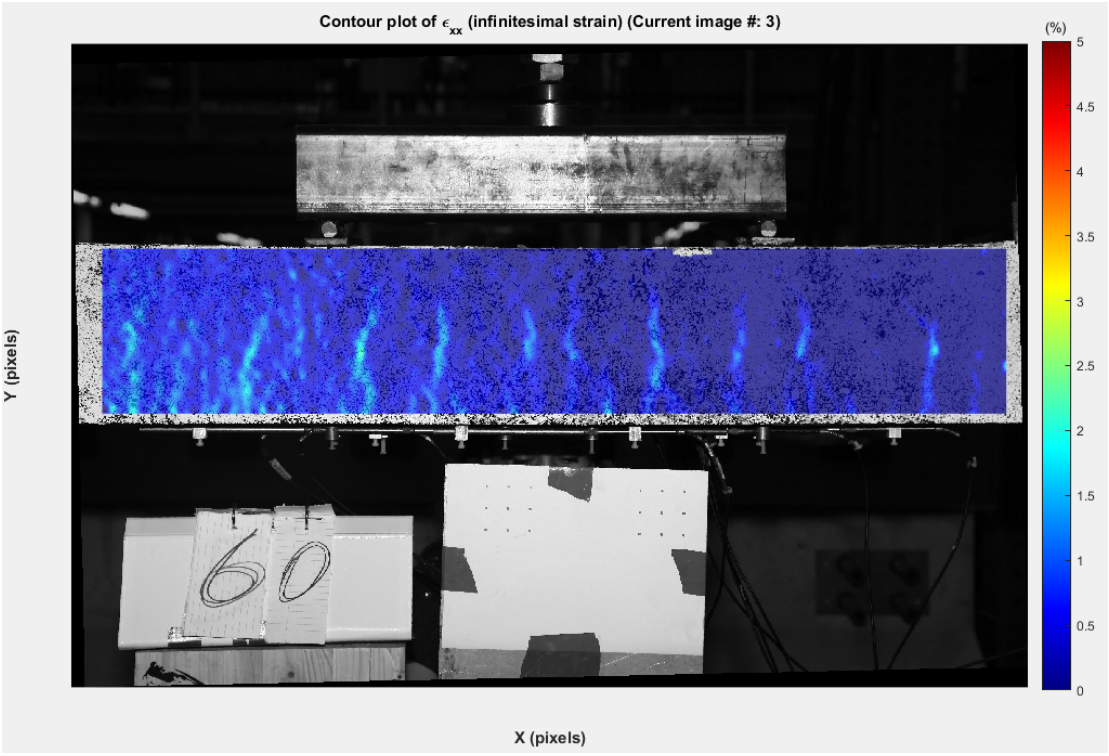

Figure 166 DIC image under 60 kN of Test 04, beam with SHCC+SH layer of 70 mm

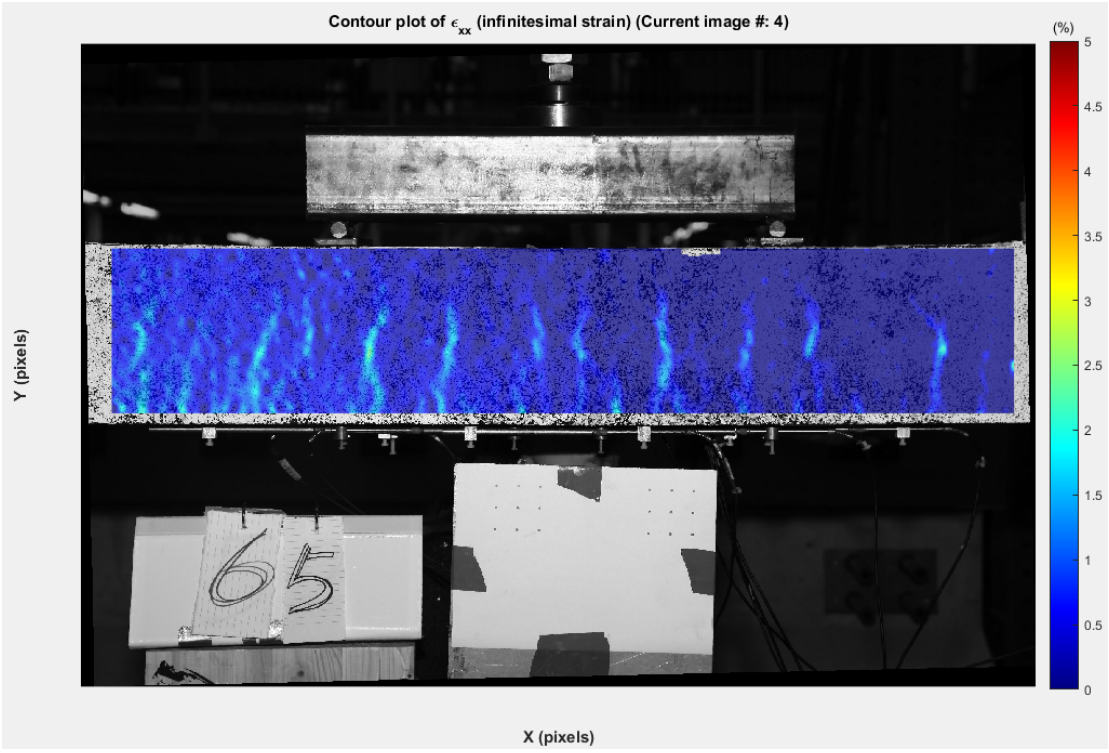

Figure 167 DIC image under 65 kN of Test 04, beam with SHCC+SH layer of 70 mm

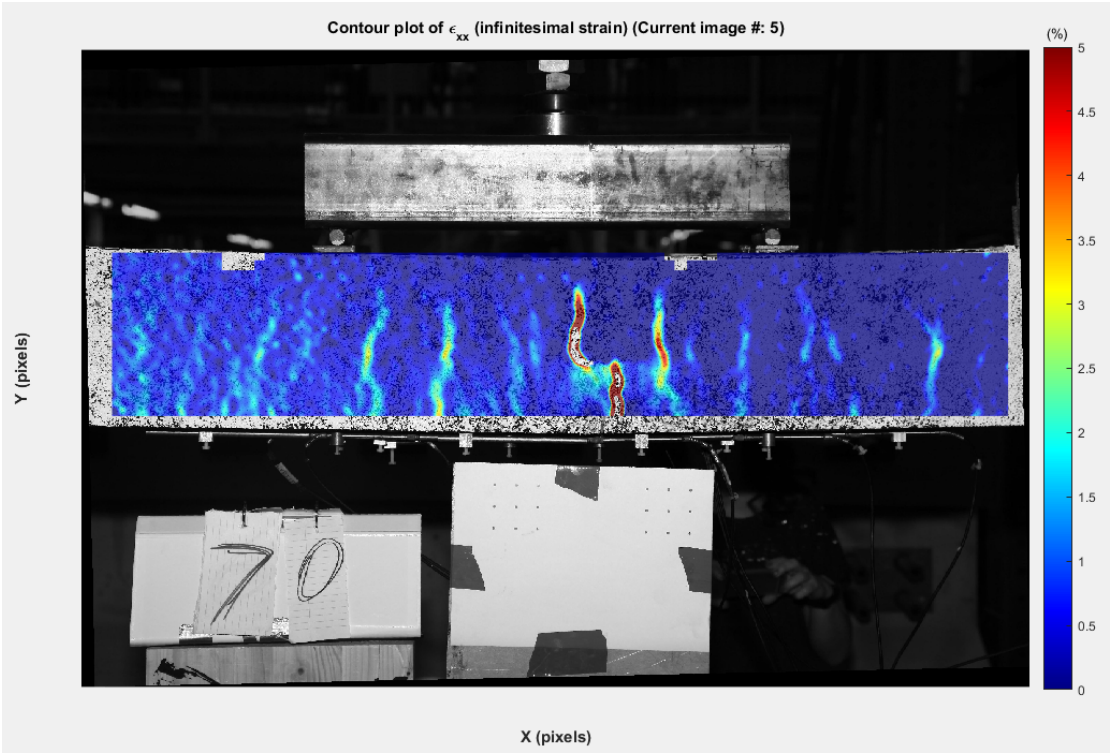

Figure 168 DIC image under 70 kN of Test 04, beam with SHCC+SH layer of 70 mm

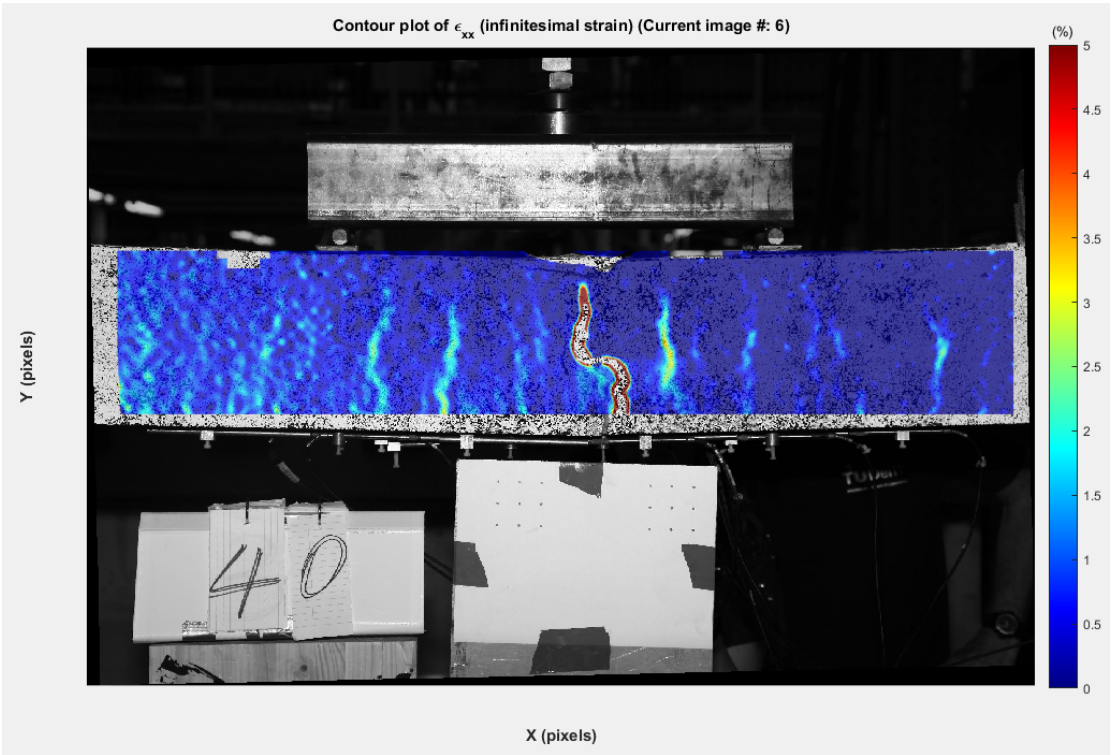

Figure 169 DIC image under 40 kN of Test 04, beam with SHCC+SH layer of 70 mm

Test 05, beam with SHCC layer of 30 mm

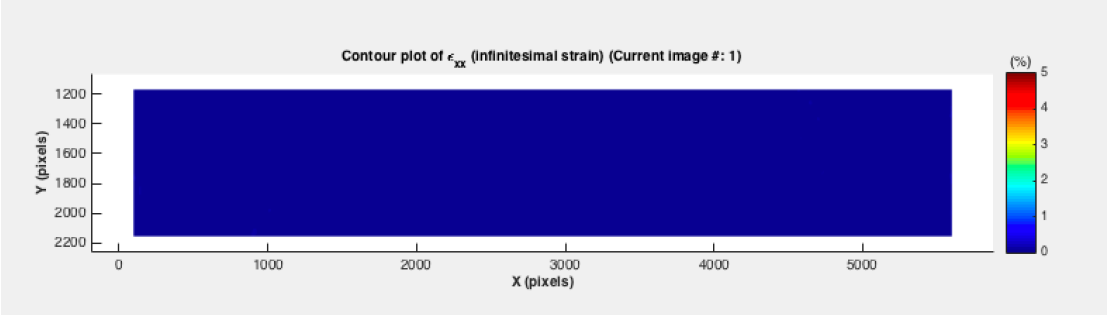

Figure 170 DIC image under 0 kN of Test 05, beam with SHCC layer of 30 mm

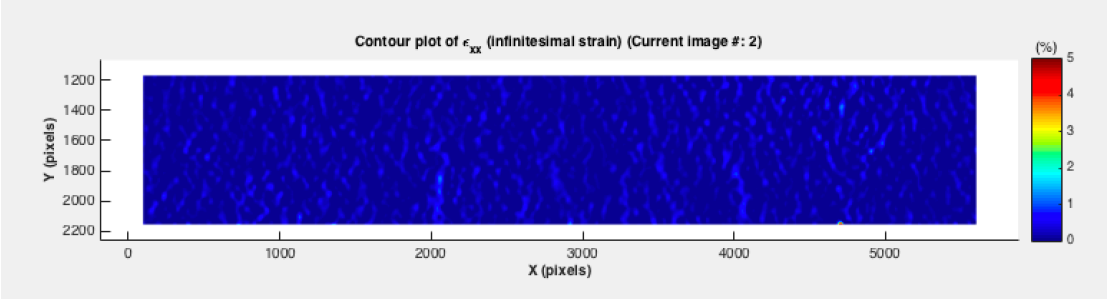

Figure 171 DIC image under 20 kN of Test 05, beam with SHCC layer of 30 mm

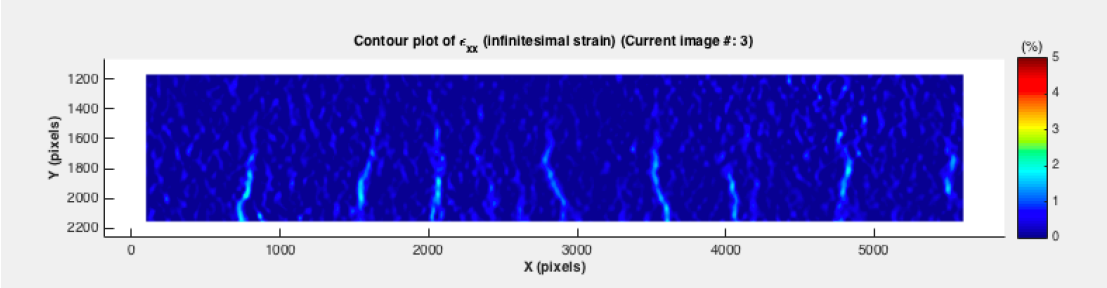

Figure 172 DIC image under 40 kN of Test 05, beam with SHCC layer of 30 mm

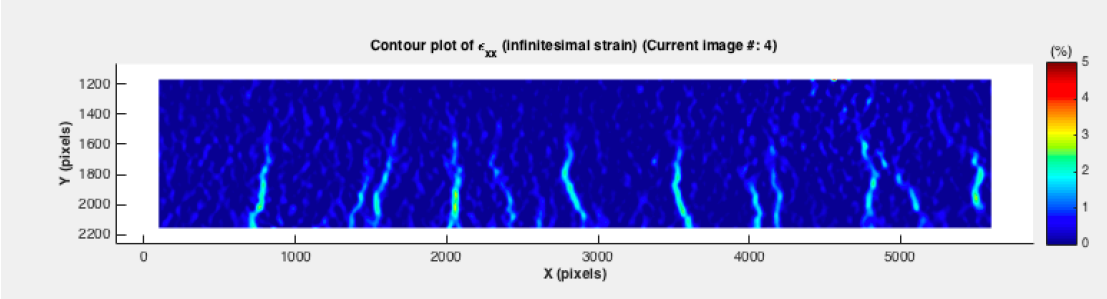

Figure 173 DIC image under 60 kN of Test 05, beam with SHCC layer of 30 mm

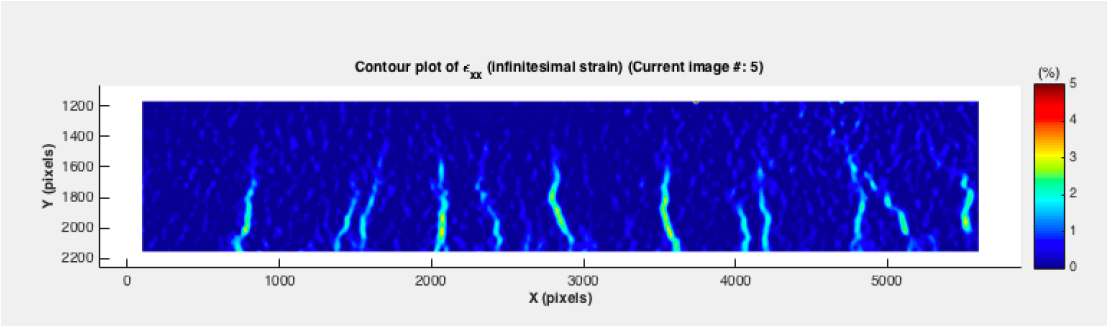

Figure 174 DIC image under 65 kN of Test 05, beam with SHCC layer of 30 mm

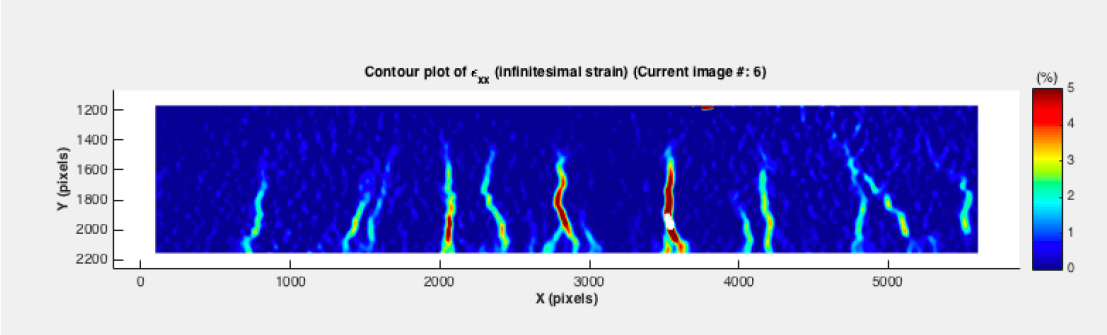

Figure 175 DIC image under 70 kN of Test 05, beam with SHCC layer of 30 mm

Test 06, RC beam with cover of 31 mm

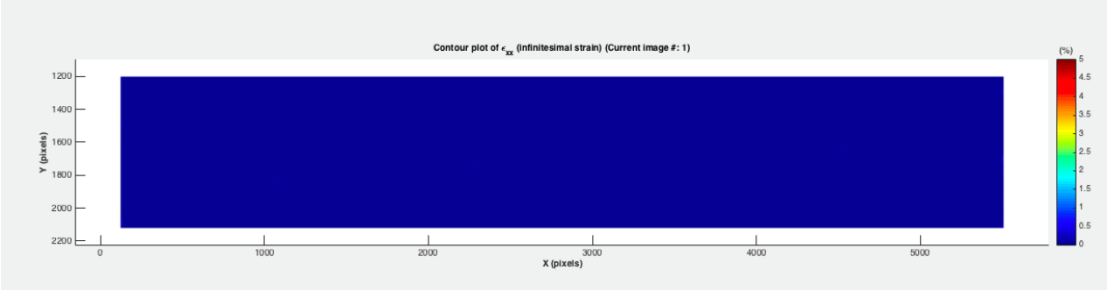

Figure 176 DIC image under 0 kN of Test 06, RC beam with cover of 31 mm

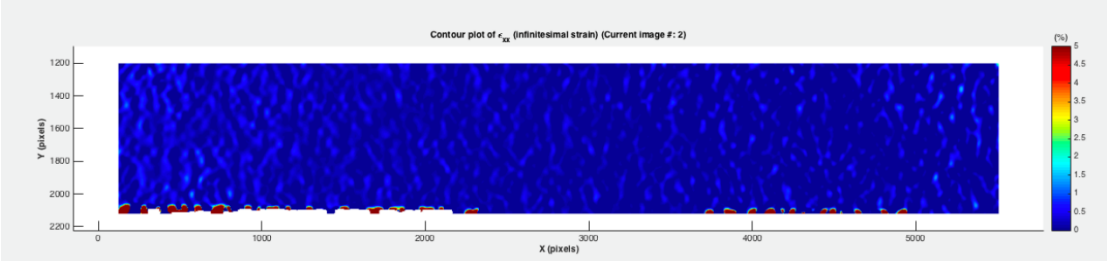

Figure 177 DIC image under 10 kN of Test 06, RC beam with cover of 31 mm

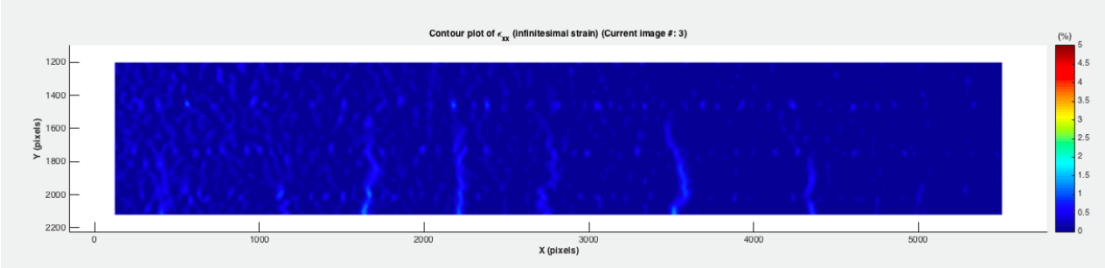

Figure 178 DIC image under 20 kN of Test 06, RC beam with cover of 31 mm

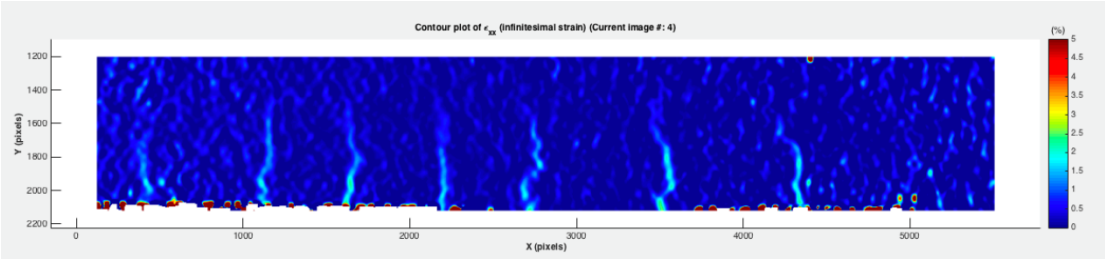

Figure 179 DIC image under 30 kN of Test 06, RC beam with cover of 31 mm

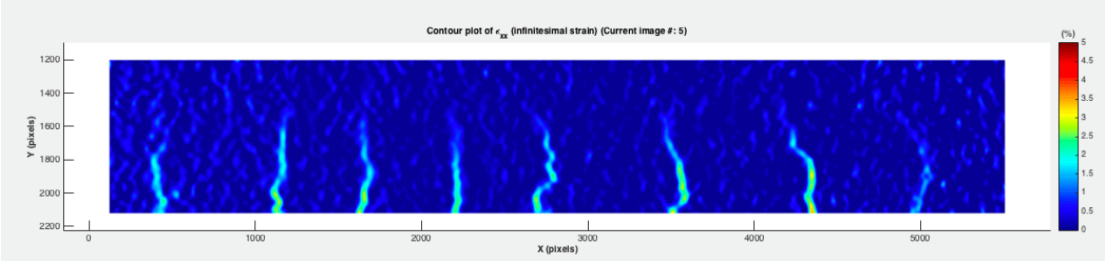

Figure 180 DIC image under 40 kN of Test 06, RC beam with cover of 31 mm

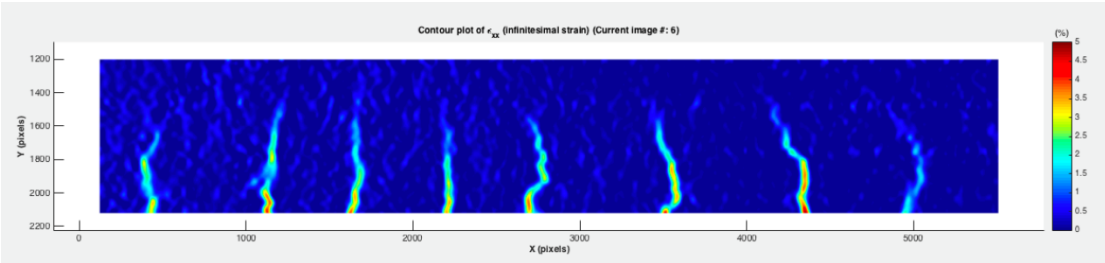

Figure 181 DIC image under 50 kN of Test 06, RC beam with cover of 31 mm

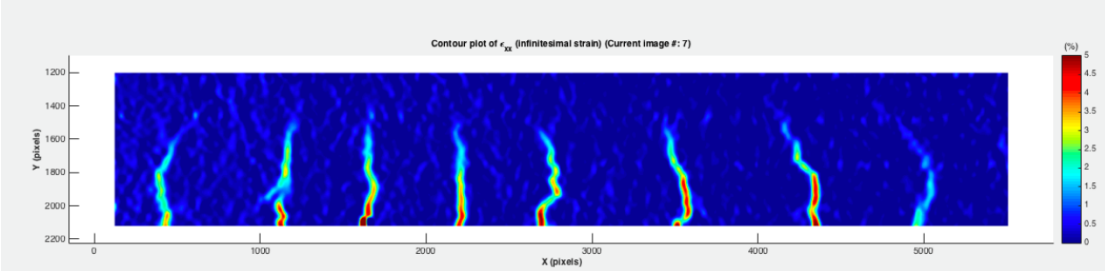

Figure 182 DIC image under 55 kN of Test 06, RC beam with cover of 31 mm

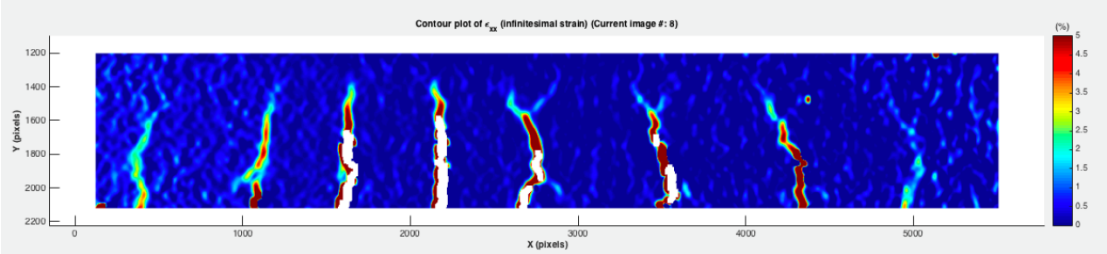

Figure 183 DIC image under 60 kN of Test 06, RC beam with cover of 31 mm

Appendix I. Theoretical and experimental crack spacings for all beams

Table 19 Calculated and experimental crack spacing of RC beam with 11 mm cover

Crack No.	Experimental Measurements [mm]	Theoretical Calculations [mm]
1-2	109.443	
2-3	74.444	
3-4	107.242	
4-5	97.286	
Mean	97.104	55.95
Min	74.444	37
Max	109.443	88.15

Table 20 Experimental crack spacing of beam with SHCC+SH layer of 30 mm

Crack No.	Experimental Measurements [mm]
1-2	62.822
2-3	43.802
3-4	82.418
4-5	63.398
5-6	56.482
6-7	72.62
Mean	63.59
Min	43.802
Max	82.418

Table 21 Experimental crack spacing of beam with SHCC layer of 30 mm

Crack No.	Experimental Measurements [mm]
1-2	91.499
2-3	136.406
3-4	88.131
4-5	76.345
Mean	98.095
Min	76.345
Max	136.406

Table 22 Calculated and experimental crack spacing of RC beam with 31 mm cover

Crack No.	Experimental Measurements [mm]	Theoretical Calculations [mm]
1-2	130.649	
2-3	149.739	
3-4	95.303	
4-5	89.485	
Mean	116.294	130.55
Min	89.485	87
Max	149.739	223.76

Table 23 Experimental crack spacing of beam with SHCC+SH layer of 70 mm

Crack No.	Experimental Measurements [mm]
1-2	73.835
2-3	66.43
3-4	51.384
4-5	76.844
5-6	78.388
6-7	68.975
Mean	69.309
Min	51.384
Max	78.388

Table 24 Experimental crack spacing of beam with SHCC layer of 70 mm

Crack No.	Experimental Measurements [mm]
1-2	71.034
2-3	25.864
3-4	33.878
4-5	62.656
5-6	44.078
6-7	65.934
7-8	102.362
Mean	57.972
Min	25.864
Max	102.362

Appendix J. Load-Deflection curves from the jack

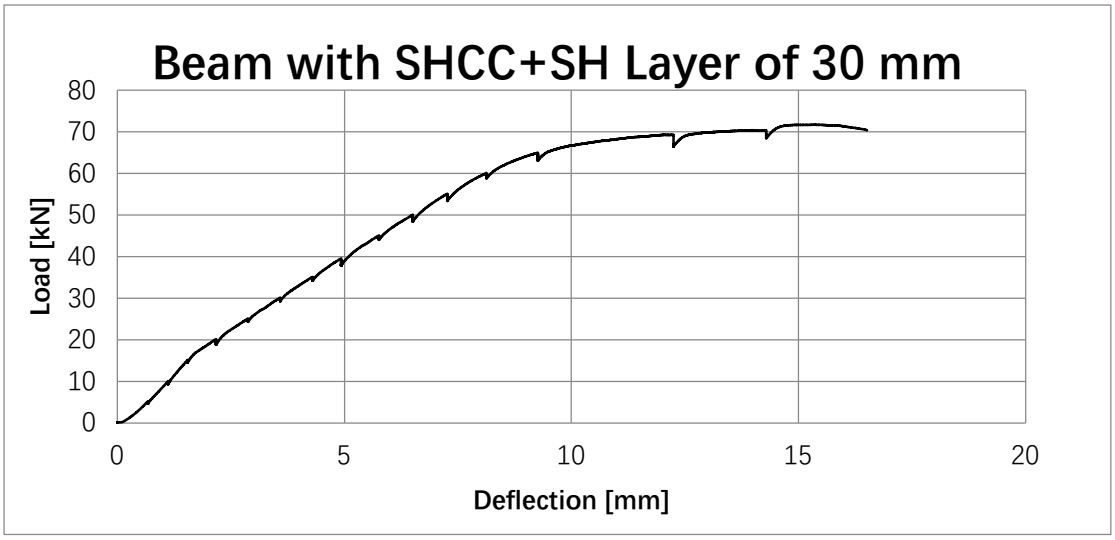

Figure 184 Load-Deflection curve of beam with SHCC+SH layer of 30 mm

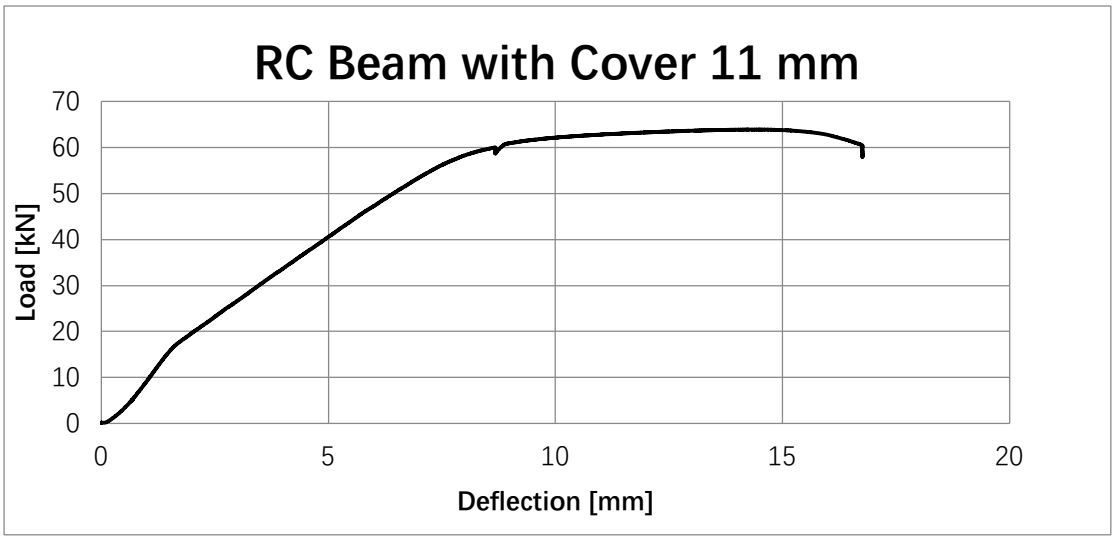

Figure 185 Load-Deflection curve of RC beam with cover of 11 mm

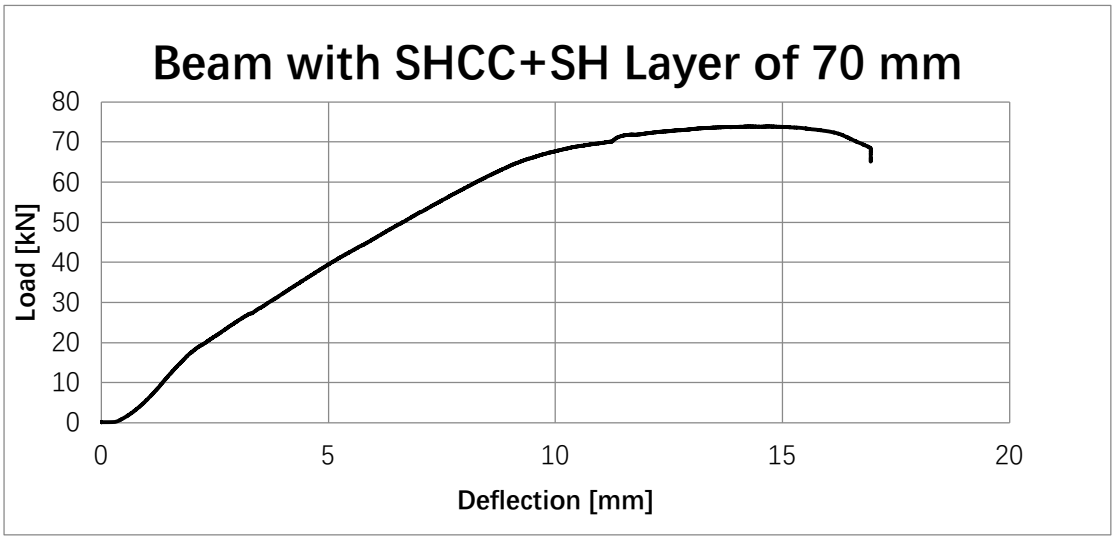

Figure 186 Load-Deflection curve of beam with SHCC+SH layer of 70 mm

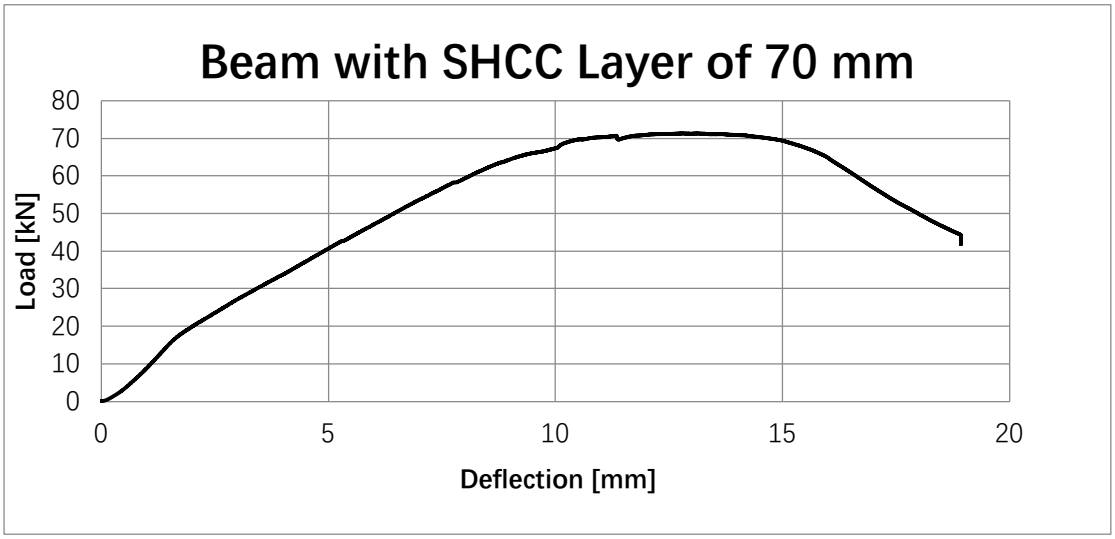

Figure 187 Load-Deflection curve of beam with SHCC layer of 70 mm

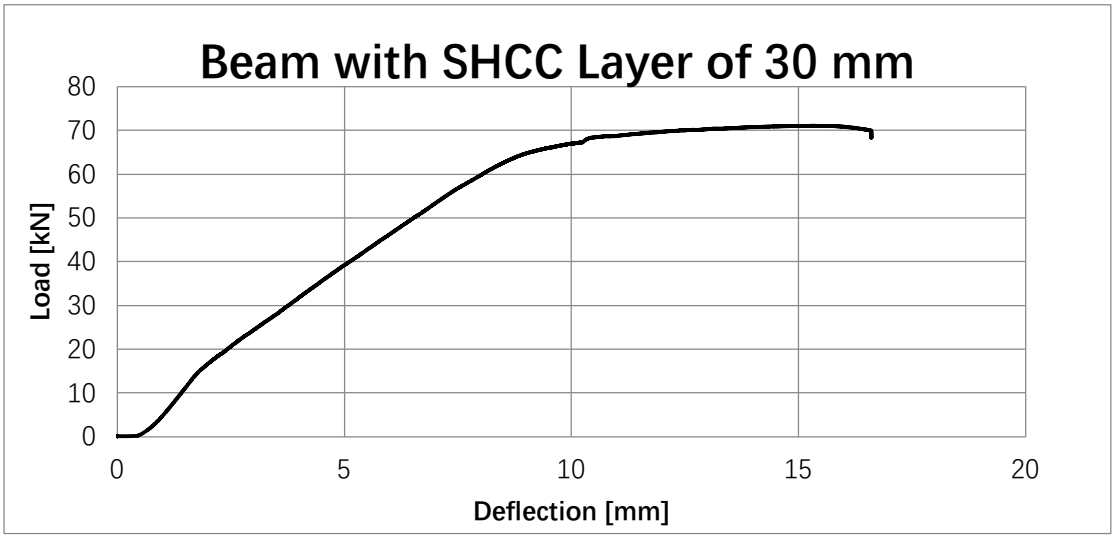

Figure 188 Load-Deflection curve of beam with SHCC layer of 30 mm

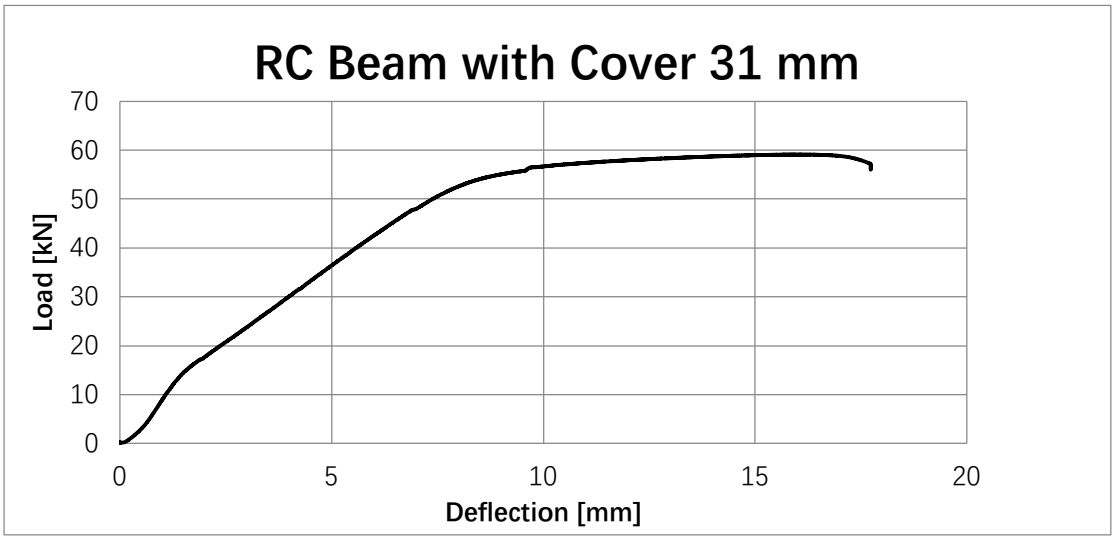

Figure 189 Load-Deflection curve of RC beam with cover of 31 mm

Appendix K. ImageJ for the beam with SHCC+SH layer of 70 mm

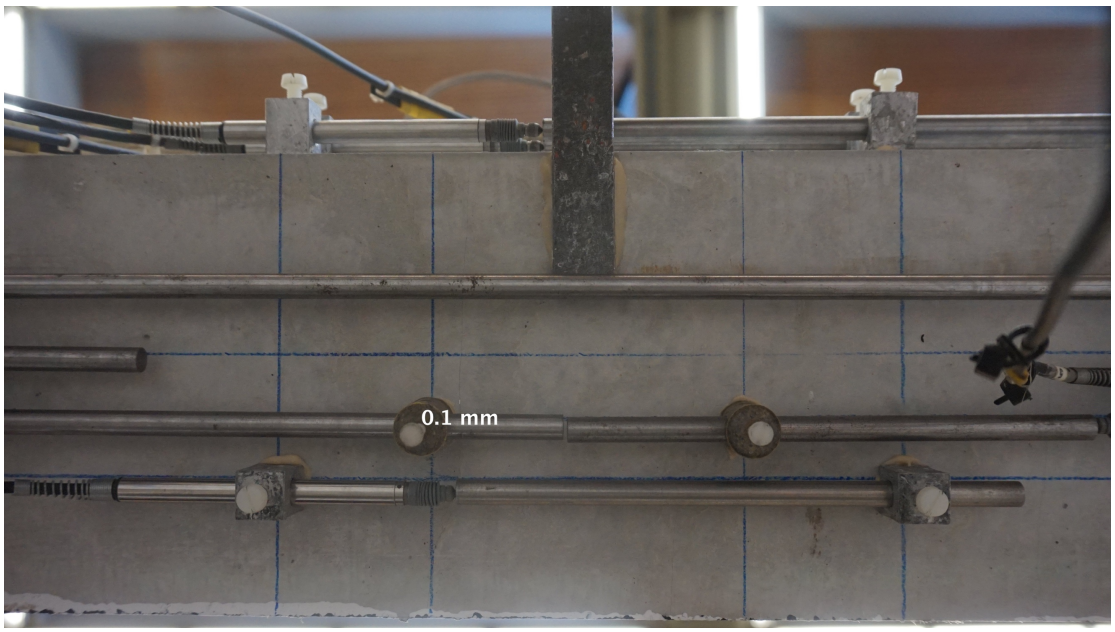

Figure 190 ImageJ measured photo of Test 04 bottom face under 0 kN

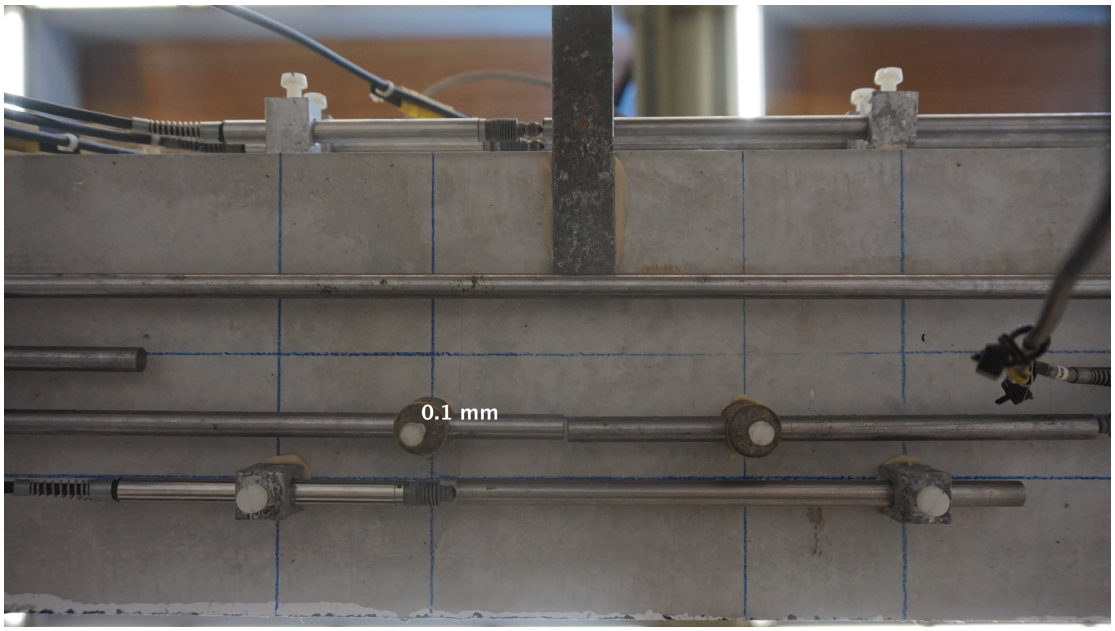

Figure 191 ImageJ measured photo of Test 04 bottom face under 7 kN

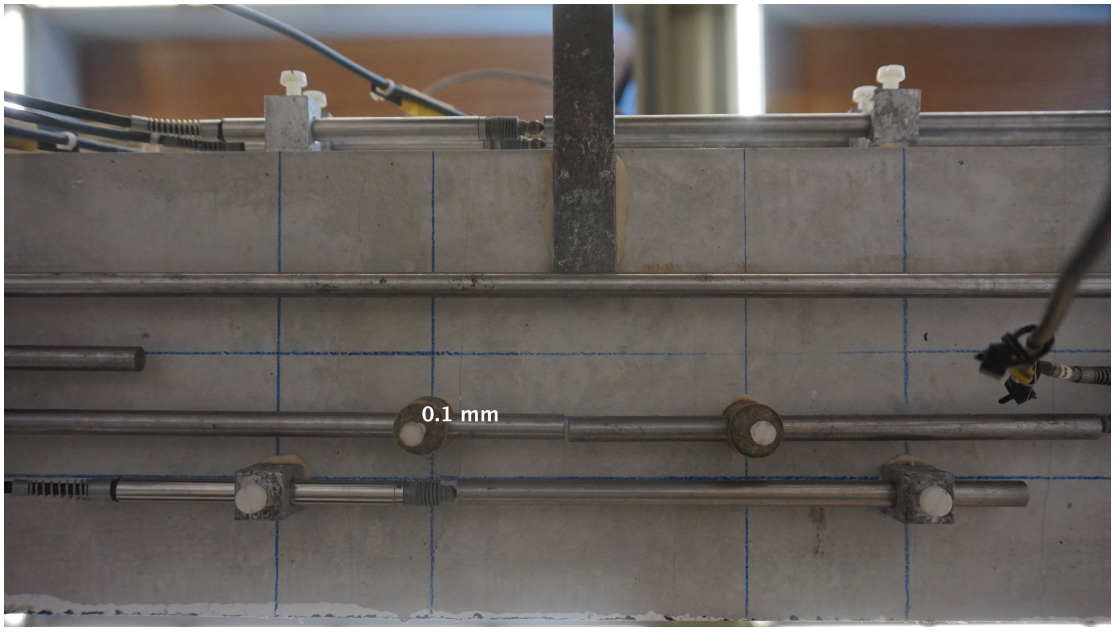

Figure 192 ImageJ measured photo of Test 04 bottom face under 20 kN

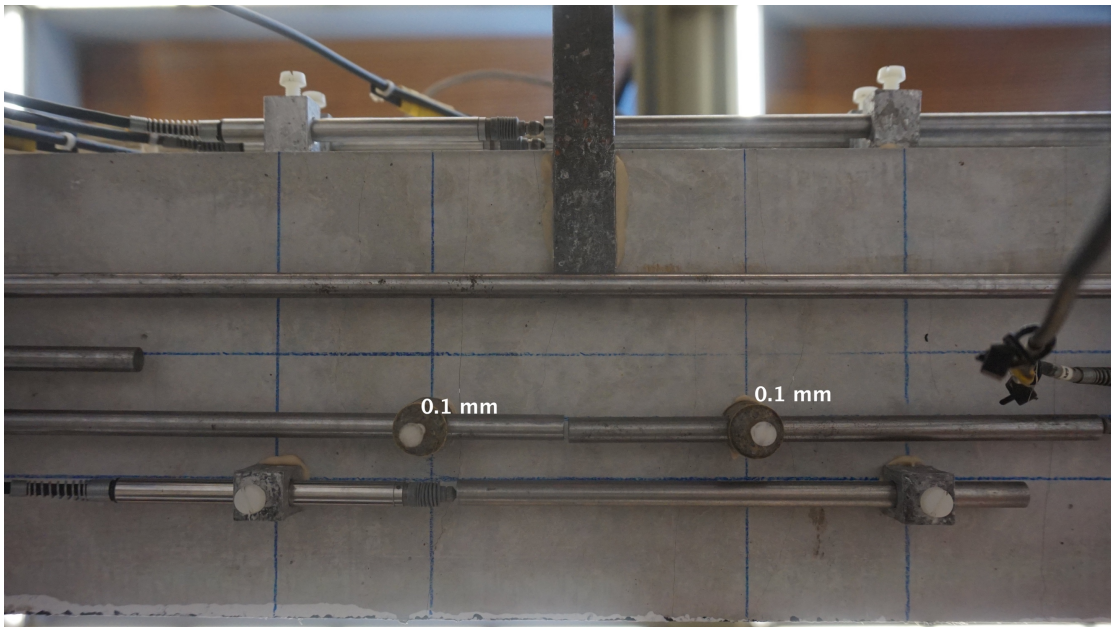

Figure 193 ImageJ measured photo of Test 04 bottom face under 30 kN

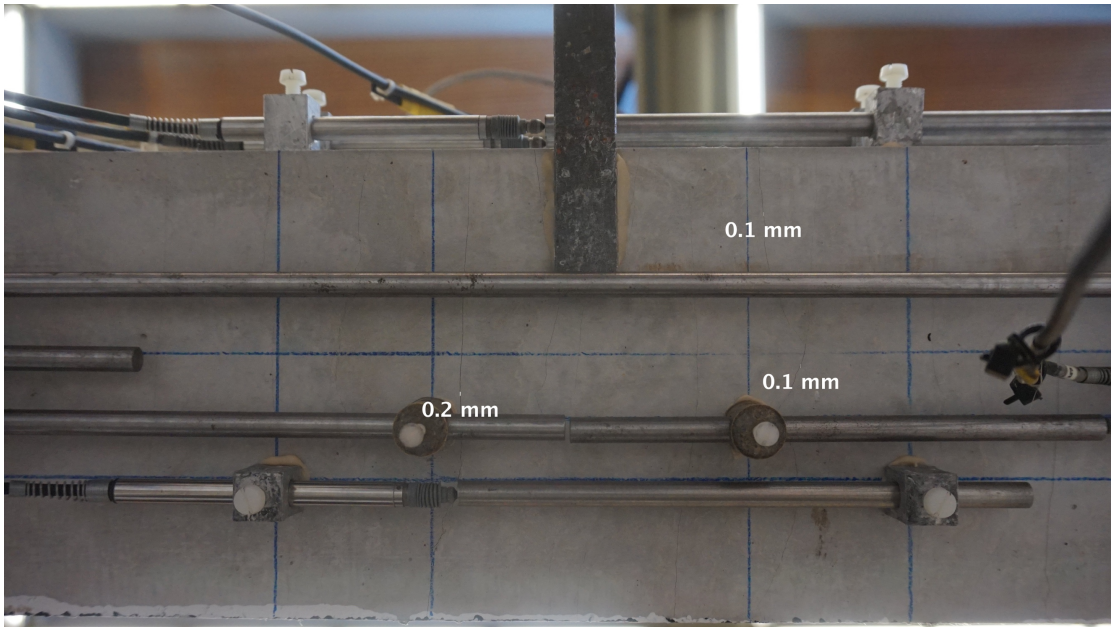

Figure 194 ImageJ measured photo of Test 04 bottom face under 37 kN

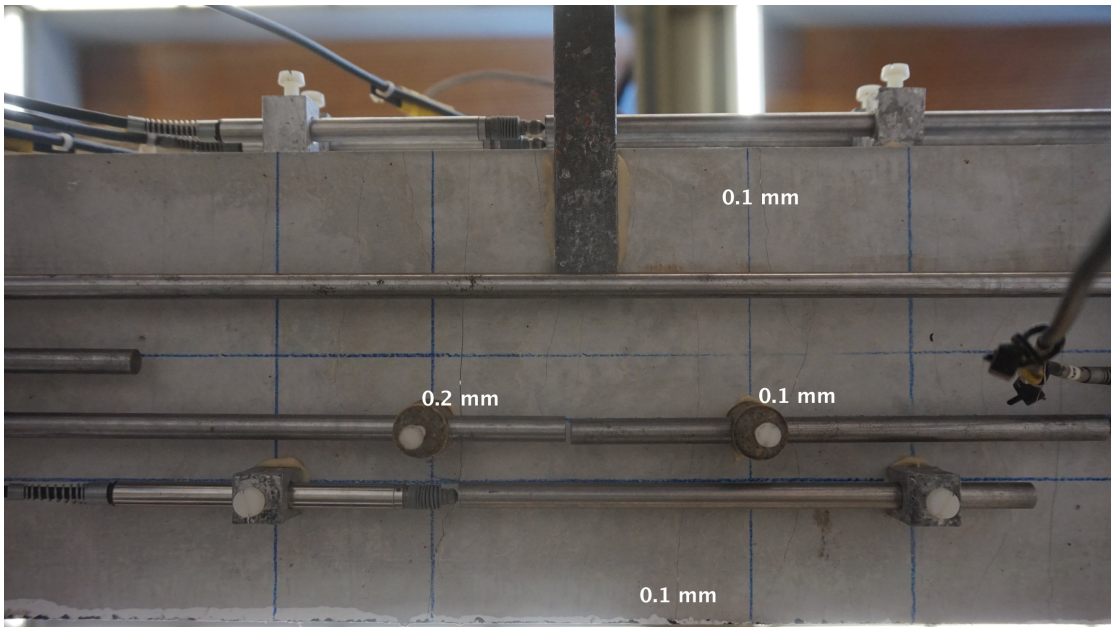

Figure 195 ImageJ measured photo of Test 04 bottom face under 50 kN

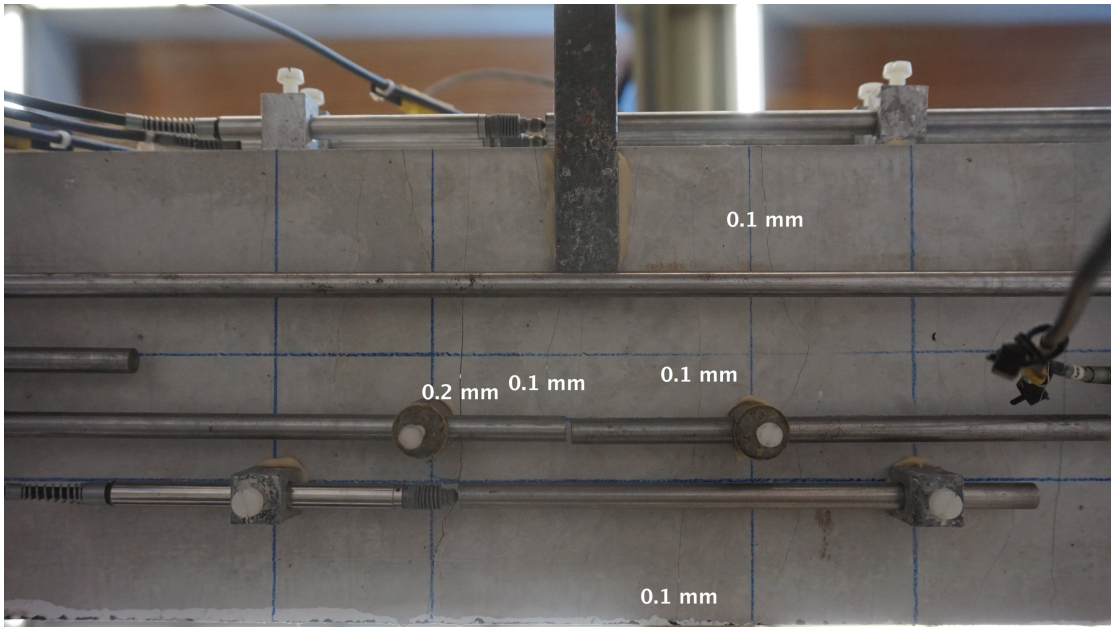

Figure 196 ImageJ measured photo of Test 04 bottom face under 55 kN

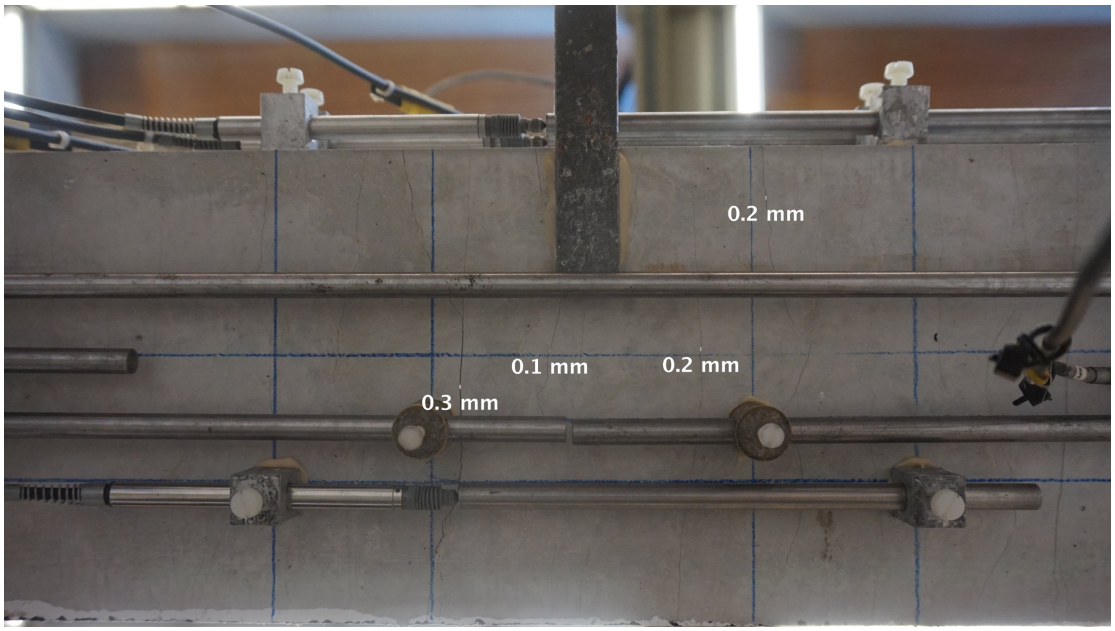

Figure 197 ImageJ measured photo of Test 04 bottom face under 62 kN

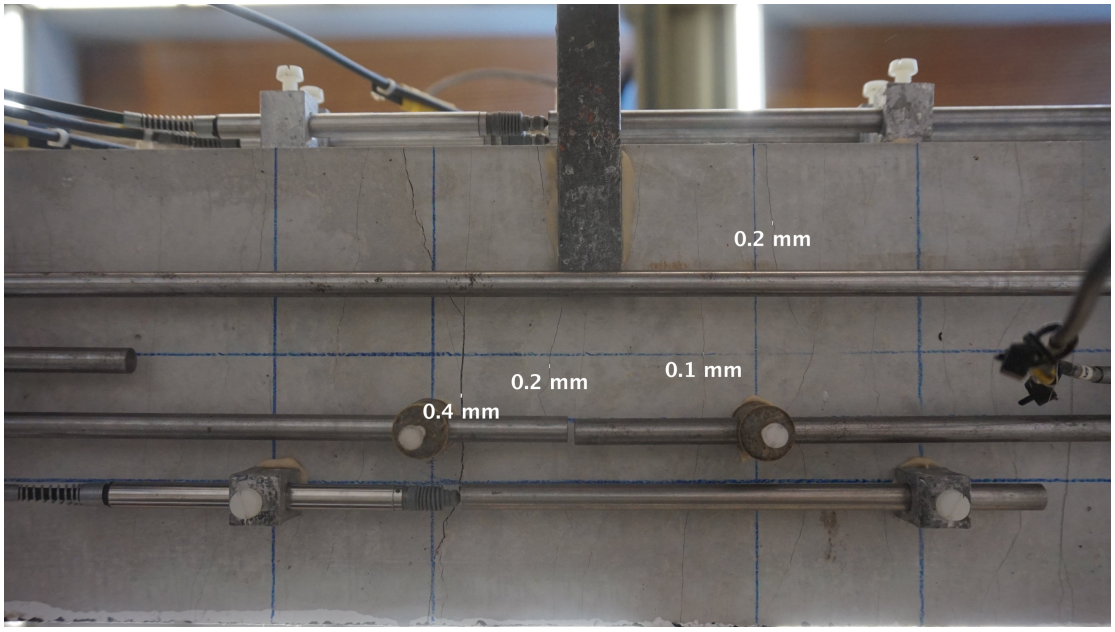

Figure 198 ImageJ measured photo of Test 04 bottom face under 67 kN

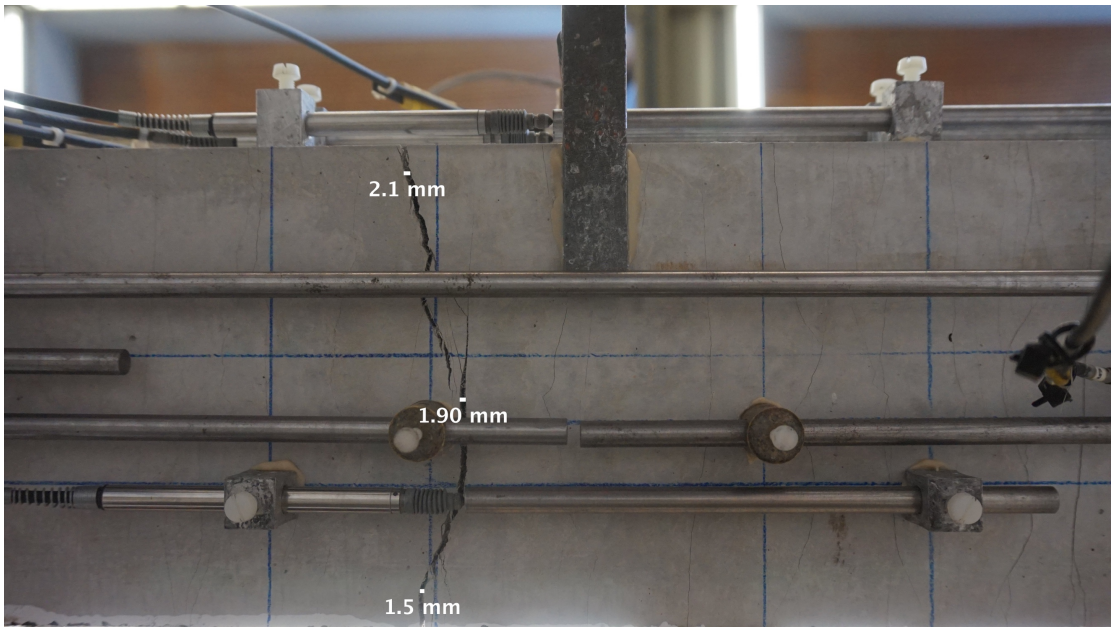

Figure 199 ImageJ measured photo of Test 04 bottom face under 70 kN

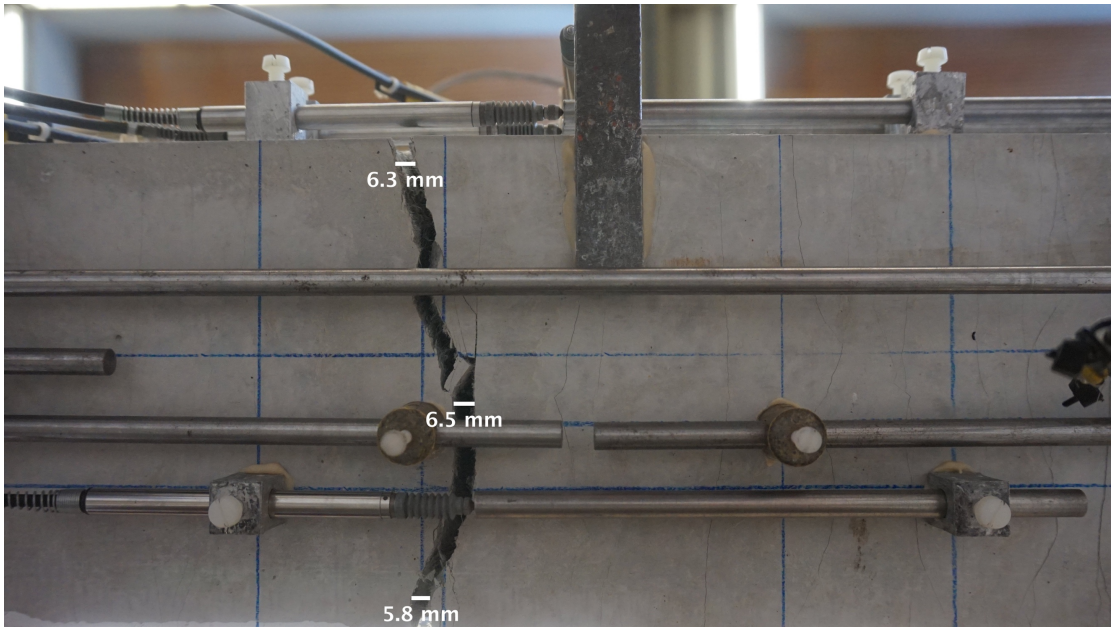

Figure 200 ImageJ measured photo of Test 04 bottom face under 42 kN